

**The role of glutamate receptors in
formation and maturation of *Drosophila*
neuromuscular synapses**

Dissertation

Zur Erlangung des Doktorgrades
der Mathematisch-Naturwissenschaftlichen Fakultäten
der Georg-August-Universität zu Göttingen

Vorgelegt von
Andreas Schmid
aus München

Göttingen, 2006

D7

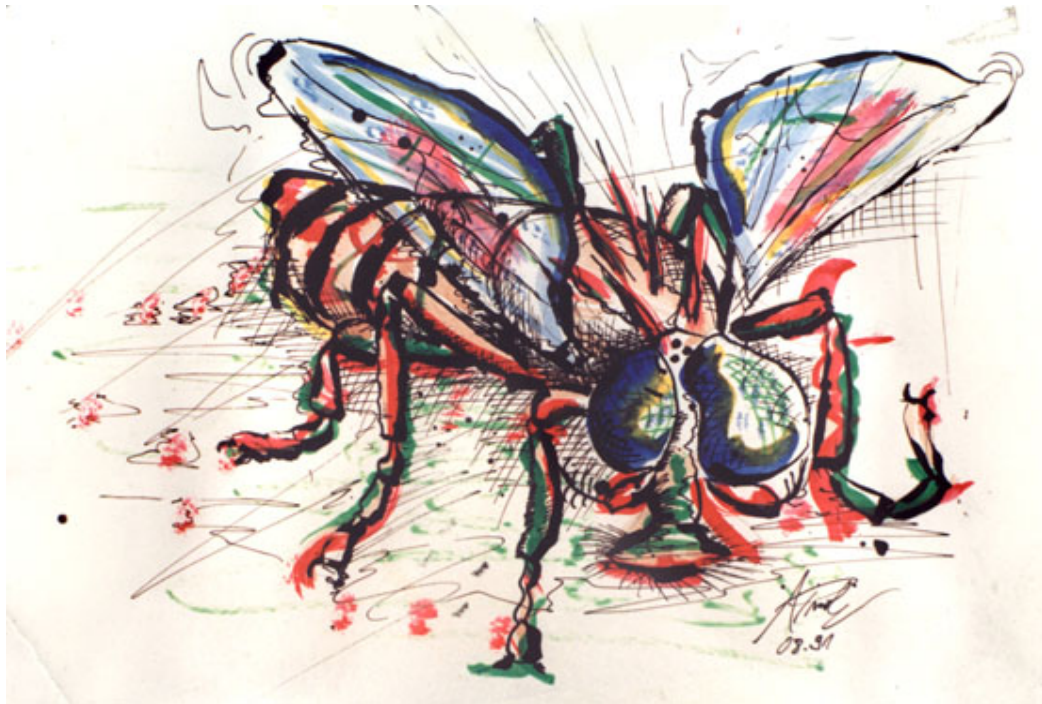
Referent: Prof. Dr. Ernst A. Wimmer

Korreferent: Prof. Dr. Ralf Heinrich

Tag der mündlichen Prüfung: 02.11.2006

The Fly – Ogden Nash
(1902-1971)

*God in his wisdom made the fly
And then forgot to tell us why.*



Andreas Prokop, 1991

Table of contents

List of figures	5
List of tables	7
Acknowledgements	8
1. Summary	10
2. Introduction	12
2.1. Structure and function of synapses	12
2.1.1. <i>Vertebrate neuromuscular synapses</i>	13
2.1.2. <i>Excitatory vertebrate CNS synapses</i>	14
2.1.2.1. Presynaptic structure.....	15
2.1.2.2. Postsynaptic structure	17
2.1.2.3. Structural synaptic plasticity and LTP	18
2.1.3. <i>Drosophila neuromuscular synapses</i>	19
2.1.3.1. <i>Drosophila melanogaster</i> as a model system	19
2.1.3.2. Properties of the <i>Drosophila</i> NMJ	20
2.1.3.3. Development of the <i>Drosophila</i> NMJ.....	22
2.1.3.4. Glutamatergic NMJ synapses	23
2.1.3.5. Activity-dependent remodeling.....	24
2.2. Structure and function of ionotropic glutamate receptors	25
2.2.1. <i>Structure and assembly of non-NMDA glutamate receptors</i>	25
2.2.2. <i>Glutamate receptor trafficking</i>	26
2.2.3. <i>Glutamate receptors at Drosophila NMJ synapses</i>	28
2.3. Study design.....	31
3. Material and Methods.....	32
3.1. Molecular biology	32
3.1.1. <i>Material</i>	32
3.1.2. <i>Transgenes</i>	32
3.1.2.1. Site-directed fluorescence-tagging of <i>gluRIIA</i> and <i>gluRIIB</i>	34
3.1.2.2. Chimeric glutamate receptor subunits.....	36
3.1.2.3. Modifications of <i>gluRIIA</i>	41
3.1.3. <i>In vitro transposition</i>	44
3.2. <i>Drosophila melanogaster</i>.....	45
3.2.1. <i>Cultivation</i>	45
3.2.2. <i>Transgenics</i>	46
3.2.3. <i>Genetics</i>	46

3.2.4. Immunohistochemistry.....	49
3.2.4.1. Larval body-wall preparation	49
3.2.4.2. Embryonic body-wall preparation	49
3.2.4.3. Fixation and staining	49
3.3. Microscopy and image analysis.....	50
3.3.1. Animal sorting.....	50
3.3.2. In vivo imaging.....	50
3.3.3. Immunostainings	52
3.3.4. Transmission electron microscopy	52
3.3.5. Quantitative image analysis.....	53
3.3.5.1. In vivo imaging – basic procedure.....	53
3.3.5.2. In vivo imaging – Tracing and development of single PSDs	55
3.3.5.3. In vivo imaging – FRAP experiments	55
3.3.5.4. NMJ parameters.....	56
3.3.5.5. Comparison of absolute signal intensities	57
3.3.5.6. Determination of intensity profiles	57
3.3.5.7. Analysis of electron micrographs	57
3.3.5.8. Statistical analysis.....	57
3.3.5.9. Software	58
3.4. Electrophysiology.....	58
3.4.1. Patch clamp recordings	58
3.4.2. Intracellular recordings	59
3.5. Styryl dye labeling	59
4. Results	60
4.1. Non-NMDA type glutamate receptors are essential for maturation but not for initial assembly of synapses at <i>Drosophila</i> NMJs.....	60
4.1.1. Formation of glutamatergic NMJ synapses deprived of postsynaptic glutamate receptors.....	60
4.1.2. Presynaptic release sites are functionally and structurally maintained at glutamate receptor deprived NMJ synapses	62
4.1.3. Early stop of postsynaptic maturation at glutamate receptor deprived NMJ synapses	64
4.1.4. Ultrastructural analysis: lack of apposition between pre- and postsynaptic membranes at NMJ synapses deprived of glutamate receptors.....	66
4.1.5. Initial molecular assembly of PSDs independent of glutamate receptors..	68

4.1.6. Neurotransmission and glutamate-triggered ionic conductance are dispensable for NMJ synapse maturation and growth.....	69
4.1.7. C-terminal truncation of GluRIIA mimics the receptor deprivation defects	72
4.1.8. Postsynaptic assembly seems to require intracellular sequence elements common to GluRIIA, IIB and IIC.....	73
4.2. Fluorophore-tagging of glutamate receptor subunits	76
4.2.1. Random insertion - In vitro transposition	77
4.2.2. Site-directed fusion.....	79
4.2.2.1. Strategy	79
4.2.2.2. Outcome.....	81
4.3. Subunit-specific targeting of glutamate receptors organizes PSD formation and maturation	82
4.3.1. Functional GFP fusions of GluRIIA and IIB to in vivo study synapse formation at developing NMJs of <i>Drosophila</i>	82
4.3.2. Simultaneous in vivo imaging of GluRIIA and GluRIIB.....	85
4.3.3. Receptor composition balances in the course of PSD growth and maturation.....	87
4.3.4. Distinct PSD incorporation behavior of GluRIIA and GluRIIB.....	89
4.3.5. The CTD of GluRIIA contributes to suppress GluRIIA incorporation at mature PSDs	90
4.3.6. Distinct PSD incorporation of GluRIIA and IIB persists in the absence of the other complex.....	92
4.3.7. GluRIIA is needed to allow efficient growth of PSDs and to define mature PSD size.....	94
4.3.8. GluRIIA dominates synaptic transmission	96
4.3.9. GluRIIA PSD content is selectively enhanced after blockade of presynaptic glutamate release.....	97
4.3.10. Receptor content per PSD can be down-regulated to allow the formation of additional synapses during experience-dependent plasticity	100
5. Discussion	104
5.1. Non-NMDA type glutamate receptors are essential for maturation but not for initial assembly of synapses at <i>Drosophila</i> NMJs	104
5.1.1. A transmission independent role of glutamate receptors in postsynaptic maturation.....	104
5.1.2. Ultrastructural and molecular maturation of NMJ synapses requires glutamate receptors.....	104

5.1.3. Glutamate receptor complexes and synaptic cell adhesion	106
5.1.4. Glutamate receptor levels in control of synapse formation.....	107
5.2. Functional fluorophore-tagging of glutamate receptor subunits	109
.....	
5.3. Subunit-specific targeting of glutamate receptors organizes PSD	111
formation and maturation	111
5.3.1. Subunit-specific glutamate receptor trafficking	111
5.3.2. Factors controlling the differential trafficking of GluRIIA and GluRIIB.	112
5.3.3. Phosphorylation and receptor trafficking	113
5.3.4. Activity-dependent PSD regulation – blocked neurotransmission	115
5.3.5. Activity-dependent PSD regulation – enhanced neurotransmission ..	116
5.3.6. Physiological relevance of GluRIIA and GluRIIB complexes.....	118
6. References	121
6.1. Scientific articles and monographies	121
6.2. World wide web	129
7. Appendix	130
7.1. Vectors	130
7.2. GluR structure and alignments	132
7.3. Constructs and transgenes	135
7.4. <i>In vivo</i> imaging device.....	138
7.5. Normalization of the PSD number and NMJ size.....	138
8. Abbreviations	139
9. List of publications	141
10. Curriculum vitae	142

List of figures

Fig. 1. Electrical and chemical synapse	12
Fig. 2. Vertebrate NMJ	13
Fig. 3. Dendritic spines	15
Fig. 4. Model of dendritic spine development.....	15
Fig. 5. Molecular components of the CAZ and the active zone.....	16
Fig. 6. Molecular components of the postsynaptic density (PSD).....	17
Fig. 7. Morphological events after LTP.....	19
Fig. 8. <i>Drosophila</i> life cycle	20
Fig. 9. <i>Drosophila</i> larval body wall muscles	21
Fig. 10. NMJ – bouton - synapse.....	21
Fig. 11. <i>Drosophila</i> NMJ development.....	22
Fig. 12. Ultrastructure of glutamatergic <i>Drosophila</i> NMJ synapses.....	24
Fig. 13. Assembly of non-NMDA glutamate receptors	26
Fig. 14. Subunit-dependent AMPA receptor insertion and recycling	28
Fig. 15. Receptor subunit composition regulates desensitization kinetics	29
Fig. 16. Overlap extension PCR	33
Fig. 17. Molecular cloning of <i>gluRIIB</i> and <i>gluRIIB^{GFP897}</i>	34
Fig. 18. <i>In vitro</i> transposition	45
Fig. 19. Image analysis steps	53
Fig. 20. Larval NMJs developing with extremely reduced levels of postsynaptic glutamate receptors.....	61
Fig. 21. Active zones and presynaptic release at glutamate receptor deprived NMJ synapses	62
Fig. 22. Signs of chronically increased release probability at glutamate receptor deprived NMJ synapses.....	63
Fig. 23. Molecular markers of postsynaptic assembly at glutamate receptor deprived NMJ synapses	65
Fig. 24. Electron microscopic analysis of glutamate receptor deprived NMJ synapses.....	67
Fig. 25. Synapse assembly at embryonic NMJs lacking all glutamate receptors	69
Fig. 26. NMJ synapse assembly after suppression of neurotransmission or glutamate receptor ligand binding	70
Fig. 27. PSD assembly defects after C-terminal truncation of GluRIIA	73
Fig. 28. GluR AA alignment: C-terminal domain (CTD).....	74
Fig. 29. <i>In vitro</i> transposition results: <i>gluRIIA</i>	78

Fig. 30. <i>In vitro</i> transposition results: <i>gluRIIB</i>	78
Fig. 31. Fluorophore-tagging of rat GluR1	80
Fig. 32. Structure of <i>gluRIIB</i> ^{GFP897}	81
Fig. 33. GluRIIB ^{GFP897}	81
Fig. 34. Analysis of GFP-tagged GluRIIA and GluRIIB	83
Fig. 35. Size-dependent divergence of PSD subunit composition.	86
Fig. 36. Absolute and relative PSD growth	87
Fig. 37. PSD subunit composition development depends on initial stage	88
Fig. 38. Differential PSD incorporation behavior of GluRIIA and GluRIIB complexes.....	89
Fig. 39. Quantification of the differential FRAP behavior	91
Fig. 40. The differential incorporation characteristics involve the receptor C-terminus – part I	92
Fig. 41. Specific incorporation behavior independent of the presence of the respective 2 nd receptor type.....	93
Fig. 42. The differential incorporation characteristics involve the receptor C-terminus – part II	94
Fig. 43. GluRIIA limits PSD growth	95
Fig. 44. Physiological characterization of GluRIIA and GluRIIB complexes.....	96
Fig. 45. Expression pattern of <i>ok319-gal4</i>	97
Fig. 46. PSD composition after blockage of presynaptic release	98
Fig. 47. FRAP in the absence of the 2 nd receptor type after presynaptic activity blockage.....	99
Fig. 48. GluRIIA and GluRIIB after activity blockage.....	100
Fig. 49. PSDs during experience-dependent plasticity	101
Fig. 50. Activity and long-term NMJ plasticity	102
Fig. 51. Model: Maturation of PSDs requires glutamate receptors	105
Fig. 52. Model: Transsynaptic interactions instructed by intracellular interactions of glutamate receptors	107
Fig. 53. Model: Differential glutamate receptor incorporation involves the cAMP cascade	114
Fig. 54. Model: Presynaptic activity, postsynaptic conductance and PSD growth	117
Fig. 55. Model: PSD growth in the sole presence of either GluRIIA or GluRIIB... ..	119
Fig. 56. pSL1180	130
Fig. 57. pUAST	131

Fig. 58. Crystal structure of glutamate bound GluR6 - S1/S2 domain.....	132
Fig. 59. GluR AA alignment: S1/S2 domain – tetramer stabilization.....	132
Fig. 60. GluR AA alignment: S1/S2 domain – beta 7,8, helix D and J	133
Fig. 61. GluR AA alignment: reentrant pore loop and M2.....	134
Fig. 62. Constructs and transgenes 1.....	135
Fig. 63. Constructs and transgenes 2.....	136
Fig. 64. Constructs and transgenes 3.....	137
Fig. 65. <i>In vivo</i> imaging device.....	138

List of tables

Table 1. Fly stocks for germ line transformation	46
Table 2. Genetics	48
Table 3. C-terminal modifications	75

Acknowledgements

Foremost, I would like to thank my supervisor Prof. Stephan Sigrist for his continuous support and advice, for fruitful scientific work and discussions and the consistent full confidence he had in me. Furthermore, I am also grateful to Prof. Ernst Wimmer and Prof. Ralf Heinrich for their valuable support as my thesis committee and to Prof. Jörg Stülke, Prof. Michael Hörner, PD Michael Hoppert and Prof. Dieter Heineke for accepting the office as further members of my examination board.

I would like to thank all the members of the ENI and especially everybody from the AG Sigrist for creating a pleasant and amicable atmosphere.

In particular thanks go to:

- my dear friend Christine Quentin for being an excellent lab manager, my lab jester, a fantastic cook, kind, straightforward and considerate
- my dear friend Philipp Gorlovoy for his reliability, solidarity and hilarity
- Carolin Wichmann for doing electron microscopy, for her numerous perusals and for hard struggles whenever we had some treats in the lab
- Robert Kittel for almost all of the electrophysiological data in this thesis
- Andreas Frölich for the rest of the electrophysiological data in this thesis
- Qin Gang for starting up the *IIA^{hypo}* project
- Manuela Schmidt for being my bench buddy and fair-minded listener
- Tobias Schwarz for his helpfulness, enjoyable lunch breaks and being the best Beckenbauer double
- Wernher Fouquet and Sara Mertel for their cooperativeness
- Carola Sigrist, Rui Tian, Laura Swan, Tobias Rasse, Ulrike Prange, Carlos Merino, Thomas Schwarzbraun and Henrike Hartung for being likeable colleagues
- Jasmin Held, Miriam Richter, Franziska Zehe and Heiko Röhse for being technical aces (TAs)
- Anne Grünewald, my former diploma student, for her dedication on the IVT screen
- Andrea Möller and Banu Colak for being fly-mommies
- Magda Krause for her consistent support and smile
- Frank Kötting for being Daniel Düsentrieb
- Ulrike Borchardt for yummy fly food
- Oliver Schade and Matthias Weyl for support whenever I thought nothing else as a sledgehammer could help my PC

- Wiebke Heinrich and Dagmar Thomiczek for their support with administrative concerns

Furthermore, I would like to thank Prof. Manfred Heckmann for his constructive advice.

Moreover, I would like to thank everybody who contributed to make my off work time in Göttingen enjoyable, diversified and prosperous: my flat-mates and neighbors, the Hochschulsport crew, the ASTA Sportreferat, the Monday evening soccer people, the Tuesday evening Spanish course, the Wednesday evening cast of the DT and especially my awesome Thursday evening Rollersoccer team, namely Tatjana and Tomi Haramina, Philipp Gorlovoy, Nicolas Bontems, Matthias Schmalisch, Hans-Matti Blencke, Fabian Commichau, Carola Eyßell, Justus Lücke, Franziska Jurk, Friederike Draber, Jörg Mertins, Dennis Rippe, Dennis Kappei, Steffen Arning, Johanna Kuhlenkampff, Monika Herold, Inga and Volker Hannstein.

Special thanks also goes to my dear friends Christian Graf and his wife Katja, Ulrich Syber and Markus Hermann, who accompanied me in an inimitable way throughout my studies.

Last but not least, I would like to thank my girlfriend Silke for her understanding, kindness and love and particularly my family and grandma for their lifelong support, dedication, frankness, guidance and faith in me.

Thanks to everybody else who accompanied me, believed in me and helped me finding the right path.

1. Summary

Ionotropic glutamate receptor channels (GluRs) are key elements for excitatory neurotransmission in the central nervous system (CNS). Both the activity-dependent as well as the activity-independent trafficking of GluRs to postsynaptic densities (PSDs) of glutamatergic synapses is meant to control synaptic plasticity in the mammalian nervous system, thereby mediating learning and memory. Whether similar processes are generally implicated into the formation and adaptation of glutamatergic synapses, e.g. throughout nervous system development, remained unknown so far. The *Drosophila* neuromuscular junction (NMJ) is a highly accessible synaptic model system, which allows extensive *in vivo* analysis of cellular and molecular mechanisms by combining efficient genetics with physiological, ultrastructural and histological analyses. Two glutamate receptor complexes, containing either the subunit GluRIIA or GluRIIB, are expressed at the NMJ. Previously, GluRIIA and GluRIIB complexes were shown to influence NMJ synapse number and strength in an antagonistic way. In this thesis, the role of GluRs and their subunit-specific incorporation in the formation and maturation of PSDs was studied *in vivo* at developing NMJs.

Following a drastic genetic reduction in the level of all postsynaptic glutamate receptors at the NMJ, PSD maturation was found to be inhibited and proteins normally excluded from PSD membranes remained at these apparently immature sites. However, initial steps of structural postsynaptic assembly proceeded and presynaptic active zones showed normal composition and ultrastructure as well as proper glutamate release. Intriguingly, synaptic transmission as well as glutamate binding to glutamate receptors appeared dispensable for synapse maturation.

In vivo imaging was then used to follow GluRIIA or GluRIIB dynamics during PSD formation and maturation. An essentially irreversible incorporation of GluRIIA was found exclusively during the growth phase of nascent PSDs. Once a sufficient presynaptic glutamate release and postsynaptic conductance through the highly conducting GluRIIA complexes was established at a maturing PSD, further GluRIIA PSD incorporation was blocked, mediated by the cytoplasmic C-terminus of the GluRIIA subunit. In contrast, the incorporation of GluRIIB complexes was reversible and uniform over all PSDs and did not cease with PSD maturation.

This thesis shows that the incorporation of GluRs into PSDs and likely their protein-protein interactions with further PSD components trigger a conversion from an initial to a mature stage of PSD assembly. Moreover, it is demonstrated that subunit-specific PSD targeting of GluRs also controls the developmental formation and maturation of glutamatergic synapses. Two GluR complexes with opposing

physiological features compete for PSD incorporation. This competition appears to be necessary to continuously adjust postsynaptic glutamate-mediated conductance and presynaptic glutamate release. In addition, the subunit-specific GluR incorporation seems to determine the final size and physiological performance of individual synapses and with it the collective transmission strength by tuning the overall synapse number per NMJ.

2. Introduction

2.1. Structure and function of synapses

The human brain harbors an exquisitely complex neuronal network consisting of 10^{10} to 10^{11} nerve cells which are interconnected via about 10^{15} synaptic contacts. Synapses are highly specialized junctions across which a nerve impulse passes to a neuron, muscle cell or gland cell. Thereby, electrical input signals of the presynaptic cell are rapidly and efficiently transmitted to the connected postsynaptic partner cell. This communication constitutes biological computation which underlies perception, cognition and memory formation.

Despite the high grade of specialization all synapses apply only one of the two basic transmission forms: electrical or chemical. At electrical synapses the transmission is regulated by passive ion flow through tight gap junctions (Fig. 1). Transmission at chemical synapses is mediated by rapid release of a neurotransmitter which triggers an ion influx into the postsynaptic cell.

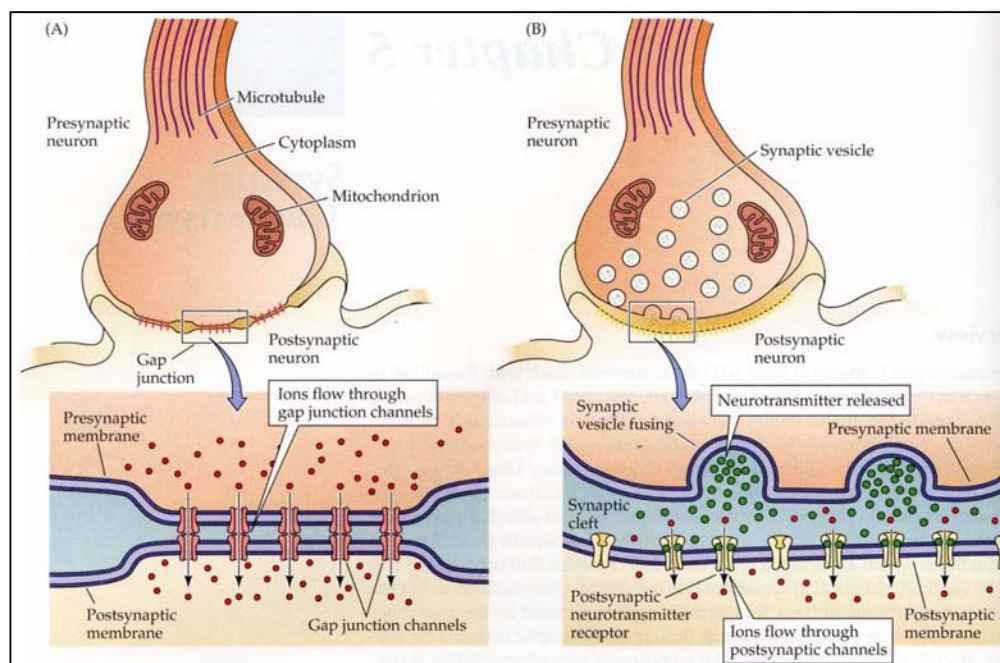


Fig. 1. Electrical and chemical synapse

A, Electrical synapse between two neurons. Gap junctions enable the passive direct ion flow from the presynaptic into the postsynaptic neuron. **B**, Chemical synapse. Synaptic vesicles filled with neurotransmitter fuse with the presynaptic plasma membrane and release the neurotransmitter into the synaptic cleft. The postsynaptic membrane harbors ion channels that bind the neurotransmitter, which results in a conformational change that allows ion influx into the postsynaptic cell. Adapted from (Purves et al., 2001).

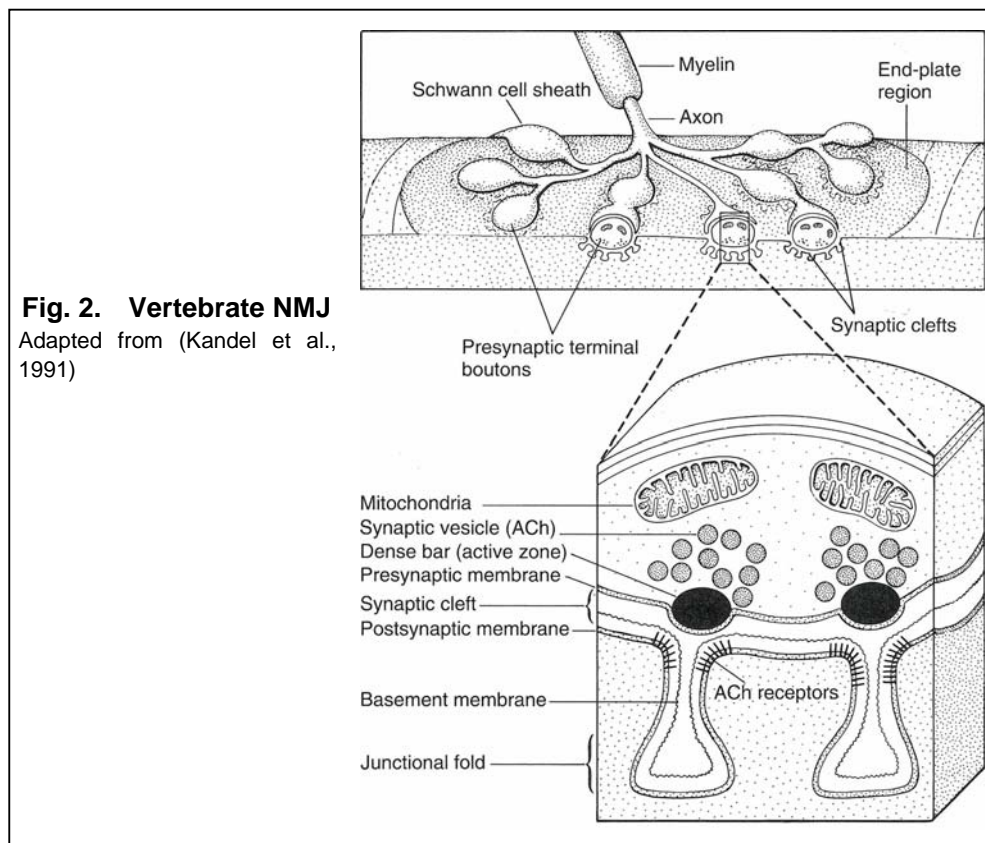
Following an action potential propagating along the presynaptic neuron, Ca^{2+} influx into the presynaptic terminal causes the fusion of synaptic vesicles with the presynaptic membrane. Thereby, the neurotransmitter molecules are released from the vesicles into the synaptic cleft. Postsynaptic ion channels specifically bind the

neurotransmitter. The binding alters the channel conformation and enables the influx of ions, which in turn establishes the signal propagation by changing the membrane potential of the postsynaptic cell (Fig. 1).

Two types of transmission at chemical synapses can be discriminated: excitatory and inhibitory. Excitatory transmission often utilizes the neurotransmitter glutamate, whereas classical inhibitory neurotransmitters are glycine or γ -aminobutyric acid (GABA). Neurotransmitters are generally categorized based on their chemical characteristics into four classes: amino acids (glutamate, aspartate, GABA, glycine, acetylcholine), peptides (e.g. vasopressin, somatostatin), monoamines (e.g. dopamine, serotonin) and other neurotransmitters (e.g. nitric oxide, CO).

In the following, three major model systems for studying chemical synapses will be presented. In each case, the general morphological structure and the pre- and postsynaptic constituents of the respective system will be outlined. Furthermore, information about their development and plastic remodeling will be given. Finally, there will be focus on the structure, function and trafficking of ionotropic glutamate receptors, which form the main subject matter of this thesis.

2.1.1. Vertebrate neuromuscular synapses



The vertebrate NMJ forms on a muscle fiber that is innervated by a myelinated axon of a motoneuron. The axon branches into many presynaptic terminal boutons that are ensheathed by Schwann cells (Fig. 2, top). Electrical impulses from the nerve terminals to the muscle are transmitted via the chemical transmitter acetylcholine (ACh). Thereby, each presynaptic bouton contains a dense body called active zone where synaptic vesicles dock and fuse, and which is positioned over a postjunctional fold (deep infolding of the sarcolemma) harboring nicotinic acetylcholine receptors (AChRs). As a specific feature of the vertebrate NMJ synapse, the pre- and postsynaptic membranes are, besides the synaptic cleft, additionally separated by a basal membrane (Fig. 2, bottom).

During muscle innervation, following the initial growth cone contact, AChRs and other synaptic signaling and structural molecules begin to cluster under the overlying nerve terminal (Hughes et al., 2006). Agrin, a heparan sulphate proteoglycan that is released from the motor nerve terminals was shown to be necessary as well as sufficient for AChR clustering. The trans-membrane muscle-specific kinase (MuSK), which is co-localized with AChRs in the postsynaptic membrane, apparently acts as Agrin receptor, although it does not seem to bind to Agrin directly (Sanes and Lichtman, 1999). Muscles of MuSK knockout mice show no signs of postsynaptic differentiation, whereas AChR genes are expressed at normal level (DeChiara et al., 1996).

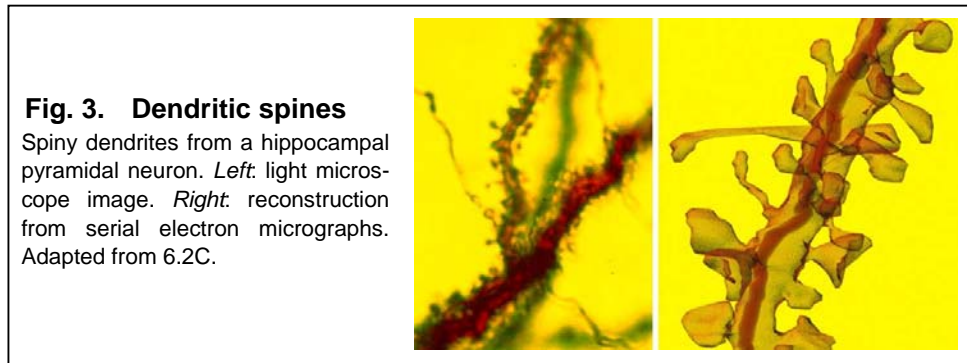
Another critical factor for AChR clustering downstream of MuSK is the cytoplasmic protein rapsyn, which is precisely co-localized with AChRs. Rapsyn deficient muscles harbor MuSK accumulations but fail to cluster AChRs, which remain atypically, diffusely distributed (Gautam et al., 1995).

Interestingly, it was also shown that the AChRs themselves are required for the clustering of postsynaptic components. Rapsyn clustering failed in zebrafish mutants deficient for AChRs (Ono et al., 2001) as well in C2 myotubes virtually lacking AChRs (Marangi et al., 2001). Moreover, in mice deficient for an adult AChR subunit the postsynaptic membrane was profoundly reorganized and largely missed the typical postjunctional folds. Additionally, several synaptic proteins were abnormally distributed forming atypical protein poor and rich regions (Missias et al., 1997). Hence, the AChRs are not only passive constituents but rather actively involved in the organization of postsynaptic assembly.

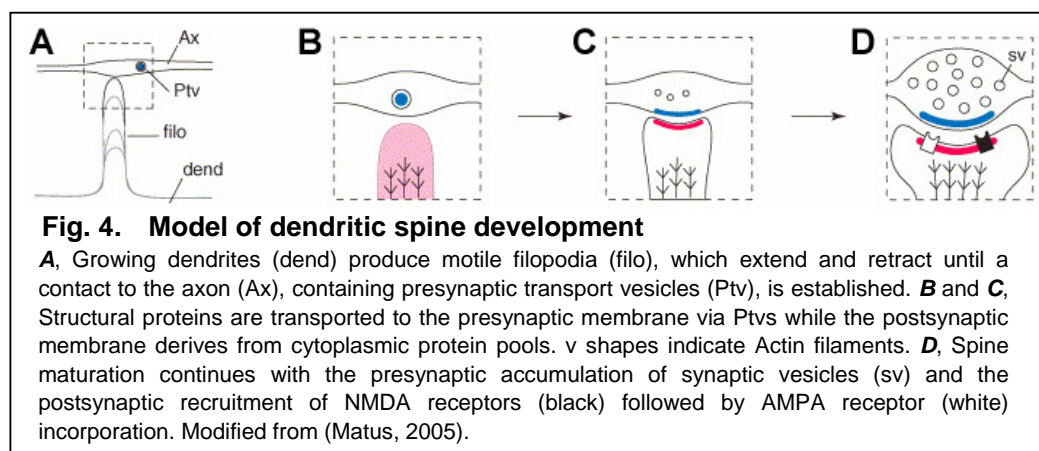
2.1.2. Excitatory vertebrate CNS synapses

Excitatory synapses in the vertebrate central nervous system are most frequently located on minute lateral dendritic protrusions, the so-called dendritic spines (Fig. 3).

The main cytoskeleton of the dendritic spines is formed by dynamic Actin filaments that make them capable of rapid morphological changes (Tada and Sheng, 2006). The formation and the morphological changes of spines are meant to play an important role in synaptogenesis and synaptic plasticity (Yuste and Bonhoeffer, 2001; Nikonenko et al., 2002; Matus, 2005).



The development of dendritic spines commences with immature dendrites producing motile filopodia that sample the neuropil for presynaptic partners to form synaptic contacts (Fig. 4A). Once an initial contact of the presynaptic axon and the postsynaptic spine is established, structural proteins accumulate at the future synaptic site (Fig. 4B). In the following, spine maturation proceeds by the accumulation of synaptic vesicles in the presynaptic terminal and the integration of glutamate receptors into the postsynaptic membrane (Fig. 4C). Mature spines, which are stable in shape, are typically characterized by an expanded head and a narrow neck (Fig. 3 and Fig. 4D). They vary strongly in size and shape (stubby, thin and mushroom-like).



2.1.2.1. Presynaptic structure

When the contact between the presynaptic axon and the postsynaptic dendritic spine has been established, structural proteins are delivered to the nascent presynaptic

membrane. Thereby, these proteins are transported via presynaptic transport vesicles (Ptv) as preassembled molecular complexes (Fig. 4A,B) (Ahmari et al., 2000; Shapira et al., 2003). Numerous scaffolding proteins of the active zone as Piccolo, Bassoon, Rim (Rab3-interacting molecule), Liprin-alpha and N-type Ca^{2+} channels (Ohtsuka et al., 2002; Kim et al., 2003; Shapira et al., 2003) as well as components of the vesicle release machinery were identified on the Ptv.

Thus, the Ptv are believed to account for the formation of the active zone itself or the cytomatrix at the active zone (CAZ) (Zhai and Bellen, 2004). The CAZ comprises a network of microfilaments and associated proteins (Zhai and Bellen, 2004) that regulates the translocation of synaptic vesicles to the active zone, the neurotransmitter release and the vesicle endocytosis (Fig. 5) (Ziv and Garner, 2004). The correct targeting of the Ptv to the nascent presynaptic membrane involves several cell adhesion molecules (CAMs) as Cadherins (Salinas and Price, 2005), Neurexin and Neuroligin (Dean and Dresbach, 2006), but also proteins of the cortical cytoskeleton like Actin and Spectrin.

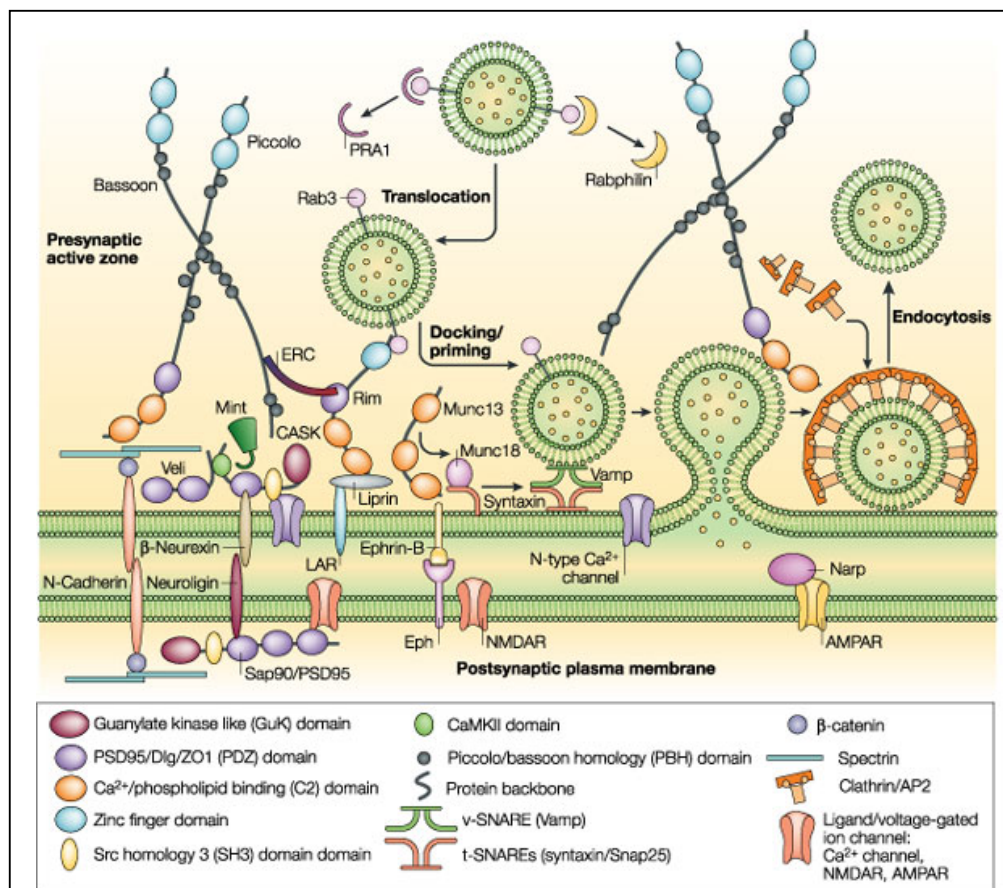


Fig. 5. Molecular components of the CAZ and the active zone

The CAZ and the active zone regulate the release of synaptic vesicles, which comprises vesicle translocation, docking and priming, membrane fusion and vesicle endocytosis. Adapted from (Ziv and Garner, 2004).

2.1.2.2. Postsynaptic structure

Excitatory synapses in the vertebrate central nervous system are primarily glutamatergic. Following presynaptic vesicle fusion the released glutamate binds to glutamate-sensitive ion channels, which can be subdivided into two groups: metabotropic and ionotropic glutamate receptors. The tetrameric ionotropic glutamate receptor complexes are further categorized in AMPA (alpha-amino-3-hydroxy-5-methyl-4-isoxazole-propionic acid), NMDA (N-methyl-D-aspartate) and kainate receptors (for details see 2.2).

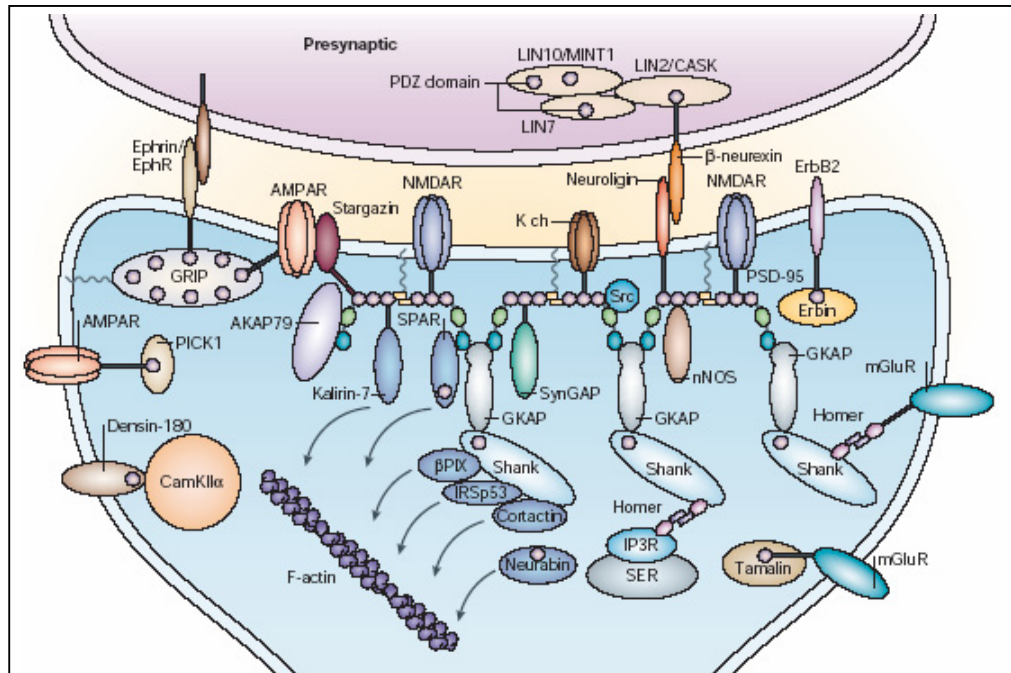


Fig. 6. Molecular components of the postsynaptic density (PSD)

Shown are the main PDZ proteins involved in the organization of the postsynaptic density. PDZ domains are indicated by small purple circles, the C-terminal cytoplasmic tails of membrane proteins by black lines. Abbreviations denote: AKAP79, A-kinase anchor protein 79; AMPAR, AMPA (α -amino-3-hydroxy-5-methyl-4-isoxazole propionic acid) receptor; β PIX, PAK-interactive exchange factor; CaMKII α , α -subunit of Ca²⁺/calmodulin-dependent protein kinase II; GK, guanylate kinase-like domain; EphR, ephrin receptor; ErbB2, EGF-related peptide receptor; GKAP, guanylate kinase-associated protein; GRIP, glutamate-receptor-interacting protein; IP3R, IP3 receptor; IRSp53, insulin-receptor substrate p53; K ch, potassium channel; LIN7, lin7 homologue; LIN10, lin10 homologue; mGluR, metabotropic glutamate receptor; NMDAR, NMDA (*N*-methyl-D-aspartate) receptor; nNOS, neuronal nitric oxide synthase; PICK1, protein interacting with C kinase 1; PSD-95, postsynaptic density protein 95; SER, smooth endoplasmic reticulum; SH3, Src homology 3 domain; Shank, SH3 and ankyrin repeat-containing protein; SPAR, spine-associated RapGAP; SynGAP, synaptic Ras GTPase-activating protein. Adapted from (Kim and Sheng, 2004).

The glutamatergic transmission is supported by a specialized postsynaptic subcellular organization, called the postsynaptic density (PSD). The PSD is involved in clustering and anchoring of postsynaptic receptors and ion channels and contains a specialized submembranous cytoskeleton with a rich collection of proteins that

serve to organize this membrane specialization (Fig. 6) (Kim and Sheng, 2004). In contrast to the assembly of presynaptic active zones involving the delivery of prefabricated transport packets (see 2.1.2.1), postsynaptic assembly seems to depend on gradual *de novo* clustering of component proteins (Bresler et al., 2004). Synaptic non-NMDA receptors may either be recruited into PSDs from a diffuse plasma membrane pool by lateral migration (Borgdorff and Choquet, 2002) or be incorporated via subunit specific constitutive or activity-dependent pathways (Bredt and Nicoll, 2003), potentially using preformed slots established at the postsynaptic membrane (Barry and Ziff, 2002). Moreover, postsynaptic glutamate receptor levels are regulated by various adaptor proteins, kinases and scaffolding molecules (McGee and Bredt, 2003). Within the PSD, scaffolding proteins containing one or more PDZ domain are highly abundant (Fig. 6) (Walikonis et al., 2000). Among them are PSD-95 (postsynaptic density protein 95) and SAP97 (synapse-associated protein 97), both membrane-associated guanylate kinases (MAGUKs), GRIP (glutamate receptor interacting protein), ABP (AMPA receptor binding protein) and PICK1 (protein interacting with C kinase).

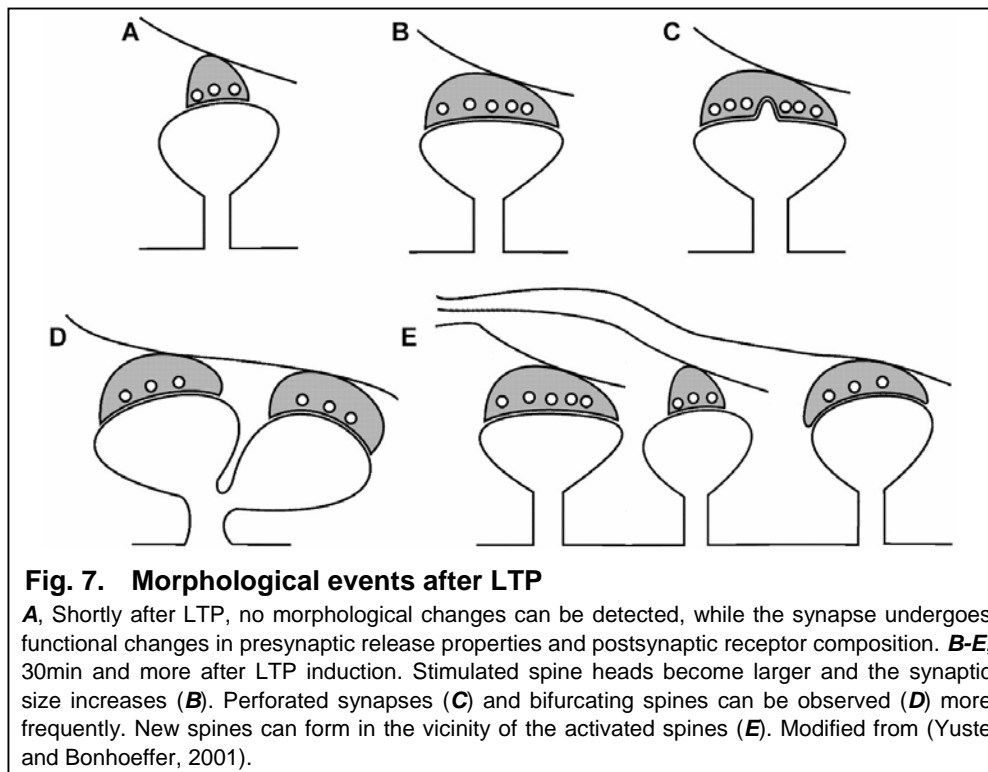
2.1.2.3. Structural synaptic plasticity and LTP

In 1949 Hebb postulated that two mechanisms were responsible for memory storage in the brain: alteration in synaptic strength and formation of novel synapses (Hebb, 1949). 24 years later, Bliss and Lomo developed a first paradigm of brief tetanic stimulation on hippocampal neurons to produce a long lasting form of synaptic plasticity which can last for hours or days, named long-term potentiation (LTP) (Bliss and Lomo, 1973). Since then, LTP was and is widely used as a cellular model for information storage at central synapses.

To establish LTP, various structural synaptic changes are conceivable. On the one hand, LTP could result from structural alterations of pre-existing synapses like the conversion from a non-functional (silent) to a functional state, synapse splitting or strengthening of pre- and/or postsynaptic structures. On the other hand, the establishment of novel synaptic contacts and thereby an increase in the overall synapse number could underlie LTP. Moreover, as dendritic spines are very mobile, changes in the spine number and morphology could as well be involved.

In fact, various changes in spine morphology can be observed following LTP induction (Fig. 7) (Yuste and Bonhoeffer, 2001; Nikonenko et al., 2002). Within the first minutes after potentiation the postsynaptic receptor composition as well as the presynaptic release properties are modified, while obvious morphological changes are not detectable (Fig. 7A). 30min after LTP induction, the swelling of spine heads

and a parallel increase in the synaptic area can be demonstrated (Fig. 7B). Moreover, perforated synapses (Fig. 7C) and bifurcating spines can be observed (Fig. 7D). Finally, new spines harboring novel synapses can emerge close to the activated spines (Fig. 7E) (Yuste and Bonhoeffer, 2001).



However, recent evidence suggests that the bifurcating spines (sdMSBs: same-dendrite, multiple-synapse boutons) do not arise from synapse and spine splitting as mature dendrites and axons were found passing through the gaps between the spine pairs (Fiala et al., 2002).

Another additional contribution to the early phase of LTP (Fig. 7A) might be the activation of silent synapses. A recent study suggests that the conversion of silent synapses to an activated state occurs 3-6h after stimulation whereas the addition of novel synapses occurred 12-18h after stimulation and might be therefore important for the late phase of LTP (Kim et al., 2003).

2.1.3. *Drosophila neuromuscular synapses*

2.1.3.1. *Drosophila melanogaster* as a model system

The fruit fly *Drosophila melanogaster* has been used as a genetic model system for almost a century. Despite its small genome of only 165Mbp distributed to four chromosome pairs, most *Drosophila* genes (about 14000 in total) are evolutionary conserved to vertebrates. One of the main advantages of *Drosophila* is its short life

cycle of about 10 days at 25°C (Fig. 8). Furthermore, the establishment and application of various transgenic and knockout strategies is simplified compared to vertebrates. Additionally, the *UAS/Gal4* system allows the ectopical and temporally defined expression of a gene of interest (Brand and Perrimon, 1993). Morphologically, most developmental stages are easily accessible with a huge variety of physiological, histological and microscopic techniques. In result, this allows vast functional *in vivo* analysis of cellular mechanisms.

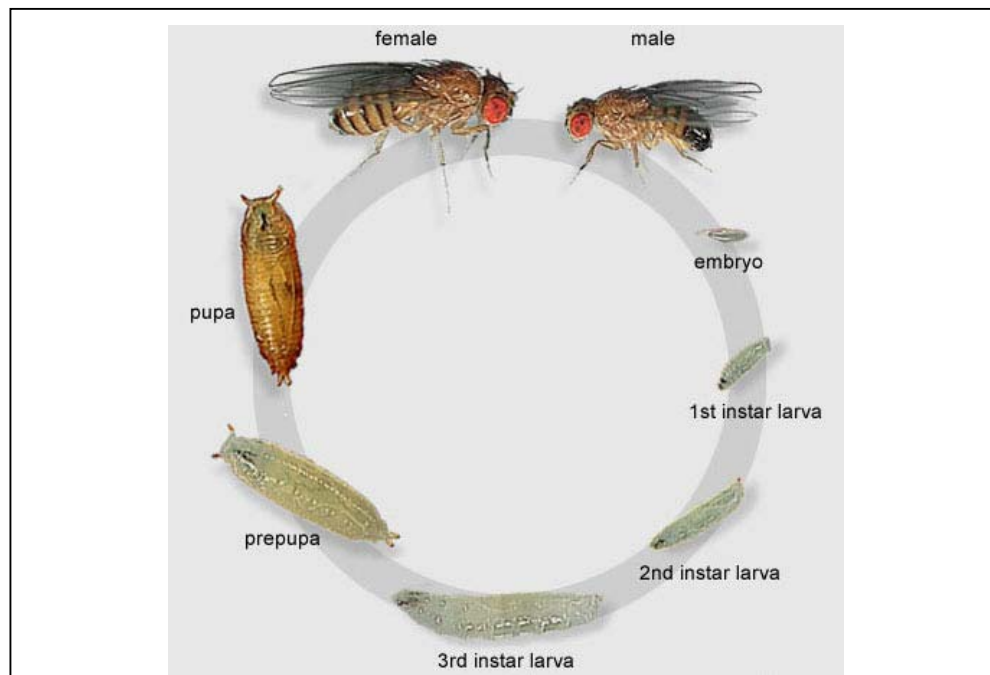


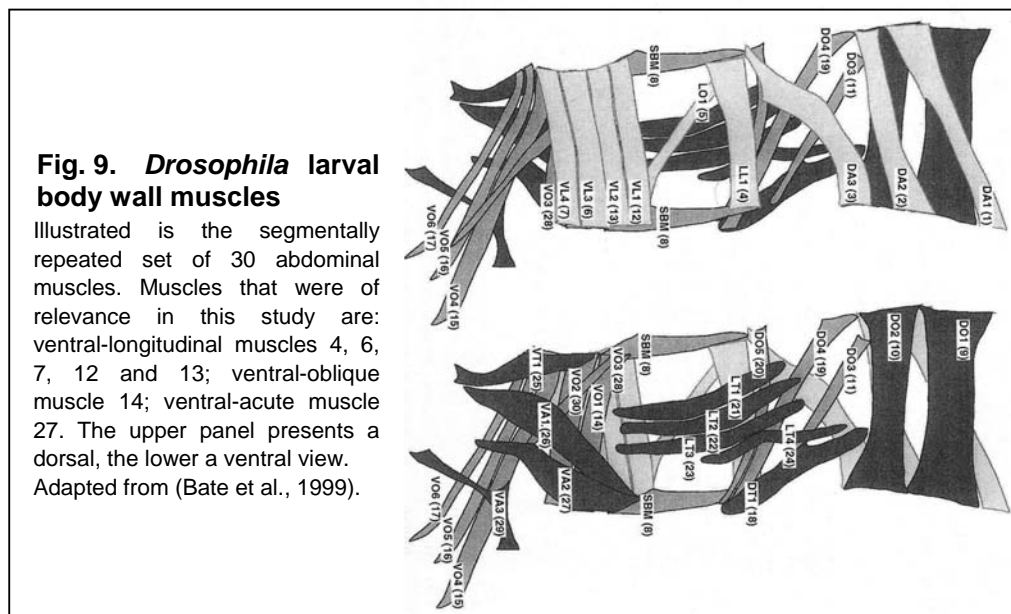
Fig. 8. *Drosophila* life cycle

After cellularization of the blastoderm, gastrulation, germ band elongation and retraction the embryo hatches about 24h after the egg laying (at 25°C). The following 1st and 2nd instar larval stages last again about one day each and end with the molt of the larva. After another two days the 3rd instar larvae reach the wandering stage, which is followed by the pupation. The subsequent metamorphosis takes three days and is finished with the eclosion and the hatching of the adult fly. The presented image originates from 6.2A.

2.1.3.2. Properties of the *Drosophila* NMJ

The neuromuscular junction of *Drosophila* (NMJ) allows efficient genetic analysis of development, plasticity and function of glutamatergic synapses (Jan and Jan, 1976; Keshishian et al., 1996; Prokop, 1999; Koh et al., 2000; Richmond and Broadie, 2002). Basic features of its synaptic function and the majority of synapse-associated proteins are evolutionary conserved with excitatory CNS synapses (see 2.1.2).

The NMJ comprises a segmentally repeated set of 30 abdominal muscle cells (Fig. 9) (Bate et al., 1999), which is innervated by 36 identified motoneurons per hemisphere branching into presynaptic varicosities (boutons) (Fig. 10) (Landgraf and Thor, 2006).



Thereby, three innervation types called type I, II and III exist. Type I presynaptic boutons (Fig. 10), which account for the excitation of the postsynaptic muscle cell, are exclusively glutamatergic and further subdivided into Ia and Ib boutons. While Ia boutons have a diameter of 1-3 μ m, Ib boutons reach a diameter of 3-5 μ m. Each Ib bouton harbors about 10-20 synapses (Atwood et al., 1993). Type II and III innervations, which were not addressed in this study, have not been associated with an electrically observable postsynaptic response so far (Rheuben et al., 1999).

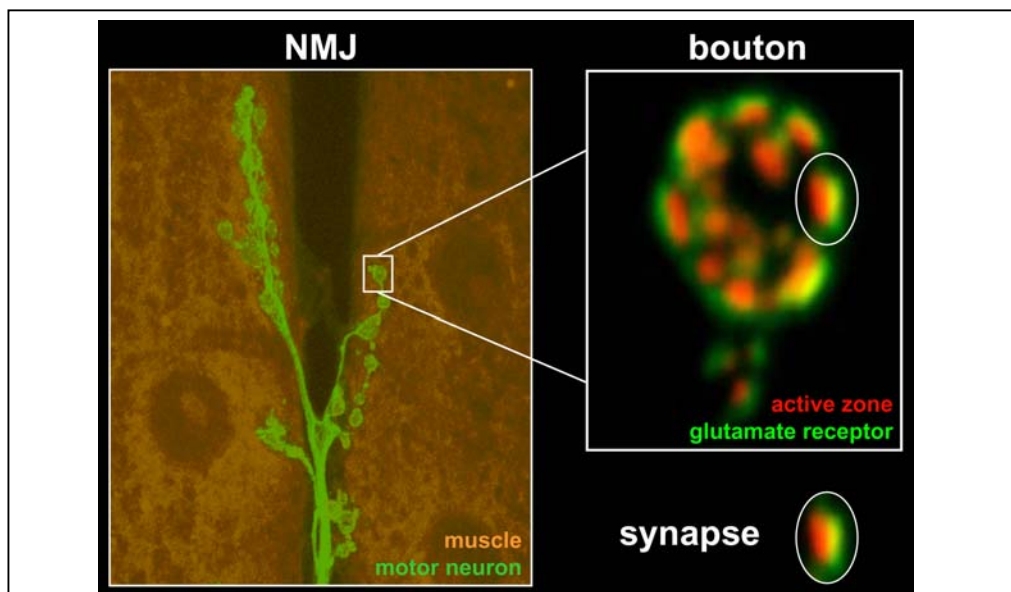
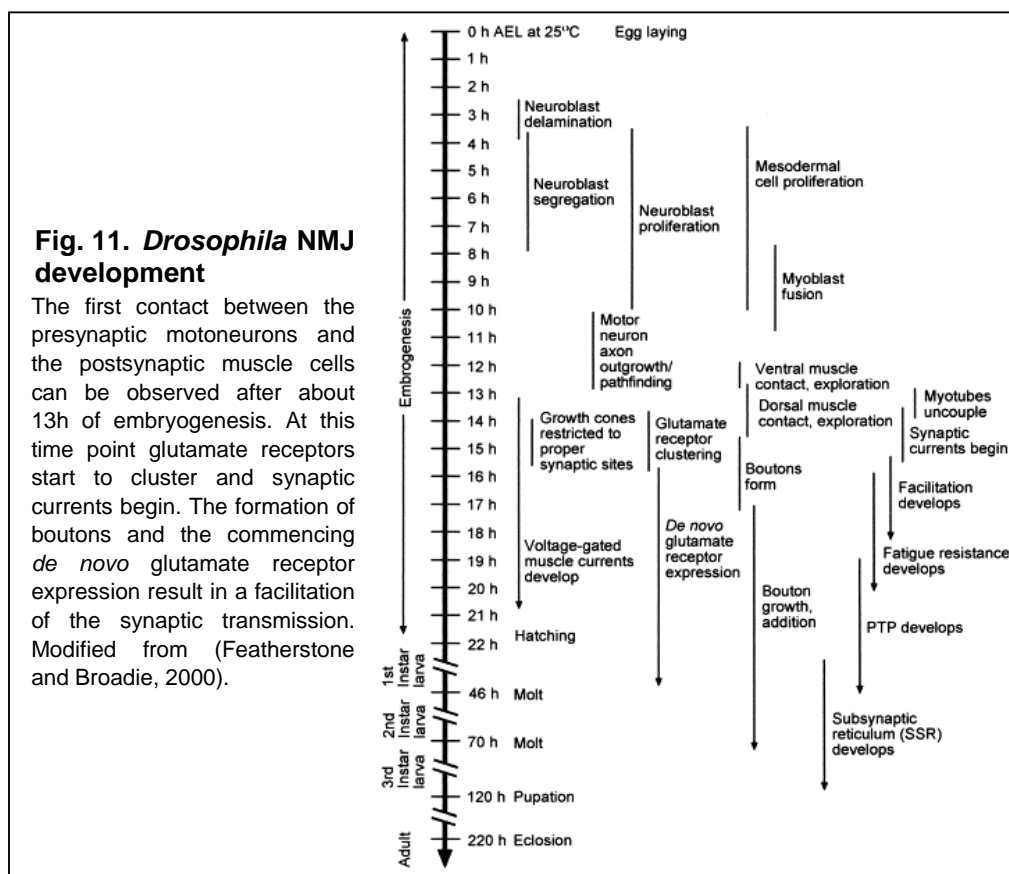


Fig. 10. NMJ – bouton - synapse

Shown are the ventral-longitudinal muscles 6 and 7 (orange) innervated by a motoneuron (green) branching into numerous varicosities called boutons (left panel). One bouton (type Ib) comprises 10-20 synapses that are characterized by postsynaptic glutamate receptors opposing the presynaptic active zone (right panel). Partially modified from J Neurosci, Vol.24 (2004).

2.1.3.3. Development of the *Drosophila* NMJ

The embryonic development of the neuromuscular junction (Fig. 11) can be separated in three stages, namely the growth cone stage, the prevaricosity stage and the varicosity stage. During the growth cone stage (13 to 16 hours after egg laying, AEL), filopodia sent out from the motoneuron growth cone contact muscle myopodia sent out from the future innervation site (Ritzenthaler et al., 2000). Thereby, inappropriate contacts are again withdrawn (Broadie and Bate, 1993). The prevaricosity stage (16h AEL) is characterized by the enlargement of the central region of the growth cone (at the nerve entry point into the muscle) and the formation of distinct branches. During the final varicosity stage (17h AEL) distinct varicosities form from the general swelling of the prevaricosity (Rheuben et al., 1999).



The initial neuromuscular contact requires stabilization mediated by several cell adhesion molecules. Among them is FasciclinII II (FasII), which is related to vertebrate NCAMs (neuronal cell adhesion molecules). It is initially strongly expressed on the surface of the innervating motoneurons and at low levels also in the muscle cell (Schuster et al., 1996). When the neuromuscular connection is established FasII is clustered at both pre- and postsynaptic membrane. The further maintenance of FasII at the neuromuscular synapses is largely mediated by Discs

large (Dlg), which is assigned to the PSD-95-type MAGUK family (Thomas et al., 1997; Zito et al., 1997).

In contrast to vertebrate NMJs where Agrin secretion from the nerve terminal initiates the clustering of postsynaptic proteins, no Agrin homologue seems to be present at the *Drosophila* NMJ. Nevertheless, recent studies showed that molecules such as Wnt and TGF β (transforming growth factor β), which act during embryo morphogenesis, are also involved in the differentiation of synapses (Packard et al., 2003).

While the presynaptic assembly of active zones can take place independent of the muscles (Prokop et al., 1996), the postsynaptic clustering of glutamate receptors requires and starts with the initial axon-muscle contact (Broadie and Bate, 1993). Notably, complete suppression of neurotransmission does not inhibit the formation of glutamate receptor clusters at the postsynaptic membrane (Featherstone and Broadie, 2000). Consistently, it could be demonstrated that embryonic synapse assembly remained apparently unaltered in Munc-13 or Munc-18 null mutant mice lacking any neurotransmission (Verhage et al., 2000; Varoqueaux et al., 2002).

2.1.3.4. Glutamatergic NMJ synapses

The principle structure of glutamatergic synapses at the *Drosophila* NMJ is similar to excitatory vertebrate CNS synapses (see 2.1.2). The synaptic ultrastructure of *Drosophila* NMJ synapses (visualized by transmission electron microscopy in Fig. 12) is characterized by a close apposition and a high electron density of the pre- and postsynaptic membranes over several hundred nanometers (synaptic cleft span: 10-20nm). Moreover, presynaptic active zones are typically associated with electron-dense specializations (T-bars) (Atwood et al., 1993; Zhai and Bellen, 2004) which are required for the efficient release of synaptic vesicles (Kittel et al., 2006). The postsynaptic density juxtaposed to the active zone provides the clustering of glutamate receptors, voltage-gated ion channels, scaffolding and regulatory molecules as PAK (p21-activated kinase) (Albin and Davis, 2004; Qin et al., 2005; Prokop and Meinertzhagen, 2006). Individual synapses are surrounded by the perisynaptic region which harbors adhesion proteins as FasII, which is linked to synaptic stabilization and growth (Schuster et al., 1996; Sone et al., 2000). Beneath the PSD the muscle membrane is highly convoluted forming the subsynaptic reticulum (SSR). Various scaffolding and adhesion proteins as Dlg, which might play a role in the structural organization and signaling mechanisms of cell adhesion molecules and ion channels, are found at the SSR membrane (Thomas et al., 1997).

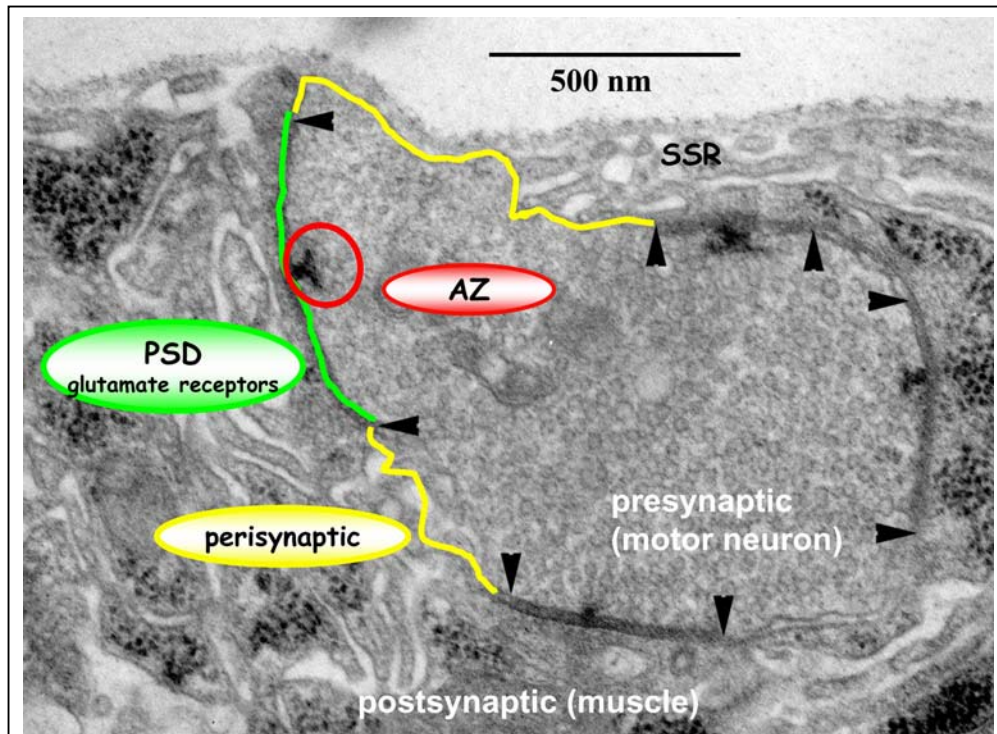


Fig. 12. Ultrastructure of glutamatergic *Drosophila* NMJ synapses

Shown is an electron microscopic cross-section through a synaptic bouton (filled with synaptic vesicles). The presynaptic active zone (red), typically characterized by the presence of an electron-dense specialization (T-bar), is in close coordination with the postsynaptic density (green) containing the glutamate receptors. Pre- and postsynaptic membranes, which are separated by a narrow synaptic cleft (10-20nm), show linear apposition and a high electron density along the synaptic region (marked by arrowheads). The perisynaptic region (yellow) surrounds the synapses. The subsynaptic reticulum (indicated as SSR) forms by pronounced folding of the muscle membrane.

2.1.3.5. Activity-dependent remodeling

Several mutants which suppress or enhance the outgrowth of the *Drosophila* NMJ have been identified. As mentioned before the cell adhesion molecule FasII mediates synaptic stabilization and growth (Schuster et al., 1996). It was shown that increased neuronal activity decreases synaptic FasII levels, and moreover, genetic FasII reduction increased the number of synapses (Schuster et al., 1996). Therefore, a weakened cell adhesion might be a prerequisite for the addition of novel synaptic contacts following activity enhancement. An elevated presynaptic activity could be genetically achieved by establishing a double mutant situation for both the Eag (ether a go-go) and Shaker (Sh) potassium channel leading to an increased frequency of nerve-evoked action potentials. This in turn resulted in elevated cAMP levels and finally enhanced morphological NMJ outgrowth (Zhong et al., 1992). The involvement of cAMP signaling in NMJ plasticity could be confirmed using the learning mutant dunce (Dudai et al., 1976; Zhong et al., 1992; Cheung et al., 1999), which lacks a cAMP phosphodiesterase and therefore accumulates cAMP (Davis

and Kauvar, 1984; Zhong et al., 1992). NMJ outgrowth could be inhibited by a concomitant knockout of *rutabaga*, which encodes for the adenylyl cyclase (Dudai and Zvi, 1985; Livingstone, 1985). Alongside with the effects on NMJ morphology, cAMP signaling also plays a role in the regulation of synaptic dimensions and structure. Whereas a genetic elimination of *rutabaga* caused a dramatic increase in synapse size but a decrease in synapse number (Renger et al., 2000; Shayan and Atwood, 2000), *dunce* mutant synapses were not different from controls (Renger et al., 2000). In turn, presynaptic overexpression of *dunce* mimicked the *rutabaga* knockout (Shayan and Atwood, 2000).

A modulation of neural activity without genetic manipulation can be achieved through chronic larval rearing at an increased temperature of 29°C, which enhances their locomotion (Sigrist et al., 2003; Zhong and Wu, 2004). The elevated locomotion resulted in increased arborization of the NMJ and a boost of bouton and synapse number (Sigrist et al., 2003; Zhong and Wu, 2004)

Besides the alterations of presynaptic neural activity, changes in glutamate receptor complex composition are implicated in long-term changes of synaptic structure and transmission (Petersen et al., 1997; DiAntonio et al., 1999; Sigrist et al., 2002). Thereby, increased expression of the glutamate receptor subunit GluRIIA (see 2.2.3) was shown to elevate the number of synapses forming per NMJ (Sigrist et al., 2002).

2.2. Structure and function of ionotropic glutamate receptors

2.2.1. Structure and assembly of non-NMDA glutamate receptors

Glutamate receptors can be subdivided into two groups, namely metabotropic GluRs, which are coupled to G-proteins, and ionotropic GluRs. Ionotropic glutamate receptors (iGluRs) mediate excitatory synaptic transmission at most mammalian CNS synapses. They are discriminated in AMPA, NMDA and Kainate receptors. Non-NMDA receptors form homo- or heterooligomers, most likely tetramers (Rosenmund et al., 1998), composed of the subunits GluR1-4 (AMPA type) and GluR5-7 and/or KA1-2 (Kainate type) (Madden, 2002). A typical glutamate receptor subunit consists of an amino terminal domain (NTD), a ligand binding domain (S1/S2; for molecular 3D structure see Fig. 58), three transmembrane domains, a reentrant pore loop and an intracellular C-terminal domain (Fig. 13, Fig. 20). The NTD, which covers about half of the protein, contributes to receptor assembly (Ayalon and Stern-Bach, 2001). Besides the ligand binding, the S1/S2 domain controls the channel closure, thereby determines the activation and desensitization behavior of the ion channel, and is involved in the dimerization and tetramerization of subunits (see Fig. 59, Fig. 60). The reentrant pore loop, which is located between the

first and second transmembrane domain, lines the channel and controls the ion gating (Madden, 2002). The C-terminal domain is involved in trafficking and transport of the receptor subunits (see 2.2.2) (Malinow and Malenka, 2002).

The assembly of the tetrameric non-NMDA glutamate receptor complexes is thought to follow the 'dimer-of-dimers' model (Fig. 13). Subunit monomers associate primarily through interactions between their amino terminal domains. The formed dimers undergo a secondary dimerization, mainly mediated by interactions between the transmembrane domains and the S2 ligand binding domain (Fig. 59) (Ayalon and Stern-Bach, 2001; Madden, 2002). The receptor assembly is taking place in the endoplasmic reticulum (ER). The preassembled complexes are sorted in the Golgi and trans-Golgi apparatus into transport vesicles and handled to the synapses (Malinow and Malenka, 2002).

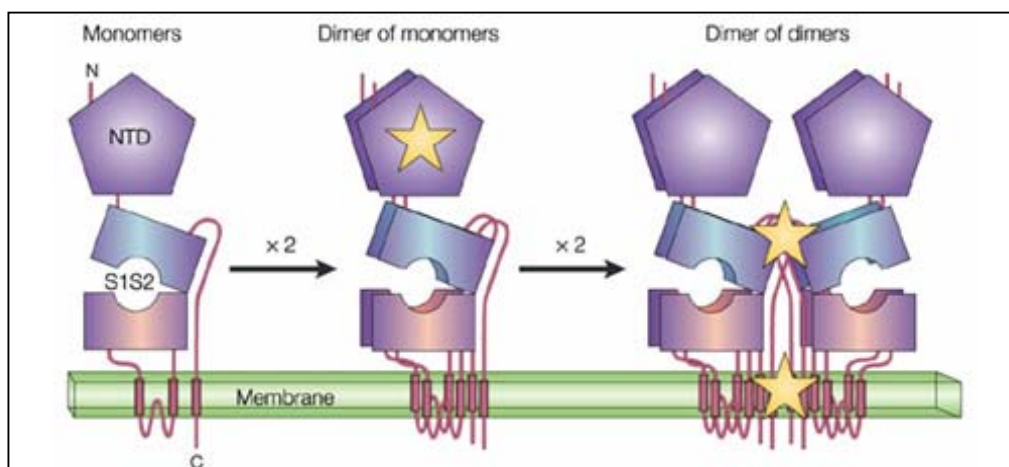


Fig. 13. Assembly of non-NMDA glutamate receptors

'Dimer-of-dimers' model of non-NMDA glutamate receptor assembly. Subunit monomers assemble mainly through N-terminal interactions to form dimers (star in the middle drawing). Dimers undergo a secondary dimerization, mediated by interactions in the transmembrane and S2 domains (stars in the right drawing). Adapted from (Madden, 2002).

2.2.2. Glutamate receptor trafficking

Long-term potentiation (LTP) and the converse long-term depression (LTD) are associated with persistent structural and functional modifications of synapses (see 2.1.2.3). Thereby, the regulated trafficking of AMPA receptor to and integration into the postsynaptic membrane plays an important role (Malinow and Malenka, 2002). Following LTP, silent synapses, which are characterized by having only NMDA receptors can be converted to active synapses by the rapid and specific functional recruitment of AMPA receptors (Fig. 14, top) (Isaac, 2003). This modulation of synaptic AMPA receptor number might involve cytoplasmic receptor-bearing vesicles and exocytotic mechanisms (Malinow and Malenka, 2002). In contrast, endocytosis

of AMPA receptors via clathrin-coated vesicles contributes to LTD (Carroll et al., 1999).

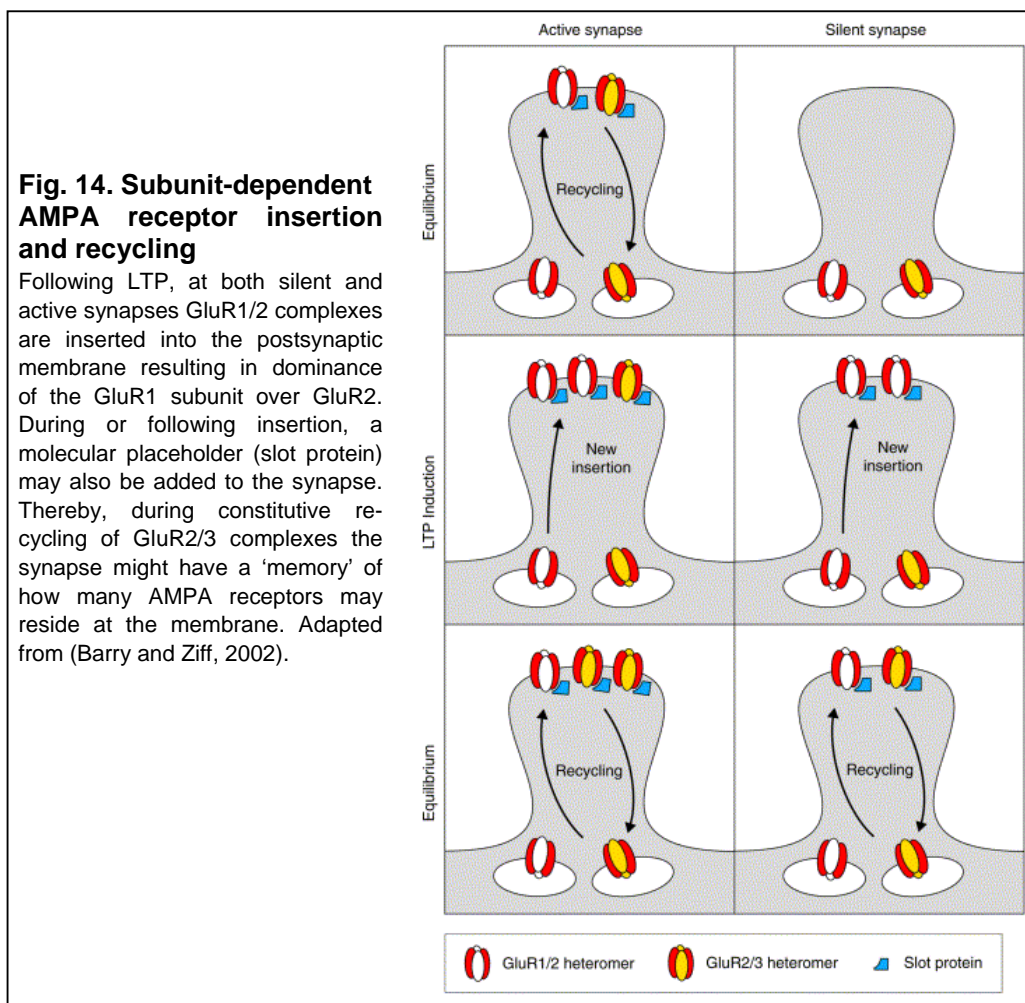
How is the AMPA receptor recruitment and drawback organized? Various, mostly C-terminal molecular interactions of AMPA receptors contributing to AMPA receptor trafficking and transport have been determined. Thereby, mostly interactions with PDZ proteins (among them: GRIP1, ABP/GRIP2, PICK1, SAP97) are of relevance (Malinow and Malenka, 2002; Kim and Sheng, 2004). Besides that, other proteins (as RIL and Band 4.1N) link the receptor complexes to the Actin cytoskeleton. In addition to that, the ATPase NSF (N-ethylmaleimide-sensitive factor), known to play a role in synaptic vesicle exocytosis (Whiteheart et al., 1994), interacts with the cytoplasmic tail of GluR2 (Nishimune et al., 1998). NSF has been reported to increase surface expression of AMPA receptors (Luscher et al., 1999) and to make them resistant to endocytosis (Shi et al., 2001).

The PDZ proteins GRIP and ABP are part of the scaffolding matrix and likely serve various functions in the delivery, stabilization and endocytosis of AMPA receptors (Malinow and Malenka, 2002). As GRIP and ABP, PICK1 interacts with a PDZ domain within the C-terminal region of GluR2 and contributes to AMPA receptor clustering (Xia et al., 1999). The interaction of SAP97 with the absolute C-terminus of GluR1 can be detected early in the secretory pathway and might be of importance for the trafficking of GluR1/2 complexes (Sans et al., 2001). Recent evidence suggested, that also Stargazin, an AMPA receptor associated transmembrane protein which interacts with the PSD-95 scaffold protein, is required for surface and synaptic expression of AMPA receptors (Chen et al., 2000; Tomita et al., 2005).

The delivery of AMPA receptors to the plasma membrane also depends on receptor phosphorylation. The phosphorylation of Ser831 on GluR1 by calmodulin-dependent kinase II (CamKII) leads to increased receptor conductance during LTP but is not required for AMPA receptor transport (Hayashi et al., 2000). Different from that, phosphorylation of Ser845 on GluR1 by protein kinase A (PKA) is necessary for synaptic delivery of GluR1-containing complexes (Malinow and Malenka, 2002). GluR2 phosphorylation on Ser880 (part of the C-terminal PDZ domain) by protein kinase C (PKC) strongly decreases the affinity of GluR2 for GRIP and ABP but not for PICK1, resulting in increased receptor internalization (Chung et al., 2000).

The specific molecular interactions of AMPA receptor subunits are the basis for the subunit-dependent AMPA receptor insertion into the postsynaptic membrane. In the most extensively studied adult rat hippocampus, assembly of AMPA receptors primarily involves heteromerization of GluR1 with GluR2, or GluR2 with GluR3 (Wenthold et al., 1996). Recent work has deciphered two general mechanisms of

postsynaptic AMPA receptor trafficking (Shi, 2001). Following LTP induction, GluR1/2 complexes are inserted *de novo* in an activity-dependent manner, thereby supporting transmission strengthening. In contrast, GluR2/3 complexes undergo a constitutive recycling largely independent of activity (Fig. 14) (Shi, 2001; Barry and Ziff, 2002)



2.2.3. Glutamate receptors at *Drosophila* NMJ synapses

The glutamate receptor subunits expressed at the *Drosophila* NMJ are related to mammalian non-NMDA type glutamate receptors. So far, five different glutamate receptor subunits (namely GluRIIA, IIB, IIC, IID and IIE) have been identified (Schuster et al., 1991; Petersen et al., 1997; Marrus et al., 2004; Featherstone et al., 2005; Qin et al., 2005). Thereby, genetic considerations suggested that the most likely tetrameric receptor complexes are formed by incorporating GluRIIC, GluRIID and GluRIIE with either GluRIIA or GluRIIB (Qin et al., 2005). The two receptor complexes, which co-exist within individual PSDs, are redundant for NMJ synapse formation (Petersen et al., 1997; DiAntonio et al., 1999; Marrus et al., 2004; Chen et

al., 2005; Qin et al., 2005). *gluRIIC^{null}*, *gluRIID^{null}* and *gluRIIE^{null}* single mutants, as well as *gluRIIA&IIB* double mutants (*gluRIIA^{null}IIB^{null}*), show embryonic lethality due to the absence of all synaptic glutamate receptors (Petersen et al., 1997; Featherstone and Brodie, 2002; Marrus et al., 2004; Qin et al., 2005).

GluRIIA and GluRIIB containing complexes differ fundamentally in their physiological properties. GluRIIB complexes show an about 10-fold faster desensitization than GluRIIA complexes, however an identical single-channel amplitude (Fig. 15) (DiAntonio et al., 1999). Accordingly, GluRIIA complexes account for the lion's share of synaptic currents at the *Drosophila* NMJ. In contrast to *gluRIIB* mutants, *gluRIIA* mutants are characterized by a strongly decreased quantal size (miniature evoked junctional current, mEJC) and concomitant compensatory increase in quantal content (Petersen et al., 1997; DiAntonio et al., 1999) This retrograde increase of presynaptic release (Davis et al., 1998) goes along with structural alterations like a smaller presynaptic terminal area with increased density of T-bars at active zones (Reiff et al., 2002).

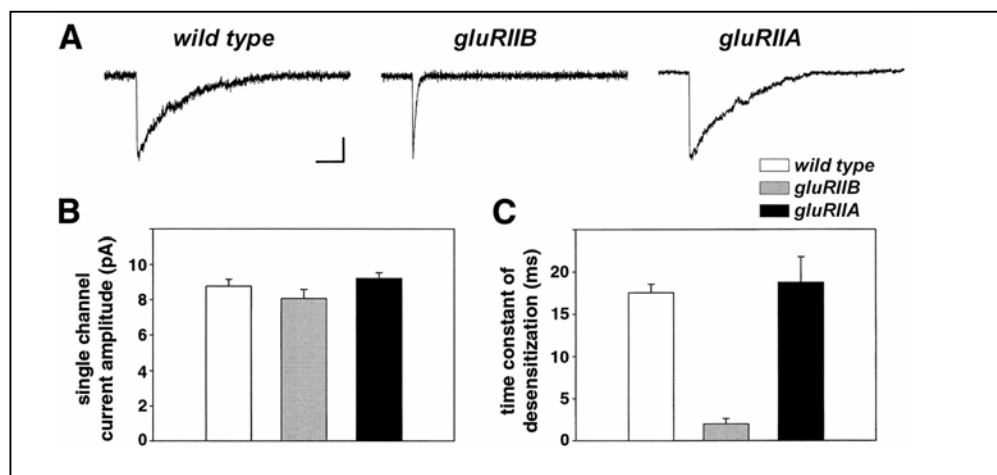


Fig. 15. Receptor subunit composition regulates desensitization kinetics

Outside-out patches were isolated from the larval muscle membrane of wild type and animals rescued by the expression of *gluRIIA* or *gluRIIB* in the *gluRIIA^{null}IIB^{null}* background. The traces show average responses (A) to the rapid application of 10mM glutamate. The single-channel current amplitude (B) was not significantly different in the three genotypes, but the time constant of desensitization (C) was much more rapid in *gluRIIB* larvae ($p < 0.005$). Calibration: 10msec, 5pA. Modified from (DiAntonio et al., 1999).

The synaptic glutamate receptor level can be regulated by PSD-associated proteins as the p21-associated kinase (PAK) (Sone et al., 2000; Albin and Davis, 2004) or the cell adhesion molecule FasII (Schuster et al., 1996). Moreover, non-vesicular glutamate release can affect glutamate receptor levels at the PSD (Featherstone et al., 2002).

The molecular mechanisms underlying the subunit-specific synaptic trafficking and anchoring of GluRIIA and GluRIIB complexes are widely unknown. However, recent

studies imply that the two receptor subtypes are likely differentially linked with membrane-associated proteins, scaffolding components or signaling molecules. GluRIIB complexes were shown to be specifically stabilized by the MAGUK Dlg (Chen and Featherstone, 2005), while GluRIIA complexes are anchored at the PSD by Coracle, a homolog to the mammalian Band 4.1N protein (Chen et al., 2005). Additionally, GluRIIA expression could be controlled by local translation (Sigrist et al., 2000). Furthermore, GluRIIA was also shown to be required for the PKA-dependent modulation of quantal size (Davis et al., 1998).

Glutamate receptor levels can control the number of synapses forming at the NMJ. Favoring GluRIIA over GluRIIB expression results in increased NMJ transmission strength and synapse number (Sigrist et al., 2000; Sigrist et al., 2002; Sigrist et al., 2003). Moreover, applying *in vivo* imaging of larval NMJ synapses, the formation and growth of individual synapses could be directly correlated with the entry of GluRIIA complexes from diffuse extra-synaptic pools (Rasse et al., 2005). Different from several other postsynaptic proteins tested, GluRIIA shows slow turnover and stably integrates into immature PSDs.

2.3. Study design

Recent reports imply mammalian non-NMDA receptors in the formation and stability of larger postsynaptic subcellular compartments such as dendritic spines independent of their ionic transmission (Kasai et al., 2003; Passafaro et al., 2003). However, whether and how non-NMDA glutamate receptors are involved in the assembly of postsynaptic specializations (PSDs) remained open.

The full absence of non-NMDA glutamate receptors at the *Drosophila* NMJ results in embryonic lethality due to the incapability of locomotion required for hatching. Nevertheless, extremely reduced levels of muscle glutamate receptors, hardly detectable by immunocytochemistry or electrophysiological recordings, were shown to be sufficient for survival (Marrus et al., 2004; Qin et al., 2005). This allowed studying effects of severe glutamate receptor deprivation on postsynaptic assembly and maturation. While the initial assembly of synapses persisted, the maturation of PSDs specifically failed. During synaptic growth glutamate receptor incorporation into the postsynaptic membrane is likely critical to enlarge PSDs by organizing cell adhesion to bring pre- and postsynaptic membranes in apposition.

The development of the larval neuromuscular system is characterized by a more than 100-fold increase in muscle surface (Jan and Jan, 1976) that goes along with a concomitant boost of evoked junctional currents (EJC), indicating a vast increase in synapse number and synaptic strength (Broadie and Bate, 1993; Schuster et al., 1996; Sigrist et al., 2003). To get an insight in the specific relevance of the two receptor complex subtypes for PSD maturation, single identified PSDs, expressing both fluorescently tagged GluRIIA- and GluRIIB-type complexes, were followed applying *in vivo* imaging of developing larval NMJs (Rasse et al., 2005). The strong dynamics of the NMJ were reflected in a massive growth of the PSD population caused by specific recruitment of either GluRIIA or GluRIIB containing complexes, which could be linked to the initial subunit composition and size of the PSD. Thereby, the incorporation behavior of the two receptor subtypes, which was analyzed by fluorescence recovery after photobleaching (FRAP) experiments, differed fundamentally. This differential recruitment, which persisted after suppression of presynaptic activity, seems to be based on the differing physiological channel properties and might be regulated by C-terminal receptor phosphorylation.

3. Material and Methods

3.1. Molecular biology

3.1.1. *Material*

The following plasmids were used for molecular cloning:

- pBNJ24.6 (generous gift of D. Sheridan, Yale University Medical School, New Haven, USA) (Sheridan et al., 2002)
- pBluescript[®] II KS + (pKS+; Stratagene, La Jolla, USA)
- pEGFP N1 (Clontech, Palo Alto, USA)
- pSL1180 (Fig. 56; Amersham Pharmacia Biotech, Buckinghamshire, England)
- pSL fa1180fa (Horn and Wimmer, 2000)
- pUAST (Fig. 57) (Brand and Perrimon, 1993)
- pUAST XL+ (produced in the lab, see 7.1)

All chemicals were, if not stated elsewhere, purchased from Roth (Karlsruhe, Germany), Sigma (St. Louis, USA) or Merck (Darmstadt, Germany). Agarose was obtained from Peqlab (Erlangen, Germany).

Alkaline phosphatase, T4 DNA ligase, T4 polynucleotide kinase, Taq Polymerase and various restriction endonucleases were purchased from Roche (Mannheim, Germany). The restriction endonuclease *Ascl* as well as Vent DNA-Polymerase was obtained from New England Biolabs (Beverly, USA). Elongase[®] enzyme mix used for overlap-extension PCRs was purchased from Invitrogen (Karlsruhe, Germany). All oligonucleotides were synthesized by MWG Biotech (Ebersberg, Germany). Unless stated elsewhere all molecular biology kits for RNA or DNA extraction and purification were obtained from Qiagen (Hilden, Germany). Chemically competent *E. coli* XL1 blue cells were produced in the lab.

All PCRs were performed with the PCR System GeneAmp 9700 (Applied Biosystems, Foster City, USA).

3.1.2. *Transgenes*

The molecular cloning of transgenes was performed, if not stated elsewhere, using standard molecular biology procedures (Sambrook et al., 1989). All constructs were double strand sequenced (MWG Biotech, Ebersberg, Germany or Qiagen, Hilden, Germany). Correct sequences were verified with MacVector[™] (Accelrys, San Diego, USA).

Overlap-extension PCRs (Fig. 16) were led through according to the Elongase[®] kit protocol (Invitrogen, Karlsruhe, Germany) with 30 ± 2 overlapping base pairs in between the two respective DNA templates.

Mixture 1:

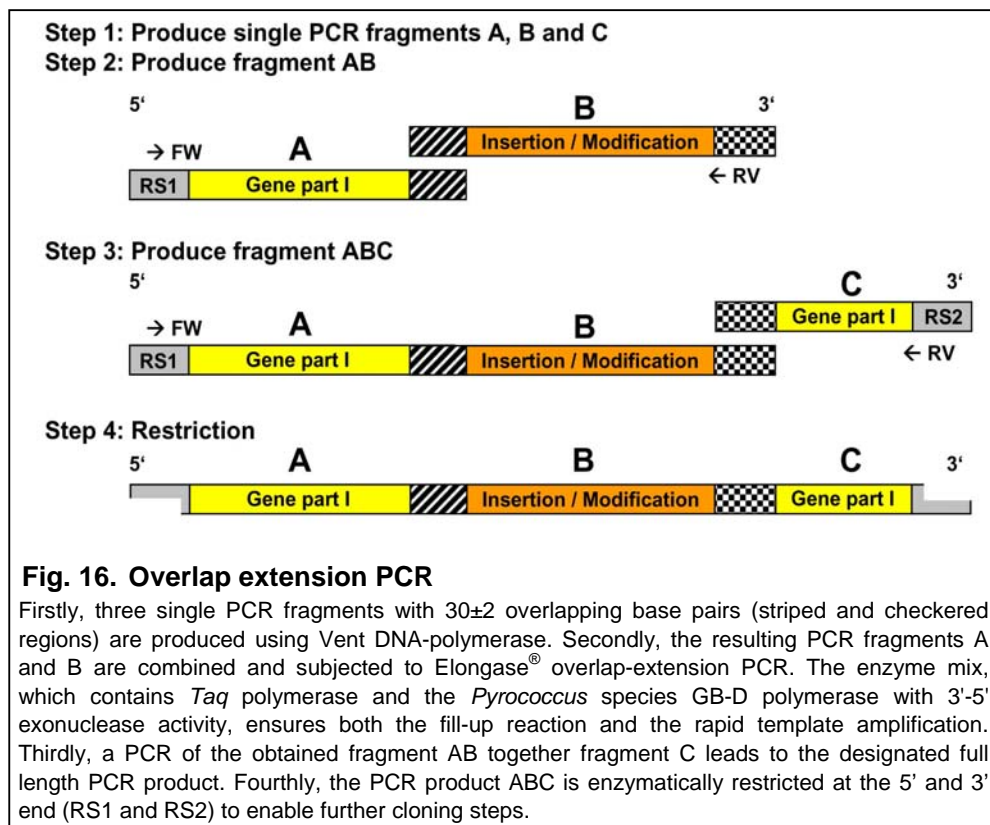
10mM	dNTP-Mix
10µM	forward primer
10µM	reverse primer
50µg	DNA template 1
50µg	DNA template 2
ad 20µl	H ₂ O

Mixture 2:

5x	buffer A	} 60mM Tris-SO ₄ (pH 9,1), 18mM (NH ₄) ₂ SO ₄ , 1-2mM MgSO ₄
5x	buffer B	
2µl	Elongase® enzyme mix	
ad 30µl	H ₂ O	

The mixtures 1 and 2 were combined and the PCR was performed as follows:

30x	Denaturation	30''	94°C
	Annealing	30''	54°C
	Extension	1' per kbp	68°C

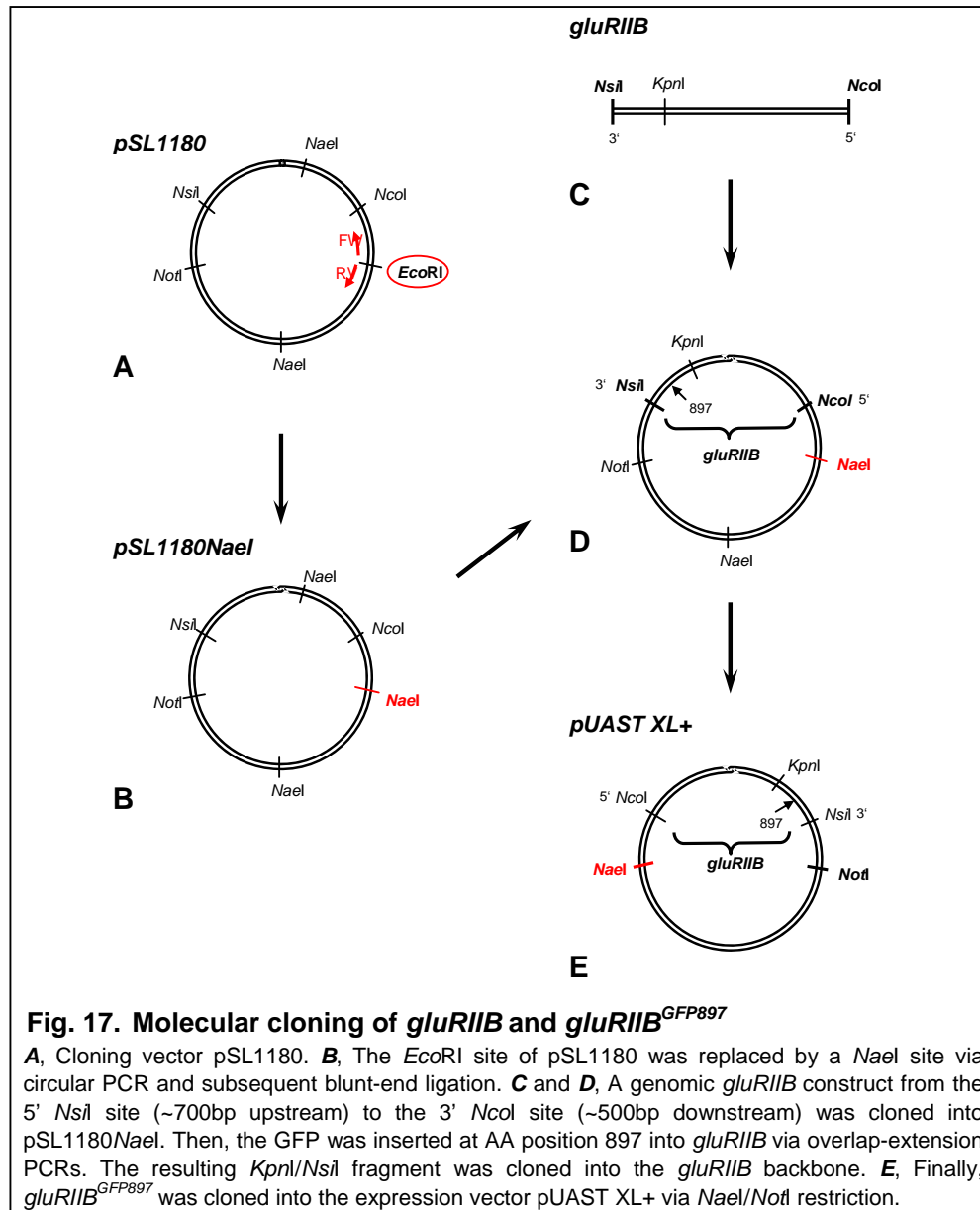


3.1.2.1. Site-directed fluorescence-tagging of *gluRIIA* and *gluRIIB*

gluRIIA^{GFP893} and *gluRIIA*^{mRFP893}.

The cloning of *gluRIIA*^{GFP893} and *gluRIIA*^{mRFP893} was described recently (Rasse et al., 2005).

gluRIIB, *gluRIIB*^{GFP897} and *gluRIIB*^{mRFP897} (Fig. 17):



Previously, a genomic *HindIII/SalI* fragment, covering the whole open reading frame of *gluRIIB* and the 3' end of *gluRIIA* was used as genomic *gluRIIB* rescue construct (DiAntonio et al., 1999). In this study, the *gluRIIA* 3' end, which is potentially translatable, was cleaved off leaving a genomic *NsiI/NcoI* construct of *gluRIIB* (*gluRIIB* coding region plus ~700bp upstream and ~500bp downstream) with unaltered rescue capability.

pSL1180NaeI:

Cloning of pSL1180NaeI (Fig. 17B):

- Circular PCR and blunt-end ligation
 - template: pSL1180 (Fig. 17A, Fig. 56)
 - forward primer: 5' CCGGCGTAATCATGGTCATAGCTGTTTCCTG 3'
 - reverse primer: 5' CGAATGGCCATGGGACGTC 3'

gluRIIB:

Cloning of pSL1180NaeI *gluRIIB* (Fig. 17C):

- Restriction: *NsiI/NcoI*
 - vector: pSL1180NaeI
 - insert: *gluRIIB*

Cloning of pUAST XL+ *gluRIIB*:

- Restriction: *NotI/NaeI*
 - vector: pUAST XL+
 - insert: *gluRIIB*

gluRIIB^{GFP897}:

The fluorophore insertion site and the linker sequences were chosen and designed as recently described (Sheridan et al., 2002; Rasse et al., 2005). Details are depicted in Fig. 32. The linker sequence is shown below in Fig. 18.

Cloning of pSL1180NaeI *gluRIIB*^{GFP897} (Fig. 17D):

- Overlap extension PCR, 3 steps (Fig. 16 and 3.1.2)
- Fragment A:
 - template: pSL1180NaeI *gluRIIB*
 - forward primer: 5' GCAAGGGTACCTATGCCTTCC 3'
 - reverse primer: 5' GGCGCGCCAGATGTGTATAAGAGACAT
GTAATTTGCTCCAGCGATGAGTAAC 3'
- Fragment B:
 - template: pEGFP N-1
 - forward primer: 5' CTCTTATACACATCTGGCGCGCCGA
GCAAGGGCGAGGAGCTGT 3'
 - reverse primer: 5' TCTGTCTCTTATACACATCTGCCCGGGCGCG
CCGCCCTTGTACAGCTCGTCCATGCC 3'
- Fragment C:
 - template: pSL1180NaeI *gluRIIB*

- forward primer: 5' GGCGGCGCGCCCGGGCAGATGTGTATAAGA
GACAGAATTACAAGTGCTTCCAGTGCGAAAA 3'
- reverse primer: 5' CCAGCATGCATTTTGCATACA 3'
- Fragment AB
 - primer: fragment A forward and B reverse
- Fragment ABC
 - primer: fragment A forward and C reverse
- Restriction: *KpnI/NsiI*
 - vector: pSL1180*NaeI gluRIIB*
 - insert: PCR product ABC

Cloning of pUAST XL+ *gluRIIB*^{GFP897} (Fig. 17E):

- Restriction: *NotI/NaeI*
 - vector: pUAST XL+
 - insert: *gluRIIB*^{GFP897}

gluRIIB^{mRFP897}:

Cloning of pUAST XL+ *gluRIIB*^{mRFP897}:

- Restriction: *Ascl*
 - vector: pUAST XL+ *gluRIIB*^{GFP897} (cleavage of GFP)
 - insert: mRFP1 with flanking *Ascl* sites (Rasse et al., 2005)

3.1.2.2. Chimeric glutamate receptor subunits

AAB (gluRIIA^{IB C-term}):

Cloning of pSL fa1180fa *AAB*:

- circular PCR of vector and blunt-end ligation with insert
- vector:
 - template: pSL fa1180fa *gluRIIA*
 - forward primer: 5' TAGGTGGTCGGAATATTGGAC 3'
 - reverse primer: 5' CCAGGATAACGCCGATGAGAAC 3'
- insert:
 - template: pKS+ *gluRIIBcDNA*
 - forward primer: 5' GCATCGCCGAGTTTTTGTGG 3'
 - reverse primer: 5' CTACTTTTCAATTCGCCTGGTCT 3'

Cloning of pUAST *AAB*:

- Restriction: *EcoRI/XhoI*
 - vector: pUAST
 - insert: *AAB*

AAB^{GFP}:Cloning of pSL fa1180fa AAB^{GFP}:

- Overlap-extension PCR, 3 steps (Fig. 16 and 3.1.2)
- Fragment A:
 - template: pSLfa1180fa *gluRIIA*
 - forward primer: 5' GGGATTAGGTTAACGCTCTTGAGTG 3'
 - reverse primer: 5' CCACAAAACTCGGCGAT
GCCCAGGATAACGCCG 3'
- Fragment B:
 - template: pSL1180NaeI *gluRIIB*^{GFP897}
 - forward primer: 5' GTTATCCTGGGCATCGCCGAGTTTTTGT
GGCACG 3'
 - reverse primer: 5' CAATATTCCGACCACCTACTTTTCAATTTCGC
CTGGTCTT 3'
- Fragment C:
 - template: pSL fa1180fa *gluRIIA*
 - forward primer: 5' CGAATTGAAAAGTAGGTGGTCGGAATATTG
GACGATTG 3'
 - reverse primer: 5' CTCGCTCGAGTGCCGCACTAAAGG 3'
- Fragment AB
 - primer: fragment A forward and B reverse
- Fragment ABC
 - primer: fragment A forward and C reverse
- Restriction: *HpaI/XhoI*
 - vector: pSL fa1180fa *gluRIIA*
 - insert: PCR product ABC

Cloning of pUAST AAB^{GFP}:

- Restriction: *EcoRI/XhoI*
 - vector: pUAST
 - insert: AAB^{GFP}

AAC (*gluRIIA*^{IIC C-term}):

Cloning of pSL fa1180fa AAC:

- circular PCR of vector and blunt-end ligation with insert
- vector:
 - template: pSL fa1180fa *gluRIIA*
 - forward primer: 5' TAGGTGGTCGGAATATTGGAC 3'

- reverse primer: 5' CCAGGATAACGCCGATGAGAAC 3'
- insert:
 - template: pSL fa1180fa *gluRIICcDNA*
 - forward primer: 5' GCATCACGGAGTTTTTGGTCTACG 3'
 - reverse primer: 5' CTAGACCCTTGCCTCCTTTTCTCC 3'

Cloning of pUAST AAC:

- Restriction: *EcoRI/XhoI*
 - vector: pUAST
 - insert: AAC

AAD (gluRIIA^{IID C-term}):

Cloning of pSL fa1180fa *AAD*:

- Overlap-extension PCR, 3 steps (Fig. 16 and 3.1.2)
- Fragment A:
 - template: pSL fa1180fa *gluRIIA*
 - forward primer: 5' CCGCCATTCCAGGATCCAGATG 3'
 - reverse primer: 5' GTAGCACCAACATAGGATGCCCAGG
ATAACGCCG 3'
- Fragment B:
 - template: pKS+ *gluRIIDcDNA*
 - forward primer: 5' GTTATCCTGGGCATCCTATGTTGGTGCTA
CTTTGTCTACAAG 3'
 - reverse primer: 5' CAATATTCCGACCACTTAATCCTCAAC
CGGCATATTTTC 3'
- Fragment C:
 - template: pSL fa1180fa *gluRIIA*
 - forward primer: 5' CCGGTTGAGGATTAAGTGGTCGGA
ATATTGGACGATTG 3'
 - reverse primer: 5' TACCCAAATGCGCTATCTGTGTTCT 3'
- Fragment AB
 - primer: fragment A forward and B reverse
- Fragment ABC
 - primer: fragment A forward and C reverse
- Restriction: *BamHI/NcoI*
 - vector: pSL fa1180fa *gluRIIA*
 - insert: PCR product ABC

Cloning of pUAST AAD:

- Restriction: *NaeI/XhoI*
 - vector: pUAST *gluRIIA*^{GFP893}
 - insert: AAD

AAE (*gluRIIA*^{IIE C-term}):

Cloning of pSL fa1180fa AAE:

- Overlap-extension PCR, 3 steps (Fig. 16 and 3.1.2)
- Fragment A:
 - template: pSL fa1180fa *gluRIIA*
 - forward primer: 5' CCGCCATTCCAGGATCCAGATG 3'
 - reverse primer: 5' CAAAACCCAGCTGATGATGCCAG
GATAACGCCG 3'
- Fragment B:
 - template: pKS+ *gluRIIEcDNA*
 - forward primer: 5' GTTATCCTGGGCATCATCAGCTGGGT
TTTGTTCGTAATG 3'
 - reverse primer: 5' CAATATTCCGACCACCTACTGCGATTCCTGGGCC 3'
- Fragment C:
 - template: pSL fa1180fa *gluRIIA*
 - forward primer: 5' CAGGAATCGCAGTAGGTGGTCGGA
ATATTGGACGATTG 3'
 - reverse primer: 5' TACCCAAATGCGCTATCTGTGTTCT 3'
- Fragment AB
 - primer: fragment A forward and B reverse
- Fragment ABC
 - Primer: fragment A forward and C reverse
- Restriction: *BamHI/NcoI*
 - vector: pSL fa1180fa *gluRIIA*
 - insert: PCR product ABC

Cloning of pUAST AAE:

- Restriction: *EcoRI/XhoI*
 - vector: pUAST
 - insert: AAE

BBA (gluRIIB^{I/A C-term}):Cloning of pUAST *BBA*:

- Overlap-extension PCR, 2 steps (Fig. 16 and 3.1.2)
- Fragment A:
 - template: pKS+ *gluRIIBcDNA*
 - forward primer: 5' GAGCAGATGTATGCACGGTGTACAGTTCCTGG 3'
 - reverse primer: 5' CCACAGGAACTCAAAGACACCGATCACGAGTCC 3'
- Fragment B:
 - template: pKS+ *gluRIIAcDNA*
 - forward primer: 5' CTCGTGATCGGTGTCTTTGAGTTCCTGTGGAACG 3'
 - reverse primer: 5' GCAGTCTAGACTAGCTAACCGTCTTGCTGCG 3'
- Fragment AB
 - primer: fragment A forward and B reverse
- Restriction: *BglI/XbaI*
 - vector: pUAST
 - insert: PCR product AB

BBA^{GFP}:Cloning of pSL1180*NaeI BBA^{GFP}*:

- Overlap extension PCR, 3 steps (Fig. 16 and 3.1.2)
- Fragment A:
 - template: pSL1180*NaeI gluRIIB*
 - forward primer: 5' GCAAGGGTACCTATGCCTTCC 3'
 - reverse primer: 5' CCACAGGAACTCAAAGACACCGATCACGAGTCC 3'
- Fragment B:
 - template: pSL fa1180fa *gluRIIA^{GFP893}*
 - forward primer: 5' CTCGTGATCGGTGTCTTTGAGTTCCTGTGGAACG 3'
 - reverse primer: 5' AGCCTTTTTACTCCCCTAGCTAACCGT
CTTGCTGCG 3'
- Fragment C:
 - template: pSL1180*NaeI gluRIIB*
 - forward primer: 5' CAAGACGGTTAGCTAGGGGAGTAAAAAGG
CTTGCGAAC 3'
 - reverse primer: 5' CCAGCATGCATTTTGCATACA 3'
- Fragment AB
 - primer: fragment A forward and B reverse

- Fragment ABC
 - primer: fragment A forward and C reverse
- Restriction: *KpnI/NsiI*
 - vector: pSL1180*NaeI gluRIIB*
 - insert: PCR product ABC

Cloning of pUAST XL+ *BBA^{GFP}*:

- Restriction: *NotI/NaeI*
 - vector: pUAST XL+
 - insert: *BBA^{GFP}*

CCA (gluRIIC^{IIA C-term}):

Cloning of pUAST *CCA*:

- Overlap-extension PCR, 2 steps (Fig. 16 and 3.1.2)
- Fragment A:
 - template: pKS+ *gluRIICcDNA*
 - forward primer: 5' GAGCAGATCTATGAAAAAAGAAGTGTCCGGAAAT 3'
 - reverse primer: 5' CCACAGGAACTCAAAAATGCCGATG
AGAAAGGCAATC 3'
- Fragment B:
 - template: pSL fa1180fa *gluRIIA*
 - forward primer: 5' TTTCTCATCGGCATTTTTGAGTTCCTGTGGAACG 3'
 - reverse primer: 5' GCAGTCTAGACTAGCTAACCGTCTTGCTGCG 3'
- Fragment AB
 - primer: fragment A forward and B reverse
- Restriction: *BglII/XbaI*
 - vector: pUAST
 - insert: PCR product AB

3.1.2.3. Modifications of *gluRIIA*

gluRIIA^{hypo}:

The cloning of *gluRIIA^{hypo}*, a genomic *gluRIIA* construct missing most of the 3' untranslated region (UTR), was described recently (Qin et al., 2005).

gluRIIA^{Q614R}:

Cloning of pSL fa1180fa *gluRIIA^{Q614R}*:

- Overlap extension PCR, 2 steps (Fig. 16 and 3.1.2)

- Fragment A:
 - template: pSL fa1180fa *gluRIIA*
 - forward primer: 5' GCAGCGCATCCACTTCAACCT 3'
 - reverse primer: 5' CTAGGCAGAATGTCGCAGCCCTGTCTCATAA
TGGAGCCCACCATCAGCCAAG 3'
 - Fragment B:
 - template: pSL fa1180fa *gluRIIA*
 - forward primer: 5' CTTGGCTGATGGTGGGCTCCATTATGAGACA
GGGCTGCGACATTCTGCCTAG 3'
 - reverse primer: 5' TACCCAAATGCGCTATCTGTGTTCT 3'
 - Fragment AB
 - primer: fragment A forward and B reverse
 - Restriction: *BglII/NcoI*
 - vector: pSL fa1180fa *gluRIIA*
 - insert: PCR product AB
- Cloning of pUAST *gluRIIA*^{Q614R}:
- Restriction: *EcoRI/XhoI*
 - vector: pUAST
 - insert: *gluRIIA*^{Q614R}

gluRIIA^{E783A}:

Cloning of pSL fa1180fa *gluRIIA*^{E783A}:

- Overlap extension PCR, 2 steps (Fig. 16 and 3.1.2)
- Fragment A:
 - template: pSL fa1180fa *gluRIIA*
 - forward primer: 5' GCAGCGCATCCACTTCAACCT 3'
 - reverse primer: 5' CATCTTCTGCAGCTCGCCCCTGGCGCTCAG
CTGGAGAATGGACACG 3'
- Fragment B:
 - template: pSL fa1180fa *gluRIIA*
 - forward primer: 5' CGTGTCCATTCTCCAGCTGAGCGCCAGGG
GCGAGCTGCAGAAGATG 3'
 - reverse primer: 5' TACCCAAATGCGCTATCTGTGTTCT 3'
- Fragment AB
 - primer: fragment A forward and B reverse
- Restriction: *BglII/NcoI*
 - vector: pSL fa1180fa *gluRIIA*

- insert: PCR product AB

Cloning of pUAST *gluRIIA*^{E783A}:

- Restriction: *EcoRI/XhoI*
 - vector: pUAST
 - insert: *gluRIIA*^{E783A}

gluRIIA^{ΔC17}:

Cloning of pUAST *gluRIIA*^{ΔC17}:

- circular PCR and blunt-end ligation
 - template: pSL fa1180fa *gluRIIA*
 - forward primer: 5' TAGGTGGTCGGAATATTGGACG 3'
 - reverse primer: 5' TGATCGCCTGGACGACGACTTG 3'
- restriction: *EcoRI/XhoI*
 - vector: pUAST
 - insert: *gluRIIA*^{ΔC17}

gluRIIA^{ΔC35}:

Cloning of pUAST *gluRIIA*^{ΔC35}:

- circular PCR and blunt-end ligation
 - template: pSL fa1180fa *gluRIIA*
 - forward primer: 5' TAGGTGGTCGGAATATTGGACG 3'
 - reverse primer: 5' GCGCACCCAAAACCTTCAGG 3'
- restriction: *EcoRI/XhoI*
 - vector: pUAST
 - insert: *gluRIIA*^{ΔC35}

gluRIIA^{ΔC44}:

Cloning of pUAST *gluRIIA*^{ΔC44}:

- circular PCR and blunt-end ligation
 - template: pSL fa1180fa *gluRIIA*
 - forward primer: 5' TAGGTGGTCGGAATATTGGACG 3'
 - reverse primer: 5' GAGCTCCGCCTTGAAAGCC 3'
- restriction: *EcoRI/XhoI*
 - vector: pUAST
 - insert: *gluRIIA*^{ΔC44}

gluRIIA^{ΔC53}:Cloning of pUAST *gluRIIA*^{ΔC53}:

- circular PCR and blunt-end ligation
 - template: pSL fa1180fa *gluRIIA*
 - forward primer: 5' TAGGTGGTCGGAATATTGGACG 3'
 - reverse primer: 5' AGTCACTCGCTCCTCCACCG 3'
- restriction: *EcoRI/XhoI*
 - vector: pUAST
 - insert: *gluRIIA*^{ΔC53}

3.1.3. *In vitro* transposition

(in collaboration with Anne Grünewald)

The *in vitro* transposition (IVT; Fig. 18, scheme for pSL1180Nael *gluRIIB*) was performed with the EZ::TNTM Transposase Kit of Epicentre (Madison, USA). To start, the transposon *TgPT-0* was amplified from pBNJ24.6 by Vent-polymerase PCR from its mosaic ends with the *TN5 ME* primer (5' CTGTCTCTTATACACATCT 3'). Then, the following reagents were mixed:

1μl	10x reaction buffer
0,2μg	target DNA (pSLfa1180fa <i>gluRIIA</i> or pSL1180Nael <i>gluRIIB</i>)
X μl	transposon <i>TgPT-0</i> (molar equivalent to target DNA)
1μl	Transposase
ad 10μl	H ₂ O

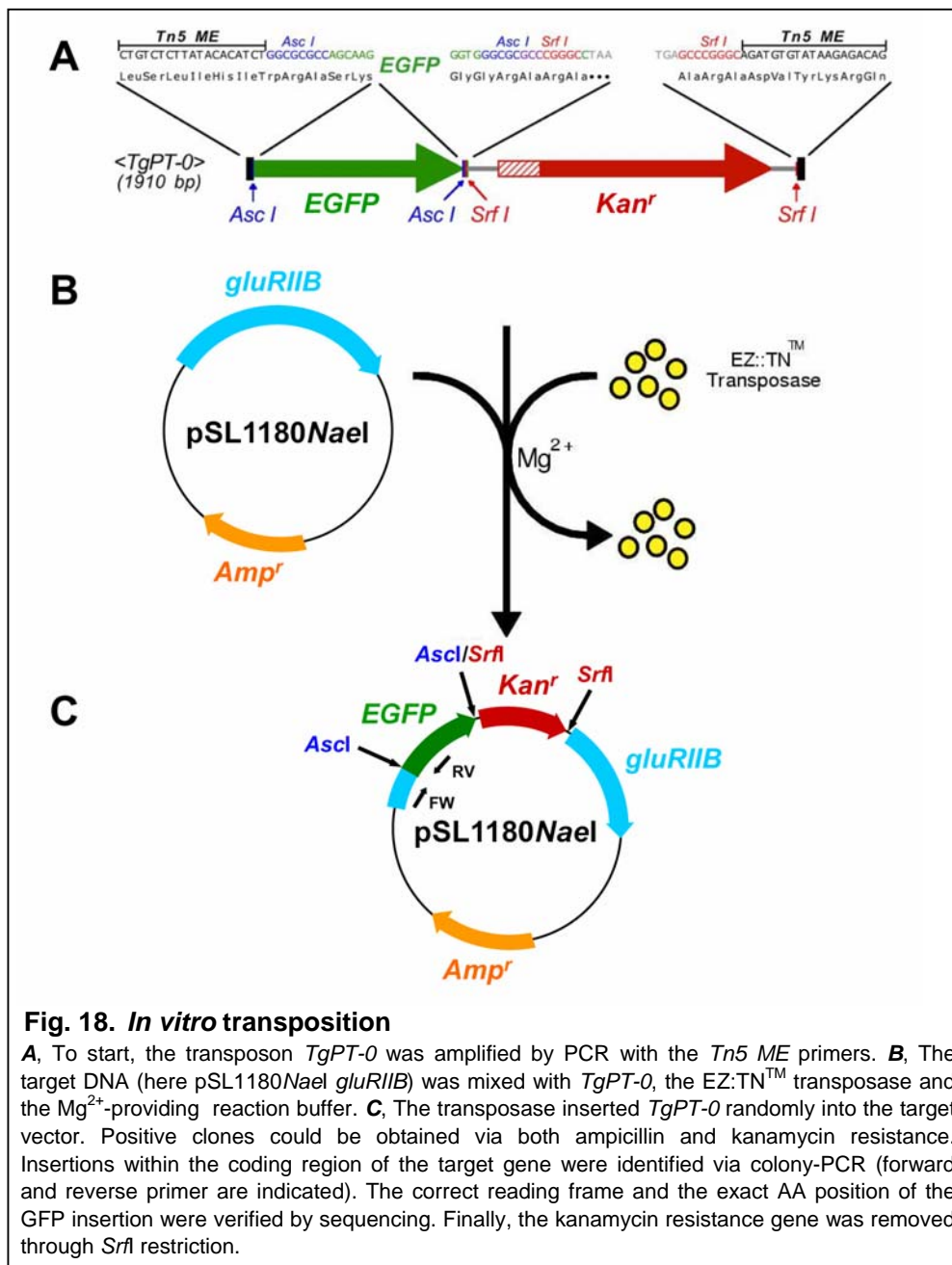
After incubation for 2h at 37°C the reaction was stopped with the provided 10x stop solution EZ::TNTM and the mixture was transformed into chemically competent *E. coli* XL1blue cells. Positive clones, containing both kanamycin and ampicillin resistance genes, were identified for insertions of *TgPT-0* within the target DNA via colony PCR using the following primer pairs:

	forward primer	5' GCTGAGATGACATTCTTGGC 3' (<i>gluRIIA</i>)
		5' CATTCACTGGTCCATTTCC 3' (<i>gluRIIB</i>)
5'3' insertion:	reverse primer	5' AACAGCTCCTCGCCCTTG 3' (within GFP)
3'5' insertion:	reverse primer	5' CCTGCCATCACGAGATTT 3' (within KanaR)

Positive samples harboring *TgPT-0* within the translated region of the target gene were sequenced to identify in frame insertions and the exact position.

Clones with 3'5' insertion were subjected to enzymatic *Ascl* digest and re-ligation to change the EGFP orientation (*gluRIIA*, which contains an internal *Ascl* site, had to be subcloned via *SalI/NcoI* restriction). Positive clones were again identified via

colony PCR. Finally, the kanamycin resistance was eliminated from all obtained clones by *SrfI* restriction and all constructs were cloned into pUAST (*gluRIIA*, via *EcoRI/XhoI*) or pUAST XL+ (*gluRIIB*, via *NotI/NaeI*).



3.2. *Drosophila melanogaster*

3.2.1. Cultivation

Fly strains were, if not otherwise stated, reared at 25°C in plastic bottles (Greiner Bio-one, Kremsmünster, Austria) containing cultivation medium (195g agar, 200g soy flour, 360g yeast, 1600g corn flour, 440g beet syrup, 1600g malt, 30g nipagine,

126ml propionic acid, ad 18l H₂O). Embryonic collections were performed in plastic cylinders placed on apple agar plates (1l apple juice, 100g saccharose, 85g agar-agar, 40ml nipagine (15%), ad 3l H₂O).

3.2.2. Transgenics

Drosophila germ line transformation was performed with an Eppendorf InjectMan (Hamburg, Germany) as described previously (Rubin and Spradling, 1982) using 300ng/μl P-element DNA (pUAST with inserted transgene) and 100ng/μl helper plasmid (pΔ2-3). Transgenic animals were established in the following genetic backgrounds:

Name	Genetics	Source
<i>w</i> ¹	$\frac{w-}{w-}; \frac{+}{+}$	(Castiglioni, 1951)
<i>dfclh</i> ⁴	$\frac{w-}{w-}; \frac{df(2L)cl^{h4}}{Gla, Bc}; \frac{+}{+}$	(Petersen et al., 1997)
<i>dfast</i> ⁴	$\frac{w-}{w-}; \frac{df(2L)ast^4}{Gla, Bc}; \frac{+}{+}$	(Marrus et al., 2004)
<i>E3</i>	$\frac{w-}{w-}; \frac{+}{+}; \frac{E3}{TM6B}$	(Qin et al., 2005)

Table 1. Fly stocks for germ line transformation

*dfclh*⁴ is a deficiency for *gluRIIA* and *gluRIIB*, *dfast*⁴ for *gluRIIC* and *E3* for *gluRIID* and *gluRIIE*.

3.2.3. Genetics

To establish a *gluRIIA&IIB* (*gluRIIA*^{null}*IIB*^{null}) double mutant situation, *dfclh*⁴ (see 3.2.2) had to be crossed to *df(2L)gluRIIA&B*^{SP22} (from here on referred to as *A22*) (Petersen et al., 1997; DiAntonio et al., 1999; Qin et al., 2005). *gluRIIC* (*gluRIII*) mutants were produced by crossing *gluRIII*¹ to *df(2L)ast*⁴ or *df(2L)ast*² (Marrus et al., 2004). Leaky expression of GluRIIC (*IIC*^{hypo}) was performed as previously described (Marrus and DiAntonio, 2004). As wild type control *w*¹ (see Table 1) was used. Rescue embryos and larvae were selected using marked balancer chromosomes (either Bc (black cell) or GFP).

The genetics of all used animals are summarized in Table 2. All transgenes (see Fig. 62, Fig. 63, Fig. 64) derived, if not stated elsewhere, from genomic constructs. In cases where the gender was genetically of no importance, females and males were chosen stochastically.

Name	Genetics
<i>IIA^{null}IIB^{null}</i>	$\frac{w-}{w-}; \frac{dfcl^{h4}}{A22}; \frac{+}{+}$
<i>IIC^{null}</i>	$\frac{w-}{w-}; \frac{dfast^4}{III^1}; \frac{+}{+}$
<i>IIA</i>	$\frac{w-}{w-}; \frac{dfcl^{h4}}{A22}; \frac{UAS - gluRIIA}{+}$
<i>IIA^{hypo}</i>	$\frac{w-}{w-}; \frac{dfcl^{h4}, UAS - gluRIIA^{hypo}}{A22}; \frac{+}{+}$
<i>IIA^{hypo} + elav-tnt</i>	$\frac{w-}{w-}; \frac{dfcl^{h4}, UAS - gluRIIA^{hypo}}{A22, UAS - tnt}; \frac{elav - gal4}{+}$
<i>IIC^{hypo}</i>	$\frac{w-}{w-}; \frac{dfast^2, UAS - gluRIICcDNA}{III^1}; \frac{+}{+}$
<i>IIA^{ΔC17}</i>	$\frac{UAS - gluRIIA^{ΔC17}}{w-}; \frac{dfcl^{h4}}{A22}; \frac{+}{+}$
<i>IIA^{ΔC35}</i>	$\frac{w-}{w-}; \frac{dfcl^{h4}}{A22}; \frac{UAS - gluRIIA^{ΔC35}}{+}$
<i>IIA^{ΔC44}</i>	$\frac{w-}{w-}; \frac{dfcl^{h4}, UAS - gluRIIA^{ΔC44}}{A22}; \frac{+}{+}$
<i>IIA^{ΔC53}</i>	$\frac{w-}{w-}; \frac{dfcl^{h4}, UAS - gluRIIA^{ΔC53}}{A22}; \frac{+}{+}$
<i>IIA^{Q614R}</i>	$\frac{w-}{w-}; \frac{dfcl^{h4}}{A22}; \frac{UAS - gluRIIA^{Q614R}}{+}$
<i>IIA^{E783A}</i>	$\frac{w-}{w-}; \frac{dfcl^{h4}, UAS - gluRIIA^{E783A}}{A22}; \frac{+}{+}$
<i>IIA^{GFP}</i>	$\frac{w-}{w-}; \frac{dfcl^{h4}}{A22}; \frac{UAS - gluRIIA^{GFP893}}{+}$
<i>2xIIA^{GFP}</i>	$\frac{w-}{w-}; \frac{dfcl^{h4}}{A22}; \frac{UAS - gluRIIA^{GFP893}}{UAS - gluRIIA^{GFP893}}$
<i>IIA^{GFP} & IIA^{mRFP}</i>	$\frac{w-}{w-}; \frac{dfcl^{h4}}{A22}; \frac{UAS - gluRIIA^{GFP893}}{UAS - gluRIIA^{mRFP893}}$
<i>IIA^{GFP} & IIA^{mRFP} + ok319-tnt</i>	$\frac{w-}{w-}; \frac{dfcl^{h4}, ok319 - gal4}{A22, UAS - tnt}; \frac{UAS - gluRIIA^{GFP893}}{UAS - gluRIIA^{mRFP893}}$
<i>IIB</i>	$\frac{w-}{w-}; \frac{dfcl^{h4}}{A22}; \frac{UAS - gluRIIB}{+}$
<i>IIB^{GFP}</i>	$\frac{w-}{w-}; \frac{dfcl^{h4}}{A22}; \frac{UAS - gluRIIB^{GFP897}}{+}$
<i>2xIIB^{GFP}</i>	$\frac{w-}{w-}; \frac{dfcl^{h4}, UAS - gluRIIB^{GFP897}}{A22}; \frac{UAS - gluRIIB^{GFP897}}{+}$
<i>IIB^{GFP} & IIB^{mRFP}</i>	$\frac{w-}{w-}; \frac{dfcl^{h4}}{A22}; \frac{UAS - gluRIIB^{GFP897}}{UAS - gluRIIB^{mRFP897}}$
<i>IIB^{GFP} & IIB^{mRFP} + ok319-tnt</i>	$\frac{w-}{w-}; \frac{dfcl^{h4}, ok319 - gal4}{A22, UAS - tnt}; \frac{UAS - gluRIIB^{GFP897}}{UAS - gluRIIA^{mRFP897}}$
<i>IIB^{GFP} & IIA^{mRFP}</i>	$\frac{w-}{w-}; \frac{dfcl^{h4}}{A22}; \frac{UAS - gluRIIB^{GFP897}}{UAS - gluRIIA^{mRFP893}}$

<i>IIB^{GFP}</i> & <i>IIA^{mRFP}</i> + <i>ok319-tnt</i>	$\frac{w-}{w-}; \frac{dfcl^{h4}, ok319-gal4}{A22, UAS-tnt}; \frac{UAS-gluRIIB^{GFP897}}{UAS-gluRIIA^{mRFP893}}$
<i>IIA^{GFP}</i> & <i>IIB^{mRFP}</i>	$\frac{w-}{w-}; \frac{dfcl^{h4}}{A22}; \frac{UAS-gluRIIA^{GFP893}}{UAS-gluRIIB^{mRFP897}}$
<i>AAB</i>	$\frac{w-}{w-}; \frac{dfcl^{h4}}{A22}; \frac{UAS-AAB}{+}$
<i>AAB^{GFP}</i> & <i>IIA^{mRFP}</i>	$\frac{w-}{w-}; \frac{dfcl^{h4}, UAS-AAB^{GFP}}{A22}; \frac{UAS-gluRIIA^{mRFP893}}{+}$
<i>AAB^{GFP}</i> & <i>IIB^{mRFP}</i>	$\frac{w-}{w-}; \frac{dfcl^{h4}, UAS-AAB^{GFP}}{A22}; \frac{UAS-gluRIIB^{mRFP897}}{+}$
<i>AAC</i>	$\frac{w-}{w-}; \frac{dfcl^{h4}}{A22}; \frac{UAS-AAC}{+}$
<i>AAD</i>	$\frac{w-}{w-}; \frac{dfcl^{h4}}{A22}; \frac{UAS-AAD}{+}$
<i>AAE</i>	$\frac{w-}{w-}; \frac{dfcl^{h4}}{A22}; \frac{UAS-AAE}{+}$
<i>BBA</i>	$\frac{w-}{w-}; \frac{dfcl^{h4}, UAS-BBAcDNA}{A22}; \frac{Mhc-gal4}{+}$
<i>BBA^{GFP}</i> & <i>IIA^{mRFP}</i>	$\frac{w-}{w-}; \frac{dfcl^{h4}, UAS-BBA^{GFP}}{A22}; \frac{UAS-gluRIIA^{mRFP893}}{+}$
<i>BBA^{GFP}</i> & <i>IIB^{mRFP}</i>	$\frac{w-}{w-}; \frac{dfcl^{h4}, UAS-BBA^{GFP}}{A22}; \frac{UAS-gluRIIB^{mRFP897}}{+}$
<i>CCA</i>	$\frac{w-}{w-}; \frac{dfcl^{h4}}{A22}; \frac{UAS-CCAcDNA}{Mhc-gal4}$
<i>ok319-2xEYFP</i>	$\frac{w-}{w-}; \frac{ok319-gal4}{+}; \frac{UAS-2xEYFP}{+}$
<i>ok319-tnt</i>	$\frac{w-}{w-}; \frac{ok319-gal4}{UAS-tnt}; \frac{+}{+}$
<i>cha-shi^{TS1}</i> (29°C)	$\frac{UAS-shi^{TS1}}{w-}; \frac{cha-gal4}{+}; \frac{+}{+}$
<i>elav-tnt</i>	$\frac{w-}{w-}; \frac{UAS-tnt}{+}; \frac{elav-gal4}{+}$
<i>shi^{TS1}</i> (32°C) *	$\frac{shi^{TS1}}{shi^{TS1}}; \frac{+}{+}; \frac{+}{+}$
<i>para^{TS}</i> (29°C)	$\frac{para^{TS}}{para^{TS}}; \frac{+}{+}; \frac{+}{+}$
<i>cac^{GFP}</i>	$\frac{w-}{w-}; \frac{ok6-gal4}{+}; \frac{UAS-cac^{GFP}}{+}$
<i>cac^{GFP}</i> + <i>IIA^{hypo}</i>	$\frac{w-}{w-}; \frac{dfcl^{h4}, UAS-gluRIIA^{hypo}}{A22, ok6-gal4}; \frac{UAS-cac^{GFP}}{+}$

Table 2. Genetics

Genetics of all used genotypes. The 4th chromosome is not illustrated. * *shi^{TS1}* embryos were collected for 2h, aged 12h at 25°C and then shifted to the restrictive temperature of 32°C until dissection. In the text, glutamate receptor genotypes also appear with the prefix *gluR*.

3.2.4. Immunohistochemistry

For all preparations hemolymph-like (HL-3) saline without Ca^{2+} (Stewart et al., 1994) was used (concentrations in mM): NaCl 70, KCl 5, MgCl_2 20, NaHCO_3 10, trehalose 5, sucrose 115, HEPES 5, pH adjusted to 7.2.

3.2.4.1. Larval body-wall preparation

2nd or 3rd instar larvae were fixed on a rubber dissection pad with fine insect pins (0.1x10mm, Thorns, Göttingen, Germany) and covered with a drop of cold HL-3 solution. Then, the larvae were opened dorsally along the midline from the posterior to the anterior end with dissection spring scissors (FST, Vancouver, Canada). Subsequently, all internal organs including the central nervous system were removed carefully with fine forceps (FST, Vancouver, Canada) and the epidermis was stretched and pinned down with two pins on each side.

3.2.4.2. Embryonic body-wall preparation

The embryos (stage 17, 20-22h after egg laying) were washed within a micro sieve and their chorion membrane was removed with 50% DanChlorix (Colgate-Palmolive, Hamburg, Germany). Next, the embryos were carefully pressed out of their vitellin membrane with fine forceps. For dissection the embryos were fixed with fine clips on a sylgard (Dow Corning, Midland, USA) plate and opened dorsally along the midline using two ultra-thin electrolytically sharpened tungsten needles (tungsten wire, 0.075mm; World Precision Instruments, Sarasota, USA). Then, internal organs were sucked off and the epidermis was pinned down with a tungsten needle on each side.

3.2.4.3. Fixation and staining

The dissected samples were fixed either for 10' with 4% paraformaldehyde (PFA) in PBS (8g NaCl, 2g KCl, 2g KH_2PO_4 , 1.15g $\text{Na}_2\text{HPO}_4 \cdot 2\text{H}_2\text{O}$, ad 1l H_2O , pH 7.4) or for 5' with ice-cold methanol (for 8B4D2 stainings). After 30' of blocking with PBT (PBS with 0.05% Triton TX100) containing 5% goat serum (NGS), the PBT/NGS solution was refreshed, primary antibodies were added and the dissections were incubated over night at 4°C. The next day the samples were washed twice shortly and three times for 20' with PBT. Then, fluorescence-labeled secondary antibodies (Dianova, Hamburg, Germany) were applied 1:500 for 2h in PBT with 5% NGS. The dissections were washed as before and mounted on an object slide in VectaShield Mounting Medium for fluorescence (Vector Laboratories, Burlingame, USA).

Primary antibodies were used at the following concentrations:

- mouse anti-GluRIIA (8B4D2; Developmental Studies Hybridoma Bank, Iowa City, USA), 1:100
- rabbit anti-GluRIIB (gift of A. DiAntonio, Washington University School of Medicine, St. Louis, USA), 1:2000
- rabbit anti-GluRIIC (Qin et al., 2005), 1:500
- rabbit anti-GluRIID (Qin et al., 2005), 1:500
- mouse Nc82 (gift of E. Buchner, University of Würzburg, Würzburg, Germany), 1:100
- rabbit anti- α -Adaptin, (gift of M. Gonzalez-Gaitan, MPI of CBG, Dresden, Germany), 1:50
- rabbit anti-PAK (gift of N. Harden, Simon Fraser University, Burnaby, Canada), 1:2000
- mouse anti-FasII (1D4; Developmental Studies Hybridoma Bank, Iowa City, USA), 1:50
- mouse anti-Dlg (4F3; Developmental Studies Hybridoma Bank, Iowa City, USA), 1:500
- mouse anti-GFP 3E6 (A-11120; Molecular Probes, Eugene, USA), 1:200
- rabbit anti-GFP (A-11122; Molecular Probes, Eugene, USA), 1:500
- goat anti-HRP cyanine 5 (Dianova, Hamburg, Germany), 1:200

To visualize the muscle morphology TRITC-coupled Phalloidine (P1951, Sigma, St. Louis, USA), which binds to Actin, was applied for 30 minutes in 1:200 dilution (together with the secondary antibodies).

3.3. Microscopy and image analysis

3.3.1. Animal sorting

The sorting of normal adult flies was performed on a self-made CO₂ frit using binocular microscopes (Stemi 2000, Zeiss, Jena, Germany) equipped with halogen lamps (KL200, Schott, Mainz, Germany).

GFP-marked embryos, larvae and adults were sorted using a binocular fluorescence microscope (FluoTM MZFLIII, Leica Biosystems, Heidelberg, Germany) equipped with a GFP filter.

3.3.2. In vivo imaging

In vivo imaging was performed on a Leica DM IRE2 inverted microscope equipped with a Leica TCS SP2 AOBS scan head and a HCX PL Apo CS 63x 1.32 NA OIL UV objective. The following settings were applied:

- GFP (green fluorescent protein):
 - excitation: 488nm (Ar/ArKr laser)
 - detection: 495 – 540nm, gain 750V
- mRFP (monomeric red fluorescent protein):
 - excitation: 561nm (He/HeNe laser)
 - detection: 570 – 630nm, gain 800V
- format: 512x512 pixel
- pixel size: 98x98nm
- z-distance: 488nm
- line averaging: 4
- pinhole: 1.5 airy units

All *in vivo* imaging experiments were done as recently presented (Rasse et al., 2005) (for an illustration of the set-up see Fig. 65). In short, early 3rd instar larvae with a standardized size of 3.0mm to 3.5mm were selected and mounted inside an airproof anaesthetization chamber between two 0.12mm coverslips, which were kept apart by a thin plastic disc with a slit in the centre. The thickness of the disc and the size of the slit were adjusted to the size of the larvae. The lower coverslip was covered with Voltalef H 10S oil (Lehman & Voss, Hamburg, Germany) to enable optimal optical access to the ventral larval body wall muscles. Finally, a metal ring was placed onto the upper coverslip to fix the animal position. To anesthetize the larvae a mixture of air and Suprane[®] containing the agent desfluran (Baxter, Unterschleißheim, Germany) was pumped into the chamber for about 10 to 12 seconds. The anesthetic freezes all internal movement, which is necessary for undisturbed imaging of the NMJ synapses. Recently it was shown, that even several rounds of anaesthetization do not interfere with further growth and function of the synaptic system (Rasse et al., 2005).

To focus on a specific NMJ (usually NMJ 27, in some cases NMJ 14), halogen light was used to identify the respective muscle. All images were taken from the abdominal segments A2-6. For FRAP (fluorescence recovery after photobleaching) experiments either the mRFP (561nm laser) or both the GFP and mRFP channel (488nm laser) were bleached until residual fluorescent signals were no longer detectable in the respective NMJ part.

After each imaging session (maximally 30 minutes) single larvae were placed inside Petri dishes containing standard fly cultivation medium and raised at 25° as before. 12 or 24 hours after the first imaging time point the same NMJs were again

subjected to confocal live imaging. Only NMJs of larvae with a net length increase of more than 10% (12h interval) or 20% (24h interval) were accepted for analysis.

3.3.3. Immunostainings

Immunostainings of embryonic or larval body-wall preparations were normally visualized with a wide field fluorescence light microscope (Axioskop 2 MOT, Zeiss, Jena, Germany) equipped with an Axiocam camera (plus Axiovision software) and either a 100x oil objective of numerical aperture 1.4 or a 40x oil objective of numerical aperture 1.3. Filters for GFP, Cy2, Cy3 and Cy5 could be switched manually. The Axioskop 2 MOT system allowed the image recording under fixed illumination conditions. Images were taken with a resolution of 2600x2060 pixels (pixel size: 34x34nm). To record z-stacks of whole NMJs confocal microscopy on a Leica NM IRE2 system was performed (see 3.3.2). Here, images were usually taken with a resolution of 2048x1024 pixels (pixel size: 98x98nm).

The images shown in Fig. 21A,B and Fig. 23E,F were produced by Qin Gang.

3.3.4. Transmission electron microscopy

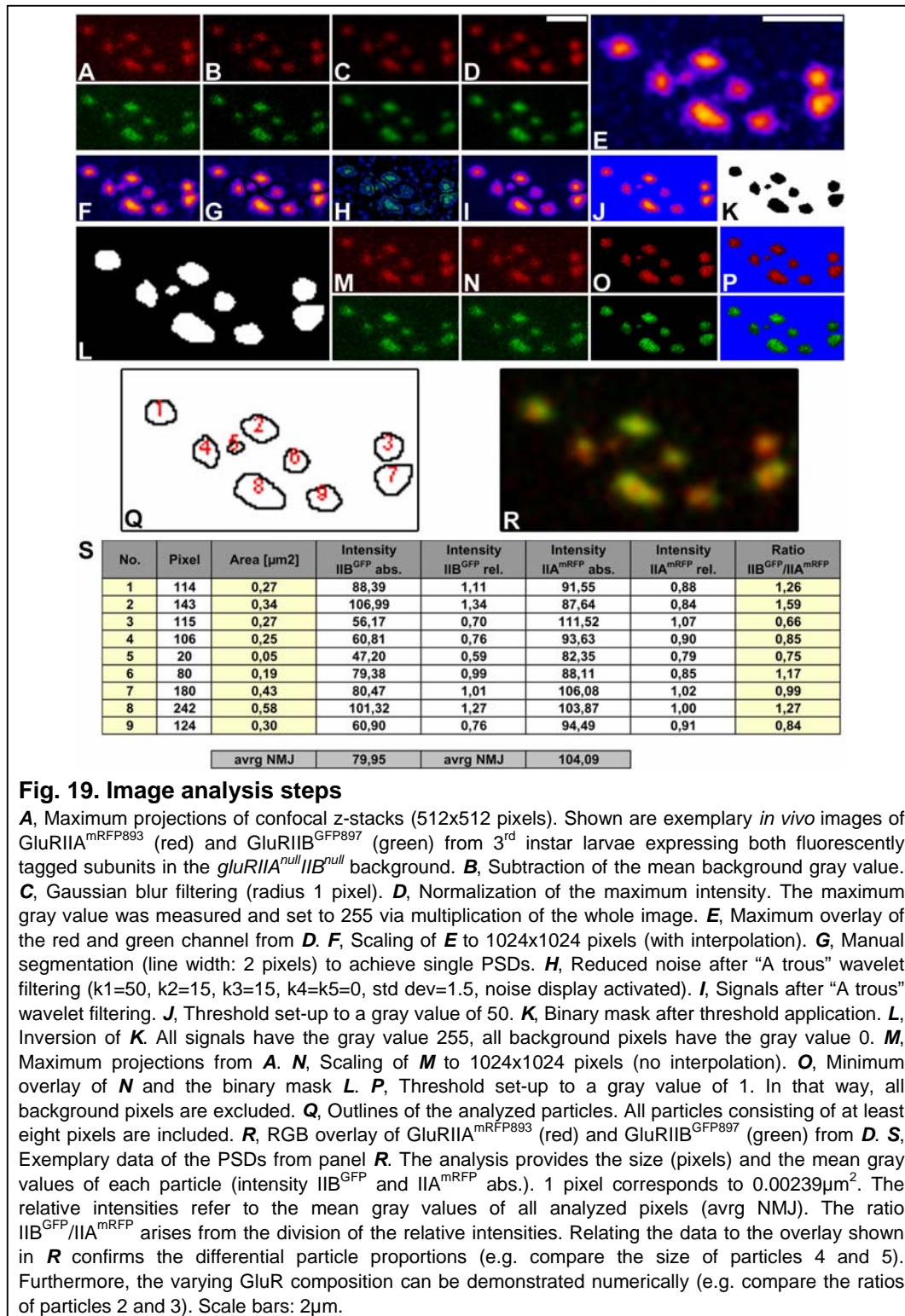
(performed by Carolin Wichmann)

Dissected preparations of 3rd instar larvae (NMJ 6/7, segment A2/A3) were primary fixed in a mixture of 4% paraformaldehyde and 0.5% glutaraldehyde in 0.1M PBS (pH 7.2) for 10' and additionally fixed 60' on ice with secondary fixative comprising 2% glutaraldehyde in 0.1M sodium cacodylate buffer (pH 7.2). Subsequently, the preparations were washed three times for 5' in sodium cacodylate buffer and post-fixed on ice for 1h with 1% osmium tetroxide (in 0.1M sodium cacodylate buffer), followed by an 1h washing step in sodium cacodylate buffer and three brief washing steps in distilled water. The samples were stained en bloc with 1% uranyl acetate in distilled water for 1h on ice. After a brief rinse with distilled water, the samples were dehydrated at room temperature in increasing ethanol concentrations, infiltrated in Epon resin (100% EtOH/Epon 1:1, 30' and 90'; 100% Epon, over night) and embedded for 24h at 85°C. The samples were trimmed, and series of 80-90nm ultra-thin sections were cut with a 35° diamond knife (Diatome, Biel, Switzerland) on a Reichert Ultracut Ultramicrotome (Leica, Nussloch, Germany) and mounted on Formvar-coated grids. The sections were stained in uranyl acetate and lead citrate. Pictures were taken with an EM 301 (Philips, Mahwah, USA) transmission electron microscope.

3.3.5. Quantitative image analysis

3.3.5.1. *In vivo* imaging – basic procedure

Quantitative image analysis was carried out manually using ImageJ (NIH, Bethesda, USA, 6.2B). All attempts to automate the image analysis with other software products proved to be unreliable.



The multi-step image processing is in detail shown and described in Fig. 19. In short, maximum z-projections of the confocal z-stacks were used to produce a binary mask. Therefore the projections were background-corrected, filtered and normalized. Next, a maximum overlay of both the GFP and mRFP channel was manually segmented to define single synaptic signals. After a further noise reduction a critical threshold was applied, resulting in the binary mask. Finally, the binary mask was superimposed (minimum overlay) with the original maximum projections and the signals were analyzed.

The following measurement parameters were therefore activated: area, mean gray value (from here on referred to as “mgv”), limit to threshold, minimum size: 8 pixel (equivalent to $0.019\mu\text{m}^2$), maximum size: not restricted, show outlines, display results, exclude edge particles.

The analysis provided data of all particles about the area and the mean gray values of both the red and green channel. The area, denoted in pixels, was converted to μm^2 while the absolute mean gray value of each channel and particle was converted to a relative intensity (referring to the mean gray value of all pixels). This allowed numerical data about the GluR composition of single PSDs, expressed by the ratio $r(n)$.

$$\boxed{\text{Int}_{GFP}(n)^{rel} = \frac{mgv_{GFP}(n) * \sum_1^n A(n)}{\sum_1^n [A(n) * mgv_{GFP}(n)]}} \quad \boxed{\text{Int}_{mRFP}(n)^{rel} = \frac{mgv_{mRFP}(n) * \sum_1^n A(n)}{\sum_1^n [A(n) * mgv_{mRFP}(n)]}}$$

- $mgv_{GFP}(n)$ mean gray value of PSD n – GFP channel
- $mgv_{mRFP}(n)$ mean gray value of PSD n – mRFP channel
- $A(n)$ area of PSD n [pixel]
- $\text{Int}_{GFP}(n)^{rel}$ relative intensity of PSD n (to NMJ mgv) – GFP channel
- $\text{Int}_{mRFP}(n)^{rel}$ relative intensity of PSD n (to NMJ mgv) – mRFP channel
- $r(n)$ ratio of relative intensities GFP/mRFP channel

$$\boxed{r(n) = \frac{\frac{mgv_{GFP}(n) * \sum_1^n A(n)}{\sum_1^n [A(n) * mgv_{GFP}(n)]}}{\frac{mgv_{mRFP}(n) * \sum_1^n A(n)}{\sum_1^n [A(n) * mgv_{mRFP}(n)]}} = \frac{mgv_{GFP}(n) * \sum_1^n [A(n) * mgv_{mRFP}(n)]}{\sum_1^n [A(n) * mgv_{GFP}(n)] * mgv_{mRFP}(n)}}$$

3.3.5.2. *In vivo* imaging – Tracing and development of single PSDs

The development of single PSDs was followed within a 12h growth interval during the 3rd instar larval stage (see 3.3.2). To start, the consecutive images of t=0h and t=12h were analyzed (according to 3.3.5.1) to obtain the pixel area, the mean gray values of both the GFP and mRFP channel and the relative intensity ratio *r* (GFP/mRFP channel) for all single PSDs.

Next, the PSDs from t=0h had to be assigned to the PSDs from t=12h. As the “Analyze Particles” option of ImageJ allocates the PSD numbers based on their *y*-position, the PSD numbering of both time points varies. Furthermore, newly formed, additional PSDs can also reform the PSD numbering. Therefore, the assignment had to be performed manually. Only PSDs which could be unambiguously identified at both time points were considered for further analysis. Cases where, e.g. two PSDs converged to one (or the other way round) due to the *z*-projection were excluded in any event.

The successful assignment made it possible to calculate the absolute and relative changes in PSD area ($\Delta A(n)$, [μm^2]), the relative intensities of the GFP and mRFP channel ($\Delta \text{Int}_{\text{GFP}}(n)^{\text{rel}}$ and $\Delta \text{Int}_{\text{mRFP}}(n)^{\text{rel}}$) and the ratio *r* ($\Delta r(n)$) of single PSDs.

3.3.5.3. *In vivo* imaging – FRAP experiments

Fluorescence recovery after photobleaching (FRAP) experiments were performed within a time window of 24h (see 3.3.2) as the fluorescence recovery of glutamate receptors is very slow (Rasse et al., 2005). The parameters area, relative intensity and ratio *r*(*n*) were again determined as outlined above (see 3.3.5.1). Importantly, the PSDs were subdivided into two groups: bleached (*bl*) and non-bleached (*non*). The FRAP of the bleached PSDs after 24h was calculated as follows identically for both the GFP and mRFP channel:

$$mgv_{bl}(0h) = \frac{\sum_1^n [A(n) * mgv(n)]}{\sum_1^n A(n)} \quad mgv_{non}(0h) = \frac{\sum_1^m [A(m) * mgv(m)]}{\sum_1^m A(m)}$$

$$mgv_{non}(24h) = \frac{\sum_1^y [A(y) * mgv(y)]}{\sum_1^n A(y)}$$

$$frap_{bl}(x, 24h) = \frac{mgv_{bl}(x, 24h)}{\frac{mgv_{non}(24h)}{mgv_{bl}(0h)}} \cdot mgv_{non}(0h)$$

- n number of PSDs within the bleached area before bleaching ($t=0h$)
- m number of PSDs within the non-bleached area before bleaching ($t=0h$)
- $mgv_{bi}(0h)$ mean gray value of all bleached PSDs before bleaching ($t=0h$)
- $mgv_{non}(0h)$ mean gray value of all non-bleached PSDs before bleaching ($t=0h$)
- $A(..)$ PSD area [pixel]
- x number of PSDs within the bleached area after recovery ($t=24h$)
- y number of PSDs within the non-bleached area after recovery ($t=24h$)
- $mgv_{bi}(x,24h)$ mean gray value of a single PSD x within the bleached area after recovery ($t=24h$)
- $mgv_{non}(24h)$ mean gray value of all non-bleached PSDs after recovery ($t=24h$)
- $frap_{bi}(x,24h)$ FRAP of a single PSD x within the bleached area after recovery ($t=24h$)

Therefore the achieved recovered intensity of the before bleached PSDs was related to the intensity of the non-bleached PSDs at the time point $t=24h$. Additionally, intensity discrepancies between the bleached and non-bleached region at $t=0h$ (before bleaching) were considered to exclude potential local differences in receptor availability.

3.3.5.4. NMJ parameters

Immunostainings of NMJs 4 or 6/7 were used for the quantitative determination of NMJ size, PSD size and PSD/synapse number. Two different protocols were used. The first measures of both protocols were identical and performed according to the steps shown in Fig. 19. To start, maximum projections of the recorded confocal z-stacks (see 3.3.3) were produced, the background was corrected, the images were filtered (Gaussian blur, radius: 2 pixels) and the maximum gray value was normalized to 255.

Protocol 1 (applied for Fig. 34G,H and Fig. 50A):

The larval NMJ size was quantified from anti-HRP (horse radish peroxidase) immunolabelings of NMJ 6/7. Thereto, a threshold of 50 was applied to the processed images and the remaining pixels were quoted and converted to μm^2 . The total PSD number shown in Fig. 34G,H was obtained from antibody (AB) stainings against GFP-tagged glutamate receptors whereas the quantification of the synapse number shown in Fig. 50A resulted from Nc82 immunostainings. In both cases, the

PSD/synapse number was counted manually with a mechanical counter. Additionally, the segment length of the respective larvae was measured on an Axioskop 2 MOT (see 3.3.3) with a scaled ocular (Zeiss, Jena, Germany) to enable animal size normalization.

Protocol 2 (applied for Fig. 23J,K):

To determine the size of single PSDs (here visualized by PAK immunostainings of NMJ 4) a manual PSD segmentation (see Fig. 19) was necessary. Subsequently, the image was filtered (A trous filter, for settings see Fig. 19) and a threshold of 50 was set. Finally, the remaining particles were counted and analyzed for their pixel number which was converted to μm^2 .

3.3.5.5. Comparison of absolute signal intensities

Wide field fluorescence microscopy (see 3.3.3) at identical stable illumination times was used for image acquisition (image dimension: 2600x2060 pixels). In each case, a cumulative intensity histogram starting from the gray value 255 was produced and the gray value of the 1000th brightest pixel was used to estimate the intensity.

3.3.5.6. Determination of intensity profiles

To quantify the distribution of FasciclinIII relative to PAK (see Fig. 23I), the intensity profile along the maximum diameter of the respective PSD was plotted (profile length, 1 μm). In each case 20 intensity profiles were put into perspective of the respective maximum absolute intensity and averaged. The FasciclinIII intensity in the PSD centre was determined with respect to the average of the two marginal, perisynaptic intensities.

3.3.5.7. Analysis of electron micrographs

Analysis of synaptic membranes visualized by electron micrographs was performed manually by classifying the pre- and postsynaptic membrane according to their electron-dense character and their linear apposition. SSR thickness was measured as previously described (Gorczyca et al., 1999) from electron micrographs of mid-bouton sections.

3.3.5.8. Statistical analysis

The nonparametric Mann-Whitney rank sum test was used for statistical analysis of all linear independent data groups. The data are reported as mean \pm s.e.m., n indicates the sample number, and p denotes the significance: * p<0.05, ** p<0.01,

*** $p < 0.001$. Linear and non-linear (Gaussian fit) regression was used to determine significant data correlation.

3.3.5.9. Software

The image analysis itself was, as mentioned above, led through with Image J (NIH, Bethesda, USA, see 6.2B). All calculations were performed with Microsoft Excel (Microsoft Corporation, Redmond, USA). Graphics and statistics were produced with Prism 4 (GraphPad Software, San Diego, USA). Image transformation and compilation was done with Adobe Acrobat and Adobe Photoshop (Adobe Systems, San Jose, USA).

3.4. Electrophysiology

3.4.1. Patch clamp recordings

(performed by Robert J. Kittel)

Mature embryos (stage 17, 20-22h AEL at 25°C) were selected for electrophysiology. All recordings were acquired at 22°C from the ventral-longitudinal muscle 6 in anterior abdominal segments A2 and A3, in the whole-cell patch clamp configuration, essentially as previously described (Broadie and Bate, 1993; Featherstone et al., 2000). Miniature EJCs were recorded in extracellular HL-3.1 saline (Feng et al., 2004), consisting of (in mM): NaCl 70, KCl 5, MgCl₂ 4, NaHCO₃ 10, trehalose 5, sucrose 115, HEPES 5, CaCl₂ 1.5, pH adjusted to 7.2. Additionally, 2µM TTX was included in the saline to block spontaneous firing of the motoneurons, as the CNS was left attached. The intracellular saline consisted of (in mM): CsCl 158, ATP-NA₂ 2, EGTA 5, HEPES 10, pH adjusted to 7.2. The preparation was viewed in transmitted light with an upright microscope (BX51WI, Olympus, Hamburg, Germany) and a 60x water-immersion lens. The patch pipettes were pulled from borosilicate glass (1.5mm outer diameter, with filament) and fire-polished to final resistances of 3-5MΩ. The input resistance of the muscle ranged from about 600MΩ to 2GΩ, and the series resistance, measured throughout the experiment, was typically between 10 and 20 MΩ. To record mEJCs, the membrane potential was clamped at -60mV. A single recording lasted for at least 3 minutes, during which the holding current never exceeded ±25pA. The signals were amplified with an Axopatch 200B (Molecular Devices, Sunnyvale, USA) patch-clamp amplifier, recorded at a sampling rate of 10kHz and low-pass filtered at 2kHz. Only events of an amplitude ≥20pA were used for subsequent analysis in Clampfit 9 (Molecular Devices, Sunnyvale, USA).

3.4.2. Intracellular recordings

(performed by Andreas Frölich and Robert J. Kittel)

Two-electrode voltage clamp (TEVC) recordings were obtained from late third instar male larvae (muscle 6, segment A2 or A3), in principle as formerly reported (Kittel et al., 2006). The composition of the extracellular hemolymph-like saline (HL-3) (Stewart et al., 1994) was (in mM): NaCl 70, KCl 5, MgCl₂ 20, NaHCO₃ 10, trehalose 5, sucrose 115, HEPES 5, CaCl₂ 1, pH adjusted to 7.2. Nerve-evoked EJC's (voltage clamp at -60 mV) were recorded with intracellular microelectrodes filled with 3M KCl to give final resistances of 12-20 MΩ.

3.5. Styryl dye labeling

FM5-95 labeling was done as previously denoted (Kuromi and Kidokoro, 2002; Rasse et al., 2005). In short, styryl dye uptake was induced by nerve stimulation with 30Hz for 5' in the presence of 20μM FM5-95 (T-23369, Molecular Probes, Eugene, USA) in normal saline. After stimulation, the preparations were washed three times with Ca²⁺-free saline (2x shortly, then 1x 15min). To destain, high-K⁺ saline was applied for 5min.

4. Results

4.1. Non-NMDA type glutamate receptors are essential for maturation but not for initial assembly of synapses at *Drosophila* NMJs

4.1.1. Formation of glutamatergic NMJ synapses deprived of postsynaptic glutamate receptors

Previous work has identified a total of five glutamate receptor subunits (Fig. 20A, scheme) within *Drosophila* muscles (GluRIIA, IIB, IIC, IID and IIE), from which two receptor complexes incorporating GluRIIC, GluRIID and GluRIIE together with either GluRIIA or GluRIIB seem to form (Fig. 20B). GluRIIA or GluRIIB containing complexes co-exist within individual synapses of the NMJ. In both *gluRIIA* or *gluRIIB* single mutants, structurally normal synapses form, meaning that either complex is *per se* dispensable for the formation of proper NMJ synapses (Petersen et al., 1997; DiAntonio et al., 1999; Marrus et al., 2004; Chen et al., 2005; Qin et al., 2005). In *gluRIIA&IIB* double mutants (*gluRIIA^{null}IIB^{null}*), however, and similarly in *gluRIIC^{null}*, *gluRIID^{null}* and *gluRIIE^{null}* single mutants, all glutamate receptor subunits are absent from the NMJ resulting in embryonic lethality (Petersen et al., 1997; Featherstone and Broadie, 2002; Marrus et al., 2004; Qin et al., 2005). However, already minimal amounts of the relevant glutamate receptors can rescue the lethality and even give rise to adult flies (Marrus and DiAntonio, 2004; Qin et al., 2005).

To start, effects of glutamate receptor deprivation were studied at the well-described larval NMJ. Here, individual synapses are considerably larger than in the embryo (Rheuben et al., 1999) and, moreover, a recent *in vivo* imaging study indicated a rate-limiting role for glutamate receptor incorporation in the formation of synapses at larval NMJs (Rasse et al., 2005). Three different situations combining a severe depression of glutamate receptor subunits still compatible with larval vitality have been described previously. When *gal4*-inducible cDNA constructs of either *gluRIIC* (Marrus and DiAntonio, 2004) or *gluRIID* (Qin et al., 2005) were brought into the corresponding single mutant background, "leaky expression" permitted larval survival in the absence of *gal4*-drivers. A strong reduction in the synaptic expression of all glutamate receptor subunits was observed for the *gluRIIC^{hypo}* (Fig. 20D) (Marrus and DiAntonio, 2004) and *gluRIID^{hypo}* (Qin et al., 2005) situation. In the third constellation, the otherwise lethal *gluRIIA^{null}IIB^{null}* situation could be rescued with a *gluRIIA* genomic transgene encoding the whole open reading frame but lacking parts of the 3'-UTR (from here on referred to as *gluRIIA^{hypo}*), resulting in less than 5% of wild type GluRIIA mRNA levels and certainly no GluRIIB (Qin et al., 2005). Some PSDs obviously still showed normal size and glutamate receptor intensity at *gluRIIC^{hypo}* NMJs (Fig. 20D, arrow) (Marrus and DiAntonio, 2004). However, at larval NMJs of

gluRIIA^{hypo} no such PSDs could be observed (Fig. 20E). In fact, only when using atypically long exposure times very faint residual accumulations of GluRIIA and GluRIIC could be visualized (Fig. 20F). Thus, because of their extreme and consistent reduction of glutamate receptors, *gluRIIA^{hypo}* larvae were used to study the formation of glutamatergic synapses largely deprived of glutamate receptors.

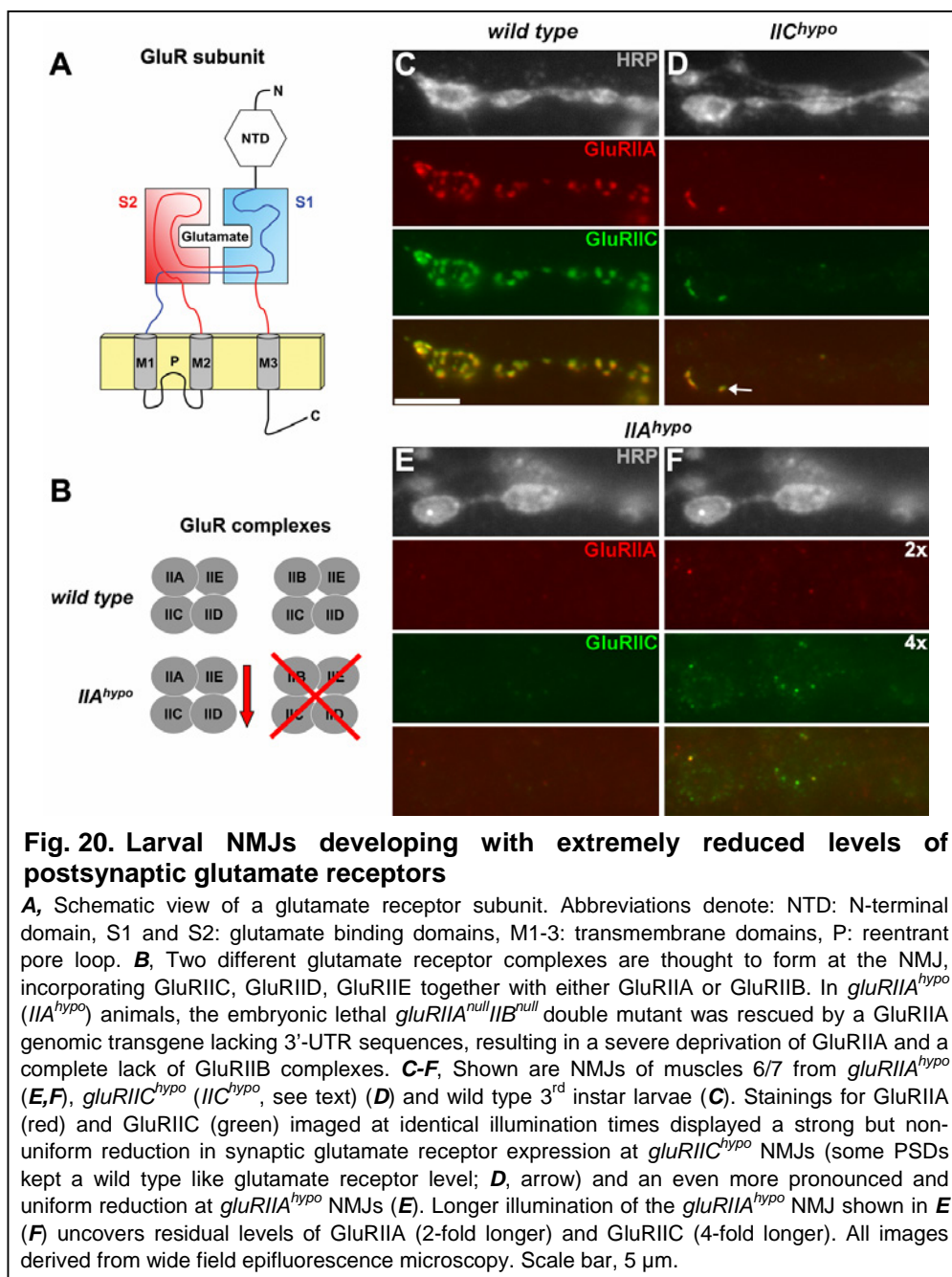
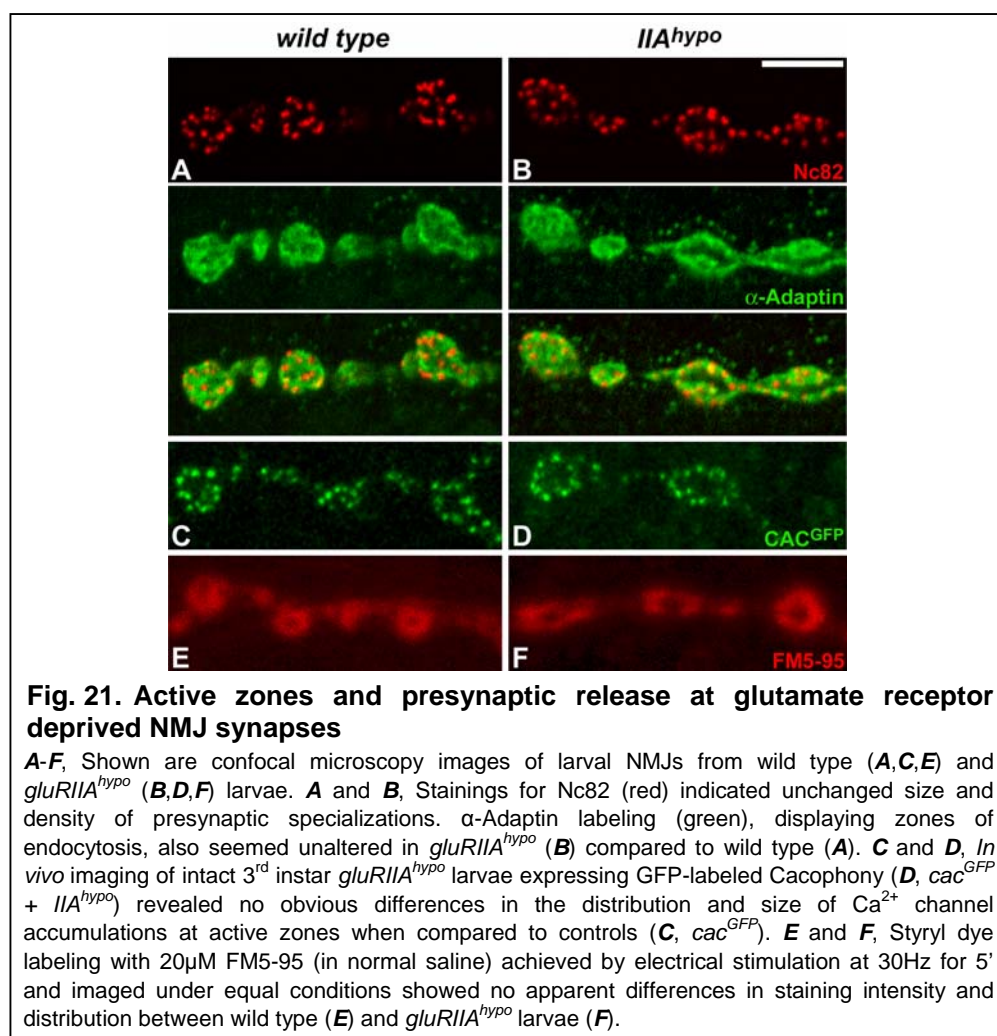


Fig. 20. Larval NMJs developing with extremely reduced levels of postsynaptic glutamate receptors

A, Schematic view of a glutamate receptor subunit. Abbreviations denote: NTD: N-terminal domain, S1 and S2: glutamate binding domains, M1-3: transmembrane domains, P: reentrant pore loop. **B**, Two different glutamate receptor complexes are thought to form at the NMJ, incorporating GluRIIC, GluRIID, GluRIIE together with either GluRIIA or GluRIIB. In *gluRIIA^{hypo}* (*IIA^{hypo}*) animals, the embryonic lethal *gluRIIA^{null} IIB^{null}* double mutant was rescued by a GluRIIA genomic transgene lacking 3'-UTR sequences, resulting in a severe deprivation of GluRIIA and a complete lack of GluRIIB complexes. **C-F**, Shown are NMJs of muscles 6/7 from *gluRIIA^{hypo}* (**E,F**), *gluRIIC^{hypo}* (*IIC^{hypo}*, see text) (**D**) and wild type 3rd instar larvae (**C**). Stainings for GluRIIA (red) and GluRIIC (green) imaged at identical illumination times displayed a strong but non-uniform reduction in synaptic glutamate receptor expression at *gluRIIC^{hypo}* NMJs (some PSDs kept a wild type like glutamate receptor level; **D**, arrow) and an even more pronounced and uniform reduction at *gluRIIA^{hypo}* NMJs (**E**). Longer illumination of the *gluRIIA^{hypo}* NMJ shown in **E** (**F**) uncovers residual levels of GluRIIA (2-fold longer) and GluRIIC (4-fold longer). All images derived from wide field epifluorescence microscopy. Scale bar, 5 μ m.

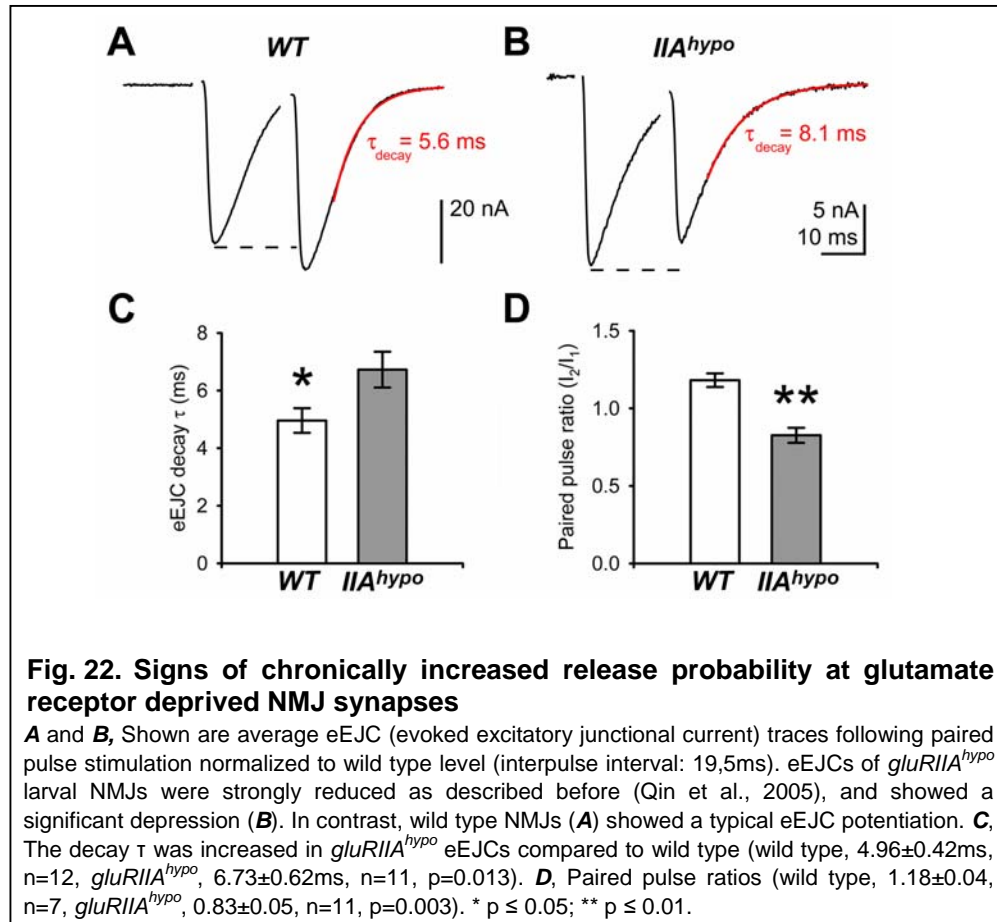
4.1.2. Presynaptic release sites are functionally and structurally maintained at glutamate receptor deprived NMJ synapses

NMJ synapses developing in the near absence of glutamate receptors were further investigated by using molecular markers. The active zone (AZ) is a specialized presynaptic region, where synaptic vesicles dock, fuse, and release their neurotransmitters (Zhai and Bellen, 2004). In *Drosophila*, AZs are associated with electron-dense specializations (T-bars) (Atwood et al., 1993; Zhai and Bellen, 2004). The monoclonal antibody Nc82 was shown to label the AZs of *Drosophila* synapses (Wucherpfennig et al., 2003) by recognizing the Bruchpilot protein (BRP), which is essential for T-bar formation (Atwood, 2006; Kittel et al., 2006; Wagh et al., 2006).



At *gluRIIA^{hypo}* synapses, the density and size of synaptic clusters of both Nc82 (Fig. 21B) and Ca²⁺-channels (Fig. 21D) appeared unaffected when compared to wild type controls (Fig. 21A,C). Thus, consistent with the presence of T-bars (see below in Fig. 24), AZ structures seemed to establish normally at *gluRIIA^{hypo}* synapses. AZs are

also surrounded by zones of endocytosis, which can be labeled in α -Adaptin stainings (Dornan et al., 1997). The distribution of α -Adaptin appeared unchanged as well (Fig. 21B). Thus, in contrast to the PSD (see below in Fig. 23 and Fig. 24), the molecular and structural composition of the presynaptic AZs seemed unaffected.



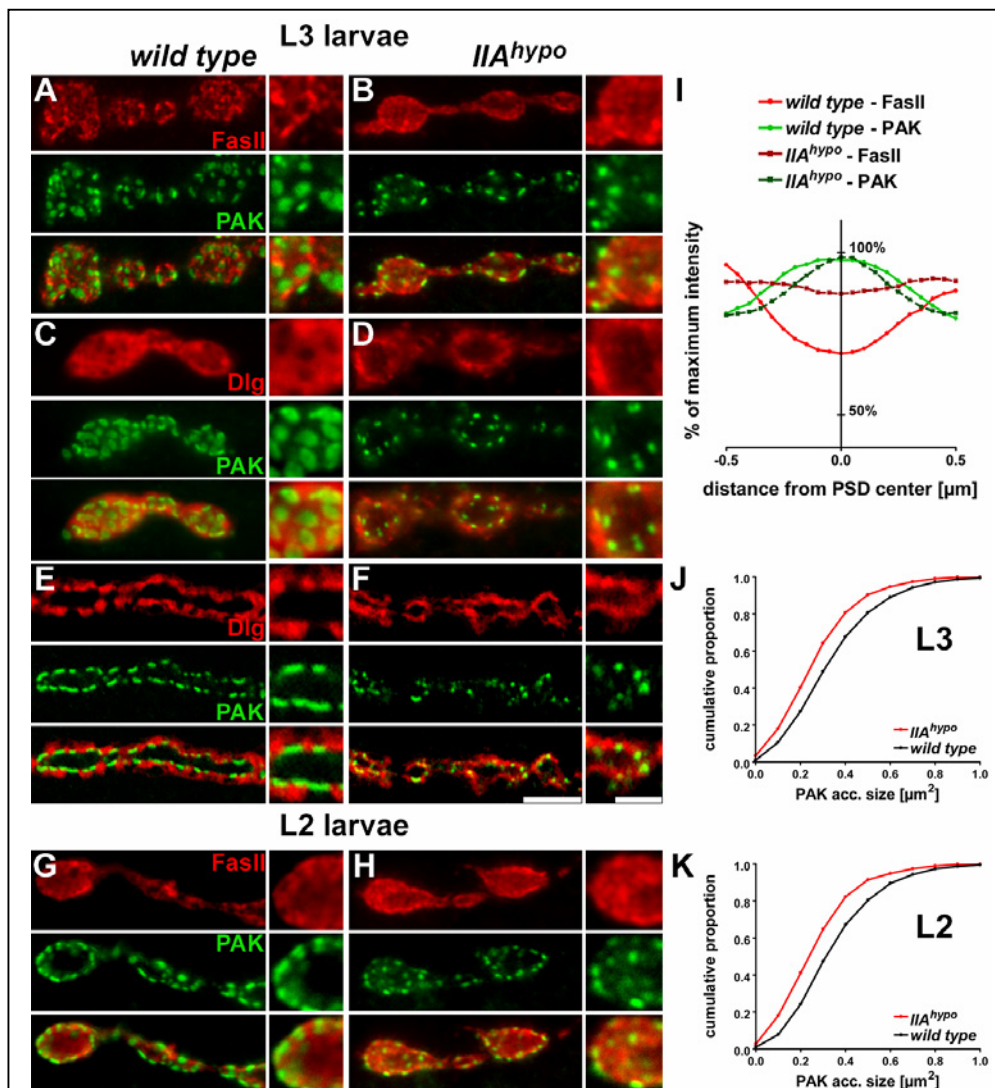
Are these AZs still functional? It could be observed that *gluRIIA^{hypo}* larvae were only moderately limited in mobility. Moreover, styryl dye (FM5-95) incorporation after high frequency stimulation (Kuromi and Kidokoro, 2002; Wucherpfennig et al., 2003) showed that vesicle release persisted at *gluRIIA^{hypo}* NMJs (Fig. 21F). In a previous electrophysiological analysis it was shown that nerve evoked EJCs at *gluRIIA^{hypo}* NMJs are reduced to about 30% of the wild type level. Notably, in this genotype miniature EJCs, indicating the postsynaptic glutamate sensitivity at individual synapses, were below the detection threshold, which can be estimated to be at about 20% of the wild type amplitude (Qin et al., 2005). Thus, following an action potential the number of presynaptically released vesicles is likely increased as part of a presynaptic compensation for reduced postsynaptic sensitivity (Petersen et al., 1997; Reiff et al., 2002). In fact, paired pulse stimulation at these junctions led to an atypical depression as would be expected for a synaptic system with a chronic

increase in presynaptic release probability (Fig. 22A,B; wild type, 1.18 ± 0.04 , $n=7$, *gluRIIA^{hypo}*, 0.83 ± 0.05 , $n=11$, $p=0.003$). In addition, the decay time constant (τ) of evoked responses was increased (Fig. 22A,B; wild type, 4.96 ± 0.42 ms, $n=12$, *gluRIIA^{hypo}*, 6.73 ± 0.62 ms, $n=11$, $p=0.013$), potentially pointing towards changes in glutamate clearance or atypical functional properties of the glutamate receptors remaining at these synapses. The rise time of evoked junctional currents was not significantly altered (wild type, 1.08 ± 0.05 ms, $n=12$, *gluRIIA^{hypo}*, 1.17 ± 0.08 ms, $n=11$, $p=0.498$). In summary, AZs still formed at the presynaptic site of NMJ synapses deprived of glutamate receptors. These AZs appeared fully active in vesicle release, and likely vesicle release is even increased to compensate for the drastically reduced postsynaptic glutamate sensitivity. Such a compensation was described before for *gluRIIA* mutants, which notably show a less drastic drop in postsynaptic glutamate sensitivity (Petersen et al., 1997).

4.1.3. Early stop of postsynaptic maturation at glutamate receptor deprived NMJ synapses

Next, postsynaptic assembly at glutamate receptor deprived synapses was examined. The PAK kinase forms a complex with PIX and Rac, involved in aspects of PSD assembly (Albin and Davis, 2004). PAK widely serves as a PSD marker at NMJ synapses and strictly co-localizes with the glutamate receptor subunit GluRIIA (Rasse et al., 2005). The size of PAK signals at individual PSDs seemed strongly reduced in *gluRIIA^{hypo}* animals (e.g. compare Fig. 23C to D). In fact, quantification of *gluRIIA^{hypo}* NMJs of mature 3rd instar larvae showed a significant reduction in the size of PAK signals (Fig. 23J; wild type, $0.385 \pm 0.005 \mu\text{m}^2$, $n=1709$, 6 NMJs, *gluRIIA^{hypo}*, $0.311 \pm 0.006 \mu\text{m}^2$, $n=1014$, 7 NMJs, $p<0.0001$), while the density of PSDs (identified as PAK spots) over the NMJ surface appeared unchanged.

In principle, the observed molecular defects in postsynaptic assembly might not reflect a genuine inability to form mature PSDs but instead a deficit in maintenance of matured PSDs (and thus “defective synapses” would have accumulated until late larval development as predominantly analyzed in this study). However, also earlier during development, in 1st (not shown) and 2nd instar *gluRIIA^{hypo}* larvae, synaptic PAK signals were identically reduced (Fig. 23H,K; quantification for 2nd instar: wild type, $0.358 \pm 0.007 \mu\text{m}^2$, $n=699$, 6 NMJs, *gluRIIA^{hypo}*, $0.280 \pm 0.006 \mu\text{m}^2$, $n=622$, 6 NMJs, $p<0.0001$).



Reduced synaptic PAK signals pointed towards defects in the molecular and/or structural assembly of the PSD region of synapses lacking glutamate receptors. FasciclinII (FasII), an NCAM-related cell adhesion molecule, and Disc Large (Dlg), founding member of the PSD-95-type MAGUK family take part in growth and maturation of the NMJ structure and interact molecularly (Schuster et al., 1996; Thomas et al., 1997; Zito et al., 1997). At wild type NMJs, FasII and Dlg are highly enriched at the “perisynaptic” muscle membrane but are clearly reduced at the actual postsynaptic membrane (Fig. 23A,C,G). In *gluRIIA^{hypo}* larvae, however, FasII and Dlg did not appear reduced at postsynaptic membranes (Fig. 23B,D,H). In fact, quantification of FasII (Fig. 23I) demonstrated a distinct reduction of FasII staining intensity at postsynaptic sites (identified by PAK labeling, also note the decreased PAK spot size in *gluRIIA^{hypo}*) for wild type but a flat distribution at *gluRIIA^{hypo}* synapses (for numbers and details see figure legend).

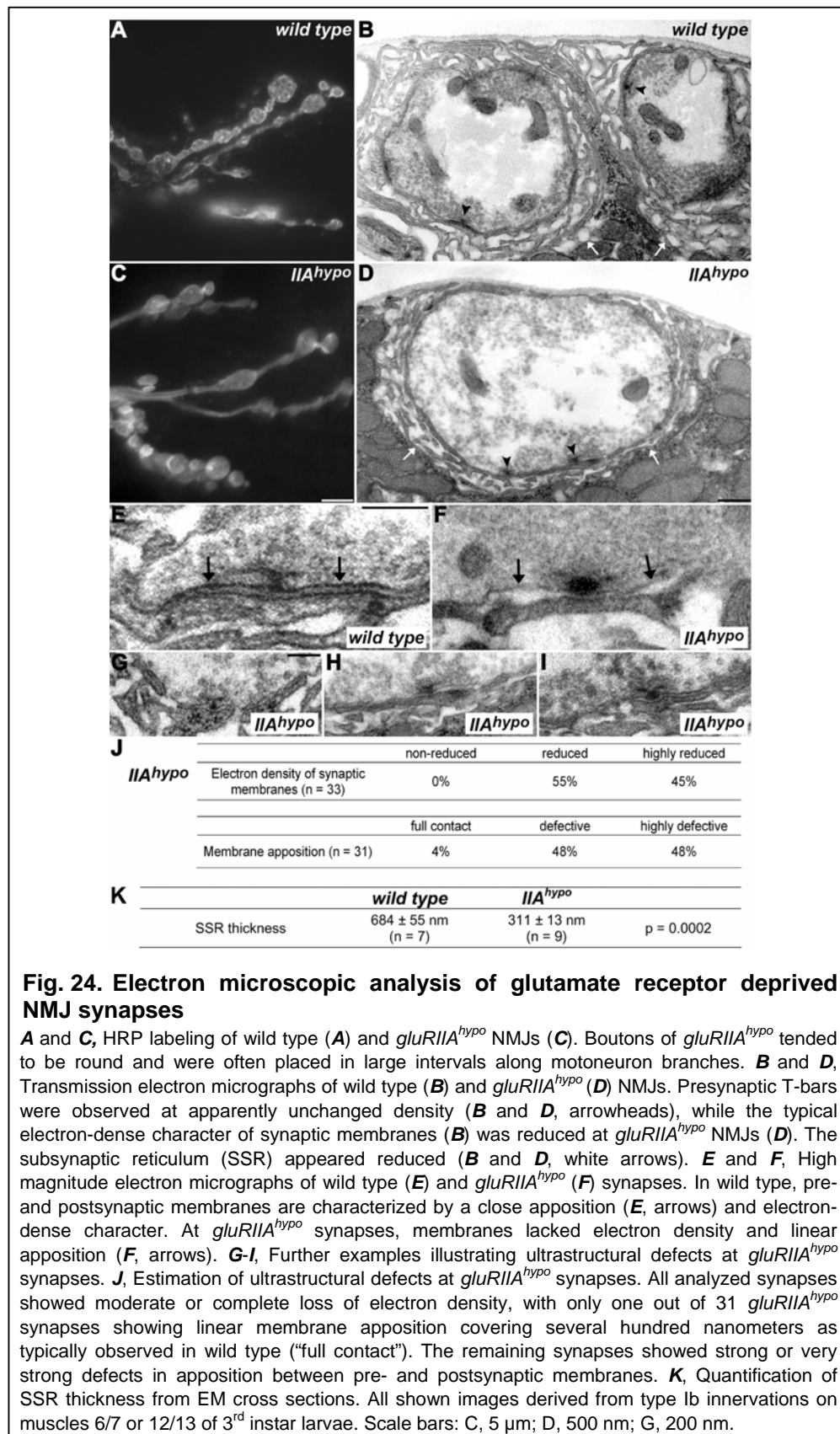
Hence, perisynaptic proteins such as the membrane protein FasII and the membrane-associated Dlg are now present in a membrane compartment normally destined to become postsynaptic membrane. It can be concluded that a lack of glutamate receptors interferes with the maturation of postsynaptic sites, and the molecular composition of these postsynaptic assemblies seemed to remain in an immature, nascent state.

4.1.4. Ultrastructural analysis: lack of apposition between pre- and postsynaptic membranes at NMJ synapses deprived of glutamate receptors

Defects in NMJ morphology became obvious in immunolabelings of *gluRIIA^{hypo}* NMJs (Fig. 24C). Both, the number of boutons as well as the number of synapses per NMJ were reduced at *gluRIIA^{hypo}* NMJs (3rd instar, NMJ 4, Ib innervation; bouton number: wild type, 26.7 ± 2.5 , $n=6$, *gluRIIA^{hypo}*, 13.3 ± 1.9 , $n=7$, $p=0.0047$; synapse number: wild type, 285 ± 16 , $n=6$, *gluRIIA^{hypo}*, 153 ± 17 , $n=7$, $p=0.0023$). In addition, boutons often appeared abnormally round (Fig. 24C) and no longer polygonal as typically observed in wild type (Fig. 24A).

To further analyze how far postsynaptic differentiation was affected by the lack of glutamate receptors, NMJs of mature *gluRIIA^{hypo}* larvae were subjected to transmission electron microscopy (EM). Within NMJ terminals, synaptic vesicles and typical organelles such as mitochondria seemed unaffected. Moreover, presynaptic T-bars were found at apparently normal frequency (per mid-bouton section: wild type, 0.88 ± 0.13 , $n=8$, *gluRIIA^{hypo}*, 0.89 ± 0.26 , $n=9$, $p=0.96$), consistent with the

preservation of AZ function (see above). T-bars also enabled an unambiguous localization of synaptic sites within electron micrographs.



Notably, the glutamate receptor deprived synapses showed severe defects in membrane organization. Normally, pre- and postsynaptic membranes are more electron-dense than neighboring extrasynaptic membranes, and show a flat and linear apposition, easily visualized in EM cross sections (Fig. 24E, arrows). This membrane apposition at mature synapses typically covers a few hundred nanometers, far exceeding the diameter of the attached T-bar (Fig. 24E). At *gluRIIA^{hypo}* NMJ synapses, however, pre- and postsynaptic membranes showed either no or only reduced electron density (Fig. 24D,F-J). Most notably, the area of close apposition between pre- and postsynaptic membrane was clearly reduced or sometimes totally absent at *gluRIIA^{hypo}* NMJ synapses (Fig. 24G-J and F, arrows). Instead, the membranes normally destined to show synapse-specific organization were of typical “perisynaptic” organization, which is characterized by the “subs synaptic reticulum” (SSR) that forms by pronounced infolding of the muscle membrane only focally contacting the presynaptic neuronal plasma membrane (Gorczyca et al., 1999). Consistent with the decreased diameter of the DLg positive area surrounding boutons (Fig. 23H), the SSR was reduced in *gluRIIA^{hypo}* larvae (compare Fig. 24B and D, white arrows; Fig. 24K, SSR thickness, type Ib boutons: wild type, 684±55nm, n=7, *gluRIIA^{hypo}*, 311±13nm, n=9, p=0.0047).

Taken together, it can be concluded that glutamate receptors are directly or indirectly needed to confer proper molecular composition to synaptic membranes. In result, the mature apposition between pre- and postsynaptic membranes normally extending over a few hundred nanometers, and likely acting as a prerequisite for properly timed neurotransmission, could no longer be observed.

4.1.5. Initial molecular assembly of PSDs independent of glutamate receptors

Above it was shown, that despite dramatic glutamate receptor deprivation a residual postsynaptic assembly of NMJ synapses demonstrated by PAK localization still took place in *gluRIIA^{hypo}* larvae. At NMJs of *gluRIIA^{hypo}* embryos, glutamate receptors were not detectable (Fig. 25C), and indistinguishable from *gluRIIA^{null}IIB^{null}* NMJs in stainings (Fig. 25B). Nevertheless, as shown above, traces of residual glutamate receptor levels could be observed at larval NMJs of *gluRIIA^{hypo}* animals (Fig. 20E,F). In principle, these minimal glutamate receptor levels could be sufficient to establish the observed residual postsynaptic assembly, which in turn could suggest a role of glutamate receptors in initial PSD formation. To address this question, PAK localization was studied at embryonic synapses fully lacking glutamate receptors (stage 17, 20-22h AEL). However, at both *gluRIIC^{null}* (Fig. 25E) as well as

gluRIIA^{null}IIIB^{null} (Fig. 25F) NMJs, PAK still accumulated opposite presynaptic active zones, identified via Nc82 labeling, similar to wild type synapses (Fig. 25D). Similarly, PAK also accumulated at NMJs of *gluRIIA^{hypo}* embryos (Fig. 25G). Thus, initial molecular assembly at prospective PSD regions still seemed possible in the absence of postsynaptic glutamate receptor complexes.

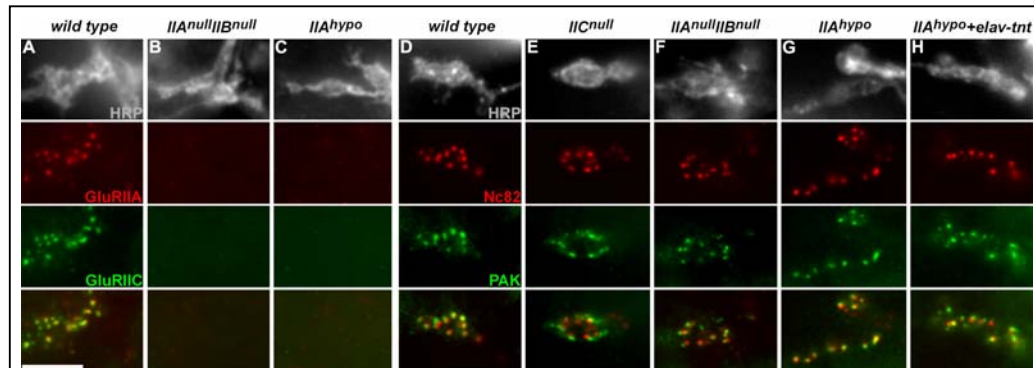


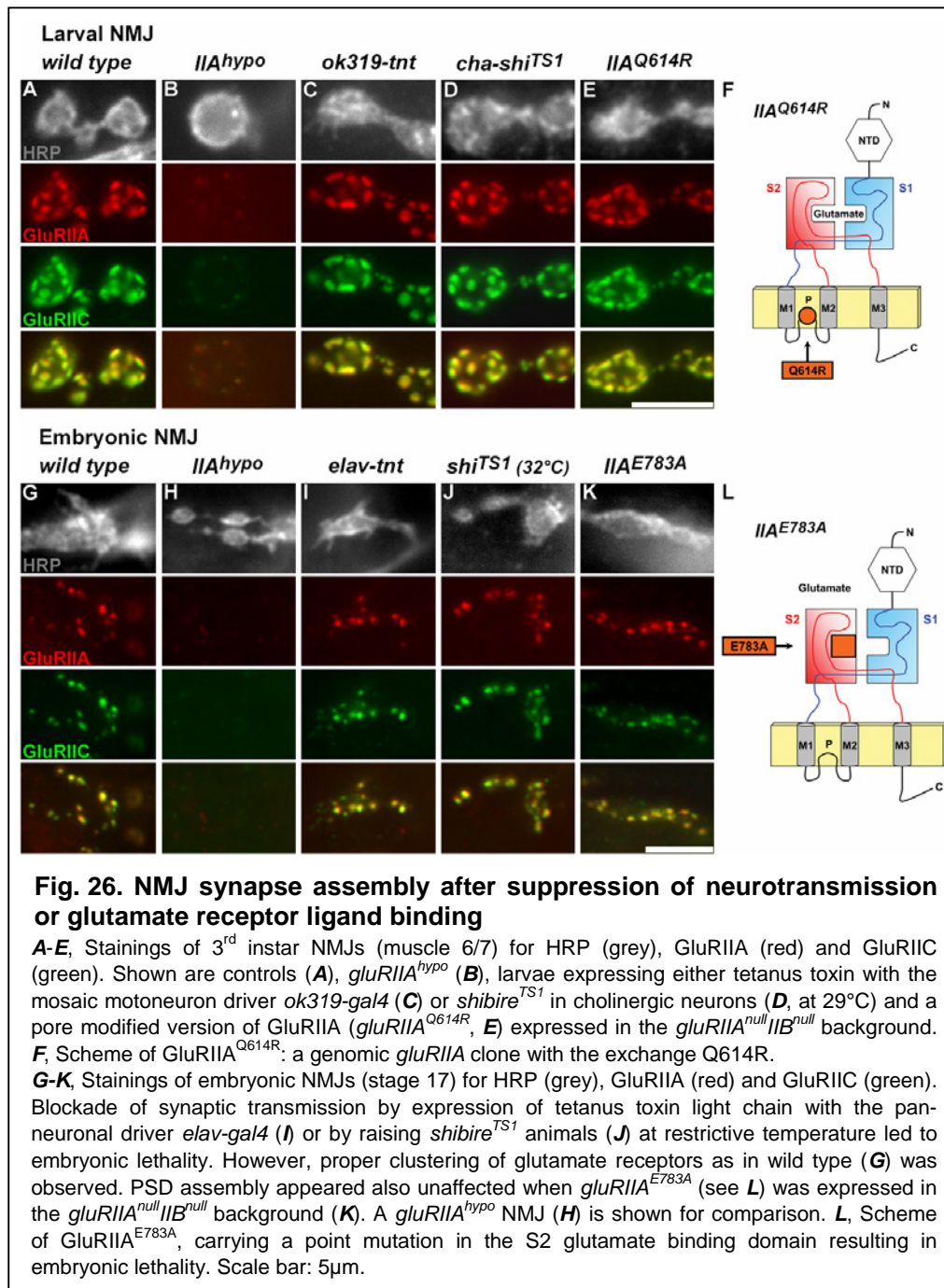
Fig. 25. Synapse assembly at embryonic NMJs lacking all glutamate receptors

A-C, Embryonic *Drosophila* NMJs (stage 17) stained for HRP (grey), GluRIIA (red) and GluRIIC (green). Wild type (**A**) NMJs showed synaptic expression of GluRIIA and GluRIIC while, as expected, glutamate receptors were absent from NMJs of *gluRIIA^{null}IIIB^{null}* embryos (**B**). In *gluRIIA^{hypo}* embryos (**C**), glutamate receptors were below detection limit as well. **D-H**, Despite the absence of glutamate receptors, embryonic NMJs of *gluRIIC^{null}* (**E**) and *gluRIIA^{null}IIIB^{null}* (**F**) animals still showed accumulations of the PSD marker PAK (green) opposite presynaptic release sites labeled with Nc82 (red) similar as in wild type (**D**). PAK also accumulated at *gluRIIA^{hypo}* NMJ synapses with (**H**) or without (**G**) a concomitant block of presynaptic activity through pan-neuronal expression of tetanus-toxin (*elav-tnt*). Scale bar: 5µm.

4.1.6. Neurotransmission and glutamate-triggered ionic conductance are dispensable for NMJ synapse maturation and growth

So far, it was shown that glutamate receptors are specifically needed to allow the maturation of the synaptic membrane organization. The question arose, whether the defects at synapses lacking glutamate receptors are mediated by the loss of synaptic transmission, resulting from the absence of glutamate receptors. To check whether a lack of synaptic transmission could in fact be responsible, several independent experimental strategies to block synaptic transmission were chosen. In larvae, tetanus toxin light chain (TNT) was expressed using the mosaic motoneuron driver line *ok319-gal4* (Sweeney et al., 1995). Such larvae appeared paralyzed, while in comparison locomotion defects in *gluRIIA^{hypo}* larvae were only moderate. However, NMJ synapses of these tetanus toxin expressing larvae had fully developed postsynaptic receptor fields (Fig. 26C). In addition, transgenic expression of temperature-sensitive, dominant-negative Dynamin (UAS-*shibire^{TS1}*) at 29°C with the *cha-gal4* driver was used to silence the cholinergic neurons “upstream” of motoneurons (Salvaterra and Kitamoto, 2001). This led to a severe paralysis of

larvae, while again mature PSDs formed (Fig. 26D). Taken together, a severe blockade of NMJ transmission did not interfere with postsynaptic assembly.



It could be argued that when tetanus toxin expression was driven by *ok319-gal4*, suppression of presynaptic release was not complete, as indicated by larval survival. Thus, it cannot be excluded that in particular residual miniature events might be present (Sweeney et al., 1995). In principle, small residual levels of spontaneous activity, as likely present in the tetanus toxin expressing larvae, might already be sufficient to allow postsynaptic assembly. In fact, miniature activity has been

implicated in the formation of postsynaptic receptor fields in the embryo (Saitoe et al., 2002). However, this finding was discussed controversially (Featherstone and Broadie, 2002; Verstreken and Bellen, 2002). Complete suppression of synaptic release at the NMJ leads to late embryonic lethality in *Drosophila*. Thus, the consequence of completely suppressing all synaptic transmission including miniature responses at the embryonic NMJ was studied. To this end, a dominant negative allele of Dynamin (*shibire*^{TS1}) which blocks both evoked as well as spontaneous synaptic transmission at restrictive temperature (Koenig et al., 1983) was used. Thereto, after 12-14h (AEL) at 25°C, embryos were transferred to 32°C 8-10h before dissection. PSDs (as judged by GluRIIA/GluRIIC co-staining) formed apparently normally in *shibire*^{TS1} mutants at restrictive temperature (Fig. 26J). The same result was obtained in embryos expressing tetanus toxin under control of the strong pan-neuronal driver *elav-gal4* (Fig. 26I). Taken together, apparently neither evoked nor spontaneous miniature responses were needed to allow normal postsynaptic assembly. Thus, it appeared unlikely that a general lack of postsynaptic conductance could underlie the postsynaptic defects at glutamate receptor deprived NMJs. In fact, PAK accumulation at PSDs was even possible when a receptor deprived situation (*gluRIIA*^{hypo}) was combined with a concomitant block of activity mediated by tetanus toxin (Fig. 25H).

It can be concluded that ionic conductance through postsynaptic glutamate receptors associated with neurotransmission did not appear to be a prerequisite for synapse assembly. Several studies have measured glutamate in the *Drosophila* hemolymph (Echalier, 1997). Thus, glutamate receptor conductance in response to such extracellular glutamate, not associated with vesicular release, could *per se* be implicated in synapse formation. However, genetic constellations meant to increase hemolymph glutamate levels were shown to decrease the size of postsynaptic glutamate receptor fields (Featherstone et al., 2002), arguing against a PSD stabilizing role of such conductances in response to extracellular glutamate. Nonetheless, the role of glutamate mediated receptor conductance was directly addressed. First, a pore-modified *gluRIIA* genomic transgene (*gluRIIA*^{Q614R}; Fig. 26F), changing the pore from MQQ to MRQ (for AA alignment see Fig. 61) (Jonas and Burnashev, 1995; Kask et al., 1998; DiAntonio et al., 1999; Aronoff et al., 2004) was engineered. This rescued the *gluRIIA*^{null}*IIB*^{null} situation and allowed the formation of apparently normal receptor fields at larval NMJs (Fig. 26E). A “complete block” of NMJ transmission, however, should result in embryonic lethality, arguing that *gluRIIA*^{Q614R} does still allow some ionic conductance when incorporated into the glutamate receptor complex (DiAntonio et al., 1999).

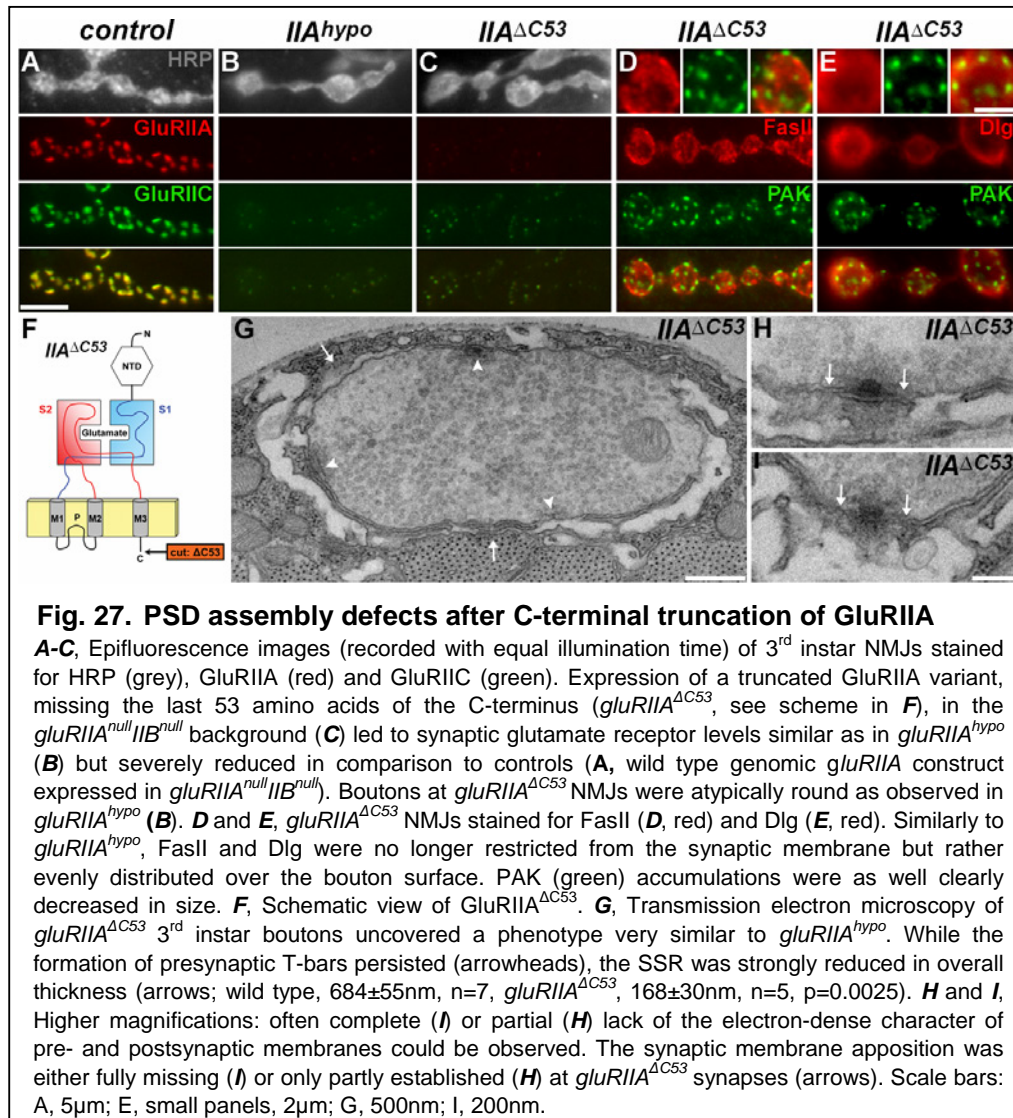
In fact, embryonic rescue of the *gluRIIA^{null}IIB^{null}* situation was no longer possible with a GluRIIA mutated in the glutamate binding pocket (*gluRIIA^{E783A}*, Fig. 26L; for AA alignment see Fig. 60) (Grunwald and Kaplan, 2003). However, at these embryonic *gluRIIA^{E783A}* NMJs wild type like patches of the glutamate receptor subunits GluRIIA and GluRIIC formed at apparently normal density (Fig. 26K). Consistently, PAK kinase and presynaptic BRP also clustered normally at these synapses (not shown), which should be most severely deprived of glutamate-triggered ionic conductance (also given that *gluRIIA^{hypo}* embryos survive despite the absence of detectable spontaneous responses). In result, a lack of glutamate receptor mediated ionic conductance is most unlikely to be responsible for the PSD defects observed at NMJ synapses lacking glutamate receptors. Instead, glutamate receptors might well be involved in postsynaptic assembly via protein-protein interactions.

4.1.7. C-terminal truncation of GluRIIA mimics the receptor deprivation defects

To determine parts of the glutamate receptor proteins involved in synapse assembly and maturation, *gluRIIA* was deleted from its C-terminus. A truncated genomic transgene (*gluRIIA^{ΔC53}*; Fig. 27F), missing the last 53 amino acids of the C-terminus, but not the 3'-UTR, was expressed in the *gluRIIA^{null}IIB^{null}* background. The rescue capability of *gluRIIA^{ΔC53}* was lower than observed for *gluRIIA^{hypo}* (24% and 43% of expected Mendelian rate of adult flies, respectively). Similar as found in *gluRIIA^{hypo}* (Fig. 27B), glutamate receptors at *gluRIIA^{ΔC53}* PSDs (Fig. 27C) were hardly detectable and drastically reduced (different from *gluRIIA^{hypo}* with only less than 5% of GluRIIA mRNA level left, the GluRIIA mRNA level of *gluRIIA^{ΔC53}* was not decreased, not shown). Alongside the reduction in synaptic glutamate receptors, NMJ morphology was clearly defective as well, harboring atypically round boutons (Fig. 27C). PSDs, visualized by labeling PAK, appeared decreased in size. As in *gluRIIA^{hypo}*, the perisynaptically expressed proteins FasII andDlg were essentially evenly distributed over the bouton surface (Fig. 27D,E). Transmission electron micrographs showed a drastic drop in the overall thickness of the SSR (Fig. 27G, arrows; wild type, 684±55nm, n=7, *gluRIIA^{ΔC53}*, 168±30nm, n=5, p=0.0025) and the number of membrane stacks appeared reduced. Importantly, membrane apposition in the synaptic region was only partly established or completely missing, and both pre- and postsynaptic membranes lacked electron-dense character (Fig. 27H,I). As for *gluRIIA^{hypo}*, presynaptic elements seemed unaffected (Fig. 27G).

In summary, the *gluRIIA^{ΔC53}* phenotype was very similar to the defects observed for *gluRIIA^{hypo}* (while even somewhat stronger). These data are consistent with the

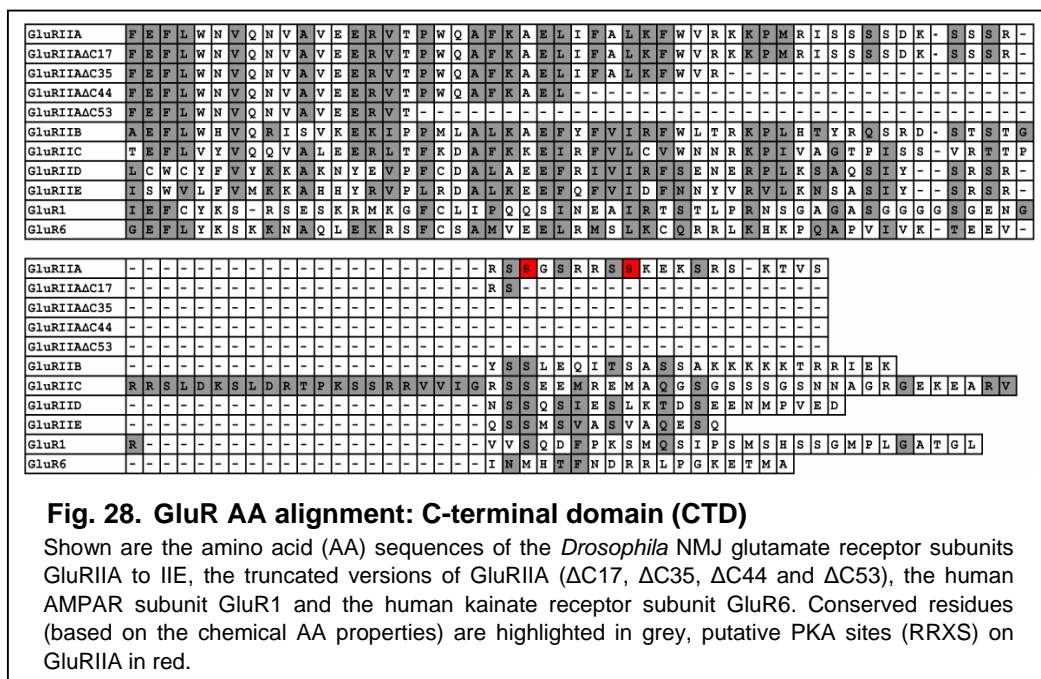
concept that a lack of interactions with other PSD components mediated by the intracellular C-terminus interferes with PSD assembly. However, lack of a C-terminal sequence could *per se* also affect initial transport and/or assembly of glutamate receptor complexes. In any case, this experiment independently shows that a lack of glutamate receptors interferes with the PSD assembly process.



4.1.8. Postsynaptic assembly seems to require intracellular sequence elements common to GluRIIA, IIB and IIC

As shown above, the C-terminal deletion *gluRIIA*^{ΔC53} mimicked the *gluRIIA*^{hypo} phenotype. The question remained, which parts of the truncated C-terminal region would be involved in postsynaptic assembly. Therefore, besides *gluRIIA*^{ΔC53}, three further genomic transgenes of *gluRIIA* missing the last 17, 35 and 44 amino acids (AAs) were expressed in the *gluRIIA*^{null}*IIB*^{null} background (Fig. 28; *gluRIIA*^{ΔC17},

gluRIIA^{ΔC35} and *gluRIIA*^{ΔC44}, respectively). The PSD status was then investigated by glutamate receptor and PAK labeling (Table 3). In *gluRIIA*^{ΔC17}, PSDs did not appear smaller than normal, while in *gluRIIA*^{ΔC35} PSD size and glutamate receptor expression level were reduced. *gluRIIA*^{ΔC44} and similarly *gluRIIA*^{ΔC53} (Fig. 27) showed most severe postsynaptic defects. As mentioned, two glutamate receptor complexes containing either GluRIIA or GluRIIB are co-expressed within individual PSDs of larval NMJ synapses. Absence of both complexes provokes embryonic lethality due to a loss of NMJ transmission (Marrus et al., 2004). Importantly, however, either of both complexes rescues the lethality, resulting in structurally normal PSDs (Petersen et al., 1997; DiAntonio et al., 1999). If protein interactions of the glutamate receptors were instructive, sequences common to both glutamate receptor complexes might well mediate the interactions relevant for PSD assembly.



In fact, it was observed that the region defined as functionally important by the GluRIIA deletion series shows a high sequence similarity to GluRIIB and IIC, but less so to GluRIID and IIE (Fig. 28). Moreover, when the C-terminus of GluRIIB or GluRIIC was placed on GluRIIA, these chimeras rescued the lethality of *gluRIIA*^{null}*IIB*^{null} double mutants and allowed the formation of proper PSDs. Similarly, GluRIIB with its C-terminus exchanged for the one of GluRIIA (GluRIIB^{IIA} C-term) rescued *gluRIIA*^{null}*IIB*^{null} and resulted in normal PSDs as judged by glutamate receptor or PAK signal. Moreover, GluRIIC^{IIA} C-term rescued the lethality of the *gluRIIC* mutant (Marrus et al., 2004), giving rise to apparently normal PSDs. Thus, within the group of GluRIIA, IIB and IIC, which are closest neighbors in terms of similarity (Qin

et al., 2005), C-termini were exchangeable without affecting the PSD assembly function of these subunits (Table 3). Furthermore, chimera of GluRIIA with GluRIID and GluRIIE, the other group of obligatory subunits of the muscle glutamate receptor complexes, which are only very distantly related to GluRIIA-IIC (Qin et al., 2005), were produced. Both C-terminal exchanges did not allow genetic rescue (Table 3). These results are thus consistent with the idea that protein interactions of the C-termini of the GluRIIA-IIC group to other PSD proteins might be essential for PSD assembly.

	Rescue activity	GluR level	PSD size
<i>gluRIIA</i>	<i>IIA^{null}B^{null}</i>	+	+
<i>gluRIIA^{hypo}</i>	<i>IIA^{null}B^{null}</i>	-	--
<i>gluRIIA^{ΔC17}</i>	<i>IIA^{null}B^{null}</i>	+	+
<i>gluRIIA^{ΔC35}</i>	<i>IIA^{null}B^{null}</i>	-	-
<i>gluRIIA^{ΔC44}</i>	<i>IIA^{null}B^{null}</i>	--	--
<i>gluRIIA^{ΔC53}</i>	<i>IIA^{null}B^{null}</i>	--	--
<i>gluRIIA^{IIB C-term} (AAB)</i>	<i>IIA^{null}B^{null}</i>	+	+
<i>gluRIIA^{IIC C-term} (AAC)</i>	<i>IIA^{null}B^{null}</i>	+	+
<i>gluRIIA^{IID C-term} (AAD)</i>	<i>IIA^{null}B^{null}</i>	o	n.a.
<i>gluRIIA^{IIE C-term} (AAE)</i>	<i>IIA^{null}B^{null}</i>	o	n.a.
<i>gluRIIB^{IIA C-term} (BBA)</i>	<i>IIA^{null}B^{null}</i>	+	+
<i>gluRIIC^{IIA C-term} (CCA)</i>	<i>IIC^{null}</i>	+	+

Table 3. C-terminal modifications
Abbreviations denote: + control level, - reduced, -- highly reduced, o none, n.a. not analyzable.

4.2. Fluorophore-tagging of glutamate receptor subunits

A massive deprivation of glutamate receptors resulted in severe ultrastructural synaptic defects characterized by the loss of proper apposition of the pre- and postsynaptic membranes, which is necessary for efficient neurotransmission. While initial PSD assembly was sustained, the maturation of PSDs was specifically inhibited. The PSDs arrested in an immature state with strongly reduced size missing the typical discrimination of peri- and postsynaptic membrane (see 4.1). Hence, glutamate receptors seem to be required for the expansion of PSDs. Indeed, *in vivo* imaging on the intact *Drosophila* larval NMJ has shown that the entry of the glutamate receptor subunit GluRIIA directly correlates with the growth of single PSDs (Rasse et al., 2005). Therefore, GluRIIA harboring a fluorophore insertion in the middle of its intracellular C-terminus (after AA S893, GluRIIA^{GFP893}) was used. Above it was shown that the C-terminal domain of GluRIIA might play a role in establishing proper membrane apposition (Fig. 27). Besides, it was shown for vertebrate AMPARs that the C-terminal domain is needed for receptor trafficking and transport to the synaptic membrane (Malinow and Malenka, 2002). Surprisingly, the C-terminal fluorophore-tagging of GluRIIA did neither interfere with proper receptor complex targeting nor affect physiological channel properties (Rasse et al., 2005). Nevertheless, extracellular tagging would be preferred for various reasons. The most striking argument for a luminal fusion is the fact that intracellular, C-terminal fluorophore-tagging of C-terminally truncated subunits is logically impossible. It would be interesting to study the dynamic involvement of e.g. the above presented GluRIIA^{ΔC53} (see 4.1.7) in PSD maturation. Furthermore, a luminal fusion would enable the usage of pH-dependent fluorophores as pHluorin to study vesicular glutamate receptor transport (Ashby et al., 2004).

As already mentioned, a previous of our laboratory focused on how the trafficking of GluRIIA organizes synapse formation at the larval NMJ (Rasse et al., 2005). Recently it was suggested that two glutamate receptor complexes incorporating GluRIIC, GluRIID and GluRIIE with either GluRIIA or GluRIIB are expressed at the *Drosophila* NMJ (Qin et al., 2005). To address how both receptor complexes are involved in *in vivo* PSD formation and maturation, GluRIIB had to be functionally tagged with EGFP.

Two different approaches, both based on a recent *in vitro* transposition screen for rat GluR1 (Sheridan et al., 2002) were chosen to tag GluRIIA and GluRIIB. On the one hand, a randomized generation of EGFP fusion proteins by *in vitro* transposition was performed. On the other hand, functional EGFP insertion sites for rat GluR1

(Sheridan et al., 2002) were transferred to the corresponding GluRIIA and GluRIIB AA positions.

4.2.1. Random insertion - *In vitro* transposition

The functional tagging of membrane proteins as glutamate receptors is often problematic. The complex 3D structure of glutamate receptor channels might favor fluorophore insertion at the very N-terminus directly after the signal peptide of the respective GluR subunit. In fact, vertebrate AMPARs were successfully labeled at this position (Shi et al., 1999; Perestenko and Henley, 2003). However, all approaches to functionally tag the *Drosophila* NMJ glutamate receptor subunits GluRIIA and GluRIIB close to their amino terminus failed.

A recent report demonstrated a rapid erratic way to generate ECFP or EGFP insertion libraries which were subsequently screened for positive clones expressing functional fusion proteins via physiological recordings on HEK293 cells (Sheridan et al., 2002).

Here, the *in vitro* transposition screen protocols were transformed to both GluRIIA and GluRIIB (see 3.1.3). Therefore, the Tn5 transposon *TgPT-0* carrying both the EGFP and a kanamycin resistance gene flanked by the Tn5 ME mosaic ends was used (Fig. 18). In the presence of Mg^{2+} the recombinant Tn5 EZ:TNTM transposase catalyzes the random transposon insertion into the target DNA. As target, genomic DNA of *gluRIIA* and *gluRIIB* (pSL fa1180fa *gluRIIA* and pSL1180Nael *gluRIIB*) was used. The successful transposon integration into the target vector could be detected via ampicillin/kanamycin co-selection as both cloning vectors pSL fa1180fa and pSL1180Nael harbor an ampicillin resistance gene.

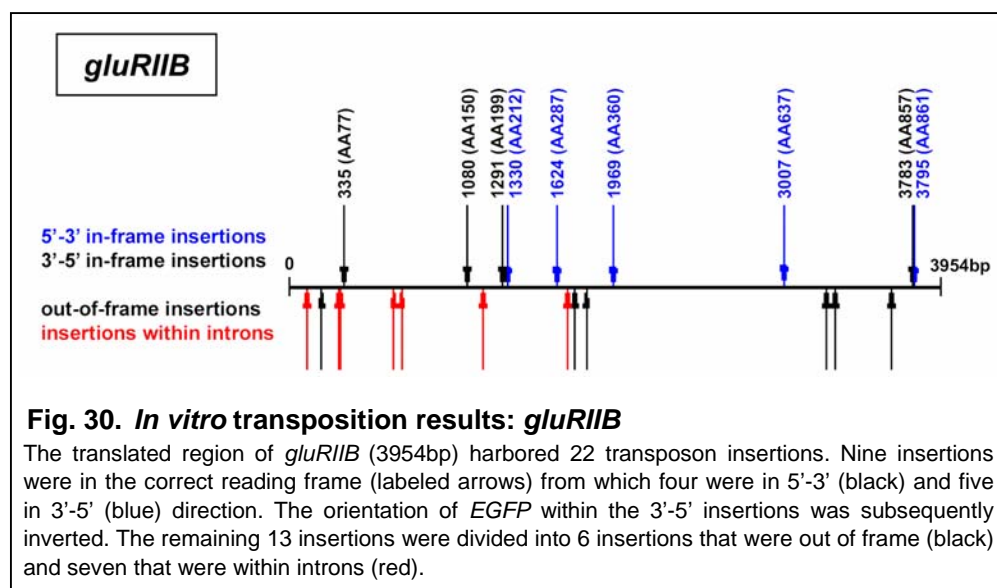
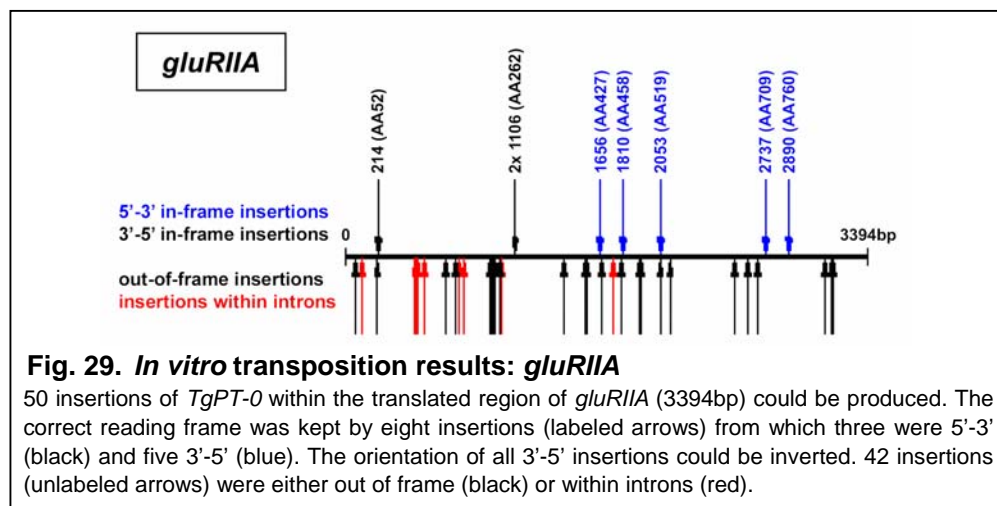
For *gluRIIA* 192 and for *gluRIIB* 96 colonies were selected and screened for a transposon insertion within the coding region of the respective gene via colony PCR (for primers see 3.1.3). To increase the rate of in frame insertions both 5'-3' and 3'-5' orientation of the transposon was accepted as a subsequent transposon inversion was possible. All clones showing PCR products were sequenced to verify insertions in the correct reading frame.

Assuming that the transposon is integrated randomly into the target DNA, the likelihood for an insertion within the genomic coding region is calculated by dividing the cDNA length by the total plasmid length (both values in bp):

$$gluRIIA \quad 2724bp / 8760bp = 31.1\%$$

$$gluRIIB \quad 2739bp / 8301bp = 33.0\%$$

Taking into consideration, that insertions within critical vector regions (as regions required for vector replication as well as the ampicillin resistance gene) might likely inhibit clone formation, the percentages from above increase to 40.4% and 43.7%, respectively. However, only one third harbors an insertion in the correct reading frame reducing the percentages to 13.5% for *gluRIIA* and 14.6% for *gluRIIB*.



From the 196 clones that were selected from the *gluRIIA in vitro* transposition reaction (Fig. 29), 72 showed PCR bands. After sequencing only eight clones with an in frame insertion were obtained (4.1%). 5 of the 8 clones harbored the transposon in 3'-5' orientation. To invert the orientation, a *Sall/NcoI* fragment was subjected to *AscI* restriction and subsequent re-ligation and brought back into the *gluRIIA* backbone. 32 clones had an insertion out of frame, 10 within introns. The remaining 22 clones were false positive.

For *gluRIIB* (Fig. 30) 35 of the 96 selected clones passed the colony PCR screening. 9 clones were positive, 6 had an insertion out of frame and 7 within introns. 13 clones were rated false positive.

The obtained positive insertions resided in the following regions (the number indicates the AA position):

<i>gluRIIA</i> ^{GFP}	NTD	52, 262 (2x)
	S1/S2	427, 458, 519, 709, 760
<i>gluRIIB</i> ^{GFP}	NTD	77, 150, 199, 212, 287, 360
	M2	637
	CTD	857, 861

Finally, all positive samples were subjected to *SrfI* restriction to eliminate the kanamycin resistance gene. The EGFP-tagged transgenes *gluRIIA*^{GFP} and *gluRIIB*^{GFP} were cloned into the expression vector pUAST (Fig. 57) or pUAST XL+ (see 7.1), respectively. The following establishment of transgenic flies was done according to 3.2.2.

All transgenics were tested for their capability to rescue the otherwise embryonically lethal *gluRIIA*^{null}/*IIB*^{null} double mutant situation (see 3.2.3). Additionally, immunostainings for GFP were performed.

None of the transgenes derived from the *in vitro* transposition screen rescued the *gluRIIA*^{null}/*IIB*^{null} lethality. Furthermore, neither synaptic nor extrasynaptic GFP signals could be observed (see Fig. 64).

4.2.2. Site-directed fusion

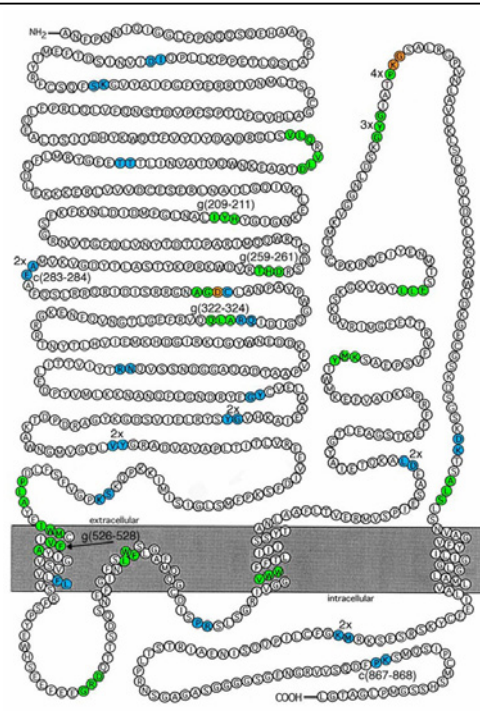
4.2.2.1. Strategy

Recently, six functional fluorophore insertion sites could be identified for rat GluR1 (Fig. 31) throughout an *in vitro* transposition screen. These findings were transformed to *Drosophila* GluRIIA and GluRIIB. The following respective AA positions could be derived and were chosen as GFP insertion sites:

rat GluR1: 211	→	GluRIIA: 255		GluRIIB:
261	→	301	→	284
284	→	319	→	309
324	→	355		
868	→	893	→	897

Fig. 31. Fluorophore-tagging of rat GluR1

In vitro transposition reactions carried out with rat GluR1 resulted in six functional ECFP (transposon *TgPT-1*) or EGFP (transposon *TgPT-0*) fusion proteins. While a random insertion of *TgPT-0* led to the duplication of three amino acids (green), a *TgPT-1* insertion is characterized by a duplication of two amino acids (blue) flanking the transposon. The highest number of the respective duplications indicates the exact AA position. Adapted from (Sheridan et al., 2002).



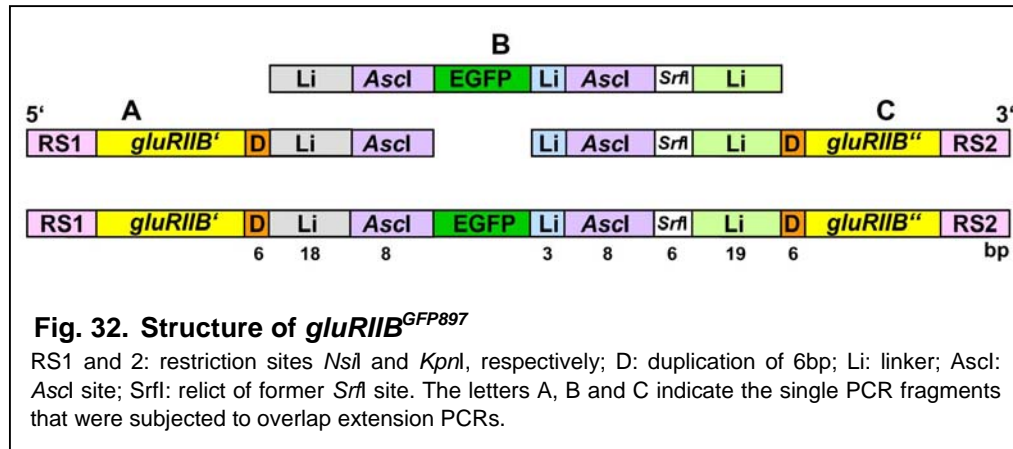
Previously, *gluRIIA*^{GFP301} and *gluRIIA*^{GFP319} have been established in our laboratory as cDNA and genomic constructs. Both proved to be non-functional. In this study, *gluRIIA*^{GFP255}, *gluRIIA*^{GFP355}, *gluRIIB*^{GFP284} and *gluRIIB*^{GFP309} were cloned. The established transgenes did not have any rescue capability for the *gluRIIA*^{null}*IIB*^{null} lethality and showed no detectable GFP signals (Fig. 64).

Recently, *gluRIIA* was functionally tagged in the middle of the intracellular C-terminus (AA position 893, see 3.1.2.1) and successfully applied to study the organization of synapse formation by *in vivo* imaging of glutamate receptors (Rasse et al., 2005).

Here, a detailed description is given for the C-terminal tagging of *gluRIIB* at the analogue AA position 897 (Fig. 17), which demonstrates the principle of all site-directed GFP fusions.

A genomic *NsiI/NcoI* fragment of *gluRIIB* (open reading frame plus ~700bp upstream and ~500bp downstream) was used as backbone. The *EGFP* insert was based on the Tn5 transposon *TgPT-0* (Fig. 18). In detail (Fig. 32), the last two amino acids before the insertion site were duplicated and the linker regions as well as the *Ascl* sites were adopted from the Tn5 transposon. To meet the correct reading frame, the 5' linker was shortened by one base pair as the *EGFP* started with the 6th base pair. The molecular cloning was performed by a three step overlap extension PCR (Fig. 16) with the restriction sites *NsiI/KpnI* flanking the final PCR product (see 3.1.2.1).

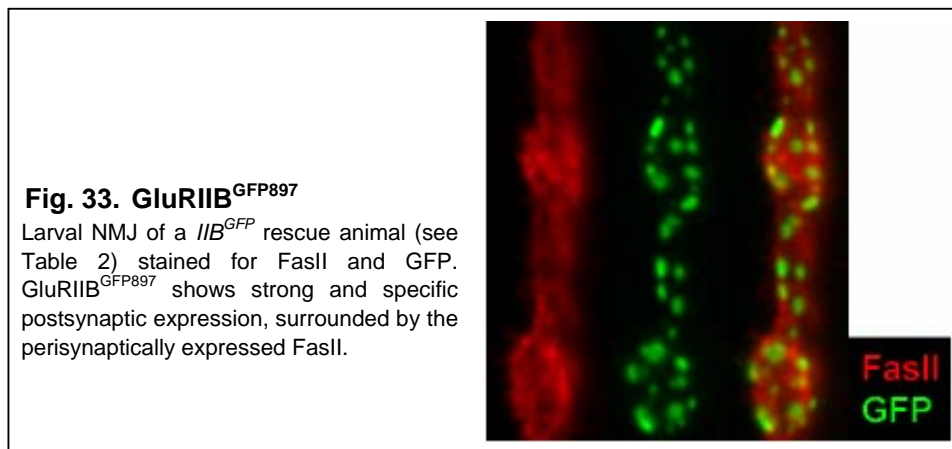
Finally, the GFP-tagged *gluRIIB*^{GFP897} was cloned into pUAST XL+ (see 7.1) and transgenics were established in *dfclh*⁴ background (see 3.2.2).



As the EGFP was flanked by Ascl sites it could be easily replaced with mRFP (see 3.1.2.1).

4.2.2.2. Outcome

Anti-GFP immunostainings of *IIB*^{GFP} larvae (*gluRIIB*^{GFP} expressed in the otherwise lethal *gluRIIA*^{null}*IIB*^{null} background) uncovered strong synaptic expression of GluRIIB^{GFP897} (Fig. 33). The same could be observed for GluRIIB^{mRFP897} (see Fig. 35 and Fig. 64).



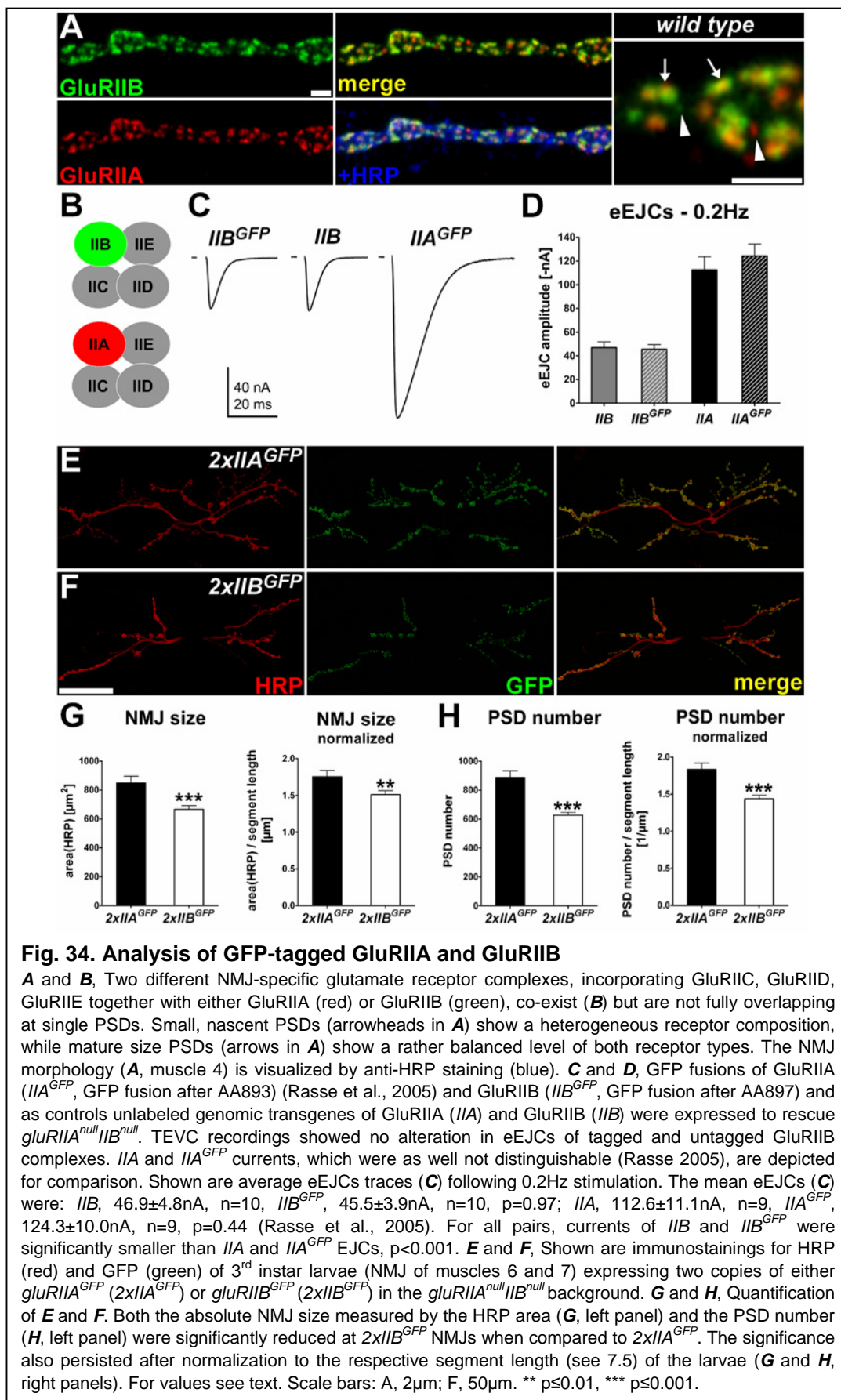
Moreover, *gluRIIB*^{GFP} was indistinguishable from the untagged *gluRIIB* concerning rescue capability and physiological properties (for details see 4.3.1).

4.3. Subunit-specific targeting of glutamate receptors organizes PSD formation and maturation

4.3.1. Functional GFP fusions of GluRIIA and IIB to *in vivo* study synapse formation at developing NMJs of *Drosophila*

Previous work has described two different glutamate receptor complexes expressed at the *Drosophila* neuromuscular junction, with each complex being sufficient for survival (DiAntonio et al., 1999). Both receptor subtypes contain either the subunit GluRIIA (but not GluRIIB) or GluRIIB (but no GluRIIA), likely together with the subunits GluRIIC, IID and IIE (Fig. 34B) (Schuster et al., 1991; Petersen et al., 1997; Marrus et al., 2004; Featherstone et al., 2005; Qin et al., 2005). As described previously (Marrus et al., 2004), GluRIIA and GluRIIB complexes (from now GluRIIA and GluRIIB) are co-expressed on the level of individual postsynaptic densities, however, were not extensively co-localized within individual PSDs (Fig. 34A). Particularly, small PSDs showed a heterogeneous GluRIIA/GluRIIB composition (often being dominated by GluRIIA, Fig. 34A, arrowheads) while mature size PSDs tended to show a more balanced receptor composition (Fig. 34A, arrows).

Previous studies indicated that GluRIIA and GluRIIB are differentially involved in long-term NMJ plasticity. When GluRIIA was favored over GluRIIB expression, both the number of synapses forming per NMJ as well as the transmission strength (measured as evoked excitatory junctional current, eEJC) increased. On the contrary, GluRIIB expression antagonized this GluRIIA mediated long-term plasticity (Sigrist et al., 2002; Sigrist et al., 2003). Moreover, recently *in vivo* imaging of fluorescently labeled GluRIIA during synapse formation of larval NMJs over extended periods was established. Small PSDs grew by a nearly irreversible incorporation of GluRIIA from diffuse pools, suggesting a rate limiting role of this incorporation for PSD assembly (Rasse et al., 2005). GluRIIB, in contrast, was not visualized *in vivo* so far. For this purpose, EGFP (Clontech, Mountain View, CA) was cloned in the middle of the intracellular C-terminus (see 3.1.2.1 and 4.2.2; after amino acid T897, homologous position as used for GluRIIA) (Rasse et al., 2005) and this GFP fusion (*gluRIIB^{GFP}*) was expressed from a genomic *gluRIIB* clone. *gluRIIB^{GFP}* was able to rescue the otherwise embryonic lethal *gluRIIA^{null}IIB^{null}* mutant as efficient as the untagged wild type genomic construct *gluRIIB* (*IIB*, 50%, *IIB^{GFP}*, 55% of expected Mendelian ratio).



Next, the NMJ physiology of 3rd instar larvae expressing either unlabeled or GFP-labeled GluRIIB in *gluRIIA^{null}IIB^{null}* background was compared (from here on referred to as *IIB* or *IIB^{GFP}*). Both mEJCs and eEJCs as measures of individual synaptic and overall NMJ transmission strength, respectively, were identical between *IIB* and *IIB^{GFP}* (Fig. 34C,D) (mEJCs: *IIB*, 0.71±0.04nA, n=10, *IIB^{GFP}*, 0.66±0.03nA, n=9, p=0.50; eEJCs: *IIB*, 46.9±4.8nA, n=10, *IIB^{GFP}*, 45.5±3.9nA, n=10, p=0.97). In contrast, as previously shown (Rasse et al., 2005) both *IIA* and *IIA^{GFP}* (rescue of *gluRIIA^{null}IIB^{null}* with either *gluRIIA* or *gluRIIA^{GFP893}*, Table 2) identically produced much higher eEJCs (Fig. 34C,D). Thus, it can be concluded that on the one hand GFP-tagging does not measurably affect the specific features of the subunits, and on the other hand that the specific differences between GluRIIA and GluRIIB for promoting NMJ transmission strength are well conserved also for the GFP-labeled subunits (being expressed in physiological levels from genomic constructs). Thus the GFP-labeled constructs were used throughout the further study.

As outlined above, favoring GluRIIA over GluRIIB expression increases the morphological size together with the number of synapses forming per NMJ (Reiff et al., 2002; Sigrist et al., 2002; Sigrist et al., 2003). To test whether these differences were also conserved for GFP-labeled GluRIIA or GluRIIB, *gluRIIA^{GFP}* or *gluRIIB^{GFP}* were expressed in the *gluRIIA^{null}IIB^{null}* background (2 genomic copies used, thus *2xIIA^{GFP}* and *2xIIB^{GFP}*, respectively). In fact, NMJs of *2xIIA^{GFP}* late 3rd instar larvae (Fig. 34E) were considerably larger than *2xIIB^{GFP}* NMJs (Fig. 34F) (HRP signal) before and after animal size normalization (Fig. 34G,H; see 3.3.5.4 and 7.5) (area(HRP) - *2xIIA^{GFP}*, 849±46µm², n=20, *2xIIB^{GFP}*, 666±25µm², n=20, p<0.001; area(HRP), normalized - *2xIIA^{GFP}*, 1.76±0.09µm, n=20, *2xIIB^{GFP}*, 1.51±0.05µm, n=20, p=0.0043). Concomitantly, *2xIIA^{GFP}* NMJs on average comprised about 30% more PSDs visualized by GFP immunostainings (PSD number - *2xIIA^{GFP}*, 888±46, n=20, *2xIIB^{GFP}*, 628±19, n=20, p<0.001; PSD number, normalized - *2xIIA^{GFP}*, 1.83±0.09 per µm, n=20, *2xIIB^{GFP}*, 1.44±0.05 per µm, n=20, p<0.001).

In summary, the physiological properties of GFP-labeled constructs could not be discriminated from their unlabeled counterparts, while the specific differences in promoting or inhibiting NMJ synapse number and transmission strength appeared well conserved when using the GFP-tagged versions. Thus, an analysis to study the above mentioned differential role of the two receptor subtypes in PSD formation and NMJ development using these functional GFP fusions could be set-up.

4.3.2. Simultaneous *in vivo* imaging of GluRIIA and GluRIIB

To allow the parallel *in vivo* imaging (see 3.3.2) of both receptor complexes expressed at the *Drosophila* NMJ, also equally functional fusions of GluRIIA (Rasse et al., 2005) and GluRIIB (Fig. 35C) with monomeric red fluorescent protein (mRFP) (Campbell et al., 2002) were used. Differentially tagged GluRIIA and GluRIIB were co-imaged at early 3rd instar larval NMJs (of the ventral-acute muscle 27, see Fig. 9; type Ib terminals) to follow the formation and maturation of individual PSDs. The analysis of the relative intensities of both GluRIIB^{GFP} and GluRIIA^{mRFP} (expressed from genomic transgenes in the *gluRIIA^{null}IIB^{null}* background, *IIB^{GFP}&IIA^{mRFP}*, Table 2) at single PSDs allowed a quantitative specification of the PSD subunit composition, indicated by the ratio r ($r = \text{Int}_{\text{rel}}(\text{IIB}^{\text{GFP}})/\text{Int}_{\text{rel}}(\text{IIA}^{\text{mRFP}})$); an exemplary ratio evaluation is shown in Fig. 19). In doing so, vast differences between the PSDs of *IIB^{GFP}&IIA^{mRFP}* NMJs became obvious. Small PSDs showed large differences in the ratio r , means in the receptor content, which converged with increased PSD size (Fig. 35A). A similar divergence in the ratio r was not observed in identically processed images of *IIA^{GFP}&IIA^{mRFP}* (Fig. 35B) and *IIB^{GFP}&IIB^{mRFP}* (Fig. 35C) NMJs (*gluRIIA^{null}IIB^{null}* background, Table 2; ratio $r = \text{Int}_{\text{rel}}(\text{IIA}^{\text{GFP}})/\text{Int}_{\text{rel}}(\text{IIA}^{\text{mRFP}})$ or $\text{Int}_{\text{rel}}(\text{IIB}^{\text{GFP}})/\text{Int}_{\text{rel}}(\text{IIB}^{\text{mRFP}})$). Accordingly, in both cases the respective GFP- and mRFP-labeled subunits almost completely overlapped at individual PSDs (Fig. 35B,C). This became also obvious when the ratio frequencies, subdivided into three ratio classes, covering GFP-rich (ratio $r > 1.2$), mRFP-rich (ratio $r < 0.8$) and balanced ($0.8 < r < 1.2$) PSDs, were analyzed. While for *IIB^{GFP}&IIA^{mRFP}* all three PSD classes were represented with at least 20%, more than 80% of *IIA^{GFP}&IIA^{mRFP}* and *IIB^{GFP}&IIB^{mRFP}* PSDs were assigned to the middle ratio class (Fig. 35D). Thus, it can be concluded that the ratio differences observed after co-imaging of GluRIIA and GluRIIB are, at least to the largest extent, due to the distinct nature of GluRIIA and GluRIIB complexes.

To study the dynamic involvement of both receptor subtypes in PSD formation and maturation, identified NMJs of early 3rd instar larvae expressing both GluRIIB^{GFP} and GluRIIA^{mRFP} were subjected to repeated *in vivo* imaging (12h time intervals, rearing temperature 25°C). *In vivo* imaging of GluRIIA had shown that new PSDs form *de novo*, often distant from the PSDs of pre-existing synapses (Rasse et al., 2005), and then grow until they reach a mature GluRIIA content. When GluRIIA^{mRFP} and GluRIIB^{GFP} were co-imaged, small, newly forming PSDs were typically rich of GluRIIA^{mRFP} (Fig. 35E, octothorpes). In contrast, small GluRIIB^{GFP}-rich PSDs were generally rather rare and frequently found in-between boutons (Fig. 35E,F, asterisks). As a strict definition of bouton and inter-bouton PSDs was not feasible, for analysis all PSDs were pooled independent of their localization at the NMJ.

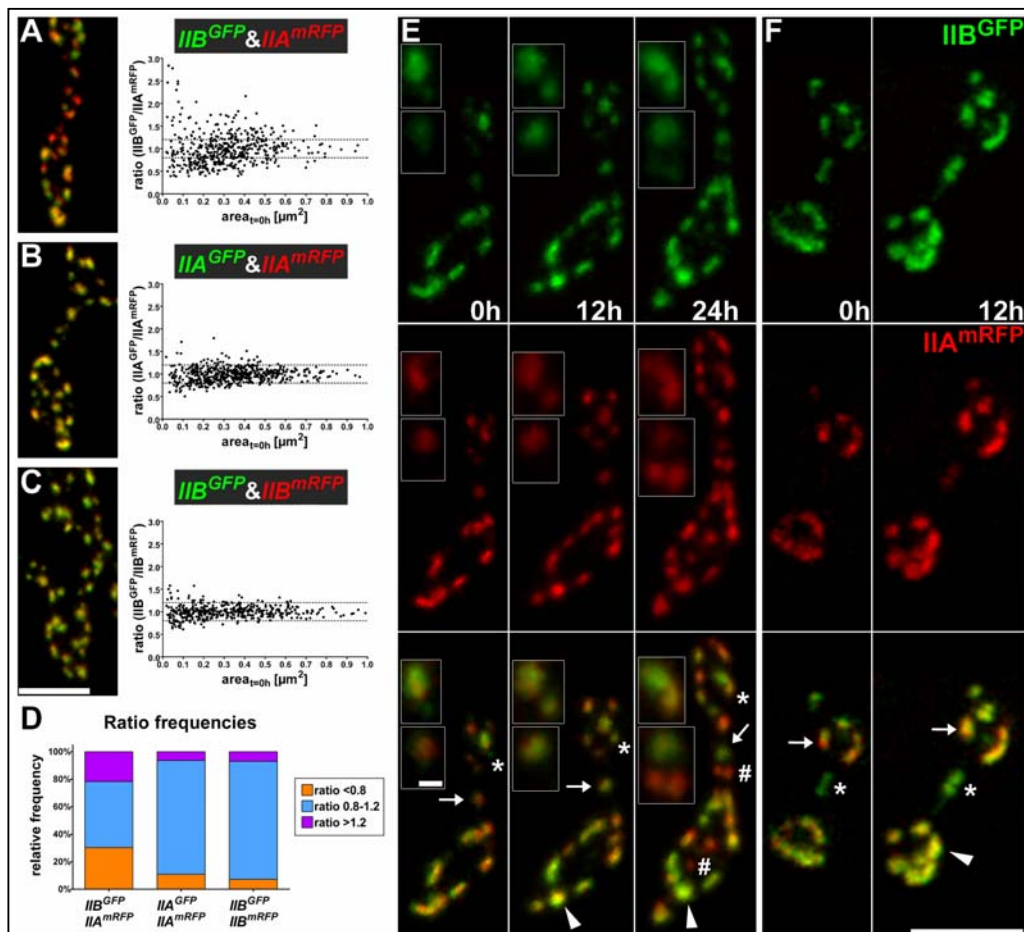


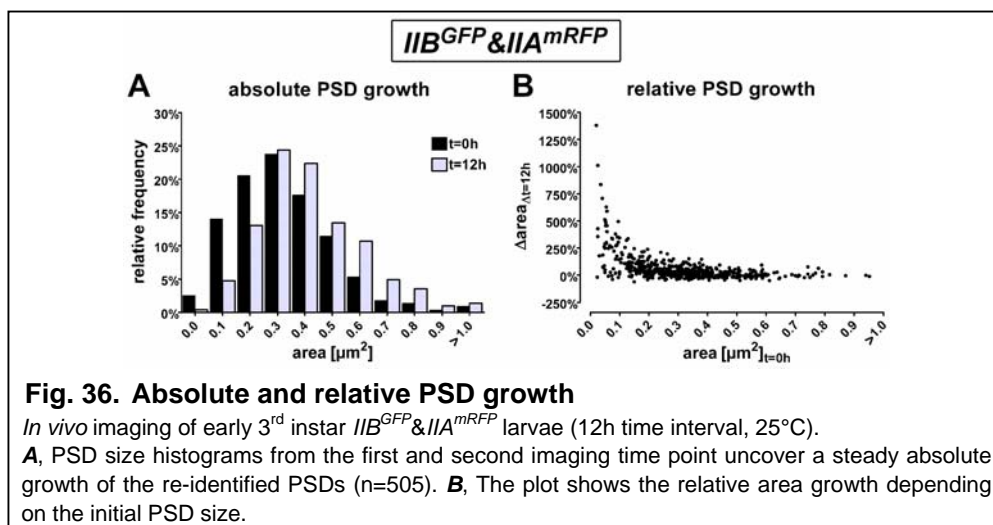
Fig. 35. Size-dependent divergence of PSD subunit composition.

A, *In vivo* imaging of 3rd instar larvae expressing *gluRIIB^{GFP}* and *gluRIIA^{mRFP}* in the lethal *gluRIIA^{null}IIB^{null}* background (*IIB^{GFP}&IIA^{mRFP}*) (12h time window; at 25°C). Single *IIB^{GFP}&IIA^{mRFP}* PSDs (image, left panel) showed differential levels of GluRIIB^{GFP} (green) and GluRIIA^{mRFP} (red). A quantification of the relative intensities of both receptor types allowed quoting the ratio of GluRIIB^{GFP} to GluRIIA^{mRFP} at individual PSDs [ratio $r = \text{Int}_{\text{rel}}(\text{IIB}^{\text{GFP}})/\text{Int}_{\text{rel}}(\text{IIA}^{\text{mRFP}})$]. Plotting the ratio r over the initial PSD area (graph, right panel) uncovered a strong divergence in subunit composition for small PSDs and a convergence in the ratio r with growing PSD size. **B** and **C**, Analogue procedure as in **A**. Using either *gluRIIA^{GFP}* and *gluRIIA^{mRFP}* or *gluRIIB^{GFP}* and *gluRIIB^{mRFP}* to rescue the *gluRIIA^{null}IIB^{null}* mutant (*IIA^{GFP}&IIA^{mRFP}* (**B**) or *IIB^{GFP}&IIB^{mRFP}* (**C**), respectively) resulted, as expected, in a complete overlap of GFP and mRFP fluorescence (images, left panels). Here, a divergence in subunit composition [ratio $r = \text{Int}_{\text{rel}}(\text{IX}^{\text{GFP}})/\text{Int}_{\text{rel}}(\text{IX}^{\text{mRFP}})$; X represents A or B] could not be observed (graphs, right panels). **D**, Quantification of the observed subunit ratios from **A-C** subdivided into ratio classes ($r < 0.8$; $0.8 < r < 1.2$; $r > 1.2$; boundaries are indicated in the respective graphs of panels **A-C**). While the vast majority of *IIA^{GFP}&IIA^{mRFP}* and *IIB^{GFP}&IIB^{mRFP}* PSDs showed balanced ratios, *IIB^{GFP}&IIA^{mRFP}* PSDs could be clearly classified into three representative classes. The relative ratio frequencies of the particular classes were: *IIB^{GFP}&IIA^{mRFP}*, $< 0.8 - 30.3\%$, $0.8-1.2 - 48.1\%$, $> 1.2 - 21.6\%$, $n=505$, 8 NMJs; *IIA^{GFP}&IIA^{mRFP}*, $< 0.8 - 10.9\%$, $0.8-1.2 - 82.8\%$, $> 1.2 - 6.3\%$, $n=559$, 8 NMJs; *IIB^{GFP}&IIB^{mRFP}*, $< 0.8 - 7.2\%$, $0.8-1.2 - 85.9\%$, $> 1.2 - 6.9\%$, $n=433$, 9 NMJs. **E** and **F**, *In vivo* imaging of *IIB^{GFP}&IIA^{mRFP}* early 3rd instar larvae during 24h (**E**) and 12h (**F**) of NMJ development. Among small, nascent PSDs, GluRIIB^{GFP} rich PSDs (green) could be rarely observed (asterisks) while GluRIIA^{mRFP} dominated PSDs (red) were particularly frequent (octothorpes). Both types showed further outgrowth and tended to equalize their differential receptor content (arrow). Mature size PSDs were characterized by a rather balanced receptor level (arrowheads). All presented images were obtained by confocal microscopy of NMJ27. Scale bars: C and F, 5μm; E, enlarged sections, 0.5μm.

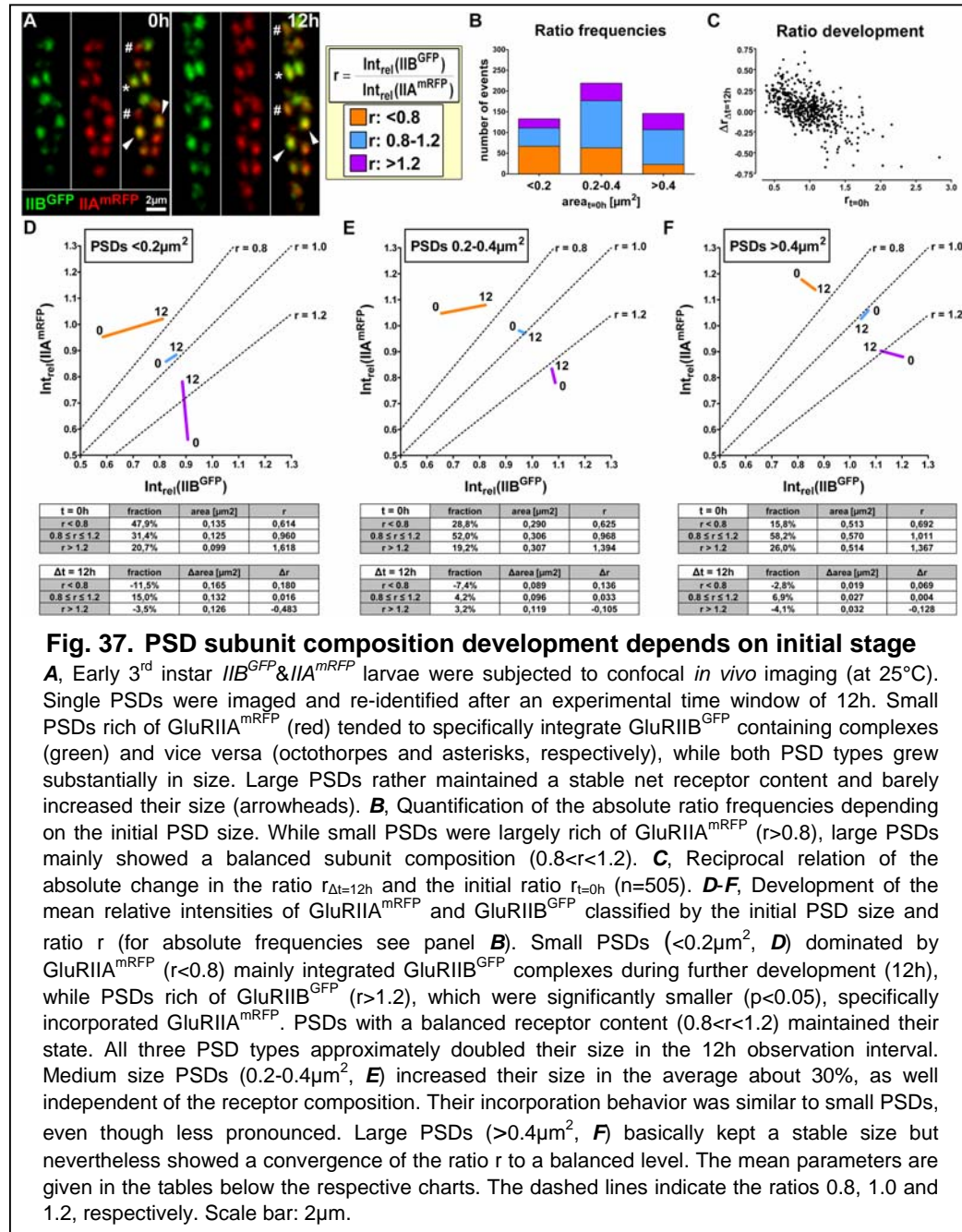
4.3.3. Receptor composition balances in the course of PSD growth and maturation

So far, it was shown that newly forming synapses are heterogeneous in glutamate receptor composition, typically being dominated by GluRIIA^{mRFP}. Throughout their further outgrowth, however, such newly forming, GluRIIA^{mRFP}-rich PSDs (arrows in Fig. 35,F) seemed to become more balanced in receptor composition at later observation time points. *Vice versa*, small PSDs initially rich of GluRIIB^{GFP} later appeared more balanced as well (Fig. 35E,F, asterisks).

To quantify this behavior, 505 individual PSDs (from 8 NMJs, muscle 27) identified at $t=0h$ and re-identified at $t=12h$ were analyzed. As expected, the PSD population (example PSDs shown in Fig. 37A) substantially increased its average size (resulting from a maximum overlay of both GluRIIA^{mRFP} and GluRIIB^{GFP}) from $0.323 \pm 0.08 \mu m^2$ to $0.414 \pm 0.09 \mu m^2$, $p < 0.001$ (Fig. 36A). Thereby, an inverse relation between the initial PSD size and the further growth could be observed (Fig. 36B). Moreover, the development of the receptor subunit composition of single PSDs, numerically quoted by the intensity ratio r ($\text{Int}_{\text{rel}}(\text{IIB}^{\text{GFP}})/\text{Int}_{\text{rel}}(\text{IIA}^{\text{mRFP}})$), was followed. Nine PSD classes, discriminated by the initial size (small, $<0.2 \mu m^2$; medium, $0.2-0.4 \mu m^2$; large, $>0.4 \mu m^2$) and ratio r (<0.8 , $0.8-1.2$, >1.2), were established (absolute numbers, see Fig. 37B; proportion, see Fig. 37D, tables). As mentioned above, among the small PSDs observed at the first time point, GluRIIA^{mRFP}-rich ones ($r < 0.8$) were most prominent while the majority of medium and large PSDs showed a balanced receptor content ($0.8 \leq r \leq 1.2$). Fig. 37C demonstrates that the change of the ratio r during the observation interval of 12h ($\Delta r_{\Delta t=12h}$) was reciprocally related to the start ratio r ($r_{t=0h}$). In other words, the PSD population showed a strong trend to balance the receptor composition over time.



The detailed analysis of the particular size classes showed that small PSDs rich of GluRIIA^{mRFP} (Fig. 37D, $r < 0.8$) specifically increased their GluRIIB^{GFP} intensity. Vice versa, small GluRIIB^{GFP}-rich PSDs (Fig. 37D, $r > 1.2$) specifically increased their GluRIIA^{mRFP} levels. PSDs harboring both receptor subtypes to a similar extent, on average maintained steady relative intensities (Fig. 37D, $0.8 \leq r \leq 1.2$). Thus, all subpopulations either converged to or kept a balanced receptor composition.



PSDs initially rich of GluRIIB^{GFP} ($r > 1.2$) were significantly smaller than those PSDs containing notable levels of GluRIIA^{mRFP} (Fig. 37D, table, $p < 0.05$). However, the growth of small PSDs ($\Delta area$) was not statistically different among the three ratio

classes (Fig. 37D, table; $p > 0.1$). Medium PSDs (Fig. 37E) still showed remarkable growth (about two thirds of the growth observed for small PSDs) apparently independent of the initial receptor composition. Similar to small PSDs, the receptor composition became more balanced. Large PSDs (Fig. 37F) experienced only minor changes in PSD size and in the intensities of the respective receptor subunits. However, the tendency to balance the levels of both receptor complexes remained. To sum up, the initial diverse glutamate receptor subtype composition balanced in the course of the maturation of individual PSDs. This was obviously accomplished by the specific incorporation of either GluRIIA or GluRIIB complexes depending on the initial receptor content of the respective PSD.

4.3.4. Distinct PSD incorporation behavior of GluRIIA and GluRIIB

Previously, fluorescence recovery after photobleaching (FRAP) experiments showed that the incorporation of GluRIIA is maximal at growing PSDs but low at mature, no longer growing PSDs (Rasse et al., 2005). These experiments have been done in the presence of unlabeled GluRIIB. To directly compare the PSD incorporation behavior of GluRIIA to GluRIIB, both $\text{GluRIIB}^{\text{GFP}}$ and $\text{GluRIIA}^{\text{mRFP}}$ (co-expressed in the $\text{gluRIIA}^{\text{null}}\text{IIB}^{\text{null}}$ background, $\text{IIB}^{\text{GFP}}\&\text{IIA}^{\text{mRFP}}$) were imaged, bleached and re-imaged after 24h recovery (Fig. 38). As expected, $\text{GluRIIA}^{\text{mRFP}}$ incorporation was strong at few synapses but very faint at the remaining synapses (Fig. 38, arrowhead and arrow, respectively). In clear contrast, $\text{GluRIIB}^{\text{GFP}}$ showed a uniform recovery over all PSDs. In result, the overlay of the FRAP signals showed a large fraction of synapses with essentially only $\text{GluRIIB}^{\text{GFP}}$ incorporation, while some PSDs were dominated by strong $\text{GluRIIA}^{\text{mRFP}}$ incorporation.

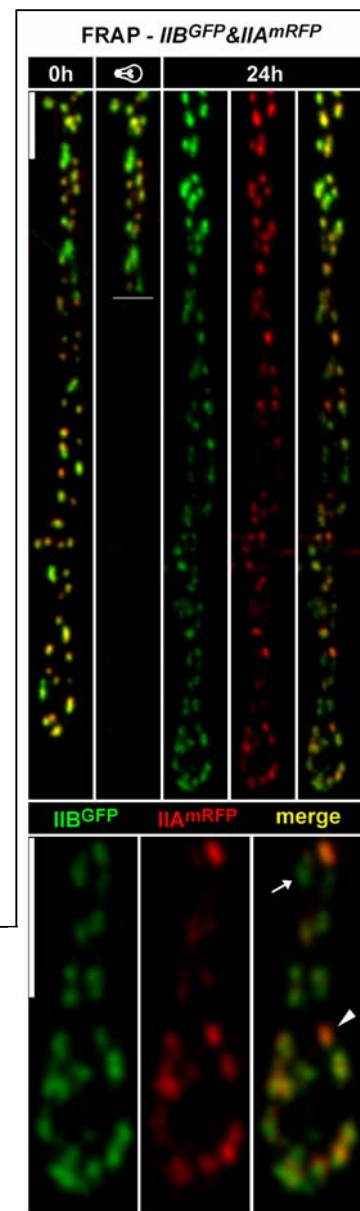


Fig. 38. Differential PSD incorporation behavior of GluRIIA and GluRIIB complexes

FRAP experiment of $\text{IIB}^{\text{GFP}}\&\text{IIA}^{\text{mRFP}}$ early 3rd instar NMJs (24h recovery time; bleaching of both the GFP and mRFP channel). $\text{GluRIIA}^{\text{mRFP}}$ (red) and $\text{GluRIIB}^{\text{GFP}}$ (green) containing complexes showed a differential incorporation behavior. While $\text{GluRIIB}^{\text{GFP}}$ recovered rather equally over all PSDs, $\text{GluRIIA}^{\text{mRFP}}$ showed strong FRAP at some PSDs (arrowhead) but almost no FRAP at the remaining PSDs (arrow). Scale bar: 5 μm .

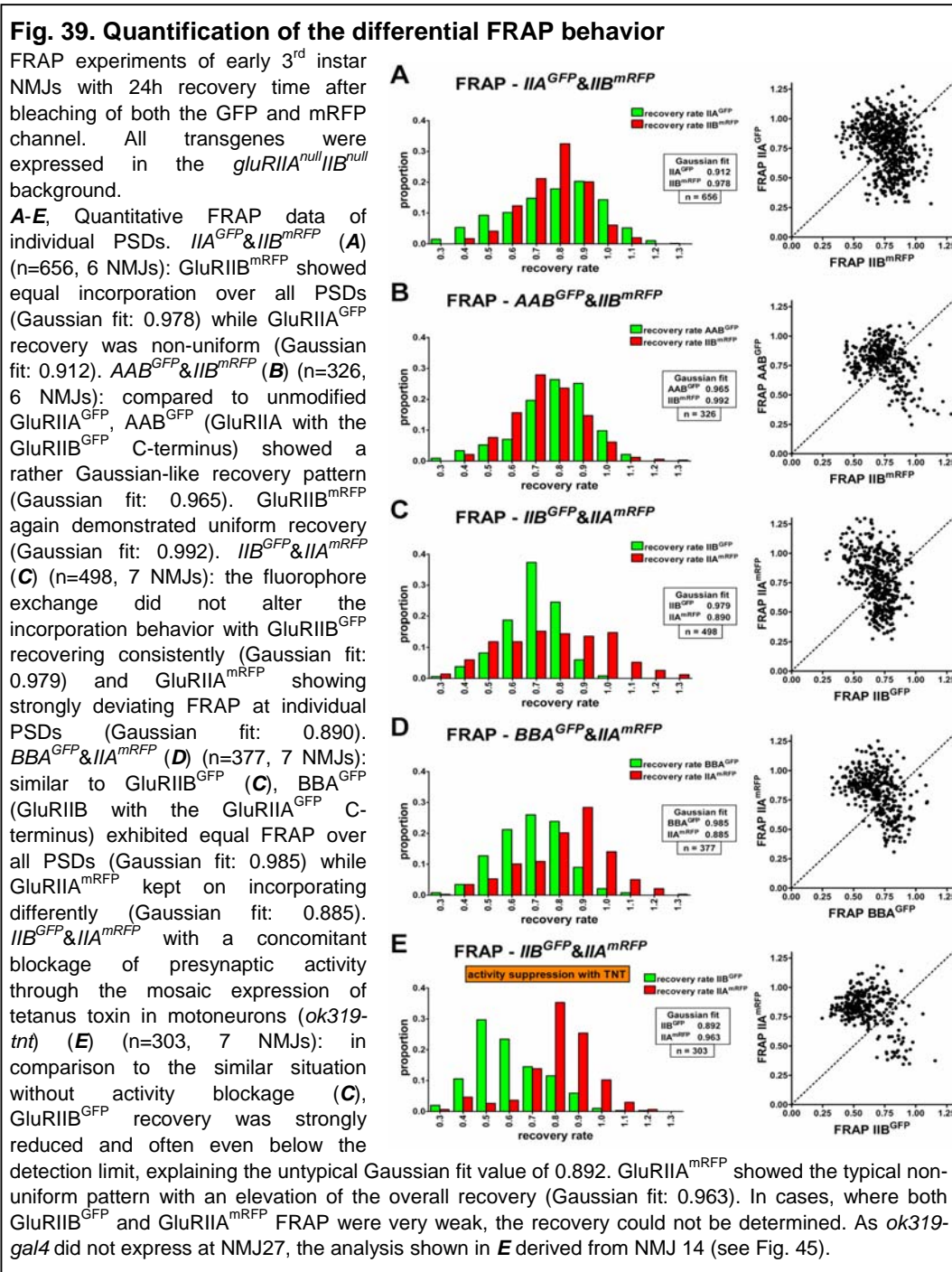
The choice of the fluorophore might have a principal effect on the FRAP behavior. Thus, GFP and mRFP were exchanged resulting in GluRIIA^{GFP} and GluRIIB^{mRFP} (again expressed in the *gluRIIA^{null}IIB^{null}* background, thus *IIA^{GFP}&IIB^{mRFP}*). Here, FRAP of GluRIIA^{GFP} was confined to few synapses (Fig. 40A) while FRAP of GluRIIB^{mRFP} exhibited uniform incorporation over the before bleached PSDs. Thus, qualitatively, GluRIIA and GluRIIB FRAP were independent of fluorophore choice. As reported before, GluRIIA incorporation was restricted to few PSDs, previously shown to represent growing PSDs (Rasse et al., 2005). In clear contrast GluRIIB apparently incorporated equally into all PSDs, both growing and matured ones.

4.3.5. The CTD of GluRIIA contributes to suppress GluRIIA incorporation at mature PSDs

To consolidate the mere optical impression, the FRAP experiments were quantified. Thereto, the FRAP intensity of the formerly bleached PSDs was related to the mean intensity of the non-bleached PSDs (t=24h) and normalized to the initial time point (t=0h), thereby forming a recovery rate (see 3.3.5.3). In both FRAP experiments (*IIB^{GFP}&IIA^{mRFP}*, Fig. 38 and *IIA^{GFP}&IIB^{mRFP}*, Fig. 40A), recovery rates of GluRIIA were very heterogeneous, with the majority of PSDs showing only little or strong recovery, not fitting a non-linear Gaussian regression (Fig. 39A and Fig. 39C, fit values: 0.912 and 0.890, respectively). In contrast, in both cases the recovery of GluRIIB followed a Gaussian distribution (Fig. 39A and Fig. 39C, fit values: 0.978 and 0.979). While the observed recovery rates varied sparsely (potentially reflecting a faster assembly of mRFP than of GFP) the specific FRAP patterns were essentially unaffected by the fluorophore exchange.

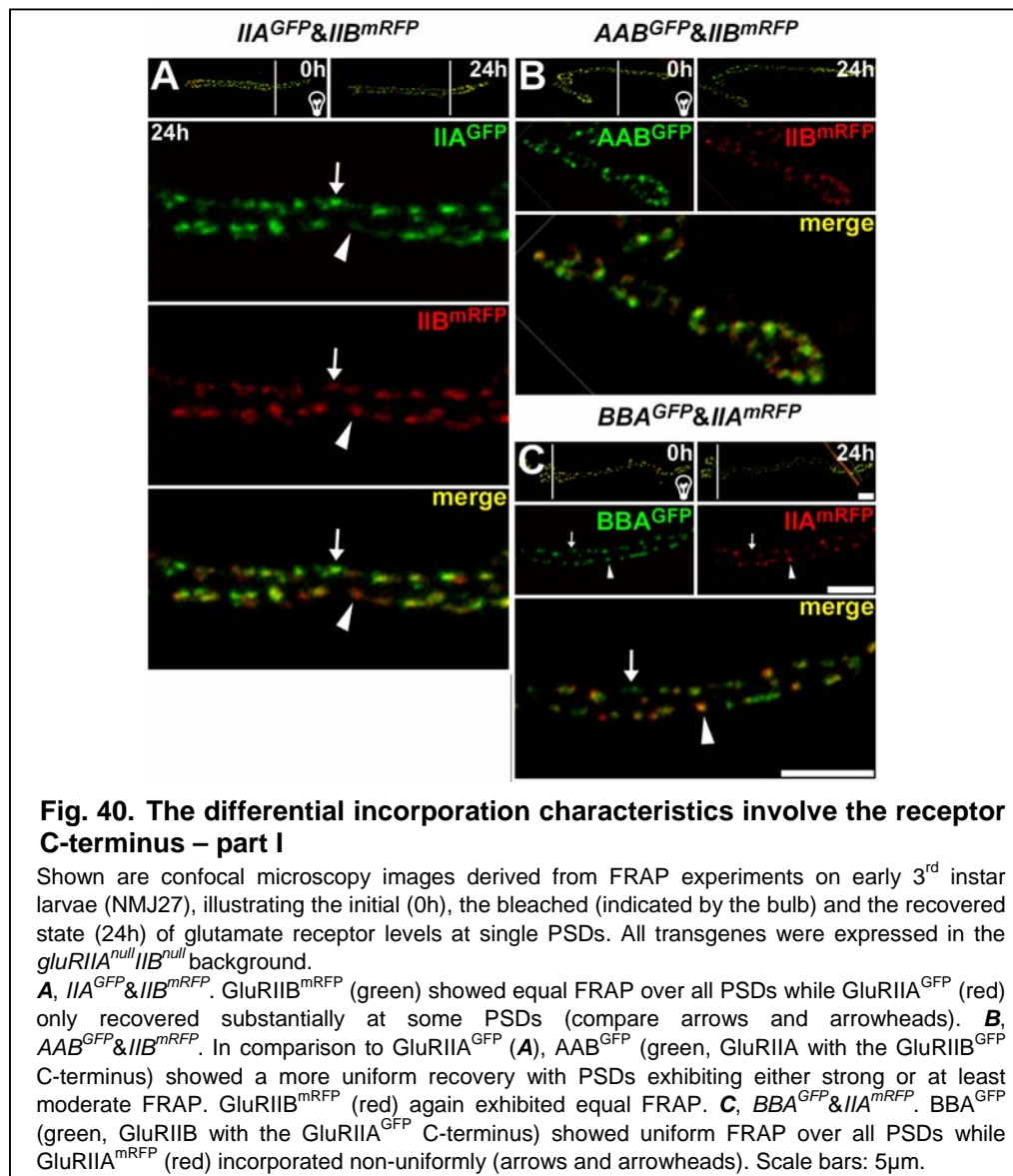
GluRIIA and GluRIIB are structurally similar subunits (Petersen et al., 1997). Which structural elements might then encode this different targeting behavior of the two receptor subtypes? The intracellular C-terminal domains (CTDs) have been directly implicated into the subunit-specific targeting behavior of mammalian glutamate receptor (Barry and Ziff, 2002; Malinow and Malenka, 2002; Bredt and Nicoll, 2003). Hence, C-terminal chimeras of GluRIIA and GluRIIB, each labeled with GFP, were established (*AAB^{GFP}* and *BBA^{GFP}*). Both chimeras rescued the otherwise lethal *gluRIIA^{null}IIB^{null}* background giving rise to adult flies. For FRAP experiments, genomic transgenes of *AAB^{GFP}* together with GluRIIB^{mRFP} (*AAB^{GFP}&IIB^{mRFP}*, Fig. 39B and Fig. 40B) and *BBA^{GFP}* together with GluRIIA^{mRFP} (*BBA^{GFP}&IIA^{mRFP}*, Fig. 39D and Fig. 40C) were expressed in the *gluRIIA^{null}IIB^{null}* background. The recovery of *AAB^{GFP}* (Fig. 39B and Fig. 40B) was more Gaussian-like (fit value: 0.965) as observed before

for GluRIIA^{GFP} (Fig. 39A), means more PSDs exhibiting moderate instead of faint FRAP could be detected.



Thus, the CTD of GluRIIA seems to contribute to suppress GluRIIA incorporation into PSDs. The recent report that GluRIIA incorporation is restricted to growing PSDs (Rasse et al., 2005) implies that the CTD of GluRIIA is involved in shutting down GluRIIA incorporation at mature PSDs. Notably, the CTD of GluRIIA was not sufficient to confer GluRIIA-type incorporation behavior to BBA^{GFP} (Fig. 39E,

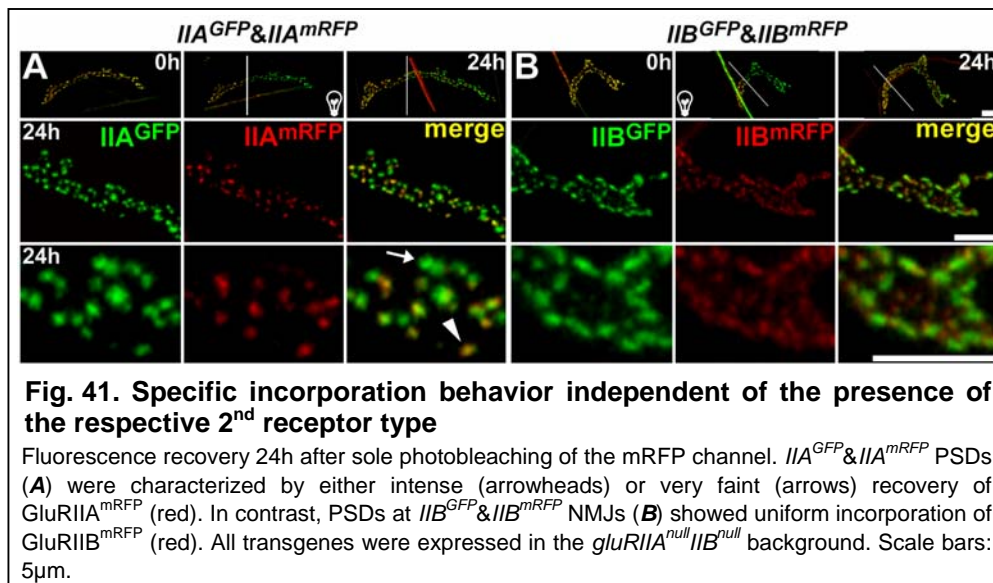
compare to Fig. 39D). In fact, BBA^{GFP} still recovered uniformly (fit value: 0.985). Moreover, the FRAP pattern of $GluRIIA^{mRFP}$ remained unaffected by the presence of BBA^{GFP} (fit value: 0.885). In summary, the C-terminal domains of $GluRIIA$ and $GluRIIB$ seem to contribute to their different PSD incorporation behavior.



4.3.6. Distinct PSD incorporation of *GluRIIA* and *IIB* persists in the absence of the other complex

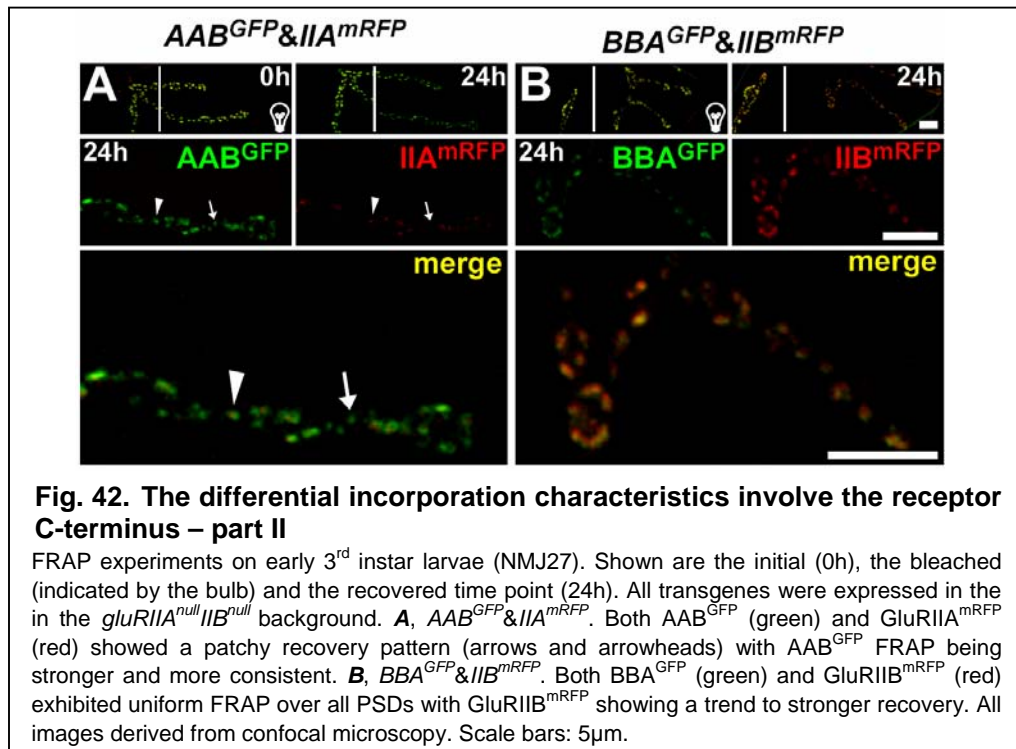
To clarify whether the differentiation of incorporation behavior between $GluRIIA$ and $GluRIIB$ would be established only if both receptor complexes were present simultaneously, FRAP experiments in the respective absence of one complex subtype were performed. For this purpose, genomic transgenes of either $GluRIIA^{GFP}$

and GluRIIA^{mRFP} (*IIA^{GFP}&IIA^{mRFP}*) or GluRIIB^{GFP} and GluRIIB^{mRFP} (*IIB^{GFP}&IIB^{mRFP}*) were expressed in the *gluRIIA^{null}IIB^{null}* background.



To score also potential PSDs showing no measurable recovery (after 24h), only the mRFP channel was bleached at $t=0h$. Interestingly, the non-uniform recovery pattern of GluRIIA complexes persisted in the absence of GluRIIB, with GluRIIA^{mRFP} showing strong recovery at some but only very faint recovery at the other PSDs (Fig. 41A, arrowhead and arrow, respectively), very similar as before seen in the presence of GluRIIB (Fig. 38 and Fig. 40A) (Rasse et al., 2005). In result, only a partial overlap between the recovered GluRIIA^{mRFP} and the non-bleached GluRIIA^{GFP} could be observed. PSDs lacking GluRIIA showed a uniform incorporation of GluRIIB^{mRFP} (Fig. 41B) that almost entirely overlapped with the non-bleached GluRIIB^{GFP}. It can thus be concluded that the subunit specific incorporation properties persisted also when the respective glutamate receptor complex was absent.

This result allowed to evaluate the role of the CTDs in additional FRAP experiments. When AAB^{GFP} and GluRIIA^{mRFP} (*AAB^{GFP}&IIA^{mRFP}*, Fig. 42A) were subjected to FRAP (bleaching of both channels), AAB^{GFP} showed a more uniform FRAP over all PSDs while GluRIIA^{mRFP} kept its typical non-uniform recovery pattern. Thus, integration of AAB^{GFP} into PSDs seemed to be favored over GluRIIA^{mRFP} incorporation, again consistent with the notion that the CTD of GluRIIA contributes to suppress GluRIIA incorporation. Similarly, FRAP of individual PSDs was compared between BBA^{GFP} and GluRIIB (*BBA^{GFP}&IIB^{mRFP}*, Fig. 42B). While both showed uniform FRAP, GluRIIB^{mRFP} incorporation seemingly outcompeted BBA^{GFP}, suggesting that the CTD of GluRIIA tends to suppress PSD incorporation also in fusion to GluRIIB.



Taken together, principal PSD incorporation behavior is not dependent on the simultaneous presence of both the GluRIIA and IIB complex, while the CTD of GluRIIA promotes suppression of GluRIIA incorporation at mature type PSDs.

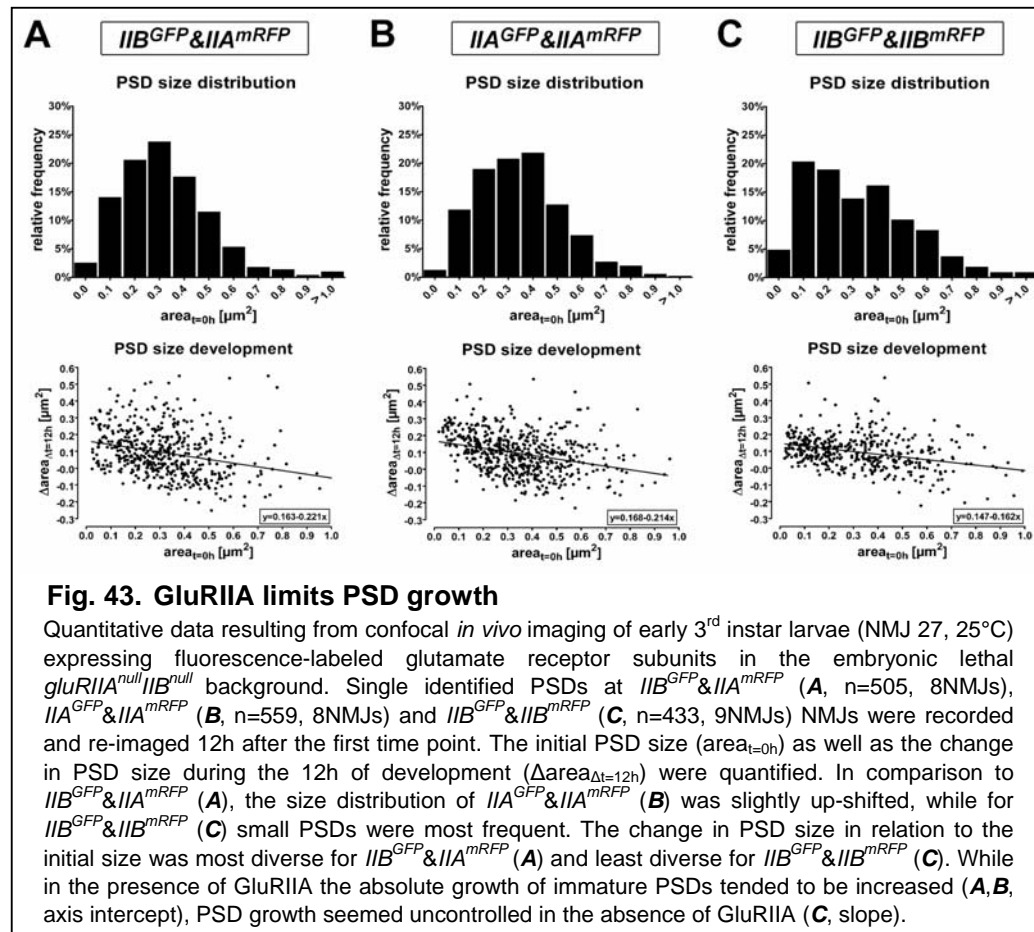
4.3.7. *GluRIIA* is needed to allow efficient growth of PSDs and to define mature PSD size

Despite the absence of growth related glutamate receptor incorporation accomplished by GluRIIA (Rasse et al., 2005), PSD populations at “GluRIIB-only NMJs” (Fig. 35C and Fig. 41B) can still form. However, the number of synapses forming per GluRIIB-only NMJ is reduced when compared to a GluRIIA-only NMJ (Fig. 34E-H), and further structural plasticity upon NMJ experience is inhibited in this situation (Sigrist et al., 2003; Zhong and Wu, 2004).

Differences in PSD growth could principally underlie this restricted structural plasticity of GluRIIB-only NMJs. Thus, the effect of the receptor composition on PSD growth was analyzed by *in vivo* imaging of NMJs over 12h, comparing GluRIIB and GluRIIA ($IIB^{GFP}&IIA^{mRFP}$, Fig. 43A), GluRIIA-only ($IIA^{GFP}&IIA^{mRFP}$, Fig. 43B) and GluRIIB-only ($IIB^{GFP}&IIB^{mRFP}$, Fig. 43C) NMJs. At $IIB^{GFP}&IIA^{mRFP}$ and $IIA^{GFP}&IIA^{mRFP}$ NMJs, the PSD size distribution was similar with a slight and significant shift towards higher PSD size at GluRIIA-only NMJs ($p=0.014$). GluRIIB-only NMJs (Fig. 43C), however, exhibited an untypical PSD size distribution, with two maxima, one at lower and one at larger PSD size (mean PSD size: $IIB^{GFP}&IIA^{mRFP}$, $0.323\pm 0.008\mu m^2$,

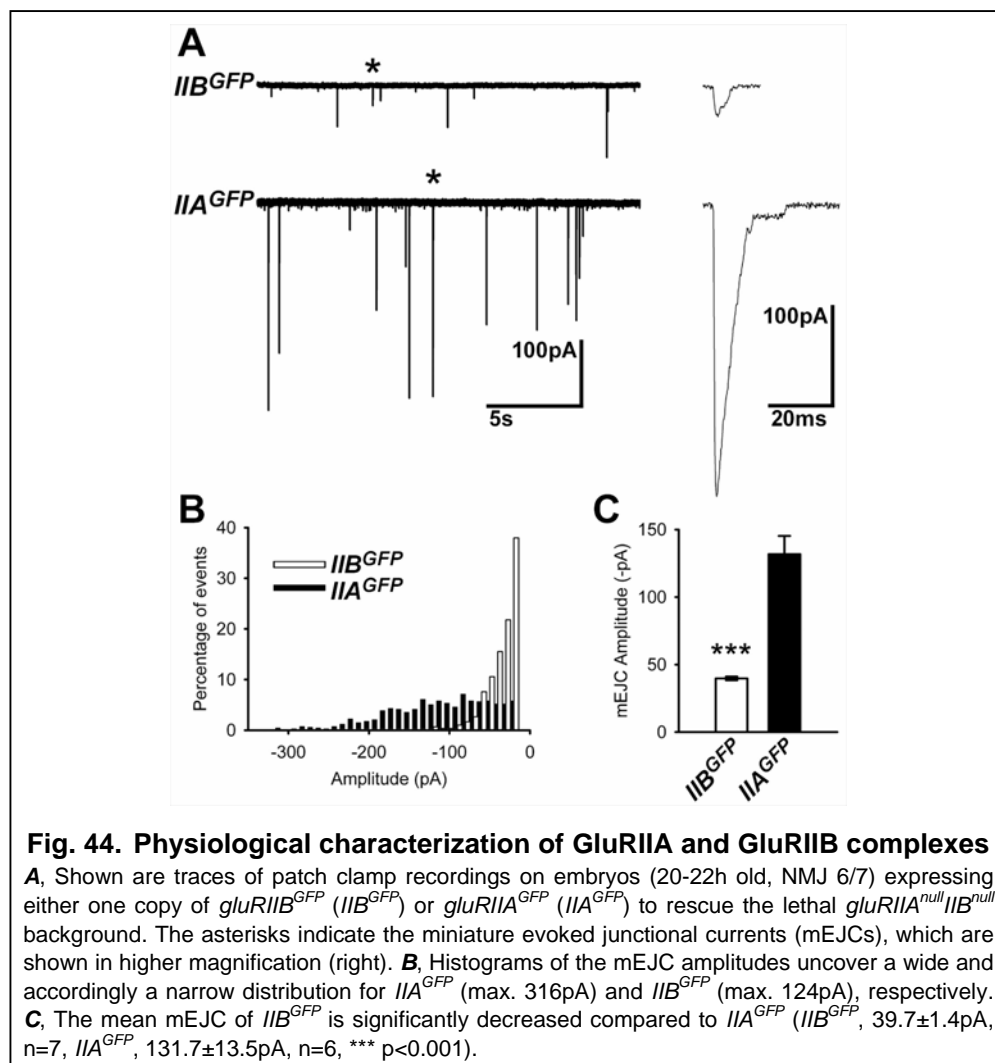
$n=505$, 8NMJs, $IIA^{GFP}&IIA^{mRFP}$, $0.346\pm 0.007\mu\text{m}^2$, $n=559$, 8NMJs, $IIB^{GFP}&IIB^{mRFP}$, $0.325\pm 0.010\mu\text{m}^2$, $n=433$, 9NMJs). The mean PSD size was as well significantly reduced compared to $IIA^{GFP}&IIA^{mRFP}$ ($p=0.010$). These data are interesting in the light of the observation that $IIB^{GFP}&IIA^{mRFP}$ larvae showed a population of particularly small GluRIIB-rich synapses (Fig. 37D, table).

Finally, PSD growth dynamics were analyzed. The relation of PSD growth to the initial PSD size appeared similar between $IIB^{GFP}&IIA^{mRFP}$ (Fig. 43A) and $IIA^{GFP}&IIA^{mRFP}$ (Fig. 43B) NMJs, with PSD growth dropping steeply with increasing PSD size. In contrast, a less pronounced drop of PSD growth could be observed at GluRIIB-only NMJs (Fig. 43C). In result, linear regression analysis indicated a larger maximum PSD size (after extrapolation) in this situation. Thus, while initial PSD growth is delayed in the absence of GluRIIA, with many small PSDs accumulating, the stop of PSD growth at a definite size seems defective in this situation as well. In other words, GluRIIA apparently fulfills two functions, promoting growth of nascent PSDs, and mediating a stop of further PSD growth once a sufficient PSD size has been reached. In the absence of GluRIIA, the number of PSDs per NMJ is reduced (Fig. 34H) and cannot be any longer adapted on different needs (Sigrist et al., 2003).



4.3.8. *GluRIIA* dominates synaptic transmission

Above it was shown that during larval NMJ development, PSDs grew to a defined size and, simultaneously, PSD receptor composition converged towards a balanced ratio of GluRIIA and GluRIIB. The question remains whether this behavior was solely explained by a “biochemical” assembly principle, or whether also the physiological properties of these receptor assemblies might be relevant here. Previously, both NMJ glutamate receptor complexes were shown to differ strongly in transmission (DiAntonio et al., 1999; Chen and Featherstone, 2005). In single channel recordings of extrasynaptic receptors, GluRIIB complexes desensitized about 10-fold faster than GluRIIA complexes (DiAntonio et al., 1999). Moreover, genetic elimination of GluRIIA (Petersen et al., 1997; Reiff et al., 2002) or over-expression of GluRIIB (DiAntonio et al., 1999) drastically reduces spontaneous responses, being a measure for the glutamate-gated ionic conductance at individual PSDs.



In order to measure spontaneous synaptic PSD currents with ideal signal-noise ratio from either GluRIIA-only or GluRIIB-only NMJs, embryonic muscles were subjected to patch clamp recording (see 3.4.1). In fact, spontaneous currents at GluRIIA-only PSDs were more than threefold higher than at GluRIIB-only PSDs (Fig. 44A,B,C; IIB^{GFP}, 39.7±1.4pA, n=7, IIA^{GFP}, 131.7±13.5pA, n=6, p<0.001). Thus, the remarkable differences in eEJCs between GluRIIA-only and GluRIIB-only NMJs (see Fig. 34C,D) are to a large extent due to an enormous difference in the conductance of synaptic GluRIIA and GluRIIB channels. Balancing the receptor composition of the PSD might therefore be important to normalize conductance during PSD maturation. The specific PSD conductance might in turn contribute to regulate the differential incorporation of the two glutamate receptor complexes. Insufficient conductance might stimulate incorporation of the high conductance species (GluRIIA) and vice versa high conductance due to mature GluRIIA content might stop further GluRIIA and favor GluRIIB incorporation.

4.3.9. *GluRIIA* PSD content is selectively enhanced after blockade of presynaptic glutamate release

If postsynaptic conductance was involved in the differential receptor incorporation, an interference with presynaptic glutamate release could affect the receptor composition of PSDs. Thus, mosaic presynaptic expression of tetanus toxin light chain (TNT) using *ok319-gal4* to suppress evoked glutamate release (Sweeney et al., 1995) was combined with *in vivo* imaging of GluRIIB^{GFP} and GluRIIA^{mRFP} (in *gluRIIA^{null}IIB^{null}* background) (Fig. 46A IIB^{GFP}&IIA^{mRFP}, NMJ 14; Fig. 46B: IIB^{GFP}&IIA^{mRFP} + *ok319-tnt*). As *ok319-gal4* did not express in the motoneuron innervating muscle 27 (usually used in this study for *in vivo* imaging), NMJs of the ventral-longitudinal muscle 14 were analyzed for this experiment (Fig. 45).

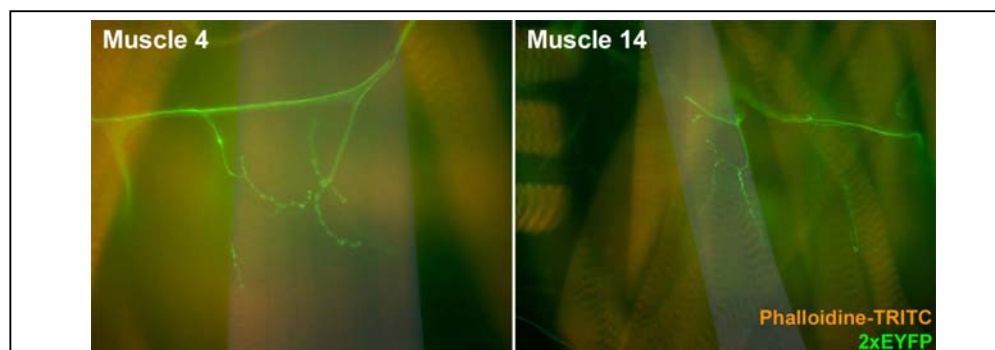
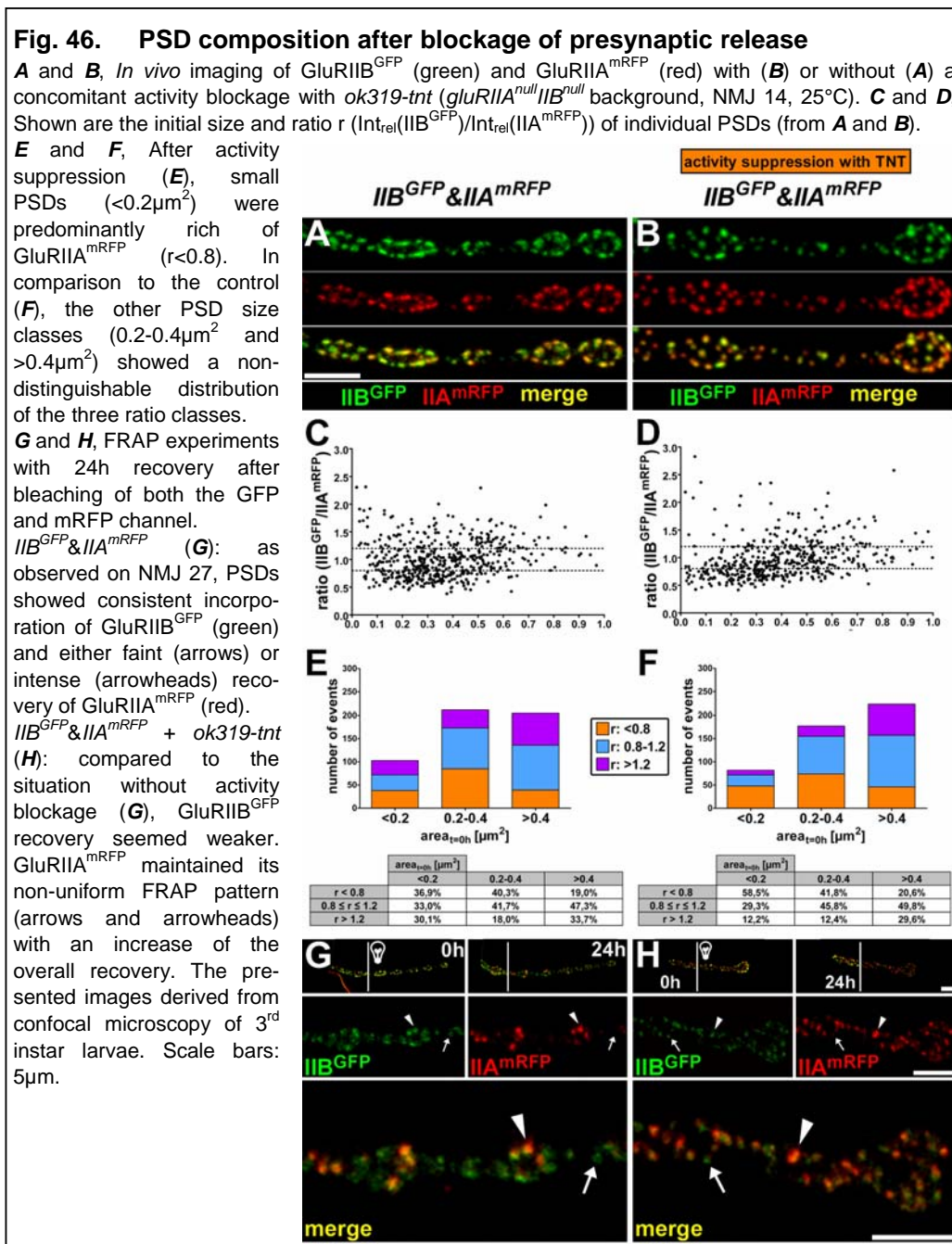


Fig. 45. Expression pattern of *ok319-gal4*

Phalloidine (TRITC-coupled, orange) staining of 3rd instar larvae expressing 2xEYFP (green) ectopically with the *ok319-gal4* driver. *ok319-gal4* showed presynaptic expression at the NMJ of the ventral-longitudinal muscle 4 (as well as at the NMJs 6/7 and 12/13, not shown) and of the ventral-oblique muscle 14 but not of the ventral-acute muscle 27 (not shown).

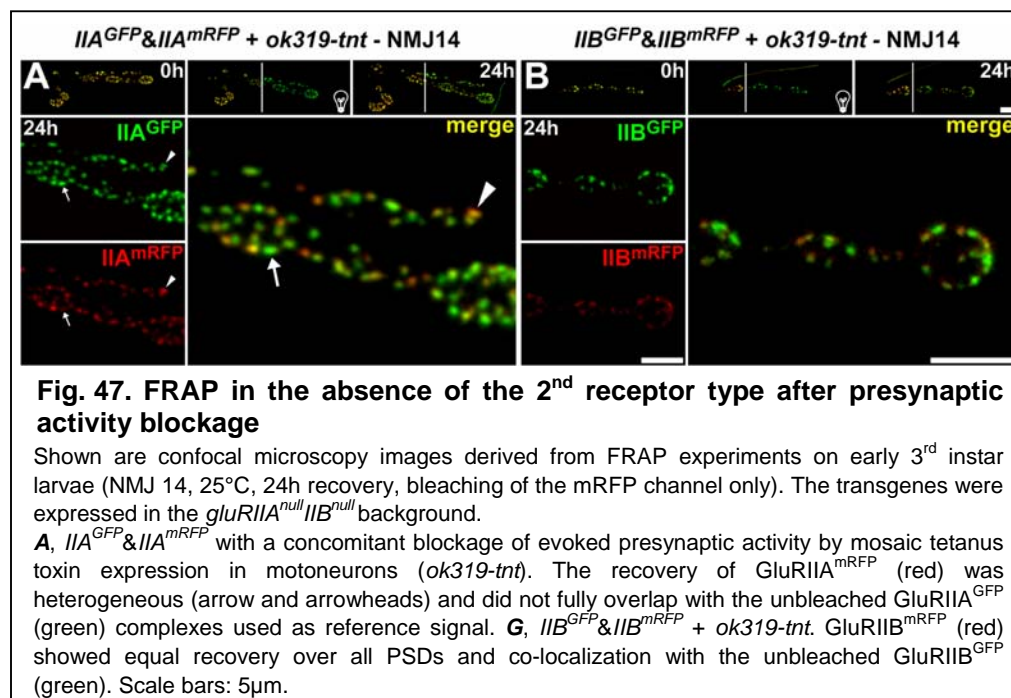
PSDs were classified according to their size and receptor composition (ratio r). At TNT expressing NMJs (Fig. 46B,D,F), small PSDs ($<0.2\mu\text{m}^2$) were particularly rich of GluRIIA^{mRFP} ($r < 0.8$), while the receptor composition at medium and large PSDs ($0.2\text{--}0.4\mu\text{m}^2$ and $>0.4\mu\text{m}^2$) appeared essentially unaffected compared to controls (Fig. 46A,C,E). To see whether a difference in GluRIIA incorporation was responsible, again FRAP experiments were performed.



At the control NMJs (Fig. 46G), recovery of GluRIIA^{mRFP} was very faint at a large fraction of PSDs but very intense at a few PSDs while GluRIIB^{GFP} exhibited uniform

FRAP, as typically observed throughout this study (Fig. 38, Fig. 39A,C, Fig. 40A). However, more PSDs appeared to efficiently incorporate GluRIIA^{mRFP} at TNT expressing NMJs (Fig. 46H), also obvious after quantitative analysis (Fig. 39E), which uncovered a rather Gaussian-like recovery distribution (fit value: 0.963). For GluRIIB^{GFP} an atypically low Gaussian fit (fit value: 0.892) could be observed. This can be explained by the reduced FRAP, which was often below the detection threshold (corresponding to a recovery rate of about 40%).

Further FRAP experiments addressed whether the influence of TNT expression was also obvious at GluRIIA-only (*IIA^{GFP}&IIA^{mRFP} + ok319-tnt*, Fig. 47A) or GluRIIB-only NMJs (*IIB^{GFP}&IIB^{mRFP} + ok319-tnt*, Fig. 47B). Again, FRAP of GluRIIA^{mRFP} appeared slightly stronger than in non-TNT expressing controls (Fig. 41A), whereas recovery of GluRIIB^{mRFP} appeared unchanged or even weaker in comparison to controls (Fig. 41B). As before, also in the presence of TNT GluRIIA and GluRIIB incorporation behavior appeared unaffected by the absence of the respective other receptor complex type.



So far, the data indicate that suppression of glutamate release and thus ionic conductance provokes a further incorporation of GluRIIA, leading to increased GluRIIA content particularly at small immature PSDs. Increased incorporation of GluRIIA in turn should provoke an increase in PSD growth (Rasse et al., 2005). In fact, after TNT expression (Fig. 46H), the mean PSD size (resulting from a maximum overlay of both GluRIIA^{mRFP} and GluRIIB^{GFP}) was significantly increased (Fig. 48C,

IIB^{GFP}&IIA^{mRFP}, NMJ14, $0.362 \pm 0.008 \mu\text{m}^2$, $n=519$, 9 NMJs, *IIB^{GFP}&IIA^{mRFP} + ok319-tnt*, $0.402 \pm 0.010 \mu\text{m}^2$, $n=482$, 8 NMJs, $p=0.0034$). Finally, GluRIIA and GluRIIB were also visualized by antibody stainings (Fig. 48A,B) using a different NMJ (NMJ 4, which also shows *ok319-gal4* expression, see Fig. 45). In fact, the GluRIIA level per PSD was increased while GluRIIB remained unchanged after TNT expression (Fig. 48C; GluRIIA: wild type, $126.3 \pm 3.5 \text{ a.u.}$, *ok319-tnt*, $149.3 \pm 9.6 \text{ a.u.}$, $p=0.028$; GluRIIB: wild type, $140.8 \pm 7.6 \text{ a.u.}$, *ok319-tnt*, $145.0 \pm 13.6 \text{ a.u.}$, $p=0.96$; $n=8$; see 3.3.5.5). Thus, suppression of presynaptic release provoked a specific increase in GluRIIA content and PSD size.

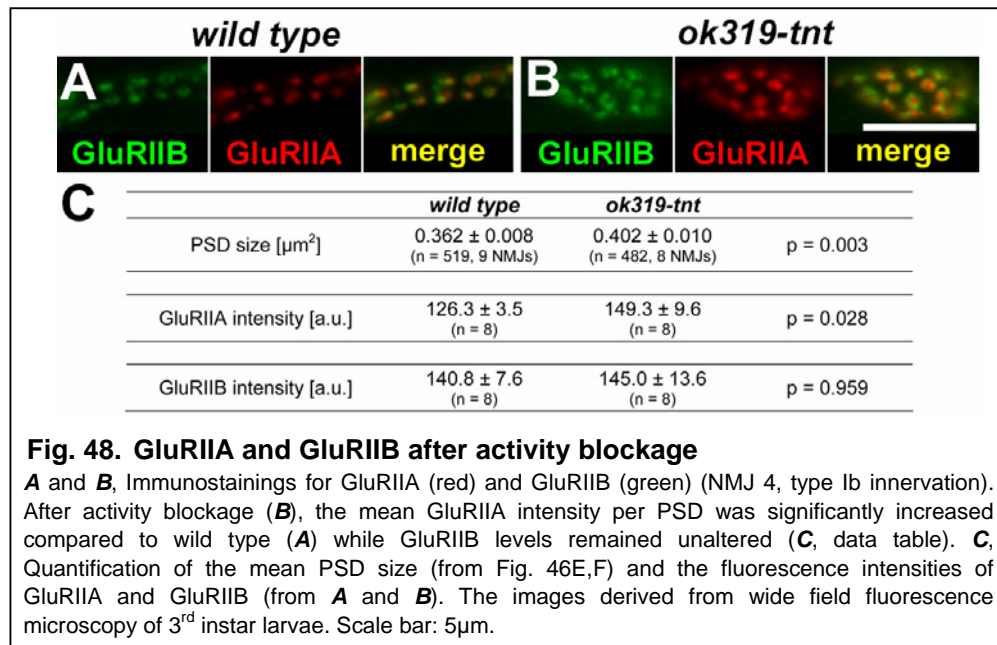


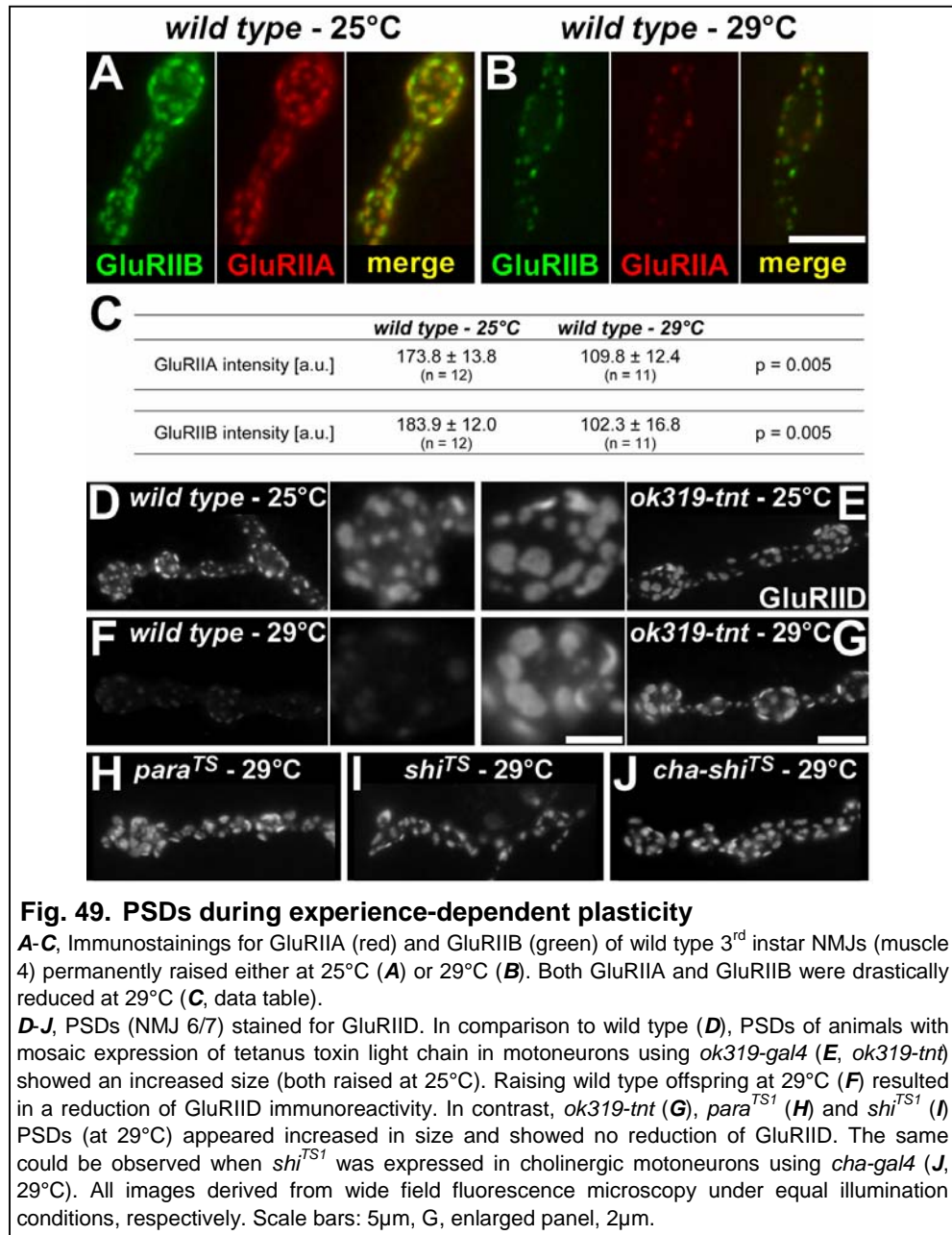
Fig. 48. GluRIIA and GluRIIB after activity blockage

A and **B**, Immunostainings for GluRIIA (red) and GluRIIB (green) (NMJ 4, type Ib innervation). After activity blockage (**B**), the mean GluRIIA intensity per PSD was significantly increased compared to wild type (**A**) while GluRIIB levels remained unaltered (**C**, data table). **C**, Quantification of the mean PSD size (from Fig. 46E,F) and the fluorescence intensities of GluRIIA and GluRIIB (from **A** and **B**). The images derived from wide field fluorescence microscopy of 3rd instar larvae. Scale bar: $5 \mu\text{m}$.

4.3.10. Receptor content per PSD can be down-regulated to allow the formation of additional synapses during experience-dependent plasticity

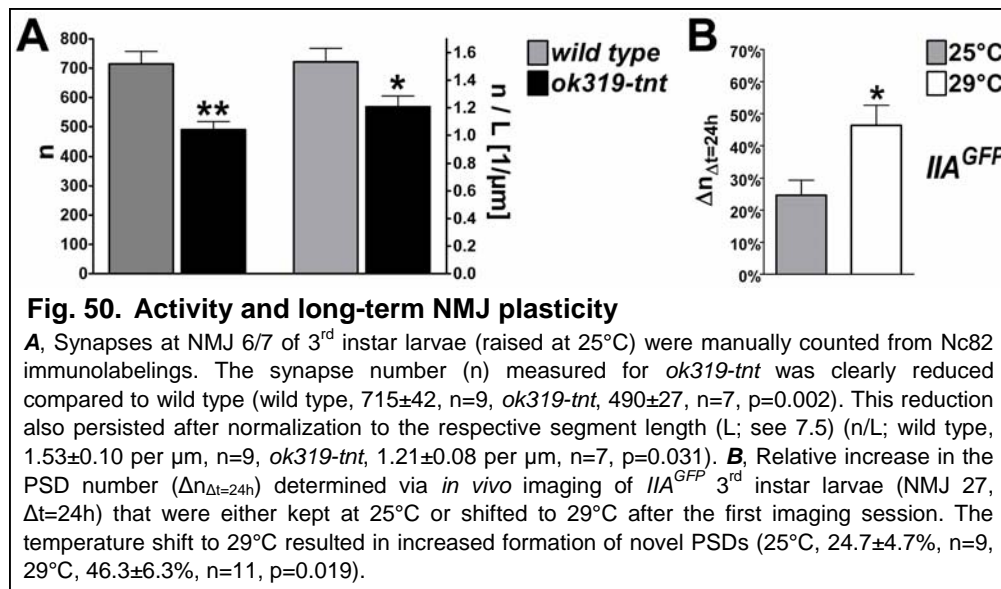
Finally, the question was addressed how glutamate receptor content per PSD would be organized when the NMJ as a system was challenged towards producing additional synapses. Previously, it was shown that an elevation of the environmental temperature is associated with increased locomotion (Sigrist et al., 2003). Thereby, the number of synaptic boutons and the NMJ transmission strength was shown to be considerably increased (Sigrist et al., 2003; Zhong and Wu, 2004). Interestingly, antibody stainings of wild type NMJs (muscle 4) exhibited an accompanying drastic reduction of both GluRIIA and GluRIIB levels at PSDs when the temperature was shifted from 25°C (Fig. 49A) to 29°C (Fig. 49B) (Fig. 49C; GluRIIA: 25°C , $173.8 \pm 13.8 \text{ a.u.}$, $n=12$, 29°C , $109.8 \pm 12.4 \text{ a.u.}$, $n=11$, $p=0.005$; GluRIIB: 25°C ,

183.9±12.0a.u., n=12, 29°C, 102.3±16.8a.u., n=11, p=0.005). Despite the coordinated reduction of both GluRIIA and GluRIIB, the amplitude of miniature excitatory currents is not significantly altered (Sigrist et al., 2003). This regulation might either be mediated by changes in postsynaptic conductivity, e.g. by posttranslational modifications of GluRIIA complexes or changes in the per vesicle glutamate content (Steinert et al., 2006) (see discussion).



The down-regulation of glutamate receptor levels at PSDs following experience-dependent plasticity was equally present in immunostainings for the subunit GluRIID, likely to be part of both GluRIIA and GluRIIB complexes (Fig. 34B). PSDs (NMJ 6/7)

of animals consistently raised at 29°C (Fig. 49F) showed strongly reduced levels of GluRIID compared to the 25°C control (Fig. 49D). To address whether this reduction was mediated by the temperature increase and the associated potentiation of presynaptic release (Sigrist et al., 2003), several situations of affecting (predominantly) evoked vesicle release at presynaptic NMJ terminals were examined. Expression of tetanus toxin light chain with the mosaic motoneuron driver *ok319-gal4* (*ok319-tnt*) (Sweeney et al., 1995) at 29°C (Fig. 49G) did not result in diminished glutamate receptor levels compared to 25°C (Fig. 49E). Compared to wild type, PSDs at *ok319-tnt* NMJs appeared clearly increased in size. Similarly, paralytic mutants *para^{TS1}* (*para* encodes a functionally predominant class of sodium channels in *Drosophila* neurons) (Loughney et al., 1989) raised at 29°C (Fig. 49H) did not exhibit a reduction in glutamate receptor density at PSDs. An identical finding could be obtained when temperature-sensitive, dominant-negative Dynamin (*UAS-shi^{TS1}*) was expressed at 29°C in cholinergic neurons upstream of motoneurons with the *cha-gal4* driver (*cha-shi^{TS1}*, Fig. 49J) (Salvatterra and Kitamoto, 2001). In addition, the PSD size tended to be increased compared to wild type (Fig. 49F) when both spontaneous and evoked transmission were impaired raising *shi^{TS1}* animals at 29°C (Fig. 49I) (Koenig et al., 1983).



Finally, the overall synapse number of wild type and *ok319-tnt* NMJs was compared (NMJ 6/7, 25°C). After activity blockage with TNT the synapse number was significantly decreased in comparison to the wild type control (Fig. 50A; for data see legend). In contrast, it was reported previously (Sigrist et al., 2003; Zhong and Wu, 2004) that NMJs of wild type larvae reared at 29°C harbored significantly more synapses than the 25°C controls. To study acute effects of elevated temperature and

with its activity on synaptic growth, *IIA^{GFP}* larvae (*gluRIIA^{GFP}* expressed in the *gluRIIA^{null}IIB^{null}* background) were subjected to *in vivo* imaging (NMJ 27). After the first imaging session the larvae were either kept at 25°C or shifted to 29°C until the second time point (24h later). For both time points the PSD number was determined and the relative increase in the PSD number ($\Delta n_{\Delta t=24h}$) was calculated. Notably, NMJs of animals shifted to 29°C produced nearly twice as many novel PSDs (Fig. 50B; $\Delta n_{\Delta t=24h}$, 25°C, 24.7±4.7%, n=9, 29°C, 46.3±6.3%, n=11, p=0.019).

In summary, an increase in the raising temperature (from 25°C to 29°C) provoked a drastic down-regulation of glutamate receptor levels that was obviously mediated by potentiated presynaptic activity. Going along with the decreased glutamate receptor density per PSD, more novel PSDs could be established. Contrary to it, activity suppression did not reduce but rather elevated the glutamate receptor number per PSD. Moreover, the number of PSDs per NMJ was clearly decreased. Thus, glutamate receptor levels at PSDs, the final PSD size and the overall number of synapses forming seem to be regulated by presynaptic activity.

5. Discussion

5.1. Non-NMDA type glutamate receptors are essential for maturation but not for initial assembly of synapses at *Drosophila* NMJs

A detailed molecular and cell-biological insight into the formation of glutamatergic synapses is important for understanding the development of excitatory neuronal circuits and also the process of long-term information storage in the CNS (Chklovskii et al., 2004). So far, studies on cultivated brain neurons analyzed mechanisms of glutamate receptor trafficking during synapse formation and have suggested a temporal sequence of pre- and postsynaptic assembly (Washbourne et al., 2002; Gundelfinger et al., 2003; Bresler et al., 2004). However, whether in turn the process of incorporating glutamate receptors is needed for the establishment of synaptic structures was hardly addressed.

5.1.1. A transmission independent role of glutamate receptors in postsynaptic maturation

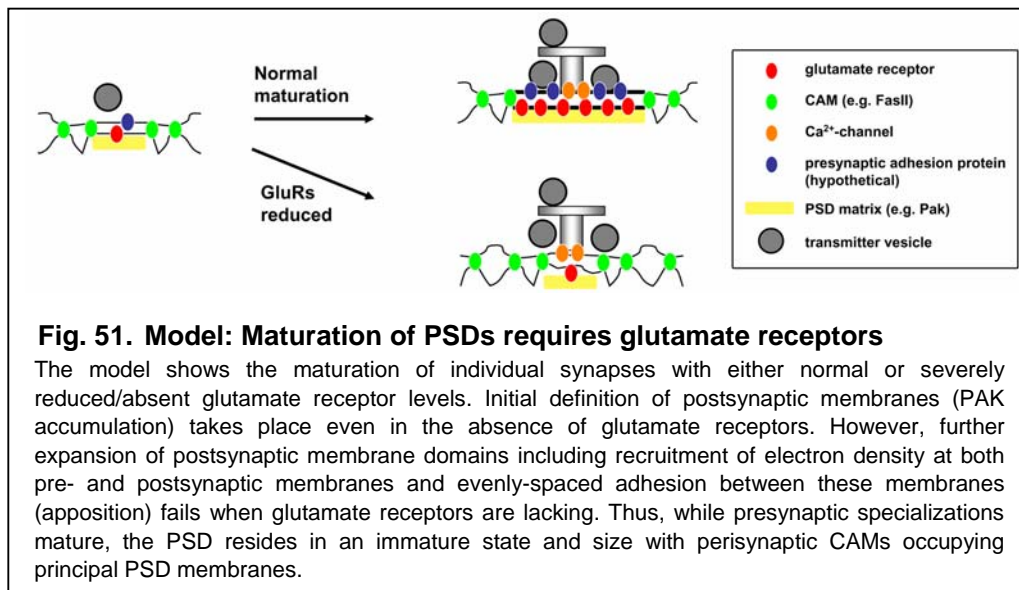
The relationship between neurotransmitter receptor incorporation and synapse assembly was addressed by genetically reducing or eliminating the expression of all neurotransmitter receptors at a certain synapse type. Consequences of eliminating *all* postsynaptic glutamate receptors expressed at a specific glutamatergic synapse had not been described previously. Here it was shown that a lack of glutamate receptors provoked a specific block in the molecular and ultrastructural maturation of PSDs.

Notably, loss of transmission due to the loss of glutamate receptor complexes seemed not involved, based on the fact that neither blocking synaptic transmission (Fig. 26C,D,I,J) nor affecting glutamate binding by site-directed mutagenesis (Fig. 26K) did provoke similar defects. Thus, consistent with studies in other synaptic systems (Harris, 1980; Verhage et al., 2000; Baines et al., 2001; Misgeld et al., 2002; Varoqueaux et al., 2002; Heeroma et al., 2003) ionic transmission through the postsynaptic neurotransmitter receptors does not appear essential for principal synapse assembly. Instead, the data clearly imply that a critical level of glutamate receptor *protein* is needed to allow synapse maturation.

5.1.2. Ultrastructural and molecular maturation of NMJ synapses requires glutamate receptors

A model for the maturation of individual NMJ synapses in either presence or absence of postsynaptic glutamate receptors is given in Fig. 51. At glutamate receptor deprived synapses, synaptic vesicles appeared normally distributed, and

their activity mediated release appeared increased, likely as part of a compensation for reduced postsynaptic sensitivity. Moreover, functional active zones with presynaptic dense bodies still formed. Thus, active zones still assemble when the mature organization of synaptic membranes (“tight planar apposition”) is not established. Consistently, previous work had shown that the formation of presynaptic dense bodies persisted even after genetic elimination of postsynaptic muscle cells (Prokop et al., 1996). On the contrary, active zone formation is severely affected in *bruchpilot* mutants, while the pre- and postsynaptic membranes remain tightly apposed (Kittel et al., 2006; Wagh et al., 2006).



At developing NMJs, newly forming “nascent” PSDs are characterized by small GluRIIA accumulations strictly co-localized with PAK kinase (Rasse et al., 2005). Even in the complete absence of glutamate receptors (*IIC^{null}* or *IIA^{null}IIB^{null}*, Fig. 25E,F), postsynaptic PAK patches, as typical for small nascent synapses still formed, indicating that principal cues for the definition of postsynaptic membrane patches persisted in this situation. Nonetheless, these PAK patches consistently failed to reach mature size (Fig. 23J,K). PAK, which mediates effects of Rho-GEF dPIX has been implicated in postsynaptic maturation, with PAK mutants showing a partial depletion of GluRIIA, and reduced SSR formation. However, neither *pak* nor *dpix* mutants have so far been reported to show defects in synaptic membrane apposition (Parnas et al., 2001; Albin and Davis, 2004). Thus, postsynaptic differentiation is not completely blocked in the absence of glutamate receptors. Instead, two postsynaptic “assembly modules” (PAK/dPIX signaling and glutamate receptor localization) appear only partly dependent on each other, with glutamate

receptor localization being essential for PSD maturation but not for initial PSD assembly.

At the cholinergic mouse NMJ, genetic deletion of the adult acetylcholine receptor subunit ϵ (AChR ϵ) led to severely reduced AChR density. Notably, a profound reorganization of AChR-associated components of the postsynaptic membrane and cytoskeleton was observed in this situation (Missias et al., 1997).

5.1.3. Glutamate receptor complexes and synaptic cell adhesion

Synaptic membranes are electron-dense and apposed to each other leaving a cleft of consistent width, likely essential for robust timing and efficacy of neurotransmission. In contrast, perisynaptic membranes are less electron-dense and tend to undulate. At NMJs lacking glutamate receptors, FasII/Dlg complexes ectopically remained at synaptic sites and membranes now appeared undulated, indicating perisynaptic type of membrane adhesion. Thus, glutamate receptors seem essential to establish the type of membrane adhesion found at the synapse, whereas usually perisynaptic adhesion molecules as FasII mediate a qualitatively different type of membrane adhesion. Notably, undulation of perisynaptic membranes was impaired at NMJs lacking glutamate receptors leading to a less developed SSR (Fig. 24D,K; Fig. 27G). Moreover, boutons often appeared atypically round (Fig. 24C; Fig. 27D,E), further indicating that membrane-membrane adhesion is fundamentally affected at NMJ terminals lacking glutamate receptors.

Several classes of cell adhesion molecules (CAMs) have been implicated in mediating membrane adhesion at synapses, particularly trans-synaptic neurexin-neurologin pairs and cadherins (Murthy and De Camilli, 2003). The specific contributions of these synaptic CAMs during initial synapse assembly and maturation are under intense investigation. The data are consistent with the idea that the C-terminal, intracellular domains of glutamate receptors might engage in interactions with other PSD components, which in turn cluster postsynaptic CAM-type membrane proteins. These would then mediate interactions to cluster presynaptic CAMs or bind components of the extracellular matrix to allow synaptic membrane apposition (Fig. 52). Alternatively, direct interactions of glutamate receptors with other membrane protein complexes, as recently demonstrated for Stargazins/TARPs (Osten and Stern-Bach, 2006), might be involved.

So far, no CAM single mutant has been reported to provoke a defect in synaptic membrane apposition as severe as the one observed here for glutamate receptor mutant situations. Thus, multivalent interactions of the heterotetrameric glutamate

receptor complexes as well as the redundant involvement of several CAM species might occur.

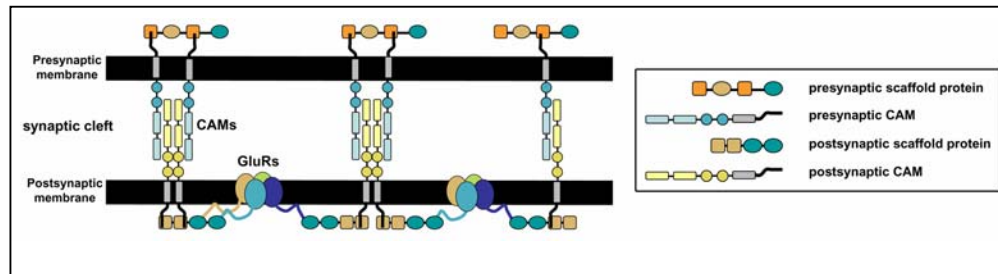


Fig. 52. Model: Transsynaptic interactions instructed by intracellular interactions of glutamate receptors

Intracellular domains of glutamate receptors interact to other PSD scaffold proteins, which in turn cluster postsynaptic CAM-type membrane proteins. Transsynaptic interactions of postsynaptic CAMs with presynaptic CAMs result in linear synaptic membrane apposition. Multivalent interactions of heterotetrameric glutamate receptor complexes might stabilize such an interaction network.

5.1.4. Glutamate receptor levels in control of synapse formation

PAK labeling suggested that initial steps in defining postsynaptic membranes persisted even in the total absence of glutamate receptors, while these initial assemblies could not mature on the ultrastructural level when glutamate receptors were lacking. Recently, *in vivo* imaging of photo-labeled GluRIIA at the developing NMJ uncovered that newly forming PSDs in fact grow by a continuous incorporation of glutamate receptors, whereby the accumulation of presynaptic active zone material (BRP) appeared slightly delayed. Thereby, the entry of GluRIIA - likely derived from cell wide plasma membrane pools via lateral diffusion - directly correlated with PSD growth. Once glutamatergic PSDs reached a certain size, they stabilized and GluRIIA was essentially immobilized. In comparison, other postsynaptic proteins showed high turnover equally over all synapses (Rasse et al., 2005). This slow turnover of glutamate receptors is consistent with the view that multiple interactions of glutamate receptors set the core of a transsynaptic interaction matrix. Several lines of genetic and experience-dependent manipulations point towards a rate-limiting role of GluRIIA levels in NMJ synapse formation (Broadie and Bate, 1993; Reiff et al., 2002; Sigrist et al., 2002; Yoshihara et al., 2005). In summary, the available data suggest that incorporation of glutamate receptors might be a key event to allow further expansion of initial postsynaptic assemblies, finally leading to mature PSDs. Thereby, the overall level of glutamate receptors available in the muscle membrane might control the total number of synapses forming per NMJ (Rasse et al., 2005).

Understanding the plasticity processes taking place at glutamatergic synapses has been a focus of attention within cellular neuroscience. Hereby, rapid changes in

synaptic receptor number were reported to mediate plastic changes of synaptic transmission, often on the time scale of tens of minutes in mammalian preparations (Malinow and Malenka, 2002; Sheng and Kim, 2002; Brecht and Nicoll, 2003; Collingridge et al., 2004). Notably, however, a recent study indicated that the cycling of synaptic glutamate receptors needed 16 hours or more (Adesnik et al., 2005). Similar timing was observed for nicotinic acetylcholine and GABA receptors (Akaaboune et al., 2002; Thomas et al., 2005). Thus, parts of the synaptic glutamate receptor population might be needed to reside stably within the PSD to maintain synapse stability. In fact, only severe receptor deprivation interfered with proper postsynaptic assembly at the NMJ, suggesting that the glutamate receptor level should not fall below a certain critical threshold.

Notably, the extracellular domain of the mammalian AMPA receptor subunit GluR2 has been shown to increase the size and density of spines in hippocampal neurons, and to induce spine formation in GABAergic interneurons normally lacking spines (Passafaro et al., 2003). It will be interesting to see whether these structural roles of glutamate receptors have a common mechanistic denominator.

Different types of synapses differ strongly in the ultrastructural detail of their postsynaptic specializations. Thus, a typical neuron of our brain, acting as a postsynaptic partner for different types of presynaptic inputs, has to establish and maintain different postsynaptic architectures, suggesting the existence of “identity molecules” allowing the self-assembly of such architectures, and potentially a match with membrane cues of the presynaptic partner cell. Obvious candidates for such molecules are the postsynaptic neurotransmitter receptors themselves. This study is consistent with such a view.

5.2. Functional fluorophore-tagging of glutamate receptor subunits

The maturation of postsynaptic densities essentially involves glutamate receptors. Thereby, subunit-specific trafficking of AMPA receptors was shown to play a major role for the activation and the maintenance of synaptic transmission (Shi, 2001). At *Drosophila* NMJ synapses, the specific incorporation of GluRIIA-type complexes, which was tracked with C-terminally labeled GluRIIA, correlated with the respective growth of single PSDs (Rasse et al., 2005). The role of the second receptor subtype (containing the subunit GluRIIB) in the dynamic PSD maturation process had so far not been addressed.

All GFP fusions of mammalian AMPA receptors were produced by inserting EGFP directly after the signal peptide of the respective glutamate receptor subunit (Shi et al., 1999; Perestenko and Henley, 2003). However, the identical position within GluRIIA and GluRIIB proved to be non-functional. To screen for other possible N-terminal fusion sites, which would ease studying the role of the C-terminal domain, GluRIIA and GluRIIB were subjected to two independent approaches for functional fluorescence-tagging.

Both fusion approaches were deduced from a recent *in vitro* transposition screen performed for rat GluR1 (Sheridan et al., 2002). The first procedure implied a transformation of the *in vitro* transposition reaction to *Drosophila*. The random integration of an EGFP transposon into the genomic transgenes *gluRIIA* and *gluRIIB* resulted in numerous insertions within the respective coding region. However, only 8 of 50 (*gluRIIA*) and accordingly 9 of 22 (*gluRIIB*) clones met the correct reading frame. 42 and respectively 13 clones carried insertions out of frame or within introns. All in frame insertions, which were spread all over the protein (Fig. 29 and Fig. 30), proved to be non-functional (no rescue of the otherwise lethal *gluRIIA^{null}IIB^{null}* situation) and showed no detectable fluorescent signals. The negative outcome is likely based on the complex structure and function of non-NMDA glutamate receptor channels (see 2.2), involving subunit-specific interactions and conformational changes upon glutamate binding and ion gating.

Specific interactions within the N-terminal domains of the glutamate receptor subunits contribute to subunit dimerization (Madden, 2002). Therefore, all N-terminal EGFP fusions most likely impede receptor complex formation. Insertions within the ligand binding domain S1/S2 can effect the organization of the glutamate binding pocket, presumably resulting in enhanced ER retention or the abolishment of synaptic transmission (Grunwald and Kaplan, 2003). Furthermore, dimer and tetramer stabilization mediated by the ligand binding domain should as well be impaired (Horning and Mayer, 2004). In one case the EGFP interrupted the

transmembrane domain M2 destructing the hydrophobic character of the lipid bilayer. Two insertions within GluRIIB resided within the CTD about 50 amino acids from the very C-term (after AA 857 and 861). As demonstrated for GluRIIA, C-terminal truncation of 53 amino acids resulted in severe defects of the postsynaptic structure (*gluRIIA*^{ΔC53}, see 4.1.7), seemingly due to the disruption of C-terminal interactions to cell adhesion molecules. Likely, this is as well the case for *gluRIIB*^{GFP857 and 861}, bearing in mind that also receptor transport to the postsynaptic membrane could be inhibited.

In a second approach functional EGFP or ECFP fusion sites within rat GluR1 (Fig. 31) (Sheridan et al., 2002) were assigned to GluRIIA and GluRIIB. Thereby, the transposon based design of the EGFP fusion, including linker sequences and internal restriction sites, was imitated.

All four N-terminal insertions (*gluRIIA*^{GFP255 and 355} as well as *gluRIIB*^{GFP284 and 309}) resulted in non-functional proteins without any rescue capability or visible GFP signals. Interestingly, these sites allowed the formation of functional GluR1 homomers (Sheridan et al., 2002) despite the crucial role of the NTD for dimer and receptor complex formation (Madden, 2002). The fact that *Drosophila* NMJ glutamate receptors are thought to form heterotetramers consisting of four different subunits (Qin et al., 2005) could account for aberrations in the N-terminal 3D structure, which eventually prevent successful GFP fusion.

In contrast, *gluRIIB*^{GFP897}, with the EGFP insertion site analogue to *gluRIIA*^{GFP893}, which was already successfully used for *in vivo* imaging of glutamate receptor dynamics (Rasse et al., 2005), showed strong and synapse-specific expression. Moreover, neither the physiological properties nor the rescue capability of *gluRIIB*^{GFP897} could be discriminated from untagged *gluRIIB*. Furthermore, both *gluRIIAGFP*⁸⁹³ and *gluRIIBGFP*⁸⁹⁷ were shown to mediate previously described long-term plasticity effects at the NMJ (see 4.3.1) (Sigrist et al., 2002). However, although no obvious hints are existing, it cannot be completely excluded that especially C-terminal interactions involved in receptor transport (Malinow and Malenka, 2002) or stabilization of the postsynaptic structure (see 4.1.7) might be effected to a certain degree. In the end, GluRIIB^{GFP897} seems to represent a fully functional glutamate receptor subunit qualified for studies on subunit-specific glutamate receptor dynamics and their role in PSD formation and maturation.

5.3. Subunit-specific targeting of glutamate receptors organizes PSD formation and maturation

5.3.1. Subunit-specific glutamate receptor trafficking

Memory formation is thought to be accomplished by activity-dependent changes in neurotransmission. Thereby, alterations in synaptic strength as well as the formation of novel synaptic contacts are of importance. The most intensively studied forms of synaptic plasticity are long-term potentiation (LTP) and long-term depression (LTD), for which trafficking of glutamatergic AMPA receptors were shown to play a critical role (Malinow and Malenka, 2002; Song and Haganir, 2002). Here, developing glutamatergic *Drosophila* NMJ synapses were used to follow the dynamics of both heterotetrameric non-NMDA type glutamate receptor complexes expressed at individual postsynaptic densities. Functional fluorescence-tagging of the two different receptor subtypes, containing either GluRIIA or GluRIIB together with GluRIIC, GluRIID and GluRIIE (Marrus et al., 2004; Chen et al., 2005; Featherstone et al., 2005; Qin et al., 2005), in combination with the recently established *in vivo* imaging technique (Rasse et al., 2005), enabled the parallel visualization and quantification of both receptor complexes during larval PSD development. As shown before for the endogenous situation (Fig. 34A) (Marrus et al., 2004), tagged GluRIIA and GluRIIB type complexes, overlapped only partially at single PSDs, with especially small PSDs showing heterogeneous receptor content, however mainly dominated by GluRIIA (Fig. 35A, Fig. 37B). During the observation time of 12h (at 25°C rearing temperature) PSDs initially rich of GluRIIA specifically incorporated GluRIIB and vice versa, striving towards a balanced level of both receptor subtypes (Fig. 37C-F). Thereby, initial PSD size and further PSD growth showed an inverse relationship (Fig. 36). Performing FRAP experiments, it could be shown that the incorporation characteristics of GluRIIA and GluRIIB complexes into PSDs was fundamentally different. GluRIIA recovery was restricted to growing PSDs (Fig. 38) (Rasse et al., 2005). In contrast, GluRIIB showed uniform FRAP over all PSDs (Fig. 38). At the mammalian glutamatergic CNS synapse, similar dynamics for AMPA receptors were shown (Shi, 2001; Barry and Ziff, 2002). Following LTP induction, GluR1/2 complexes were specifically delivered to the postsynaptic plasma membrane to potentiate synaptic transmission. In contrast, the maintenance of synaptic transmission involved the constitutive recycling of GluR2/3 complexes independent of neuronal activity. Several studies showed that currents mediated by GluRIIA are the dominant component of transmission at the *Drosophila* NMJ synapse whereas GluRIIB currents are low (Petersen et al., 1997; DiAntonio et al., 1999; Reiff et al., 2002; Haghighi et al., 2003). Thereby, specific GluRIIA incorporation into growing

PSDs would result in long-term strengthening of synaptic transmission similar to the specific integration of GluR1 containing receptors underlying LTP. AMPA receptors at glutamatergic CNS were thought to traffic from intracellular stores to the cell surface within tens of minutes (Liao et al., 1995; Durand et al., 1996; Isaac, 2003). However, a recent study on native AMPA receptors, which are thought to be dimers of GluR1/2 and GluR2/3 dimers (Madden, 2002), suggested a time scale of at least 16h for an exchange of the synaptic AMPA receptor population (Adesnik et al., 2005). Similarly, it could be demonstrated that at *Drosophila* neuromuscular synapses glutamate receptor exchange is slow (maximally 80% fluorescence recovery after 24h), much slower than the FRAP of various other synaptic proteins (Rasse et al., 2005).

5.3.2. Factors controlling the differential trafficking of GluRIIA and GluRIIB

AMPA receptor complexes, being associated with a large protein network, the postsynaptic density, are targeted to the synaptic plasma membrane via subunit specific interactions. Thereby, various, mostly C-terminal interactions and phosphorylation (discussed below) were shown to be responsible for receptor trafficking. The transport of GluR1 containing complexes involves the specific interaction with SAP97, which can be detected already early in the secretory pathway (Sans et al., 2001). Moreover, the protein 4.1N is thought to link GluR1 complexes to the Actin cytoskeleton (Song and Huganir, 2002). GluR2 interactions are predominantly mediated by a PDZ motif at the very C-terminus. The PDZ proteins GRIP, ABP and PICK1 likely serve diverse functions in transport, clustering and endocytosis of GluR2/3 complexes (Malinow and Malenka, 2002). Additionally, NSF interaction to the cytoplasmic tail of GluR2 likely increases receptor surface expression (Luscher et al., 1999) and their resistance to endocytosis (Shi et al., 2001). Recent evidence also suggests that Stargazin is required for the surface expression of AMPA receptors (Chen et al., 2000). The molecular mechanisms underlying glutamate receptor trafficking at the *Drosophila* NMJ are largely unknown. Here, a fundamentally different incorporation behavior of the two NMJ expressed glutamate receptor complexes was demonstrated. While GluRIIA complexes were apparently immobilized at the postsynaptic membrane, GluRIIB complexes seemed to cycle continuously. Thereby, the C-terminal domain of GluRIIA was involved in the heterogeneous receptor complex incorporation (Fig. 39A,B), restricted only to growing PSDs (Rasse et al., 2005). In contrast, the CTD of GluRIIA was not sufficient to confer GluRIIA type FRAP behavior to GluRIIB (Fig. 39C,D). However,

no specific C-terminal interactions of GluRIIA or GluRIIB, which could orchestrate this differential incorporation, have been verified so far. Previous studies imply that the two receptor complexes are trafficked via independent pathways (and phosphorylation, see below). While synaptic expression of GluRIIA involves the protein 4.1N homologue Coracle (Chen et al., 2005), the MAGUK protein Dlg specifically alters synaptic GluRIIB levels (Chen and Featherstone, 2005). Furthermore, GluRIIA expression was shown to be controlled by local translation (Sigrist et al., 2000). Future work should shed more light on the numerous factors (more than 50 mutants affecting synaptic GluRIIA levels were presented recently) (Liebl and Featherstone, 2005) organizing receptor transport at the *Drosophila* NMJ.

5.3.3. Phosphorylation and receptor trafficking

The direct C-terminal phosphorylation of glutamate receptors plays an important role for the regulated receptor incorporation during LTD and LTP. Whereas CamKII phosphorylation of S831 on GluR1 is not necessary for AMPA receptor transport (Hayashi et al., 2000), PKA phosphorylation of S845 (Malinow and Malenka, 2002) and PKC phosphorylation of S818 (Boehm et al., 2006) were shown to be needed for synaptic delivery of GluR1 during LTP. During LTD, S845 (Lee et al., 2000) on GluR1 is dephosphorylated. Moreover, LTD induction goes along with PKC phosphorylation of S880 on GluR2, resulting in increased receptor internalization due to the lowered affinity for GRIP and ABP, but not for PICK1 (Chung et al., 2000). Furthermore, PKA phosphorylation of GluR4 was shown to be sufficient for synaptic incorporation of GluR4 containing complexes (Esteban et al., 2003). The *Drosophila* NMJ glutamate receptor subunits GluRIIA and GluRIIB contain various putative phosphorylation sites within the CTD. While GluRIIA harbors two potential PKA phosphorylation sites at S891 and S897 (see Fig. 28), no such motifs can be found within GluRIIB. Indeed, various studies associated GluRIIA incorporation with the cAMP second messenger pathway (see below) (Davis et al., 1998; Haghghi et al., 2003; Morimoto-Tanifuji et al., 2004). GluRIIB instead contains a PKC motif at the homologue position to S818 of GluR1, which was recently linked to synaptic delivery of GluR1/2 complexes (Boehm et al., 2006).

While at vertebrate glutamatergic CNS synapses Ca^{2+} influx into the postsynaptic cell occurs through NMDA receptor channels (Barry and Ziff, 2002), NMDA receptors were so far not described at the glutamatergic *Drosophila* NMJ synapses. Thus, the non-NMDA type glutamate receptors account for the Ca^{2+} influx (Chang et al., 1994), which activates the calmodulin-dependent cAMP cascade, at last resulting in activation of PKA. Thereby, the conductance of GluRIIB complexes, which show an

about ten times faster desensitization than GluRIIA containing channels but a comparable single-channel amplitude (DiAntonio et al., 1999; Chen and Featherstone, 2005), is virtually negligible, means probably Ca^{2+} influx predominantly occurs through GluRIIA complexes (Fig. 44). Ca^{2+} is intracellularly sensed by Calmodulin, which subsequently activates the adenylyl cyclase Rutabaga. Rutabaga converts ATP to cAMP, which in turn activates PKA. PKA is thought to specifically phosphorylate the CTD of GluRIIA but not GluRIIB, thereby controlling GluRIIA incorporation characteristics.

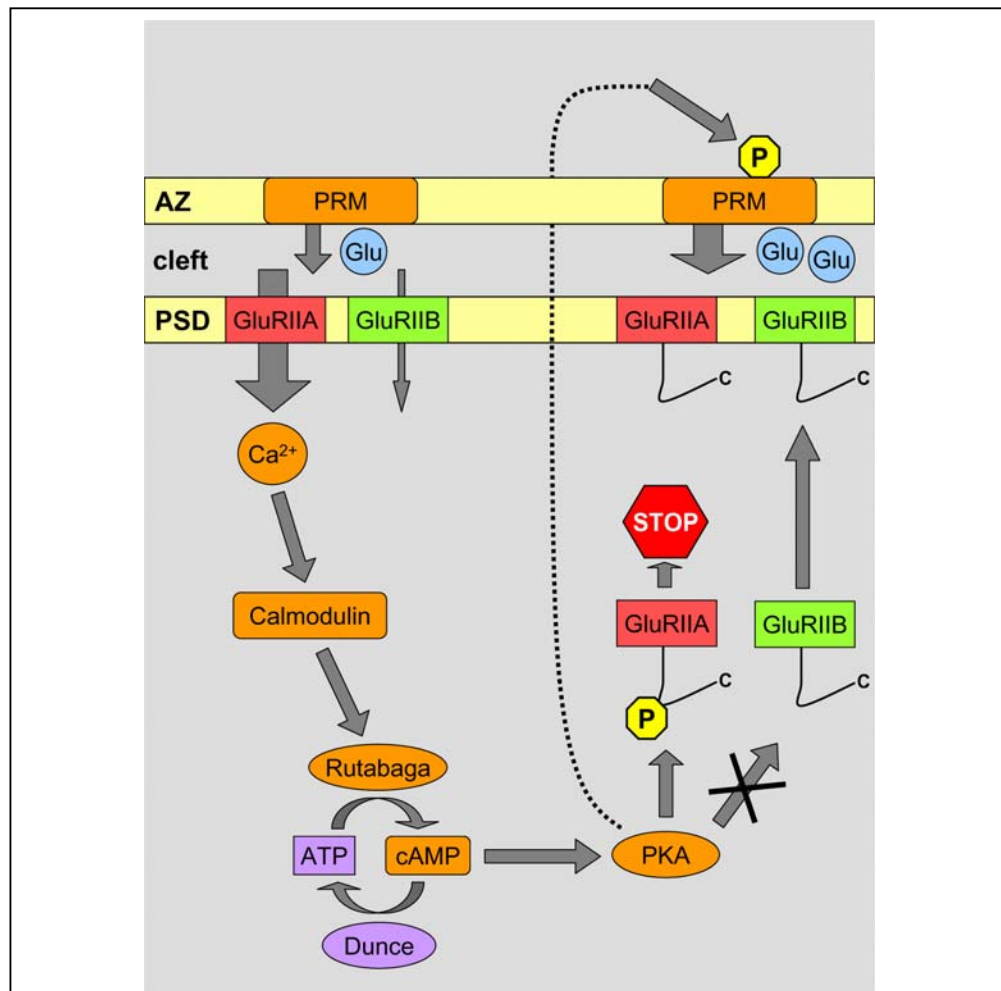


Fig. 53. Model: Differential glutamate receptor incorporation involves the cAMP cascade

GluRIIA complexes show an about 10-fold higher conductivity than GluRIIB and predominantly account for the Ca^{2+} influx into the postsynaptic muscle cell. Ca^{2+} is intracellularly sensed by Calmodulin, which activates the adenylyl cyclase Rutabaga. Rutabaga activation results in cAMP production, which in turn activates PKA. PKA phosphorylation of the GluRIIA CTD inhibits further incorporation of GluRIIA into mature PSDs. In contrast, GluRIIB is not sensitive to phosphorylation and incorporates uniformly over all PSDs. The retrograde PKA signal regulating presynaptic transmitter release is indicated by the dashed line. Abbreviations denote: PRM – presynaptic release machinery, P – phosphorylation, Glu – glutamate-filled synaptic vesicle.

Based on the presented model (Fig. 53), PSDs rich of GluRIIA complexes show substantial Ca^{2+} influx into the postsynaptic muscle cell. This results in high cAMP production, increased PKA activation and thus phosphorylation of GluRIIA, which inhibits further incorporation of GluRIIA complexes. In that way, a maximum conductance value of the whole PSD could be set. In contrast, PSDs rich of GluRIIB complexes show very low Ca^{2+} influx into the postsynaptic muscle cell, at last hardly resulting in GluRIIA phosphorylation. Thus, incorporation of (dephosphorylated) GluRIIA is favored, finally leading to a balanced level of both receptor subtypes at individual PSDs (Fig. 39C-F). A previous study on postsynaptic PKA supports this interpretation (Davis et al., 1998). Postsynaptic expression of a constitutively active form of PKA resulted in reduced quantal size going along with a retrograde increase in presynaptic transmitter release. Contrary to it, inhibiting PKA activity led to an increase in quantal size. In both cases the PKA-dependent modulation of the quantal size required the presence of GluRIIA, clearly indicating PKA regulation of GluRIIA trafficking. The retrograde modulation of synaptic transmission was also shown to be controlled by postsynaptic CamKII (Haghighi et al., 2003). Thereby, strong Ca^{2+} influx mediated by GluRIIA complexes results in CamKII autophosphorylation and activation which impedes the retrograde increase in presynaptic activity. A recent study implies that GluRIIA levels might be as well regulated by CamKII (Morimoto-Tanifuji et al., 2004). Postsynaptic CamKII overexpression on 1st instar NMJs resulted in slightly reduced GluRIIA immunoreactivity. Moreover, both pre- and postsynaptic expression of a constitutively active form of the alpha subunit of the heterotrimeric G protein (Gas), which positively regulates the activity of Rutabaga, resulted in strongly decreased synaptic GluRIIA levels (Renden and Broadie, 2003). However, the same phenomenon could be observed after genetic elimination of Gas, possibly mediated by compensatory activation of the cAMP cascade.

5.3.4. Activity-dependent PSD regulation – blocked neurotransmission

Synaptic vesicle release is supposed to trigger Ca^{2+} influx into the postsynaptic muscle cell (Guerrero et al., 2005), which seems to involve into glutamate receptor trafficking at the PSD. In the absence of neurotransmission the initial formation of neuronal circuits and synapses persists (Verhage et al., 2000; Baines et al., 2001; Varoqueaux et al., 2002; Heeroma et al., 2003). At the vertebrate NMJ, a cutback of activity resulted in increased nerve-terminal sprouting with varying effects on the end-plate length (Wilson and Deschenes, 2005). Moreover, fast internalization of acetylcholine receptors could be observed when neurotransmission was blocked (Akaaboune et al., 1999). Here, glutamatergic synapses at the *Drosophila* NMJ were

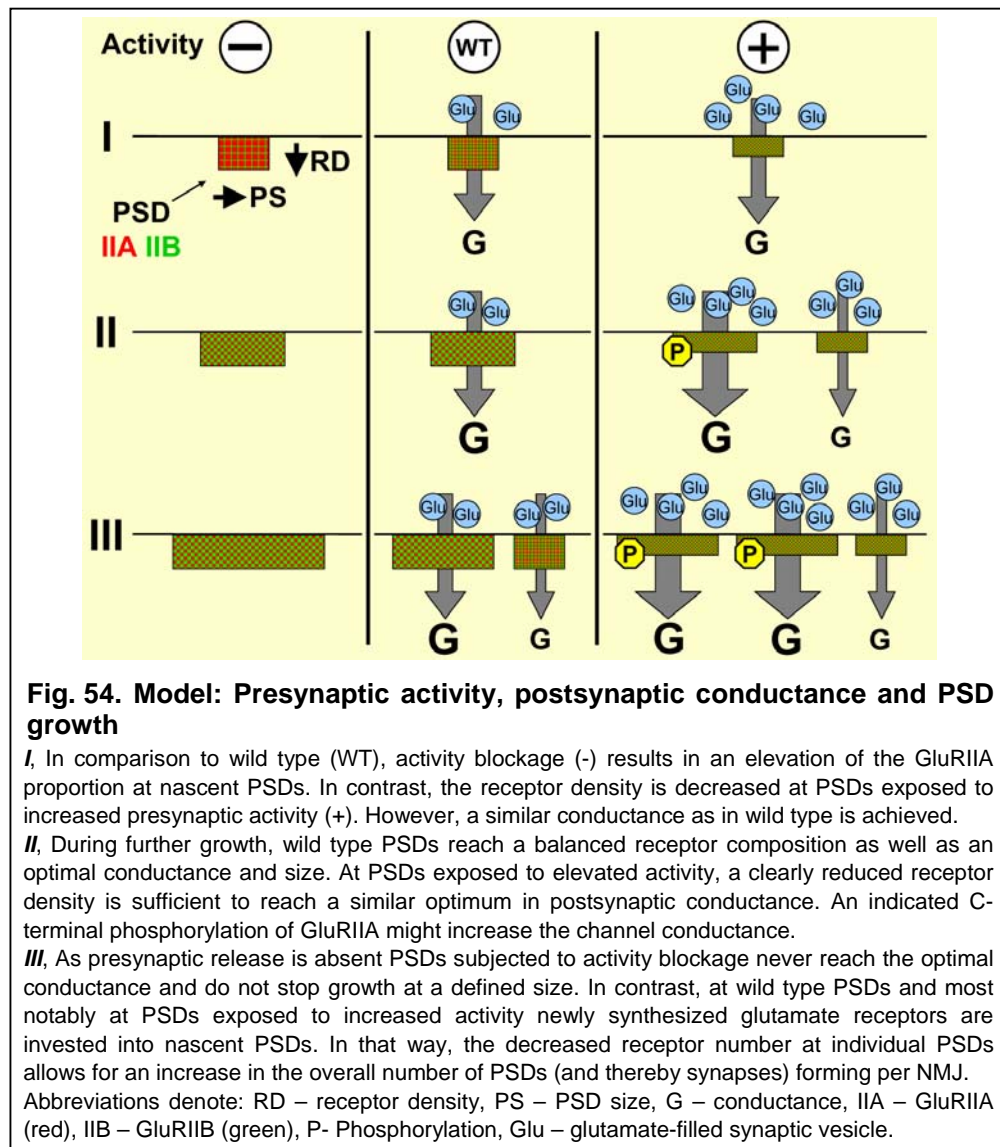
studied under activity suppression by mosaic TNT expression, which largely abolishes evoked junctional responses (Sweeney et al., 1995). *In vivo* imaging (Fig. 46A-F) and immunostainings (Fig. 48) showed that GluRIIA accumulation was increased, predominantly at small PSDs, while GluRIIB remained unaffected. Consistently, no reduction in synaptic glutamate receptor levels could be observed (Fig. 49E). Moreover, the average PSD size (determined via glutamate receptor abundance) was significantly increased after activity blockage (Fig. 48C).

A working model for the activity suppressed situation is provided in Fig. 54. The initial formation of PSDs subjected to activity blockage, is primarily dominated by GluRIIA accumulation. As nerve-evoked currents are absent, only residual miniature currents and non-vesicular glutamate release can account for some minimal Ca^{2+} influx. However, non-vesicular glutamate release, which was shown to regulate glutamate receptor levels and PSD size (Featherstone et al., 2002), had no obvious effects in this assay. Based on the above presented model (Fig. 53), Ca^{2+} influx is required for the activation of the cAMP cascade and receptor phosphorylation. Therefore, in the activity suppressed background GluRIIA would, as observed, no longer be restricted from incorporation into mature PSDs and show more uniform FRAP (Fig. 39E, Fig. 46H). As the synaptic transmission strength cannot reach mature status, receptors likely keep on incorporating, reflected in the increased PSD size (Fig. 48C). Similarly, in mutants for the adenylyl cyclase *Rutabaga* (Renger et al., 2000; Shayan and Atwood, 2000) the PSD size was strongly increased, further indicating a role of PKA phosphorylation for the limitation of PSD growth and receptor incorporation.

5.3.5. Activity-dependent PSD regulation – enhanced neurotransmission

Previously enormous morphological outgrowth of larval NMJs going along with potentiation of synaptic transmission was linked with an increase in the breeding temperature (Sigrist et al., 2003; Zhong and Wu, 2004). Similarly, activity elevation was shown to increase the nerve terminal and postsynaptic area at vertebrate NMJs (Wilson and Deschenes, 2005). Here, shifting the rearing temperature from 25°C to 29°C resulted in a dramatic reduction in the synaptic expression of both GluRIIA and GluRIIB complexes (Fig. 49A-C). In contrast, PSDs of activity suppressed larvae raised at 29°C showed no drop in receptor content (Fig. 49G-J). Interestingly, miniature currents measured at 29°C animals are not significantly altered, whereas both evoked currents and quantal content are increased (Sigrist et al., 2003). Consequently, a reduced number of glutamate receptors must account for

unchanged transmission strength at an individual synapse (Fig. 54), calling for a role of posttranslational modifications on channel function. Notably, GluRIIA levels were previously shown to be elevated (Sigrist et al., 2003) while here an enormous reduction at 29°C was observed. The answer to this problem could be different anti-GluRIIA antibodies. While the initially used antibody was generated against a C-terminal sequence of GluRIIA (likely in a dephosphorylated state; S. Sigrist, personal communication), the antibody used in this study was developed based on an extracellular epitope, which is independent of C-terminal phosphorylation.



Besides its role in receptor trafficking, phosphorylation involves as well into the regulation of the ion channel function. Phosphorylation of GluR1 at S831 and S845 during LTP was shown to potentiate the channel function, means either increasing the channel open probability or the conductance (Song and Huganir, 2002). While a

modulation of the channel conductance was mediated by PKA phosphorylation of S845 (Banke et al., 2000), the open probability can be modified by CamKII phosphorylation on S831 (Derkach et al., 1999). As mentioned above, GluRIIA harbors two putative PKA phosphorylation sites, while neither GluRIIA nor GluRIIB contain a homologous motif for CamKII phosphorylation (see Fig. 28). Accordingly, one possible mechanism could be that the two PKA sites serve to fulfill different roles. While phosphorylation of the first site might inhibit further GluRIIA incorporation into mature PSDs (Fig. 53), the second PKA site might involve into the modulation of the channel conductance (Fig. 54). However, both PKA sites are not necessary for the principal targeting of GluRIIA complexes to the postsynaptic membrane. After truncation of the last 17 amino acids of the GluRIIA C-terminal domain (*gluRIIA^{ΔC17}*) and thereby eliminating both putative PKA sites, synaptic glutamate receptor levels appeared unaltered compared to controls (see Table 3). Additional *in vivo* experiments are clearly required to certify the ultimate role of receptor phosphorylation. Basis for these future studies would be a luminal fluorophore fusion, which would allow studying C-terminal modifications with *in vivo* imaging. However, several attempts to produce functional luminal GFP fusions of GluRIIA were to no avail (see 4.2).

5.3.6. Physiological relevance of GluRIIA and GluRIIB complexes

Several previous studies have addressed the principal physiological properties of the two NMJ expressed glutamate receptor complexes. Thereby, as mentioned above, GluRIIA was shown to be predominantly responsible for the overall postsynaptic conductance (Petersen et al., 1997; DiAntonio et al., 1999; Reiff et al., 2002; Sigrist et al., 2002). Whereas the positive retrograde control of presynaptic release by PKA required the presence of GluRIIA (Davis et al., 1998), the negative control by CamKII was demonstrated for the *gluRIIA* mutant (Haghighi et al., 2003). However, both mechanisms are based on Ca^{2+} influx into the postsynaptic compartment, which is strongly dependent on GluRIIA levels. Notably, both *gluRIIA* and *gluRIIB* are redundant for viability (Petersen et al., 1997; DiAntonio et al., 1999; Marrus et al., 2004; Qin et al., 2005). Thus, the question remains what physiological relevance GluRIIB complexes have?

FRAP experiments in the respective absence of the other receptor subtype uncovered that the specific incorporation pattern of GluRIIA persisted (Fig. 41A) while GluRIIB kept on continuously recycling (Fig. 41B), obviously independent of the PSD status. However, differences in the development of the PSD sizes could be uncovered (Fig. 43). In the absence of GluRIIA, PSD growth was slower but

seemingly less limited. Consistently, an atypical size distribution with a majority of small PSDs was observed. PSDs solely expressing GluRIIA grew faster, matching the recent finding that GluRIIA incorporation is directly correlated to PSD growth (Rasse et al., 2005). Moreover, mere GluRIIA presence should support a faster convergence to the optimal conductance, thereby allocating more receptor complexes for the establishment of novel synaptic contacts (Fig. 55).

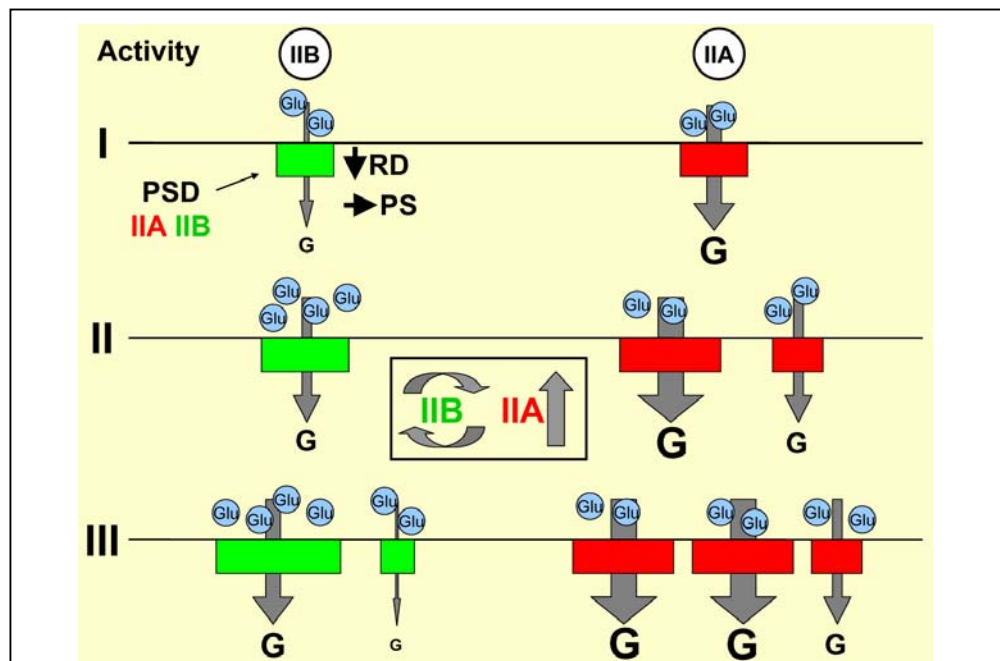


Fig. 55. Model: PSD growth in the sole presence of either GluRIIA or GluRIIB

I, Nascent PSDs at GluRIIB-only (IIB) NMJs tend to be smaller than PSDs at GluRIIA-only (IIA) NMJs. In comparison to GluRIIB, GluRIIA complexes feature a strongly increased conductance.

II, As GluRIIA incorporation directly correlates with PSD growth GluRIIA-only PSDs reach an optimal conductance, shutting down further GluRIIA incorporation at mature PSDs. In contrast, GluRIIB keeps continuously recycling independent of the PSD status.

III, In the sole presence of GluRIIB, PSDs hardly reach the optimal conductance. Thus, GluRIIB keeps on incorporating, with the final PSD size being less bounded above. Besides, the GluRIIB-only situation is accompanied by a compensatory increase in presynaptic transmitter release. At GluRIIA-only NMJs PSDs reach a standardized conductance and size. This size restriction increases the availability of GluRIIA for the establishment of novel PSDs. At GluRIIB-only NMJs novel PSDs form as well, however less frequently, reflected in a reduction in the number of synapses forming per NMJ.

Abbreviations denote: RD – receptor density, PS – PSD size, G – conductance, IIA – GluRIIA (red), IIB – GluRIIB (green), P- Phosphorylation, Glu – glutamate-filled synaptic vesicle.

Indeed, overexpression of GluRIIA (Sigrist et al., 2002) or absence of GluRIIB (Fig. 34) was shown to increase the number of synapses forming per NMJ. Similarly, an elevation of the raising temperature dramatically increased the bouton number and the overall NMJ transmission strength (Sigrist et al., 2003; Zhong and Wu, 2004). Here, it could be shown that in the absence of GluRIIB, means in an already potentiated background, more new PSDs formed after further activity enhancement

(rearing at 29°C, Fig. 50B). In contrast, activity suppression resulted in a reduction of synaptic contacts per NMJ (Fig. 50A). Thereby, a regulated interplay of glutamate receptor conductance and retrograde modulation of presynaptic release seems to define the PSD receptor composition, the PSD size and the number of synapses forming per NMJ. While for the most part GluRIIA complexes ensure the synaptic transmission, GluRIIB complexes might be responsible for the fine tuning of the pre- and postsynaptic communication. The faster desensitization and likely reactivation of GluRIIB receptors could be valuable during persistent high-frequency motor activity to maintain a solid level of muscle action.

6. References

6.1. Scientific articles and monographies

- Adesnik H, Nicoll RA, England PM (2005) Photoinactivation of native AMPA receptors reveals their real-time trafficking. *Neuron* 48:977-985.
- Ahmari SE, Buchanan J, Smith SJ (2000) Assembly of presynaptic active zones from cytoplasmic transport packets. *Nat Neurosci* 3:445-451.
- Akaaboune M, Culican SM, Turney SG, Lichtman JW (1999) Rapid and reversible effects of activity on acetylcholine receptor density at the neuromuscular junction in vivo. *Science* 286:503-507.
- Akaaboune M, Grady RM, Turney S, Sanes JR, Lichtman JW (2002) Neurotransmitter receptor dynamics studied in vivo by reversible photo-unbinding of fluorescent ligands. *Neuron* 34:865-876.
- Albin SD, Davis GW (2004) Coordinating structural and functional synapse development: postsynaptic p21-activated kinase independently specifies glutamate receptor abundance and postsynaptic morphology. *J Neurosci* 24:6871-6879.
- Aronoff R, Mellem JE, Maricq AV, Sprengel R, Seeburg PH (2004) Neuronal toxicity in *Caenorhabditis elegans* from an editing site mutant in glutamate receptor channels. *J Neurosci* 24:8135-8140.
- Ashby MC, Ibaraki K, Henley JM (2004) It's green outside: tracking cell surface proteins with pH-sensitive GFP. *Trends Neurosci* 27:257-261.
- Atwood HL (2006) Neuroscience. Gatekeeper at the synapse. *Science* 312:1008-1009.
- Atwood HL, Govind CK, Wu CF (1993) Differential ultrastructure of synaptic terminals on ventral longitudinal abdominal muscles in *Drosophila* larvae. *J Neurobiol* 24:1008-1024.
- Ayalon G, Stern-Bach Y (2001) Functional assembly of AMPA and kainate receptors is mediated by several discrete protein-protein interactions. *Neuron* 31:103-113.
- Baines RA, Uhler JP, Thompson A, Sweeney ST, Bate M (2001) Altered electrical properties in *Drosophila* neurons developing without synaptic transmission. *J Neurosci* 21:1523-1531.
- Banke TG, Bowie D, Lee H, Hugarir RL, Schousboe A, Traynelis SF (2000) Control of GluR1 AMPA receptor function by cAMP-dependent protein kinase. *J Neurosci* 20:89-102.
- Barry MF, Ziff EB (2002) Receptor trafficking and the plasticity of excitatory synapses. *Curr Opin Neurobiol* 12:279-286.
- Bate M, Landgraf M, Ruiz Gomez Bate M (1999) Development of larval body wall muscles. *Int Rev Neurobiol* 43:25-44.
- Bliss TV, Lomo T (1973) Long-lasting potentiation of synaptic transmission in the dentate area of the anaesthetized rabbit following stimulation of the perforant path. *J Physiol* 232:331-356.
- Boehm J, Kang MG, Johnson RC, Esteban J, Hugarir RL, Malinow R (2006) Synaptic incorporation of AMPA receptors during LTP is controlled by a PKC phosphorylation site on GluR1. *Neuron* 51:213-225.
- Borgdorff AJ, Choquet D (2002) Regulation of AMPA receptor lateral movements. *Nature* 417:649-653.
- Brand AH, Perrimon N (1993) Targeted gene expression as a means of altering cell fates and generating dominant phenotypes. *Development* 118:401-415.
- Bredt DS, Nicoll RA (2003) AMPA receptor trafficking at excitatory synapses. *Neuron* 40:361-379.
- Bresler T, Shapira M, Boeckers T, Dresbach T, Futter M, Garner CC, Rosenblum K, Gundelfinger ED, Ziv NE (2004) Postsynaptic density assembly is

- fundamentally different from presynaptic active zone assembly. *J Neurosci* 24:1507-1520.
- Broadie K, Bate M (1993) Innervation directs receptor synthesis and localization in *Drosophila* embryo synaptogenesis. *Nature* 361:350-353.
- Broadie KS, Bate M (1993) Development of the embryonic neuromuscular synapse of *Drosophila melanogaster*. *J Neurosci* 13:144-166.
- Campbell RE, Tour O, Palmer AE, Steinbach PA, Baird GS, Zacharias DA, Tsien RY (2002) A monomeric red fluorescent protein. *Proc Natl Acad Sci U S A* 99:7877-7882.
- Carroll RC, Lissin DV, von Zastrow M, Nicoll RA, Malenka RC (1999) Rapid redistribution of glutamate receptors contributes to long-term depression in hippocampal cultures. *Nat Neurosci* 2:454-460.
- Castiglioni MC (1951) [Distribution of pigments in the eye of alleles of white and their compounds in *Drosophila melanogaster*.]. *Sci Genet* 4:57-60.
- Chang H, Ciani S, Kidokoro Y (1994) Ion permeation properties of the glutamate receptor channel in cultured embryonic *Drosophila* myotubes. *J Physiol* 476:1-16.
- Chen K, Featherstone DE (2005) Discs-large (DLG) is clustered by presynaptic innervation and regulates postsynaptic glutamate receptor subunit composition in *Drosophila*. *BMC Biol* 3:1.
- Chen K, Merino C, Sigrist SJ, Featherstone DE (2005) The 4.1 protein coracle mediates subunit-selective anchoring of *Drosophila* glutamate receptors to the postsynaptic actin cytoskeleton. *J Neurosci* 25:6667-6675.
- Chen L, Chetkovich DM, Petralia RS, Sweeney NT, Kawasaki Y, Wenthold RJ, Brecht DS, Nicoll RA (2000) Stargazin regulates synaptic targeting of AMPA receptors by two distinct mechanisms. *Nature* 408:936-943.
- Cheung US, Shayan AJ, Boulianne GL, Atwood HL (1999) *Drosophila* larval neuromuscular junction's responses to reduction of cAMP in the nervous system. *J Neurobiol* 40:1-13.
- Chklovskii DB, Mel BW, Svoboda K (2004) Cortical rewiring and information storage. *Nature* 431:782-788.
- Chung HJ, Xia J, Scannevin RH, Zhang X, Huganir RL (2000) Phosphorylation of the AMPA receptor subunit GluR2 differentially regulates its interaction with PDZ domain-containing proteins. *J Neurosci* 20:7258-7267.
- Collingridge GL, Isaac JT, Wang YT (2004) Receptor trafficking and synaptic plasticity. *Nat Rev Neurosci* 5:952-962.
- Davis GW, DiAntonio A, Petersen SA, Goodman CS (1998) Postsynaptic PKA controls quantal size and reveals a retrograde signal that regulates presynaptic transmitter release in *Drosophila*. *Neuron* 20:305-315.
- Davis RL, Kauvar LM (1984) *Drosophila* cyclic nucleotide phosphodiesterases. *Adv Cyclic Nucleotide Protein Phosphorylation Res* 16:393-402.
- Dean C, Dresbach T (2006) Neuroligins and neuroligins: linking cell adhesion, synapse formation and cognitive function. *Trends Neurosci* 29:21-29.
- DeChiara TM, Bowen DC, Valenzuela DM, Simmons MV, Poueymirou WT, Thomas S, Kinetz E, Compton DL, Rojas E, Park JS, Smith C, DiStefano PS, Glass DJ, Burden SJ, Yancopoulos GD (1996) The receptor tyrosine kinase MuSK is required for neuromuscular junction formation in vivo. *Cell* 85:501-512.
- Derkach V, Barria A, Soderling TR (1999) Ca²⁺/calmodulin-kinase II enhances channel conductance of alpha-amino-3-hydroxy-5-methyl-4-isoxazolepropionate type glutamate receptors. *Proc Natl Acad Sci U S A* 96:3269-3274.
- DiAntonio A, Petersen SA, Heckmann M, Goodman CS (1999) Glutamate receptor expression regulates quantal size and quantal content at the *Drosophila* neuromuscular junction. *J Neurosci* 19:3023-3032.

- Dornan S, Jackson AP, Gay NJ (1997) Alpha-adaptin, a marker for endocytosis, is expressed in complex patterns during *Drosophila* development. *Mol Biol Cell* 8:1391-1403.
- Dudai Y, Zvi S (1985) Multiple defects in the activity of adenylate cyclase from the *Drosophila* memory mutant *rutabaga*. *J Neurochem* 45:355-364.
- Dudai Y, Jan YN, Byers D, Quinn WG, Benzer S (1976) *dunce*, a mutant of *Drosophila* deficient in learning. *Proc Natl Acad Sci U S A* 73:1684-1688.
- Durand GM, Kovalchuk Y, Konnerth A (1996) Long-term potentiation and functional synapse induction in developing hippocampus. *Nature* 381:71-75.
- Echalier G (1997) *Drosophila: Cells in Culture*, 1st Edition. New York: Academic Press.
- Esteban JA, Shi SH, Wilson C, Nuriya M, Hugarir RL, Malinow R (2003) PKA phosphorylation of AMPA receptor subunits controls synaptic trafficking underlying plasticity. *Nat Neurosci* 6:136-143.
- Featherstone D, Broadie K (2002) Response: meaningless minis? *Trends Neurosci* 25:386-387.
- Featherstone DE, Broadie K (2000) Surprises from *Drosophila*: genetic mechanisms of synaptic development and plasticity. *Brain Res Bull* 53:501-511.
- Featherstone DE, Rushton E, Broadie K (2002) Developmental regulation of glutamate receptor field size by nonvesicular glutamate release. *Nat Neurosci* 5:141-146.
- Featherstone DE, Rushton EM, Hilderbrand-Chae M, Phillips AM, Jackson FR, Broadie K (2000) Presynaptic glutamic acid decarboxylase is required for induction of the postsynaptic receptor field at a glutamatergic synapse. *Neuron* 27:71-84.
- Featherstone DE, Rushton E, Rohrbough J, Liebl F, Karr J, Sheng Q, Rodesch CK, Broadie K (2005) An essential *Drosophila* glutamate receptor subunit that functions in both central neuropil and neuromuscular junction. *J Neurosci* 25:3199-3208.
- Feng Y, Ueda A, Wu CF (2004) A modified minimal hemolymph-like solution, HL3.1, for physiological recordings at the neuromuscular junctions of normal and mutant *Drosophila* larvae. *J Neurogenet* 18:377-402.
- Fiala JC, Allwardt B, Harris KM (2002) Dendritic spines do not split during hippocampal LTP or maturation. *Nat Neurosci* 5:297-298.
- Gautam M, Noakes PG, Mudd J, Nichol M, Chu GC, Sanes JR, Merlie JP (1995) Failure of postsynaptic specialization to develop at neuromuscular junctions of rapsyn-deficient mice. *Nature* 377:232-236.
- Gorczyca M, Popova E, Jia XX, Budnik V (1999) The gene *mod(mdg4)* affects synapse specificity and structure in *Drosophila*. *J Neurobiol* 39:447-460.
- Grunwald ME, Kaplan JM (2003) Mutations in the ligand-binding and pore domains control exit of glutamate receptors from the endoplasmic reticulum in *C. elegans*. *Neuropharmacology* 45:768-776.
- Guerrero G, Reiff DF, Agarwal G, Ball RW, Borst A, Goodman CS, Isacoff EY (2005) Heterogeneity in synaptic transmission along a *Drosophila* larval motor axon. *Nat Neurosci* 8:1188-1196.
- Gundelfinger ED, Kessels MM, Qualmann B (2003) Temporal and spatial coordination of exocytosis and endocytosis. *Nat Rev Mol Cell Biol* 4:127-139.
- Haghighi AP, McCabe BD, Fetter RD, Palmer JE, Hom S, Goodman CS (2003) Retrograde control of synaptic transmission by postsynaptic CaMKII at the *Drosophila* neuromuscular junction. *Neuron* 39:255-267.
- Harris WA (1980) The effects of eliminating impulse activity on the development of the retinotectal projection in salamanders. *J Comp Neurol* 194:303-317.

- Hayashi Y, Shi SH, Esteban JA, Piccini A, Poncer JC, Malinow R (2000) Driving AMPA receptors into synapses by LTP and CaMKII: requirement for GluR1 and PDZ domain interaction. *Science* 287:2262-2267.
- Hebb D (1949) *The organization of behaviour*. New York, NY: Wiley.
- Heeroma JH, Plomp JJ, Roubos EW, Verhage M (2003) Development of the mouse neuromuscular junction in the absence of regulated secretion. *Neuroscience* 120:733-744.
- Horn C, Wimmer EA (2000) A versatile vector set for animal transgenesis. *Dev Genes Evol* 210:630-637.
- Horning MS, Mayer ML (2004) Regulation of AMPA receptor gating by ligand binding core dimers. *Neuron* 41:379-388.
- Hughes BW, Kusner LL, Kaminski HJ (2006) Molecular architecture of the neuromuscular junction. *Muscle Nerve* 33:445-461.
- Isaac JT (2003) Postsynaptic silent synapses: evidence and mechanisms. *Neuropharmacology* 45:450-460.
- Jan LY, Jan YN (1976) Properties of the larval neuromuscular junction in *Drosophila melanogaster*. *J Physiol* 262:189-214.
- Jonas P, Burnashev N (1995) Molecular mechanisms controlling calcium entry through AMPA-type glutamate receptor channels. *Neuron* 15:987-990.
- Kandel E, Schwartz J, Jessell T (1991) *Principles of neural science*, 3rd Edition. East Norwalk, CT: Appleton & Lange.
- Kasai H, Matsuzaki M, Noguchi J, Yasumatsu N, Nakahara H (2003) Structure-stability-function relationships of dendritic spines. *Trends Neurosci* 26:360-368.
- Kask K, Zamanillo D, Rozov A, Burnashev N, Sprengel R, Seeburg PH (1998) The AMPA receptor subunit GluR-B in its Q/R site-unedited form is not essential for brain development and function. *Proc Natl Acad Sci U S A* 95:13777-13782.
- Keshishian H, Broadie K, Chiba A, Bate M (1996) The drosophila neuromuscular junction: a model system for studying synaptic development and function. *Annu Rev Neurosci* 19:545-575.
- Kim E, Sheng M (2004) PDZ domain proteins of synapses. *Nat Rev Neurosci* 5:771-781.
- Kim JH, Udo H, Li HL, Youn TY, Chen M, Kandel ER, Bailey CH (2003) Presynaptic activation of silent synapses and growth of new synapses contribute to intermediate and long-term facilitation in *Aplysia*. *Neuron* 40:151-165.
- Kim S, Ko J, Shin H, Lee JR, Lim C, Han JH, Altmock WD, Garner CC, Gundelfinger ED, Premont RT, Kaang BK, Kim E (2003) The GIT family of proteins forms multimers and associates with the presynaptic cytomatrix protein Piccolo. *J Biol Chem* 278:6291-6300.
- Kittel RJ, Wichmann C, Rasse TM, Fouquet W, Schmidt M, Schmid A, Wagh DA, Pawlu C, Kellner RR, Willig KI, Hell SW, Buchner E, Heckmann M, Sigrist SJ (2006) Bruchpilot promotes active zone assembly, Ca²⁺ channel clustering, and vesicle release. *Science* 312:1051-1054.
- Koenig JH, Saito K, Ikeda K (1983) Reversible control of synaptic transmission in a single gene mutant of *Drosophila melanogaster*. *J Cell Biol* 96:1517-1522.
- Koh YH, Gramates LS, Budnik V (2000) *Drosophila* larval neuromuscular junction: molecular components and mechanisms underlying synaptic plasticity. *Microsc Res Tech* 49:14-25.
- Kuromi H, Kidokoro Y (2002) Selective replenishment of two vesicle pools depends on the source of Ca²⁺ at the *Drosophila* synapse. *Neuron* 35:333-343.
- Landgraf M, Thor S (2006) Development of *Drosophila* motoneurons: specification and morphology. *Semin Cell Dev Biol* 17:3-11.
- Lee HK, Barbarosie M, Kameyama K, Bear MF, Haganir RL (2000) Regulation of distinct AMPA receptor phosphorylation sites during bidirectional synaptic plasticity. *Nature* 405:955-959.

- Liao D, Hessler NA, Malinow R (1995) Activation of postsynaptically silent synapses during pairing-induced LTP in CA1 region of hippocampal slice. *Nature* 375:400-404.
- Liebl FL, Featherstone DE (2005) Genes involved in *Drosophila* glutamate receptor expression and localization. *BMC Neurosci* 6:44.
- Livingstone MS (1985) Genetic dissection of *Drosophila* adenylate cyclase. *Proc Natl Acad Sci U S A* 82:5992-5996.
- Loughney K, Kreber R, Ganetzky B (1989) Molecular analysis of the para locus, a sodium channel gene in *Drosophila*. *Cell* 58:1143-1154.
- Luscher C, Xia H, Beattie EC, Carroll RC, von Zastrow M, Malenka RC, Nicoll RA (1999) Role of AMPA receptor cycling in synaptic transmission and plasticity. *Neuron* 24:649-658.
- Madden DR (2002) The structure and function of glutamate receptor ion channels. *Nat Rev Neurosci* 3:91-101.
- Malinow R, Malenka RC (2002) AMPA receptor trafficking and synaptic plasticity. *Annu Rev Neurosci* 25:103-126.
- Marangi PA, Forsayeth JR, Mittaud P, Erb-Vogtli S, Blake DJ, Moransard M, Sander A, Fuhrer C (2001) Acetylcholine receptors are required for agrin-induced clustering of postsynaptic proteins. *Embo J* 20:7060-7073.
- Marrus SB, DiAntonio A (2004) Preferential localization of glutamate receptors opposite sites of high presynaptic release. *Curr Biol* 14:924-931.
- Marrus SB, Portman SL, Allen MJ, Moffat KG, DiAntonio A (2004) Differential localization of glutamate receptor subunits at the *Drosophila* neuromuscular junction. *J Neurosci* 24:1406-1415.
- Matus A (2005) Growth of dendritic spines: a continuing story. *Curr Opin Neurobiol* 15:67-72.
- Mayer ML (2005) Crystal structures of the GluR5 and GluR6 ligand binding cores: molecular mechanisms underlying kainate receptor selectivity. *Neuron* 45:539-552.
- McGee AW, Brecht DS (2003) Assembly and plasticity of the glutamatergic postsynaptic specialization. *Curr Opin Neurobiol* 13:111-118.
- Misgeld T, Burgess RW, Lewis RM, Cunningham JM, Lichtman JW, Sanes JR (2002) Roles of neurotransmitter in synapse formation: development of neuromuscular junctions lacking choline acetyltransferase. *Neuron* 36:635-648.
- Missias AC, Mudd J, Cunningham JM, Steinbach JH, Merlie JP, Sanes JR (1997) Deficient development and maintenance of postsynaptic specializations in mutant mice lacking an 'adult' acetylcholine receptor subunit. *Development* 124:5075-5086.
- Morimoto-Tanifuji T, Kazama H, Nose A (2004) Developmental stage-dependent modulation of synapses by postsynaptic expression of activated calcium/calmodulin-dependent protein kinase II. *Neuroscience* 128:797-806.
- Murthy VN, De Camilli P (2003) Cell biology of the presynaptic terminal. *Annu Rev Neurosci* 26:701-728.
- Nikonenko I, Jourdain P, Alberi S, Toni N, Muller D (2002) Activity-induced changes of spine morphology. *Hippocampus* 12:585-591.
- Nishimune A, Isaac JT, Molnar E, Noel J, Nash SR, Tagaya M, Collingridge GL, Nakanishi S, Henley JM (1998) NSF binding to GluR2 regulates synaptic transmission. *Neuron* 21:87-97.
- Ohtsuka T, Takao-Rikitsu E, Inoue E, Inoue M, Takeuchi M, Matsubara K, Deguchi-Tawarada M, Satoh K, Morimoto K, Nakanishi H, Takai Y (2002) Cast: a novel protein of the cytomatrix at the active zone of synapses that forms a ternary complex with RIM1 and munc13-1. *J Cell Biol* 158:577-590.

- Ono F, Higashijima S, Shcherbatko A, Fetcho JR, Brehm P (2001) Paralytic zebrafish lacking acetylcholine receptors fail to localize rapsyn clusters to the synapse. *J Neurosci* 21:5439-5448.
- Osten P, Stern-Bach Y (2006) Learning from stargazin: the mouse, the phenotype and the unexpected. *Curr Opin Neurobiol*.
- Packard M, Mathew D, Budnik V (2003) Wnts and TGF beta in synaptogenesis: old friends signalling at new places. *Nat Rev Neurosci* 4:113-120.
- Parnas D, Haghighi AP, Fetter RD, Kim SW, Goodman CS (2001) Regulation of postsynaptic structure and protein localization by the Rho-type guanine nucleotide exchange factor dPix. *Neuron* 32:415-424.
- Partin KM (2001) Domain interactions regulating ampa receptor desensitization. *J Neurosci* 21:1939-1948.
- Passafaro M, Nakagawa T, Sala C, Sheng M (2003) Induction of dendritic spines by an extracellular domain of AMPA receptor subunit GluR2. *Nature* 424:677-681.
- Perestenko PV, Henley JM (2003) Characterization of the intracellular transport of GluR1 and GluR2 alpha-amino-3-hydroxy-5-methyl-4-isoxazole propionic acid receptor subunits in hippocampal neurons. *J Biol Chem* 278:43525-43532.
- Petersen SA, Fetter RD, Noordermeer JN, Goodman CS, DiAntonio A (1997) Genetic analysis of glutamate receptors in *Drosophila* reveals a retrograde signal regulating presynaptic transmitter release. *Neuron* 19:1237-1248.
- Prokop A (1999) Integrating bits and pieces: synapse structure and formation in *Drosophila* embryos. *Cell Tissue Res* 297:169-186.
- Prokop A, Meinertzhagen IA (2006) Development and structure of synaptic contacts in *Drosophila*. *Semin Cell Dev Biol* 17:20-30.
- Prokop A, Landgraf M, Rushton E, Broadie K, Bate M (1996) Presynaptic development at the *Drosophila* neuromuscular junction: assembly and localization of presynaptic active zones. *Neuron* 17:617-626.
- Purves D, Augustine G, Fitzpatrick D, Katz L, LaMantia A, McNamara J, Williams S (2001) *Neuroscience*, 2nd Edition. Sunderland, MA: Sinauer Associates.
- Qin G, Schwarz T, Kittel RJ, Schmid A, Rasse TM, Kappei D, Ponimaskin E, Heckmann M, Sigrist SJ (2005) Four different subunits are essential for expressing the synaptic glutamate receptor at neuromuscular junctions of *Drosophila*. *J Neurosci* 25:3209-3218.
- Rasse TM, Fouquet W, Schmid A, Kittel RJ, Mertel S, Sigrist CB, Schmidt M, Guzman A, Merino C, Qin G, Quentin C, Madeo FF, Heckmann M, Sigrist SJ (2005) Glutamate receptor dynamics organizing synapse formation in vivo. *Nat Neurosci* 8:898-905.
- Reiff DF, Thiel PR, Schuster CM (2002) Differential regulation of active zone density during long-term strengthening of *Drosophila* neuromuscular junctions. *J Neurosci* 22:9399-9409.
- Renden RB, Broadie K (2003) Mutation and activation of Galpha s similarly alters pre- and postsynaptic mechanisms modulating neurotransmission. *J Neurophysiol* 89:2620-2638.
- Renger JJ, Ueda A, Atwood HL, Govind CK, Wu CF (2000) Role of cAMP cascade in synaptic stability and plasticity: ultrastructural and physiological analyses of individual synaptic boutons in *Drosophila* memory mutants. *J Neurosci* 20:3980-3992.
- Rheuben MB, Yoshihara M, Kidokoro Y (1999) Ultrastructural correlates of neuromuscular junction development. *Int Rev Neurobiol* 43:69-92.
- Richmond JE, Broadie KS (2002) The synaptic vesicle cycle: exocytosis and endocytosis in *Drosophila* and *C. elegans*. *Curr Opin Neurobiol* 12:499-507.
- Ritzenthaler S, Suzuki E, Chiba A (2000) Postsynaptic filopodia in muscle cells interact with innervating motoneuron axons. *Nat Neurosci* 3:1012-1017.

- Rosenmund C, Stern-Bach Y, Stevens CF (1998) The tetrameric structure of a glutamate receptor channel. *Science* 280:1596-1599.
- Rubin GM, Spradling AC (1982) Genetic transformation of *Drosophila* with transposable element vectors. *Science* 218:348-353.
- Saitoe M, Schwarz TL, Umbach JA, Gundersen CB, Kidokoro Y (2002) Response: meaningless minis? *Trends Neurosci* 25:385-386.
- Salinas PC, Price SR (2005) Cadherins and catenins in synapse development. *Curr Opin Neurobiol* 15:73-80.
- Salvaterra PM, Kitamoto T (2001) *Drosophila* cholinergic neurons and processes visualized with Gal4/UAS-GFP. *Brain Res Gene Expr Patterns* 1:73-82.
- Sambrook J, Fritsch E, Maniatis T (1989) *Molecular cloning: A laboratory manual*, 2nd Edition. Cold Spring Harbor, NY: Cold Spring Harbor Laboratory Press.
- Sanes JR, Lichtman JW (1999) Development of the vertebrate neuromuscular junction. *Annu Rev Neurosci* 22:389-442.
- Sans N, Racca C, Petralia RS, Wang YX, McCallum J, Wenthold RJ (2001) Synapse-associated protein 97 selectively associates with a subset of AMPA receptors early in their biosynthetic pathway. *J Neurosci* 21:7506-7516.
- Schuster CM, Davis GW, Fetter RD, Goodman CS (1996) Genetic dissection of structural and functional components of synaptic plasticity. II. Fasciclin II controls presynaptic structural plasticity. *Neuron* 17:655-667.
- Schuster CM, Davis GW, Fetter RD, Goodman CS (1996) Genetic dissection of structural and functional components of synaptic plasticity. I. Fasciclin II controls synaptic stabilization and growth. *Neuron* 17:641-654.
- Schuster CM, Davis GW, Fetter RD, Goodman CS (1996) Genetic dissection of structural and functional components of synaptic plasticity. I. Fasciclin II controls synaptic stabilization and growth. *Neuron* 17:641-654.
- Schuster CM, Ultsch A, Schloss P, Cox JA, Schmitt B, Betz H (1991) Molecular cloning of an invertebrate glutamate receptor subunit expressed in *Drosophila* muscle. *Science* 254:112-114.
- Shapira M, Zhai RG, Dresbach T, Bresler T, Torres VI, Gundelfinger ED, Ziv NE, Garner CC (2003) Unitary assembly of presynaptic active zones from Piccolo-Bassoon transport vesicles. *Neuron* 38:237-252.
- Shayan AJ, Atwood HL (2000) Synaptic ultrastructure in nerve terminals of *Drosophila* larvae overexpressing the learning gene *dunce*. *J Neurobiol* 43:89-97.
- Sheng M, Kim MJ (2002) Postsynaptic signaling and plasticity mechanisms. *Science* 298:776-780.
- Sheridan DL, Berlot CH, Robert A, Inglis FM, Jakobsdottir KB, Howe JR, Hughes TE (2002) A new way to rapidly create functional, fluorescent fusion proteins: random insertion of GFP with an in vitro transposition reaction. *BMC Neurosci* 3:7.
- Shi S, Hayashi Y, Esteban JA, Malinow R (2001) Subunit-specific rules governing AMPA receptor trafficking to synapses in hippocampal pyramidal neurons. *Cell* 105:331-343.
- Shi SH (2001) Amersham Biosciences & Science Prize. AMPA receptor dynamics and synaptic plasticity. *Science* 294:1851-1852.
- Shi SH, Hayashi Y, Petralia RS, Zaman SH, Wenthold RJ, Svoboda K, Malinow R (1999) Rapid spine delivery and redistribution of AMPA receptors after synaptic NMDA receptor activation. *Science* 284:1811-1816.
- Sigrist SJ, Thiel PR, Reiff DF, Schuster CM (2002) The postsynaptic glutamate receptor subunit DGluR-IIA mediates long-term plasticity in *Drosophila*. *J Neurosci* 22:7362-7372.

- Sigrist SJ, Reiff DF, Thiel PR, Steinert JR, Schuster CM (2003) Experience-dependent strengthening of *Drosophila* neuromuscular junctions. *J Neurosci* 23:6546-6556.
- Sigrist SJ, Thiel PR, Reiff DF, Lachance PE, Lasko P, Schuster CM (2000) Postsynaptic translation affects the efficacy and morphology of neuromuscular junctions. *Nature* 405:1062-1065.
- Sone M, Suzuki E, Hoshino M, Hou D, Kuromi H, Fukata M, Kuroda S, Kaibuchi K, Nabeshima Y, Hama C (2000) Synaptic development is controlled in the periaxonal zones of *Drosophila* synapses. *Development* 127:4157-4168.
- Song I, Huganir RL (2002) Regulation of AMPA receptors during synaptic plasticity. *Trends Neurosci* 25:578-588.
- Steinert JR, Kuromi H, Hellwig A, Knirr M, Wyatt AW, Kidokoro Y, Schuster CM (2006) Experience-dependent formation and recruitment of large vesicles from reserve pool. *Neuron* 50:723-733.
- Stewart BA, Atwood HL, Renger JJ, Wang J, Wu CF (1994) Improved stability of *Drosophila* larval neuromuscular preparations in haemolymph-like physiological solutions. *J Comp Physiol [A]* 175:179-191.
- Sweeney ST, Broadie K, Keane J, Niemann H, O'Kane CJ (1995) Targeted expression of tetanus toxin light chain in *Drosophila* specifically eliminates synaptic transmission and causes behavioral defects. *Neuron* 14:341-351.
- Tada T, Sheng M (2006) Molecular mechanisms of dendritic spine morphogenesis. *Curr Opin Neurobiol* 16:95-101.
- Thomas P, Mortensen M, Hosie AM, Smart TG (2005) Dynamic mobility of functional GABAA receptors at inhibitory synapses. *Nat Neurosci* 8:889-897.
- Thomas U, Kim E, Kuhlendahl S, Koh YH, Gundelfinger ED, Sheng M, Garner CC, Budnik V (1997) Synaptic clustering of the cell adhesion molecule fasciclin II by discs-large and its role in the regulation of presynaptic structure. *Neuron* 19:787-799.
- Thomas U, Kim E, Kuhlendahl S, Koh YH, Gundelfinger ED, Sheng M, Garner CC, Budnik V (1997) Synaptic clustering of the cell adhesion molecule fasciclin II by discs-large and its role in the regulation of presynaptic structure. *Neuron* 19:787-799.
- Tomita S, Adesnik H, Sekiguchi M, Zhang W, Wada K, Howe JR, Nicoll RA, Brecht DS (2005) Stargazin modulates AMPA receptor gating and trafficking by distinct domains. *Nature* 435:1052-1058.
- Varoqueaux F, Sigler A, Rhee JS, Brose N, Enk C, Reim K, Rosenmund C (2002) Total arrest of spontaneous and evoked synaptic transmission but normal synaptogenesis in the absence of Munc13-mediated vesicle priming. *Proc Natl Acad Sci U S A* 99:9037-9042.
- Verhage M, Maia AS, Plomp JJ, Brussaard AB, Heeroma JH, Vermeer H, Toonen RF, Hammer RE, van den Berg TK, Missler M, Geuze HJ, Südhof TC (2000) Synaptic assembly of the brain in the absence of neurotransmitter secretion. *Science* 287:864-869.
- Verstreken P, Bellen HJ (2002) Meaningless minis? Mechanisms of neurotransmitter-receptor clustering. *Trends Neurosci* 25:383-385.
- Wagh DA, Rasse TM, Asan E, Hofbauer A, Schwenkert I, Durrbeck H, Buchner S, Dabauvalle MC, Schmidt M, Qin G, Wichmann C, Kittel R, Sigrist SJ, Buchner E (2006) Bruchpilot, a protein with homology to ELKS/CAST, is required for structural integrity and function of synaptic active zones in *Drosophila*. *Neuron* 49:833-844.
- Walikonis RS, Jensen ON, Mann M, Provance DW, Jr., Mercer JA, Kennedy MB (2000) Identification of proteins in the postsynaptic density fraction by mass spectrometry. *J Neurosci* 20:4069-4080.

- Washbourne P, Bennett JE, McAllister AK (2002) Rapid recruitment of NMDA receptor transport packets to nascent synapses. *Nat Neurosci* 5:751-759.
- Wenthold RJ, Petralia RS, Blahos J, II, Niedzielski AS (1996) Evidence for multiple AMPA receptor complexes in hippocampal CA1/CA2 neurons. *J Neurosci* 16:1982-1989.
- Whiteheart SW, Rossmagel K, Buhrow SA, Brunner M, Jaenicke R, Rothman JE (1994) N-ethylmaleimide-sensitive fusion protein: a trimeric ATPase whose hydrolysis of ATP is required for membrane fusion. *J Cell Biol* 126:945-954.
- Wilson MH, Deschenes MR (2005) The neuromuscular junction: anatomical features and adaptations to various forms of increased, or decreased neuromuscular activity. *Int J Neurosci* 115:803-828.
- Wollmuth LP, Sobolevsky AI (2004) Structure and gating of the glutamate receptor ion channel. *Trends Neurosci* 27:321-328.
- Wucherpennig T, Wilsch-Brauninger M, Gonzalez-Gaitan M (2003) Role of *Drosophila* Rab5 during endosomal trafficking at the synapse and evoked neurotransmitter release. *J Cell Biol* 161:609-624.
- Xia J, Zhang X, Staudinger J, Haganir RL (1999) Clustering of AMPA receptors by the synaptic PDZ domain-containing protein PICK1. *Neuron* 22:179-187.
- Yoshihara M, Adolfsen B, Galle KT, Littleton JT (2005) Retrograde signaling by Syt 4 induces presynaptic release and synapse-specific growth. *Science* 310:858-863.
- Yuste R, Bonhoeffer T (2001) Morphological changes in dendritic spines associated with long-term synaptic plasticity. *Annu Rev Neurosci* 24:1071-1089.
- Zhai RG, Bellen HJ (2004) The architecture of the active zone in the presynaptic nerve terminal. *Physiology (Bethesda)* 19:262-270.
- Zhong Y, Wu CF (2004) Neuronal activity and adenylyl cyclase in environment-dependent plasticity of axonal outgrowth in *Drosophila*. *J Neurosci* 24:1439-1445.
- Zhong Y, Budnik V, Wu CF (1992) Synaptic plasticity in *Drosophila* memory and hyperexcitable mutants: role of cAMP cascade. *J Neurosci* 12:644-651.
- Zito K, Fetter RD, Goodman CS, Isacoff EY (1997) Synaptic clustering of Fascilin II and Shaker: essential targeting sequences and role ofDlg. *Neuron* 19:1007-1016.
- Zito K, Fetter RD, Goodman CS, Isacoff EY (1997) Synaptic clustering of Fascilin II and Shaker: essential targeting sequences and role ofDlg. *Neuron* 19:1007-1016.
- Ziv NE, Garner CC (2004) Cellular and molecular mechanisms of presynaptic assembly. *Nat Rev Neurosci* 5:385-399.

6.2. World wide web

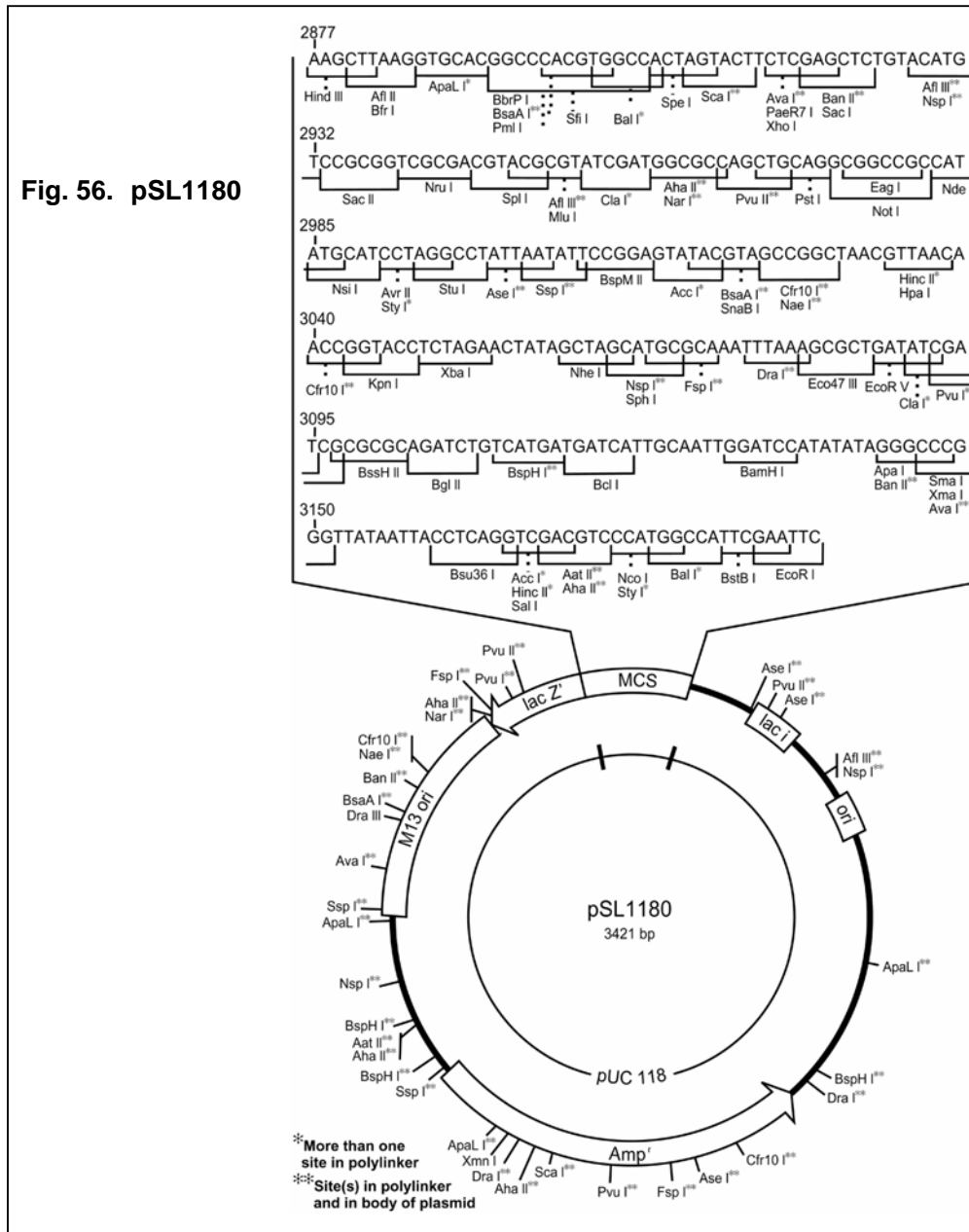
- A flymove.uni-muenster.de/Genetics-Flies-LifeCycle-LifeCyclePict-life_cycle.jpg (07/11/2006)
- B <http://rsb.info.nih.gov/ij/download.html> (07/11/2006)
- C <http://synapses.mcg.edu/anatomy/dendrite/dendrite.stm> (07/18/2006)

7. Appendix

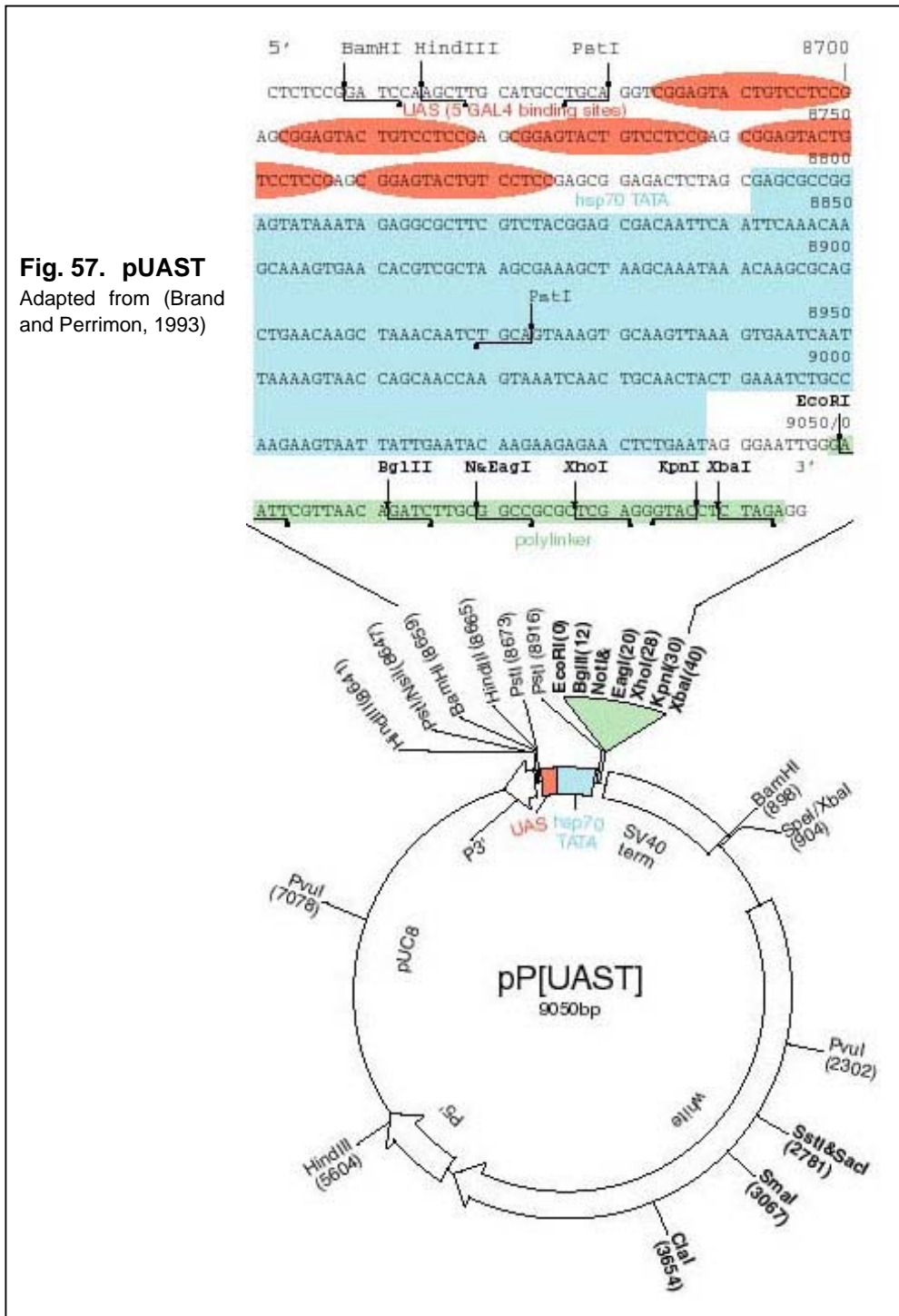
7.1. Vectors

pSL1180:

(Amersham Pharmacia Biotech, Buckinghamshire, England)



pUAST:

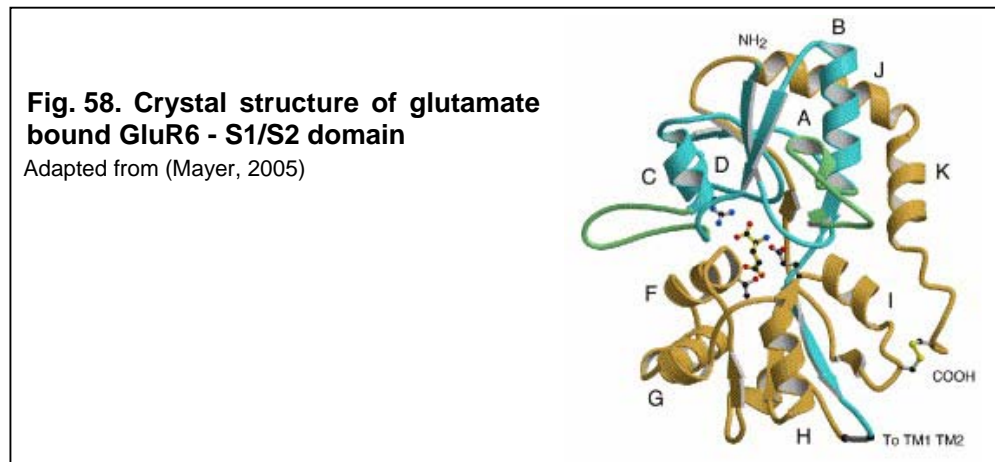


pUAST XL+:

pUAST XL+ is a modified version of pUAST (Fig. 57).

Multiple cloning site:

5' GAATTCGTTTAACTAGTGGCCGGCCTTAATTAAGGCGCGCCATTTAA
ATGAATTCGTTAACGATCTGCGGCCGGCTCGAGGGTACCTCTAGA 3'

7.2. GluR structure and alignments

	444	445	Loop1				Hel. F	Helix G				Helix K																				
			451			457	588	590	594			705	791	796																		
IIA melano	E	D	H	G	R	E	K	Y	S	G	F	S	E	T	D	Y	Q	R	A	W	N	Q	M	K	D	K	N	K	W	W	K	
IIA pseudo	E	D	H	G	R	E	K	Y	S	G	F	S	E	T	D	Y	Q	R	A	W	N	Q	M	K	D	K	N	K	W	W	K	
IIA mojaven	Q	D	H	G	Q	E	K	Y	F	S	E	T	D	Y	Q	R	A	W	N	Q	M	K	S			K	N	K	W	W	K	
IIB melano	E	E	P	G	N	E	R	F	F	S	E	T	D	N	R	M	A	W	N	K	M	L	S			R	N	K	W	F	N	
IIB pseudo	D	E	P	G	N	E	R	F	F	S	E	T	E	N	R	M	A	W	N	K	M	L	S			R	N	K	W	F	N	
IIB mojaven	K	E	P	G	N	E	R	F	F	S	E	T	E	N	R	M	A	W	N	K	M	L	S			K	S	K	W	F	N	
IIC melano	E	T	A	G	N	A	L	Y	Q	G	L	A	D	T	V	Y	R	L	A	F	N	L	M	N	N		K	Q	K	W	W	K
IIC pseudo	E	T	A	G	N	A	I	Y	Q	G	L	A	D	T	T	Y	R	L	A	F	N	L	M	N	N		K	Q	K	W	W	K
IID melano	E	S	I	G	N	N	Q	F	Q	G	F	S	T	P	I	Y	I	K	M	N	E	Y	L	N	A		K	N	K	W	W	N
IID pseudo	D	S	I	G	N	N	Q	Y	Q	G	F	L	T	P	I	Y	M	K	M	N	E	Y	M	T	N		K	N	K	W	W	N
IIE melano	E	T	Y	G	N	S	Q	Y	Q	G	F	M	T	E	R	Y	K	K	M	N	K	F	M	S	E		K	N	K	W	W	N
IIE pseudo	E	T	F	G	N	S	Q	Y	Q	G	F	L	T	E	R	Y	K	K	M	N	K	F	M	T	E		K	N	K	W	W	N
GluR1, human	K	N	A	G	N	D	R	Y	G	F	R	R	A	V	F	E	K	M	W	T	Y	M	K	S		K	S	K	W	W	Y	
GluR2, human	K	N	H	G	N	E	R	Y	G	F	R	R	A	V	F	D	K	M	W	T	Y	M	R	S		K	N	K	W	W	Y	
GluR3, human	K	N	H	G	N	E	R	Y	G	F	R	R	A	V	F	E	K	M	W	S	Y	M	K	S		K	N	K	W	W	Y	
GluR4, human	K	N	H	G	N	D	K	Y	G	F	R	R	A	V	Y	E	K	M	W	T	Y	M	R	S		K	N	K	W	W	Y	
GluR6, human	K	S	D	G	N	D	R	F	G	F	K	K	S	T	Y	D	K	M	W	A	F	M	S	S		K	E	K	W	W	R	
KA2, human	P	N	F	G	N	E	R	F	G	F	Q	N	Q	T	Y	Q	R	M	W	N	Y	M	Q	S		K	R	K	W	W	E	
NR2A, human	N	S	T	V	K	K	C	C	K	G	S	T	E	-	-	I	R	N	N	Y	P	Y	M	H	Q		E	T	L	W	L	T

Tetramer - hydrogen bond ↑
 Tetramer - salt bridge ↑
 Tetramer - salt bridge ↑
 Tetramer - salt bridge ↑
 Tetramer - salt bridge ↑
 Tetramer - salt bridge ↑
 Tetramer - salt bridge ↑

Fig. 59. GluR AA alignment: S1/S2 domain – tetramer stabilization

Summarized from (Partin, 2001; Horning and Mayer, 2004). The marked amino acid residues within the S1/S2 domain (see Fig. 58) are involved in the tetramer stabilization within the glutamate receptor complex. Abbreviations denote: melano – *Drosophila melanogaster*, pseudo – *Drosophila pseudoobscura*, mojaven – *Drosophila mojavensis*. The numbers indicate the AA position of GluRIIA.

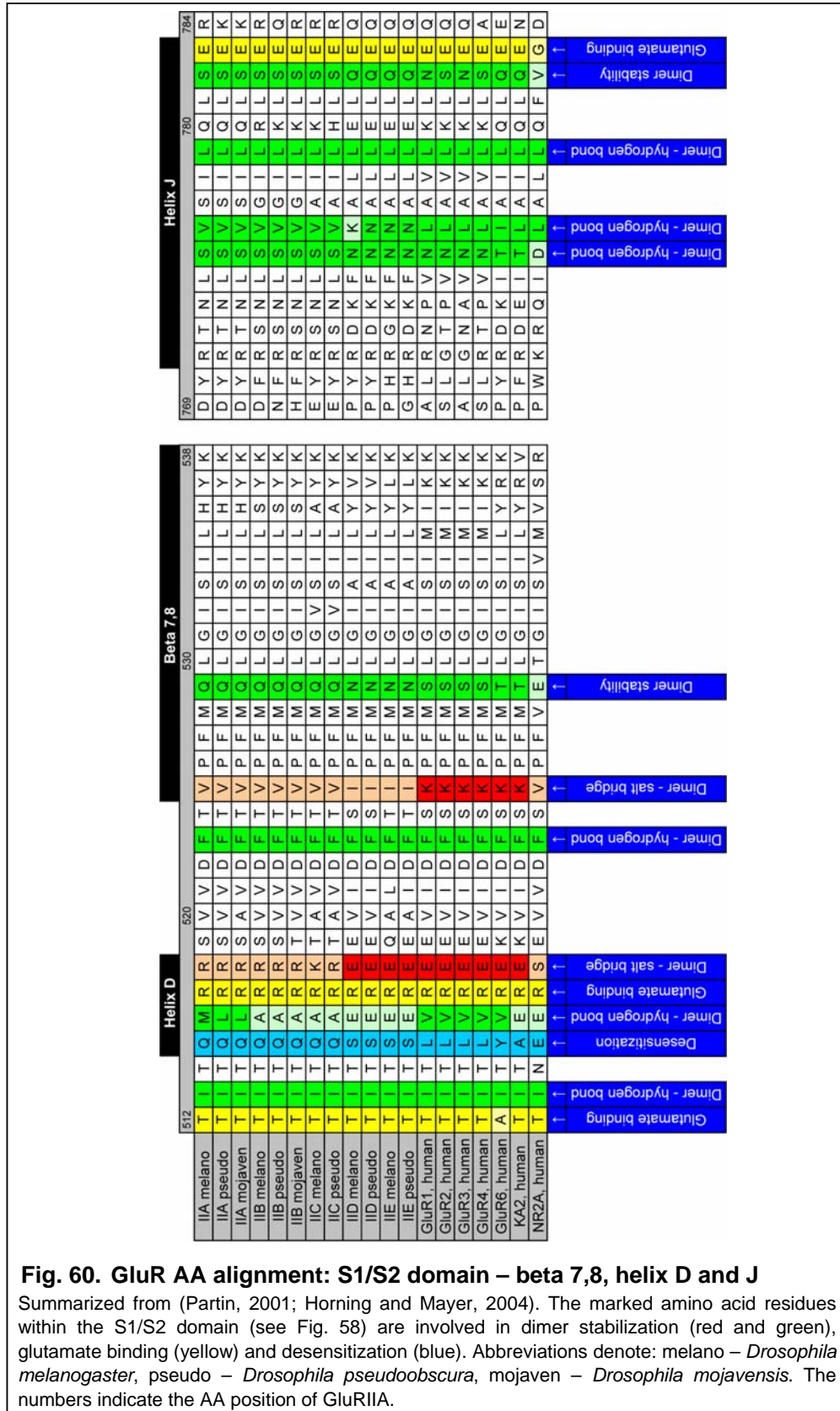


Fig. 60. GluR AA alignment: S1/S2 domain – beta 7,8, helix D and J

Summarized from (Partin, 2001; Horning and Mayer, 2004). The marked amino acid residues within the S1/S2 domain (see Fig. 58) are involved in dimer stabilization (red and green), glutamate binding (yellow) and desensitization (blue). Abbreviations denote: melano – *Drosophila melanogaster*, pseudo – *Drosophila pseudoobscura*, mojaven – *Drosophila mojavenensis*. The numbers indicate the AA position of GluRIIA.

Fig. 61. GluR AA alignment: reentrant pore loop and M2

Summarized from (Wollmuth and Sobolevsky, 2004). The marked amino acid residues are involved in ion gating (blue) and desensitization (red). The lurcher mutation residue (alanine to threonine) is indicated (red).

Abbreviations denote: melano – *Drosophila melanogaster*, pseudo – *Drosophila pseudoobscura*, mojaven – *Drosophila mojagensis*. The numbers indicate the AA position of GluRIIA.

597	600	603	606	609	610	reentrant pore loop	613	616	619	622	625	628	631	634	M2	650	653	656	659	662	665	668	671	674	677																																															
I/A melano	E	N	I	W	N	N	S	T	W	L	M	V	G	S	I	M	G	C	D	I	L	P	-	R	G	P	H	M	R	I	L	T	G	M	W	W	F	F	A	L	M	M	L	S	T	Y	T	A	N	L	A	A	F	L	T	S	N	K	W	Q	S	S	T									
I/A pseudo	E	N	I	W	N	N	S	T	W	L	M	V	G	S	I	M	G	C	D	I	L	P	-	R	G	P	H	M	R	I	L	T	G	M	W	W	F	F	A	L	M	M	L	S	T	Y	T	A	N	L	A	A	F	L	T	S	N	K	W	Q	S	S	T									
I/A mojaven	E	N	I	W	N	N	S	T	W	L	M	V	G	S	I	M	G	C	D	I	L	P	-	R	G	P	H	M	R	I	L	T	G	M	W	W	F	F	A	L	M	M	L	S	T	Y	T	A	N	L	A	A	F	L	T	S	N	K	W	Q	S	S	T									
I/B melano	Q	N	I	H	L	S	N	A	L	W	L	V	L	G	S	I	M	N	O	G	C	D	L	L	P	-	R	G	L	P	M	R	L	L	T	A	F	W	W	I	F	A	L	L	I	S	Q	T	Y	I	A	K	L	A	A	F	I	T	S	S	K	I	A	G	D							
I/B pseudo	H	N	I	W	N	H	N	T	M	W	L	V	L	G	S	I	L	T	O	G	C	D	L	L	P	-	R	G	L	P	M	R	L	L	T	A	F	W	W	I	F	A	L	L	I	S	Q	T	Y	I	A	K	L	A	A	F	I	T	S	S	K	I	A	G	D							
I/B mojaven	E	N	I	W	N	H	N	T	M	W	L	V	L	G	S	I	L	T	O	G	C	D	L	L	P	-	R	G	L	P	M	R	L	L	T	A	F	W	W	I	F	A	L	L	I	S	Q	T	Y	I	A	K	L	A	A	F	I	T	S	S	K	I	A	G	D							
I/C melano	E	N	I	W	R	I	H	N	T	G	W	L	V	A	S	I	M	T	A	G	C	D	I	L	P	-	R	S	P	Q	V	R	M	F	E	A	T	W	W	I	F	A	I	I	A	N	S	Y	T	A	N	L	A	A	F	L	T	S	S	K	M	T	G	N								
I/C pseudo	E	N	I	W	R	I	H	N	T	G	W	L	V	A	S	I	M	T	A	G	C	D	I	L	P	-	R	S	P	Q	V	R	M	F	E	A	T	W	W	I	F	A	I	I	A	N	S	Y	T	A	N	L	A	A	F	L	T	S	S	K	M	E	G	S								
I/C mojaven	E	N	I	W	R	I	H	N	T	G	W	L	V	A	S	I	M	T	A	G	C	D	I	L	P	-	R	S	P	Q	V	R	M	F	E	A	T	W	W	I	F	A	I	I	A	N	S	Y	T	A	N	L	A	A	F	L	T	S	S	K	M	E	G	S								
I/D melano	E	N	I	W	R	I	H	N	T	G	W	L	V	A	S	I	M	T	A	G	C	D	I	L	P	-	R	S	P	Q	V	R	M	F	E	A	T	W	W	I	F	A	I	I	A	N	S	Y	T	A	N	L	A	A	F	L	T	S	S	K	M	E	G	S								
I/D pseudo	E	N	I	W	R	I	H	N	T	G	W	L	V	A	S	I	M	T	A	G	C	D	I	L	P	-	R	S	P	Q	V	R	M	F	E	A	T	W	W	I	F	A	I	I	A	N	S	Y	T	A	N	L	A	A	F	L	T	S	S	K	M	E	G	S								
I/D mojaven	E	N	I	W	R	I	H	N	T	G	W	L	V	A	S	I	M	T	A	G	C	D	I	L	P	-	R	S	P	Q	V	R	M	F	E	A	T	W	W	I	F	A	I	I	A	N	S	Y	T	A	N	L	A	A	F	L	T	S	S	K	M	E	G	S								
I/E melano	E	N	I	W	N	N	S	L	W	F	T	G	A	L	L	O	G	S	E	I	A	P	-	K	A	L	S	T	R	T	I	A	I	W	W	F	F	T	L	I	M	V	S	Y	T	A	N	L	A	A	F	L	T	I	E	N	P	T	S	P												
I/E pseudo	E	N	I	W	N	N	S	L	W	F	T	G	A	L	L	O	G	S	E	I	A	P	-	K	A	L	S	T	R	T	I	A	I	W	W	F	F	T	L	I	M	V	S	Y	T	A	N	L	A	A	F	L	T	I	E	N	P	T	S	P												
I/E mojaven	E	N	I	W	N	N	S	L	W	F	T	G	A	L	L	O	G	S	E	I	A	P	-	K	A	L	S	T	R	T	I	A	I	W	W	F	F	T	L	I	M	V	S	Y	T	A	N	L	A	A	F	L	T	I	E	K	P	Q	S	L												
GluR1, human	S	N	E	F	G	I	F	N	S	L	W	F	S	L	G	A	F	M	R	O	G	C	D	I	S	P	-	R	S	L	S	G	R	I	V	G	V	W	W	F	F	T	L	I	I	S	S	Y	T	A	N	L	A	A	F	L	T	V	E	R	M	V	S	P								
GluR3, human	P	N	E	F	G	I	F	N	S	L	W	F	S	L	G	A	F	M	R	O	G	C	D	I	S	P	-	R	S	L	S	G	R	I	V	G	V	W	W	F	F	T	L	I	I	S	S	Y	T	A	N	L	A	A	F	L	T	V	E	R	M	V	S	P								
GluR4, human	P	N	E	F	G	I	F	N	S	L	W	F	S	L	G	A	F	M	R	O	G	C	D	I	S	P	-	R	S	L	S	G	R	I	V	G	V	W	W	F	F	T	L	I	I	S	S	Y	T	A	N	L	A	A	F	L	T	V	E	R	M	V	S	P								
GluR6, human	E	N	I	N	F	T	L	L	N	S	F	F	G	V	G	A	L	L	O	G	S	E	L	I	M	P	-	R	A	L	S	T	R	I	V	G	V	W	W	F	F	T	L	I	I	S	S	Y	T	A	N	L	A	A	F	L	T	V	E	R	M	E	S	P								
K42, human	E	N	I	Q	Y	T	L	L	N	S	L	W	F	P	V	G	F	L	O	G	S	E	L	I	M	P	-	R	A	L	S	T	R	C	V	S	G	V	W	W	A	F	T	L	I	I	S	S	Y	T	A	N	L	A	A	F	L	T	V	Q	R	M	E	V	P							
NR2A, human	G	P	S	F	T	I	G	K	A	I	W	L	L	W	G	L	V	F	N	N	S	V	P	Q	N	P	-	K	I	G	T	T	S	K	I	I	M	V	S	V	W	A	I	F	A	V	I	F	L	A	S	Y	T	A	N	L	A	A	F	L	T	M	I	Q	I	E	E	F	V	D	Q	

7.3. Constructs and transgenes

Construct	gen/cDNA	5'UTR	SP	N1	N2	N3	N4	S1	Pore	S2	C	3'UTR	Status	Gen. Backgr.	Rescue	Ratio	Rec	PSD	Phys
IIA	gen	A	A	A	A	A	A	A	A	A	A	A	Transgenic	Dich4	yes	0	0	0	0
IIA	cDNA	A	A	A	A	A	A	A	A	A	A	A	Transgenic	Dich4/WT	yes				
IIA hyp9 (Δ3'UTR)	gen	A	A	A	A	A	A	A	A	A	A	A	Transgenic	Dich4	yes	-	--	--	--
IIA S897A S897A	gen	A	A	A	A	A	A	A	A	A	A	A	Transgenic	Dich4	yes	0	0	0	0
IIA ΔC17	gen	A	A	A	A	A	A	A	A	A	A	A	Transgenic	Dich4	yes	0	0	0	0
IIA ΔC15-26	gen	A	A	A	A	A	A	A	A	A	A	A	Transgenic	Dich4	yes	0	0	0	0
IIA ΔC35	gen	A	A	A	A	A	A	A	A	A	A	A	Transgenic	Dich4	yes	-	-	-	-
IIA ΔC44	gen	A	A	A	A	A	A	A	A	A	A	A	Transgenic	Dich4	yes	0	0	0	0
IIA ΔC53	gen	A	A	A	A	A	A	A	A	A	A	A	Transgenic	Dich4	yes	--	--	--	--
AAB	gen	A	A	A	A	A	A	A	A	A	B	A	Transgenic	Dich4	yes	0	0	0	0
AABGFP	gen	A	A	A	A	A	A	A	A	A	B-GFP	A	Transgenic	Dich4	yes	0	0	0	0
AAC	gen	A	A	A	A	A	A	A	A	A	C	A	Transgenic	Dich4	yes	0	0	0	0
AAD	gen	A	A	A	A	A	A	A	A	A	D	A	Transgenic	Dich4	yes	0	0	0	0
AAE	gen	A	A	A	A	A	A	A	A	A	E	A	Transgenic	Dich4	no				
ACC	cDNA	A	A	A	A	A	A	C	C	C	C	A	Transgenic	Dich4	no				
AEE	cDNA	A	A	A	A	A	A	E	E	E	E	A	Transgenic	Dich4/E3	no				
IIA E763A	gen	A	A	A	A	A	A	A	A	A	A	A	Transgenic	Dich4	no				
IIA lucifer	gen	A	A	A	A	A	A	A	A	A	A	A	Transgenic	Dich4	no				
IIA poreMDQ	gen	A	A	A	A	A	A	A	A	A	A	A	Transgenic	Dich4	yes	-	-	-	-
IIA poreMRQ	gen	A	A	A	A	A	A	A	A	A	A	A	Transgenic	Dich4	yes	0	+	0	0
AAABAGFP	gen	A	A	A	A	A	A	A	A	A	A-GFP	A	Transgenic	Dich4	yes	--	--	--	--
ABABA	gen	A	A	A	A	A	A	A	A	A	B	A	Transgenic	Dich4	no				
ABAAAGFP	gen	A	A	A	A	A	A	A	A	A	B	A	Transgenic	Dich4	yes	0	0	0	0
ABAA	gen	A	A	A	A	A	A	A	A	A	A	A	Transgenic	Dich4	yes	-	-	-	-
A(NMT1)-BAGFP	gen	A	A	A	A	A	A	A	A	A	A-GFP	A	Transgenic	Dich4	no				
BBAAAGFP	gen	A	A	B	B	B	B	B	B	B	A-GFP	A	Transgenic	Dich4	no				
IIA ΔNTD	gen	A	A	A	A	A	A	A	A	A	A	A	Transgenic	Dich4	no				
BAA	gen	A	A	A	A	A	A	A	A	A	A	A	Transgenic	Dich4	no				
N(AAB)BAGFP	gen	A	A	A	A	A	A	A	A	A	A-GFP	A	Transgenic	Dich4	yes	0	0	0	0

Fig. 62. Constructs and transgenes 1

Abbreviations denote: SP – signal peptide, N1-4 – NTD sub-region 1-4, C – CTD, Rec – glutamate receptor level, PSD – PSD size, Phys – eEJC currents, A (yellow) – GluRIIA, B (orange) – GluRIIB, C (red) – GluRIIC, D (purple) – GluRIID, E (blue) - GluRIIE, GFP – insertion of GFP, o → normal, - → reduced, -- → strongly reduced, + → increased.

Construct	gen/cDNA	5'UTR	SP	N1	N2	N3	N4	S*	Pore	S2	C	SUTR	Status	Seq. Accogr.	Risks	Relia	Rec	PSD	Phys
N4A-BAY-GFP	gen	A	A	A	A	B	A	A	A	A	A-GFP	A	Transgenic	D3A4	NO				
N4B-AU-GFP	gen	A	A	A	B	A	A	A	A	A	A-GFP	A	Transgenic	D3A4	NO				
N4B-AU-GFP	gen	A	A	E	A	A	A	A	A	A	A-GFP	A	Transgenic	D3A4	YES	-	C	-	
A in B	gen	B	A	A	A	A	A	A	A	A	A	B	Transgenic	D3A4	YES	-	C	O	
AGFP in B	gen	B	A	A	A	A	A	A	A	A	A-GFP	B	Transgenic	D3A4	YES	O	C	O	
IIB	gen	B	B	B	B	B	B	B	B	B	B	B	Transgenic	D3A4	NO				O
IIB	cDNA	B	B	B	B	B	B	B	B	B	B	B	Transgenic	D3A4	NO				O
EE cesaryV	gen	B	B	B	B	B	B	B	B	B	B	B	Transgenic	D3A4	NO				
I B-AQ15M	gen	B	B	B	B	B	B	B	B	B	B	B	Transgenic	D3A4	YES	-	C	-	
BBA	cDNA	B	B	B	B	B	B	B	B	B	A	A	Transgenic	D3A4	YES	-	C	O	
EBAGFP	gen	B	B	B	B	B	B	B	B	B	A-GFP	B	Transgenic	D3A4	YES	O	C	O	
BAA	cDNA	B	B	B	B	B	B	A	A	A	A	A	Transgenic	D3A4	NO				
SABAB	gen	B	B	B	B	B	B	B	A	B	B	B	Transgenic	D3A4	NO				
ABB	gen	B	B	B	A	A	A	B	B	B	B	B	Transgenic	D3A4	NO				
B in A	gen	A	B	B	B	B	B	B	B	B	B	A	Transgenic	D3A4	YES	-	C	-	
AGFP in B	gen	A	B	B	B	B	B	B	B	B	B-GFP	A	Transgenic	D3A4	YES	-	C	O	
IIC	gen	C	C	C	C	C	C	C	C	C	C	C	Transgenic	D4A2	YES	O	C	O	
IIC	cDNA	C	C	C	C	C	C	C	C	C	C	C	Transgenic	D4A2	YES	O	C	O	
ICAEARN	gen	C	C	C	C	C	C	C	C	C	C	C	Transgenic	D4A2	YES	O	C	O	
IICGFP AEARN	gen	C	C	C	C	C-GFP	C	C	C	C	C	C	Transgenic	D4A2	YES	O	C	O	
CCB	cDNA	C	C	C	C	C	C	C	C	C	A	A	Transgenic	D4A2	YES	O	C	O	
CNC	cDNA	C	C	C	C	C	C	C	A	A	C	C	Transgenic	D4A2	NO				
CNA	cDNA	C	C	C	C	C	C	C	A	A	C	C	Transgenic	D4A2	NO				
CCB	cDNA	C	C	C	C	C	C	C	B	B	B	B	Transgenic	E3/77	YES				
IIB	gen	D	B	B	D	D	D	D	D	D	D	D	Transgenic	E3	YES	O	C	O	
IIB	cDNA	D	B	B	D	D	D	D	D	D	D	D	Transgenic	E3	YES	O	C	O	
D3C	gen	D	B	B	D	D	D	D	D	D	C	C	Transgenic	E3	YES	-	---	---	
D3E	cDNA	D	B	B	D	D	D	D	D	D	E	E	Transgenic	E3	YES	-	---	---	
IIB E75A	gen	D	B	B	D	D	D	D	D	D	D	D	Transgenic	E3	YES	-	---	---	
IIC lurcher	cDNA	D	D	D	D	D	D	D	D	D	D	D	Transgenic	E3WT					
IID 20x10Q	gen	D	D	D	D	D	D	D	D	D	D	D	Transgenic	E3	YES	-	---	---	
IID 10x10Q	gen	D	D	D	D	D	D	D	D	D	D	D	Transgenic	E3	YES	-	---	---	
D3E	cDNA	E	E	E	E	E	E	E	E	E	E	E	Transgenic	E3	NO				
IIE	gen	E	E	E	E	E	E	E	E	E	E	E	Transgenic	E3	YES	O	O	O	O
IIE	cDNA	E	E	E	E	E	E	E	E	E	E	E	Transgenic	E3	YES	O	O	O	O
EED	cDNA	E	E	E	E	E	E	E	E	E	D	D	Transgenic	E3	NO				
IIE lurcher	cDNA	E	E	E	E	E	E	E	E	E	E	E	Transgenic	E3WT					
EDD	cDNA	E	E	E	E	E	E	E	D	D	D	D	Transgenic	E3	NO				

Fig. 63. Constructs and transgenes 2

Abbreviations denote: SP – signal peptide, N1-4 – NTD sub-region 1-4, C – CTD, Rec – glutamate receptor level, PSD – PSD size, Phys – eEJC currents, A (yellow) – GluRIIA, B (orange) – GluRIIB, C (red) – GluRIIC, D (purple) – GluRIID, E (blue) - GluRIIE, GFP – insertion of GFP, o → normal, - → reduced, -- → strongly reduced.

Construct	Insertion site	Location	DNA	Linker	Method	Backgr.	Status	Rescue	Signal	Comments
IIA GFP	28	N1	gen	3xSGGGG	directed	Dfclh4	Transgenic	no	no	
	52	N1	gen	TGPT-0	IVT	Dfclh4	Transgenic	no	no	
	255	N2	gen	TGPT-0	directed	Dfclh4	Transgenic	no	no	
	262	N2	gen	TGPT-0	IVT	Dfclh4	Transgenic	no	no	
	301	N3	cDNA	TGPT-0	directed	Dfclh4	Transgenic	no	no	
	301	N3	gen	TGPT-0	directed	Dfclh4	Transgenic	no	no	
	319	N3	cDNA	TGPT-1	directed	Dfclh4	Transgenic	no	no	
	319	N3	gen	TGPT-1	directed	Dfclh4	Transgenic	no	no	
	355	N3	gen	TGPT-0	directed	Dfclh4	Transgenic	no	no	
	427	S1	gen	TGPT-0	IVT	Dfclh4	Transgenic	no	no	
	458	S1	gen	TGPT-0	IVT	Dfclh4	Transgenic	no	no	
	519	S1	gen	TGPT-0	IVT	Dfclh4	Transgenic	no	no	
	709	S2	gen	TGPT-0	IVT	Dfclh4	Transgenic	no	no	
	760	S2	gen	TGPT-0	IVT	Dfclh4	Transgenic	no	no	
	893	C	gen	TGPT-1	directed	Dfclh4	Transgenic	yes	yes	Strong signal, Phys as untagged
IIA mRFP	893	C	gen	TGPT-1	directed	Dfclh4	Transgenic	yes	yes	Strong signal
IIA PAGFP	893	C	gen	TGPT-1	directed	Dfclh4	Transgenic	yes	yes	Strong signal
IIA Cameleon 3.1	893	C	gen	TGPT-1	directed	Dfclh4	Transgenic	yes	yes	Strong signal
IIA Cameleon null	893	C	gen	TGPT-1	directed	Dfclh4	Transgenic	yes	yes	Strong signal
IIA TN-XL	893	C	gen	TGPT-1	directed	Dfclh4	Transgenic	yes	yes	Very weak rescue and signal
IIB GFP	77	N1	gen	TGPT-0	IVT	Dfclh4	Transgenic	no	no	
	150	N2	gen	TGPT-0	IVT	Dfclh4	Transgenic	no	no	
	199	N2	gen	TGPT-0	IVT	Dfclh4	Transgenic	no	no	
	284	N3	gen	TGPT-0	directed	Dfclh4	Transgenic	no	no	
	287	N3	gen	TGPT-0	IVT	Dfclh4	Transgenic	no	no	
	309	N3	gen	TGPT-0	directed	Dfclh4	Transgenic	no	no	
	360	N4	gen	TGPT-0	IVT	Dfclh4	Transgenic	no	no	
	637	Pore	gen	TGPT-0	IVT	Dfclh4	Transgenic	no	no	
	857	C	gen	TGPT-0	IVT	Dfclh4	Transgenic	no	no	
	861	C	gen	TGPT-0	IVT	Dfclh4	Transgenic	no	no	
	897	C	gen	TGPT-1	directed	Dfclh4	Transgenic	yes	yes	Strong signal, Phys as untagged
IIB mRFP	897	C	gen	TGPT-0	directed	Dfclh4	Transgenic	yes	yes	Strong signal
IIB PAGFP	897	C	gen	TGPT-0	directed	Dfclh4	Transgenic	yes	yes	Rather weak signal
IIC GFP	321	N3	cDNA	TGPT-0	directed	Dfast4	Transgenic	yes	yes	Strong signal
	321	N3	gen	TGPT-0	directed	Dfast4	Transgenic	no	no	
	344	N3	cDNA	TGPT-1	directed	WT	Transgenic		no	
	921	C	cDNA	TGPT-1	directed	Dfast4	Transgenic	yes	yes	Strong signal
IIC mRFP	321	N3	cDNA	TGPT-0	directed	Dfast4	Transgenic	yes	yes	Strong signal
	921	C	cDNA	TGPT-1	directed	Dfast4	Transgenic	yes	yes	Strong signal
IIC ecliptic pHluorin	321	N3	cDNA	TGPT-0	directed	Dfast4	Transgenic	yes	yes	Strong signal
	921	C	cDNA	TGPT-1	directed	Dfast4	Transgenic	yes	yes	Strong signal
PAK GFP	C-term	C	cDNA	none	directed	WT	Transgenic		yes	(Too) strong signal
PAK mRFP	C-term	C	cDNA	none	directed	WT	Cloning failed			
Synaptophysin 2xpHluorin	internal	?	cDNA	?	restriction	WT	Transgenic		yes	Specific signal

Fig. 64. Constructs and transgenes 3

Abbreviations denote: N1-4 – NTD sub-region 1-4, S1/2 – glutamate binding domain, C – CTD, IVT – *in vitro* transposition, PAGFP – photoactivatable GFP, TGPT-0/1 – transposon type (Sheridan et al., 2002), Phys – physiology, WT – wild type. For information on genetic background (Backgr.) see 3.2.2 .

7.4. *In vivo* imaging device

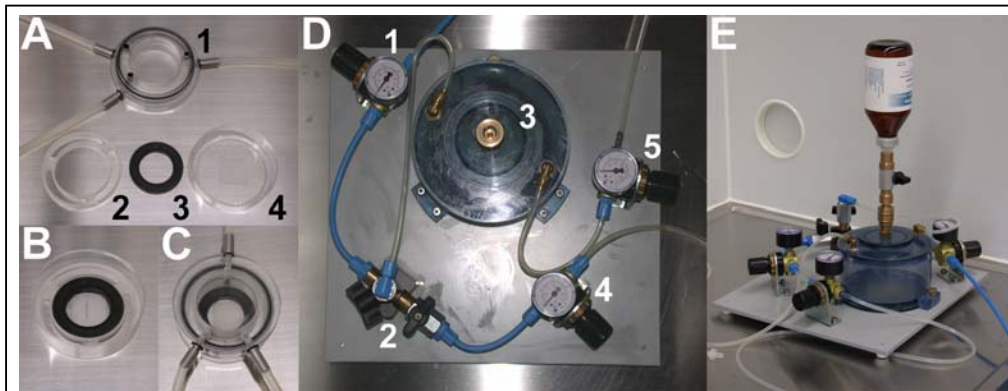


Fig. 65. *In vivo* imaging device

A, Components of the imaging chamber: cover plate with three hose connections (1), plastic guide ring (2), iron ring (3), Petri dish with coverslip bottom and plastic disc with slit (4). **B**, Assembled imaging chamber without the cover plate. **C**, Completely assembled chamber. **D**, Anesthetization device: Compressed-air supply (1), two-way valve (2), vaporization chamber (3), air supply (4), anesthetic supply (5). **E**, Anesthetization device with Suprane supply via an outlet adapter.

7.5. Normalization of the PSD number and NMJ size

In two independent experiments (wild type and *IIA^{hypo}*, see Fig. 23J,K) the development of the PSD number from 2nd to 3rd instar larval stage was followed (NMJ 6/7, at least 6 animals per stage). On the average the PSD number (*n*) nearly doubled (1.92-fold). In parallel, the body wall muscles increased in size: length (*L*), 1.82-fold, width (*W*), 1.95-fold, area (*A*), 3.59-fold. While the quotients *n/L* and *n/W* remained stable (1.03-fold and 0.95-fold, respectively), the quotient *n/A* halved (0.51-fold). Bearing in mind that the mean PSD size increased only about 0.03 μm^2 from 2nd to 3rd instar (see Fig. 23J,K), the average transmission strength of an individual synapse stays rather stable. Thus, normalization of the PSD number to the muscle area, which ends up in a reduction from 2nd to 3rd instar, is misleading as an activation of a larger muscle does not suit a reduced synapse density. At last, normalization to the segment length seems to be a more appropriate way.

8. Abbreviations

- AA – amino acid
- AB – antibody
- ABP – AMPA receptor binding protein
- AChR – acetylcholine receptor
- AEL – after egg laying
- AMPA – alpha-amino-3-hydroxy-5-methyl-4-isoxazole-propionic acid
- a.u. – arbitrary unit
- AZ – active zone
- bp – base pairs
- BRP - Brurchpilot protein
- cac – cacophony
- CAM – cell adhesion molecule
- CaMKII – calmodulin-dependent kinase II
- cAMP – cyclic adenosine monophosphate
- CAZ – cytomatrix at the active zone
- CNS – central nervous system
- CTD – C-terminal domain
- Dlg – Discs large
- eEJC – evoked excitatory junctional current
- EGFP – enhanced green fluorescent protein
- EM – electron microscopy
- ER – endoplasmatic reticulum
- FasII – FasciilinII
- FRAP – fluorescence recovery after photobleaching
- GABA – γ-aminobutyric acid
- GAL4 - galactosidase 4 protein
- GFP – green fluorescent protein
- GluR – glutamate receptor
- GRIP – glutamate receptor interacting protein
- HRP – horse radish peroxidase
- iGluR – ionotropic glutamate receptor
- Int_{rel} – relative intensity
- IVT – in vitro transposition
- LTD – long-term depression
- LTP – long-term potential

-
- MAGUK – membrane-associated guanylate kinase
 - mEJC – miniature excitatory junctional current
 - mgv – mean gray value
 - Mhc – myosin heavy chain
 - mRFP – monomeric red fluorescent protein
 - MuSK – muscle-specific kinase
 - NCAM – neural cell adhesion molecule
 - NGS – natural goat serum
 - NSF – N-ethylmaleimide-sensitive factor
 - NMDA – N-methyl-D-aspartate
 - NMJ – neuromuscular junction
 - PAK – p21-activated kinase
 - PFA – paraformalaldehyde
 - PICK1 – protein interacting with C-kinase 1
 - PIX – PAK-interacting exchange factor
 - PKA – protein kinase A
 - PKC – protein kinase C
 - PSD – postsynaptic density
 - PSD-95 – postsynaptic density protein 95
 - Ptv – presynaptic transport vesicle
 - SAP97 – synapse-associated protein 97
 - SSR – subsynaptic reticulum
 - TEVC – two-electrode voltage clamp
 - TNT – tetanus toxin light chain
 - UAS – upstream activating sequence
 - UTR – un-translated region

9. List of publications

- Swan LE, Wichmann C, Prange U, Schmid A, Schmidt M, Schwarz T, Ponimaskin E, Madeo F, Vorbruggen G, Sigrist SJ (2004) A glutamate receptor-interacting protein homolog organizes muscle guidance in *Drosophila*. *Genes Dev* 18:223-237.
- Qin G, Schwarz T, Kittel RJ, Schmid A, Rasse TM, Kappei D, Ponimaskin E, Heckmann M, Sigrist SJ (2005) Four different subunits are essential for expressing the synaptic glutamate receptor at neuromuscular junctions of *Drosophila*. *J Neurosci* 25:3209-3218.
- Rasse TM, Fouquet W, Schmid A, Kittel RJ, Mertel S, Sigrist CB, Schmidt M, Guzman A, Merino C, Qin G, Quentin C, Madeo FF, Heckmann M, Sigrist SJ (2005) Glutamate receptor dynamics organizing synapse formation in vivo. *Nat Neurosci* 8:898-905.
- Kittel RJ, Wichmann C, Rasse TM, Fouquet W, Schmidt M, Schmid A, Wagh DA, Pawlu C, Kellner RR, Willig KI, Hell SW, Buchner E, Heckmann M, Sigrist SJ (2006) Bruchpilot promotes active zone assembly, Ca²⁺ channel clustering, and vesicle release. *Science* 312:1051-1054.
- Schmid A, Qin G, Wichmann C, Kittel RJ, Mertel S, Fouquet W, Schmidt M, Heckmann M, Sigrist SJ (in revision) Non-NMDA type glutamate receptors are essential for maturation but not for initial assembly of synapses at *Drosophila* NMJs. *J Neurosci*.
- Schmid A, Sigrist SJ (in press) "Analysis of neuromuscular junctions: histology and in vivo imaging" in "Methods in Molecular Biology, Volume: *Drosophila*". Totawa, NJ: Humana Press.

10. Curriculum vitae

Am 22. September 1977 wurde ich in München geboren. Ich besitze die deutsche Staatsangehörigkeit. Von 1988 bis 1997 besuchte ich das Willibald-Gluck-Gymnasium in Neumarkt i.d.OPf., das ich 1997 mit der allgemeinen Hochschulreife abschloss. Von Oktober 1997 bis September 1998 leistete ich Ersatzdienst am Krankenhaus Rummelsberg, Schwarzenbruck. Parallel dazu absolvierte ich an der Krankenpflegehilfeschule Rummelsberg eine Ausbildung zum Krankenpflegehelfer, die ich im September 1998 abschloss. Im Oktober 1998 begann ich an der Fachhochschule Weihenstephan mein Studium zur Biotechnologie. Im März 2003 erlangte ich den Grad Dipl.-Ing.(FH). Im April 2003 begann ich in der Abteilung von Prof. Dr. Stephan Sigrist am European Neuroscience Institute in Göttingen unter der Anleitung von Prof. Dr. Ernst Wimmer die Arbeit an meiner Dissertation mit dem Titel "The role of glutamate receptors in formation and maturation of *Drosophila* neuromuscular synapses".